ISSN (1230-0322)
2026, Vol. 76, No. 2

Food

Polish Journal of Food and Nutrition Sciences

formerly Acta Alimentaria Polonica

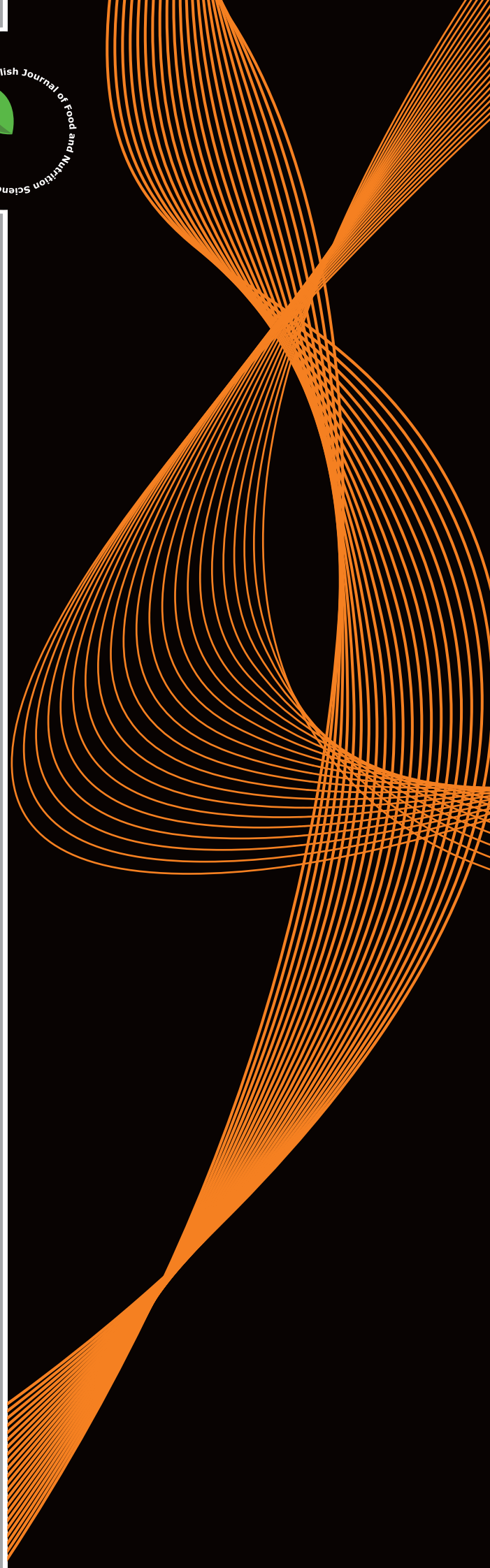

Published

by InLife Institute of Animal Reproduction and Food Research, Polish Academy of Sciences, Olsztyn

Published since 1957 as
Roczniki Chemii i Technologii Żywności and Acta Alimentaria Polonica (1975–1991)

SCOPE: The Journal covers fundamental and applied research in food area and nutrition sciences with a stress on interdisciplinary studies in the areas of food, nutrition and related subjects.

POLICY: Editors select submitted manuscripts in relation to their relevance to the scope. Reviewers are selected from the Advisory Board and from Polish and international scientific centres. Identity of reviewers is kept confidential.

AUTHORSHIP FORMS referring to Authorship Responsibility, Conflict of Interest and Financial Disclosure, Copyright Transfer and Acknowledgement, and Ethical Approval of Studies are required for all authors.

FREQUENCY: Quarterly – one volume in four issues (March, June, September, December).

COVERED by Web of Science, Current Contents/Agriculture, Biology & Environmental Sciences, Journal Citation Reports and Science Citation Index Expanded, BIOSIS (Biological Abstracts), SCOPUS, FSTA (formerly: Food Science and Technology Abstracts), CAS (Chemical Abstracts), AGRICOLA, AGRO-LIBREX data base, EBSCO, FOODLINE, Leatherhead FOOD RA data base FROSTI, AGRIS, Biblioteka Nauki ICM, Biblioteka Narodowa – POLONA, and any www browser; ProQuest: The Summon, Bacteriology Abstracts, Immunology Abstracts.

EDITORIAL AND BUSINESS CORRESPONDENCE: Submit contributions (see Instructions to Authors) and address all communications regarding subscriptions, changes of address, etc. to:

CORRESPONDENCE TO: Ms. Joanna Molga
Polish Journal of Food and Nutrition Sciences
InLife Institute of Animal Reproduction and Food Research,
Polish Academy of Sciences,
ul. Trylińskiego 18, 10-683 Olsztyn, Poland
e-mail: pjfns@pan.olsztyn.pl; http://journal.pan.olsztyn.pl

Polish Journal of Food and Nutrition Sciences

ADVISORY BOARD OF PJFNS 2023–2026

Contents

ORIGINAL PAPERS

covered by CURRENT CONTENTS/AGRICULTURE, BIOLOGY & ENVIRONMENTAL SCIENCES, JOURNAL CITATION REPORTS AND SCIENCE CITATION INDEX EXPANDED, BIOSIS, SCOPUS, IFIS Publishing and CAS abstracts, and AGRO-Librex, FROSTI, PSJC and AGRIS data bases

Subscription
Since 2025, PJFNS is published only on-line. Past issues can be ordered as previously. One volume,
four issues per volume. Annual subscription rates are: Poland 150 PLN, all other countries 80 EUR.
Prices are subject to exchange rate fluctuation. Subscription payments should be made by direct bank transfer to
Bank Gospodarki Żywnościowej, Olsztyn, Poland, account No 17203000451110000000452110 SWIFT code: GOPZPLWOLA
with corresponding banks preferably. Subscription and advertising offices at the Institute of Animal Reproduction
and Food Research of Polish Academy of Sciences, ul. Trylińskiego 18, 10-683 Olsztyn, Poland, tel./fax (48 89) 5003245,
e-mail: pjfns@pan.olsztyn.pl; http://journal.pan.olsztyn.pl

Wersja pierwotna (referencyjna) kwartalnika PJFNS: wersja on-line (eISSN 2083-6007)
Ark. wyd. 17,5
Skład: ITEM

ORIGINAL ARTICLE
http://journal.pan.olsztyn.pl

Polish Journal of Food and Nutrition Sciences
2026, Vol. 76, No. 2, 120–134
DOI: 10.31883/pjfns/220155
ISSN 1230-0322, e-ISSN 2083-6007

Development of a Vegan Soybean-Based Yoghurt Alternative Using *Levilactobacillus brevis* QD-1 and *Saccharomyces cerevisiae* as the Starter Culture for Improved Texture and Aroma Profile

Thanh-Sang Nguyen[1], Quoc-Duy Nguyen[2], Hong-Tham Truong-Thi[2,3], Hieu Vu-Quang[2], Anh D. Do[4]*

[1]Food Technology Faculty, Saigon Technology University, Ho Chi Minh City, Vietnam
[2]Faculty of Applied Science and Technology (FAST), Nguyen Tat Thanh University, Ho Chi Minh City, Vietnam
[3]VINACROP Company Limited, Ho Chi Minh City, Vietnam
[4]CIRTech Institute, HUTECH University, Ho Chi Minh City, Vietnam

This study aimed to develop a vegan soybean yoghurt alternative using co-cultures of *Levilactobacillus brevis* QD-1 and *Saccharomyces cerevisiae*, and to evaluate their effects on textural properties, protein structure, and aroma profile of the end product. Filtered and concentrated soybean slurry was fermented using varying inoculum densities (10^3–10^5 CFU/mL) of *L. brevis* alone and in combination with *S. cerevisiae*. Visible coagulation occurred at approximately 9 h of fermentation, when pH reached 5.12–5.68. Co-cultured samples exhibited significantly improved textural attributes, including increased hardness and gumminess, and water-holding capacity, which were associated with elevated exopolysaccharide (EPS) production primarily attributable to *L. brevis*. In particular, the soybean yoghurt alternatives produced by co-cultured fermentation using an inoculum density of 10^4 and 10^5 CFU/mL showed the highest EPS contents (201–216 mg/L), along with increased hardness (1.48–1.58 N) and gumminess (0.74–0.77 N). Sodium dodecyl sulfate–polyacrylamide gel electrophoresis analysis demonstrated more extensive degradation of allergenic soy proteins, including β-conglycinin and glycinin, in the co-fermented samples. Fourier-transform infrared spectroscopy indicated favourable modifications in protein secondary structure, notably an increased α-helix content, consistent with improved gel network formation. In addition, the volatile organic compound profile was characterised by shifts in the relative abundances of acetic acid, 2,3-butanediol, and phenethyl alcohol in the presence of yeast. At the highest co-culture level, ethanol content decreased to 69.55% of total volatile organic compounds, while contents of acetic acid, 2,3-butanediol, and phenethyl alcohol increased to 15.42%, 9.46%, and 1.87%, respectively. Collectively, these findings indicate that lactic acid bacteria and yeast co-fermentation may represent a promising approach to produce high-quality plant-based yoghurt with enhanced nutritional and sensory characteristics.

Keywords: exopolysaccharides, lactic acid bacteria–yeast interaction, plant-based fermentation, protein structural modification, volatile compounds

INTRODUCTION

Vegan food alternatives to conventional dairy products present both nutritional advantages and limitations, as reported in multiple studies. Plant-based dairy alternatives (PBDAs) generally contain higher levels of dietary fibre and lower amounts of saturated fat than traditional dairy products, which may

***Corresponding Author:**
E-mail: **da.duy93@hutech.edu.vn** (Dr. Anh Duy Do)

Submitted: 31 December 2025
Accepted: 30 March 2026
Published on-line: 13 April 2026

contribute to an improved overall diet quality and a reduced saturated fat intake [Marchese *et al*., 2024; Moshtaghian *et al*., 2024]. However, most PBDAs tend to provide a lower protein content, with the notable exception of soy-based products, which can match or exceed the protein levels typically found in dairy products [Moshtaghian *et al*., 2024]. Nevertheless, PBDAs may still be nutritionally limited in terms of micronutrients that are naturally abundant in dairy products, including iodine and vitamin B_2, unless appropriate fortification strategies are applied [Medici *et al*., 2023]. From an environmental perspective, PBDAs offer substantial benefits, including reduced greenhouse gas emissions and lower land and water requirements relative to dairy production, rendering them an attractive option for consumers seeking more sustainable dietary choices [Craig *et al*., 2023].

A soybean yoghurt alternative offers several nutritional advantages over traditional dairy yoghurt, largely attributable to its distinctive composition and the fermentation process involved. A key benefit is its suitability for individuals with lactose intolerance and those adhering to a vegan diet, as it is entirely plant-based and free from lactose. From a nutritional perspective, a soybean yoghurt alternative is rich in proteins, vitamins, and minerals, with reported increases in B vitamins and unsaturated fatty acids compared to an unfermented soybean substrate used for its production, which are associated with cardiovascular health benefits [Mehaya *et al*., 2023]. Fermentation further enhances soybean nutrient bioavailability, including that of isoflavones, which have been implicated in the modulation of hyperglycaemic disorders [Langa *et al*., 2023]. In addition, soybean yoghurt has been shown to positively influence gut microbiota composition, an important determinant of digestive health, by promoting beneficial genera, such as *Lactobacillus* and *Bifidobacterium* [Park & Mannaa, 2025]. The presence of γ-aminobutyric acid (GABA) in certain soybean yoghurt formulations may further contribute to health-promoting effects, particularly with respect to glucose regulation and gut health [Weng *et al*., 2023]. Moreover, substitution of cow's milk with a soybean substrate in yoghurt production does not appear to substantially compromise micronutrient content, as mineral and vitamin levels in the soybean yoghurt alternative are comparable to those of conventional yoghurt [Otolowo *et al*., 2022]. Finally, fermentation with selected lactic acid bacteria strains has been reported to enhance mineral bioavailability, which may be beneficial for bone health [Gan *et al*., 2023].

Co-cultivation of lactic acid bacteria (LAB) and yeast during fermentation of soybean-based substrates represents a promising strategy for enhancing the nutritional and functional properties of the final product. The combined use of LAB and yeast has been reported to improve nutrient and mineral bioavailability, as evidenced by enhanced mineral bioaccessibility and solubility, along with the degradation of phytate-mineral and protein-mineral complexes into smaller, more readily bioavailable forms during LAB-mediated fermentation [Gan *et al*., 2023]. In particular, fermentation of soybean substrate using *Saccharomyces boulardii* in combination with *Lactobacillus plantarum* has been shown to enhance the nutritional profile, including elevated levels of B vitamins, unsaturated fatty acids, and antioxidant activity, compared with LAB-only fermentation [Mehaya *et al*., 2023]. In addition, co-cultivation of selected yeasts with LAB may confer distinctive aromatic and functional attributes to soy-based fermented beverages, as demonstrated by yeast consortia that increase phenolic content and antioxidant capacity while maintaining probiotic viability [Agarbati *et al*., 2023]. The synergistic interactions between LAB and yeast are further supported by reports of improved carbohydrate utilisation and metabolite release, resulting in increased lactic acid production and enhanced probiotic growth [do Amaral Santos *et al*., 2014]. Moreover, co-cultivation strategies may mitigate undesirable off-flavours and improve sensory characteristics, as LAB are capable of producing flavour-enhancing volatile compounds [Lee *et al*., 2024]. These positive microbial interactions are considered critical for optimising substrate conversion and improving the nutritional and sensory quality of fermented soy products [Canon *et al*., 2020]. Nevertheless, the specific effects of LAB–yeast co-cultivation on soybean yoghurt alternative quality parameters, including texture, protein structure, and aroma profile, remain insufficiently explored.

This study investigated the effects of co-fermentation of *Levilactobacillus brevis* and *Saccharomyces cerevisiae* on the physicochemical and structural properties of soybean-based yoghurt. By modulating initial inoculation densities, the influence of microbial interactions on gel formation, protein secondary structure, exopolysaccharide (EPS) production, and volatile organic compound profiles was systematically examined.

MATERIALS AND METHODS

Microorganism strains and culture conditions

The bacterial strain *L. brevis* QD-1 (NCBI accession number: PRJNA1121961) and the yeast strain *S. cerevisiae* (NCBI accession number: PP116084) were previously isolated from kombucha [Nguyen & Nguyen, 2024] and maintained in the microbial culture collection of the Department of Food Technology, Faculty of Applied Science and Technology (FAST), Nguyen Tat Thanh University, Ho Chi Minh City, Vietnam. *L. brevis* QD-1 was maintained on De Man–Rogosa–Sharpe agar (MRS; HiMedia Laboratories Pvt. Ltd., Mumbai, India), while *S. cerevisiae* was cultivated on yeast extract–peptone–dextrose agar (YPD; HiMedia Laboratories Pvt. Ltd., Mumbai, India). Prior to fermentation, *L. brevis* was propagated in MRS broth at 37°C for 18 h under anaerobic conditions, and *S. cerevisiae* was cultured in YPD broth at 30°C for 24 h under aerobic conditions. Preliminary growth curve experiments (data not shown) confirmed that these incubation times corresponded to late exponential phase. Following incubation, both cultures were harvested by centrifugation at 10,000×*g* for 5 min and washed twice with phosphate-buffered saline (PBS). The washed cell pellets were resuspended in sterile PBS and adjusted to an optical density of 1.0 measured at 600 nm (OD_{600}), corresponding to approximately 1×10^8 CFU/mL, to obtain standardised stock suspensions for subsequent inoculation.

Fermentation of soybean water slurry by a mixed culture of *Levilactobacillus brevis* QD-1 and *Saccharomyces cerevisiae*

High-quality, mould-free soybeans were procured from Choice L Ltd., Ho Chi Minh City, Vietnam. According to the manufacturer's specifications, the raw soybeans contained approximately 34 g of protein, 18.4 g of lipids, 24.6 g of carbohydrates, and 4.5 g of dietary fibre *per* 100 g (dry weight basis). The soybeans were soaked in water for 8 h, dehulled, and ground with water at a ratio of 1:2 (g/mL). The resulting slurry was filtered through a cloth and heat-treated at 85°C until the extract reached a total solid content of 17% and an initial pH of 6.75±0.05, as measured using an Mi150 pH meter (Milwaukee Instruments, Szeged, Hungary). Following cooling to 37°C, the soybean extract was inoculated with a mixed culture of *L. brevis* QD-1 and *S. cerevisiae* at a 1:1 ratio (based on CFU counts), at final inoculation levels for each strain being 10^3 CFU/mL (LB+S_3), 10^4 CFU/mL (LB+S_4), and 10^5 CFU/mL (LB+S_5). The inoculum was added as a washed cell suspension at 1% (*v/v*) of the soybean extract volume. Control samples were inoculated with *L. brevis* QD-1 alone at the same cell densities and designated LB_3, LB_4, and LB_5, respectively. Fermentation was conducted at 37°C for 16 h in accordance with the procedure described by Nguyen *et al*. [2024].

Analytical methods

pH and total acidity determination

The pH was measured using a Mi150 pH meter (Milwaukee Instruments). Total titratable acidity (TTA) was determined by titrating 10 mL of the sample with 0.1 M NaOH to an endpoint of pH 8.3, using 1% (*w/v*) phenolphthalein as an indicator. Titratable acidity was expressed as grams of lactic acid equivalent *per* litre (g/L) and calculated using the following Equation (1):

$$TTA = (V_{NaOH} \times 0.009 \times 1{,}000)/V_{sample} \quad (1)$$

where: V_{NaOH} is the volume of 0.1 M NaOH consumed during titration (mL), V_{sample} is the sample volume (mL), and 0.009 is the conversion factor for a lactic acid equivalent [Nielsen, 2017].

Surface morphology observation during fermentation

Surface morphology was evaluated macroscopically throughout fermentation by visual observation and photographic recording of the sample surface at different fermentation times, with particular attention to coagulation onset and the appearance of surface cracks [Nguyen *et al*., 2024].

Microbial density determination

Microbial density was quantified by the serial dilution plate count method. For *L. brevis*, appropriate dilutions were spread on MRS agar and incubated anaerobically at 37°C for 48 h. For *S. cerevisiae*, samples were plated on YPD agar supplemented with 1% chloramphenicol to inhibit bacterial growth and incubated aerobically at 37°C for 48 h. Colony counts were recorded and expressed as log CFU/mL [Van *et al*., 2023].

Exopolysaccharide quantification

Exopolysaccharides (EPS) were isolated from soybean yoghurt alternative samples using a modified method based on the protocol described by Lin & Chien [2007]. Proteins and bacterial cells were precipitated by the addition of an equal volume of 40% trichloroacetic acid, followed by centrifugation at 10,000×*g* for 15 min at 4°C. The resulting supernatant was mixed with an equal volume of ethanol and stored at 4°C for 24 h to allow EPS precipitation. The crude EPS was transferred into dialysis tube (10–14 kDa molecular weight cut-off) and dialysed against distilled water at 4°C for 24–48 h to remove residual medium components and other low-molecular-weight impurities. Following centrifugation under identical conditions, the EPS pellet was collected and resuspended in distilled water. The total neutral glycoside content was subsequently quantified using the phenol-sulphuric acid method, where 1 mL of the sample was mixed with 1 mL of a 5% phenol solution, followed by the rapid addition of 5 mL of concentrated sulphuric acid, incubated at room temperature for 10–30 min, and absorbance was measured at 490 nm using a glucose standard curve, with results expressed as glucose equivalents [Urshev *et al*., 2007].

Water-holding capacity and syneresis determination

Water-holding capacity (WHC) was determined by centrifuging 5 g of the soybean yoghurt alternative at 3,000×*g* for 10 min. WHC (%) was calculated using Equation (2):

$$WHC = (1 - W_2/W_1) \times 100 \quad (2)$$

where: W_1 is the initial sample weight and W_2 denotes the weight of the supernatant obtained after centrifugation.

Syneresis was determined by storing 30 g of the soybean yoghurt alternative at 4°C for 2 h. This duration was established through preliminary trials to monitor initial whey separation while minimising confounding effects from long-term structural rearrangements. The percentage of syneresis was calculated as the mass of the expelled whey, relative to the initial sample weight [Dönmez *et al*., 2017].

Texture profile analysis

Texture profile analysis (TPA) was performed using a CT3 texture analyser (AMETEK Brookfield Inc., Middleboro, MA, USA) fitted with a cylindrical probe (TA4/1000; diameter 38.1 mm). The test conditions were as follows: probe-to-sample distance of 30 mm, trigger load of 7 g, and test and return speeds of 0.5 mm/s. Each sample was subjected to two consecutive compression cycles, with a total test duration of approximately 170 s and no recovery between cycles, allowing the acquisition of two positive force regions. Textural parameters, including hardness, cohesiveness, springiness, gumminess, and adhesiveness, were recorded and analysed using Text Proc CT V1.3 software (AMETEK Brookfield Inc., Middleboro, MA, USA). Hardness and gumminess were expressed in Newtons (N), converted from gram-force using the factor of 0.009807 N/g.

Sodium dodecyl sulfate–polyacrylamide gel electrophoresis

The protein composition of soybean yoghurt alternative samples was analysed by sodium dodecyl sulfate–polyacrylamide gel electrophoresis (SDS-PAGE) using 10% resolving gels [Laemmli, 1970]. Prior to electrophoresis, the samples were denatured by mixing with a sample buffer at a ratio of 4:1 (*v/v*), followed by heating at 100°C for 3 min and cooling for 2 min. Subsequently, 20 µL of the denatured sample were loaded into wells of a 4% stacking gel prepared with the following composition: 0.65 mL of 30% acrylamide, 1.75 mL of 0.5 mM Tris-HCl buffer (pH 6.8), 3 mL of distilled water, 100 µL of 10% SDS, 100 µL of 10% ammonium persulfate (APS), and 10 µL of *N,N,N',N'*-tetramethylethylenediamine (TEMED). Electrophoresis was performed at 80 V until the proteins migrated through the stacking gel, after which the voltage was increased to 120 V for separation in the 10% resolving gel, composed of 3.3 mL of 30% acrylamide, 2.5 mL of 0.5 mM Tris-HCl buffer (pH 8.8), 4 mL of distilled water, 100 µL of 10% SDS, 100 µL of 10% APS, and 4 µL of TEMED. Following electrophoresis, the gels were stained with 0.23% Coomassie Brilliant Blue R-250 for 30 min and subsequently destained in a solution containing 10% methanol and 10% acetic acid until a clear background was achieved. Protein bands were visualised using a BioDoc-It UVP imaging system (Analytik Jena AG, Jena, Germany). Protein molecular weights were estimated by comparison with standard protein molecular weights ranging from 10 to 250 kDa (PageRuler Plus prestained protein ladder 26619, Thermo Fisher Scientific, Waltham, MA, USA). Results were expressed as qualitative band intensity comparisons.

Determination of secondary structure of protein by Fourier transform infrared spectroscopy

Lyophilised soybean yoghurt alternative samples (1 mg) were mixed with 100 mg of KBr and pressed into pellets. Fourier transform infrared (FTIR) spectroscopy was employed to characterise protein secondary structure. FTIR spectra were acquired over the wavenumber range of 400–4,000 cm^{-1} using an MIR Frontier FTIR spectrometer (PerkinElmer, Waltham, MA, USA) at a spectral resolution of 4 cm^{-1}. Protein secondary structures were evaluated by focusing on the amide I region (1,600–1,700 cm^{-1}), which is highly sensitive to backbone conformations. Prior to analysis, spectra were baseline-corrected using a second-order polynomial function. Fourier self-deconvolution (FSD) and second derivative methods were subsequently applied to enhance spectral resolution and identify underlying component peaks. Peak deconvolution and curve fitting were performed using OriginPro 2017 (Multiple Peak Fit module; OriginLab Corporation, Northampton, MA, USA), employing Gaussian functions to resolve overlapping bands. Peak positions were assigned based on established literature, corresponding to α-helix (1,650–1,658 cm^{-1}), β-sheet (1,620–1,640 cm^{-1} and 1,670–1,690 cm^{-1}), β-turn (1,660–1,680 cm^{-1}), and random coil (1,640–1,650 cm^{-1}) structures [Nguyen *et al*., 2026]. Fitting parameters were constrained within reasonable bandwidth limits (typically 10–30 cm^{-1}), and iterative optimization was conducted until satisfactory fitting quality was achieved (R^2>0.99). The relative proportion of each secondary structural element was calculated from the integrated area of individual peaks and expressed as a percentage of the total amide I band area [Yang *et al*., 2015].

Determination of volatile organic compounds by headspace solid-phase microextraction coupled with gas chromatography–mass spectrometry

Volatile organic compound profiles of lyophilised yoghurt alternative samples were analysed using a Nexis GC-2030 gas chromatography-mass spectrometry (GC-MS) system (Shimadzu Corporation, Kyoto, Japan) equipped with a DB-5MS capillary column (30 m × 0.25 mm × 0.25 µm) and coupled to an HS-20NX headspace sampler. Briefly, 1.0 g of each sample was placed in a 20 mL headspace glass vial, followed by the addition of 2 µL of the internal standard, 2-methyl-3-heptanone (Sigma-Aldrich, St. Louis, MO, USA). A 50/30 µm divinylbenzene/carboxen/polydimethylsiloxane (DVB/CAR/PDMS) fiber was used for extraction at 60°C for 30 min. After extraction and introduction of the headspace sample into the GC-MS system, the oven temperature programme was set as follows: initial heating to 40°C for 3 min, followed by an increase to 60°C at 10°C/min, then to 150°C at 3°C/min, and subsequently to 250°C at 20°C/min, where it was held for 5 min. Helium was used as a carrier gas at a flow rate of 1.0 mL/min, with a split ratio of 15:1. Mass spectra were acquired in a scan mode over an *m/z* range of 10–500. Volatile organic compounds were identified by comparison with the NIST 14L mass spectral library and semi-quantified using the internal standard, with results expressed as relative percentages (%) of the total detected volatile compounds.

Statistical analysis

All experiments were performed using independent biological replicates, and each measurement was conducted in technical triplicate. Data are presented as mean and standard deviation. Normality of the data distribution was assessed using the Shapiro–Wilk test, and homogeneity of variances was evaluated using Levene's test. Differences among yoghurt variants were determined by one-way analysis of variance (ANOVA), followed by Tukey's post hoc test where appropriate. Statistical significance was established at p<0.05.

RESULTS AND DISCUSSION

Changes in pH, total titratable acidity, and surface morphology during soybean yoghurt alternative production

Coagulation of soybean yoghurt alternative proteins is governed by microbial activity, acidification, and enzymatic interactions. Fermentation of soybean water slurry with *L. brevis* and *S. cerevisiae* was monitored over a 16-h period, with changes in pH and total titratable acidity presented in **Figure 1**. During the initial 5 h of fermentation, pH values remained relatively stable (6.12–6.29), indicating limited metabolic activity. Between the

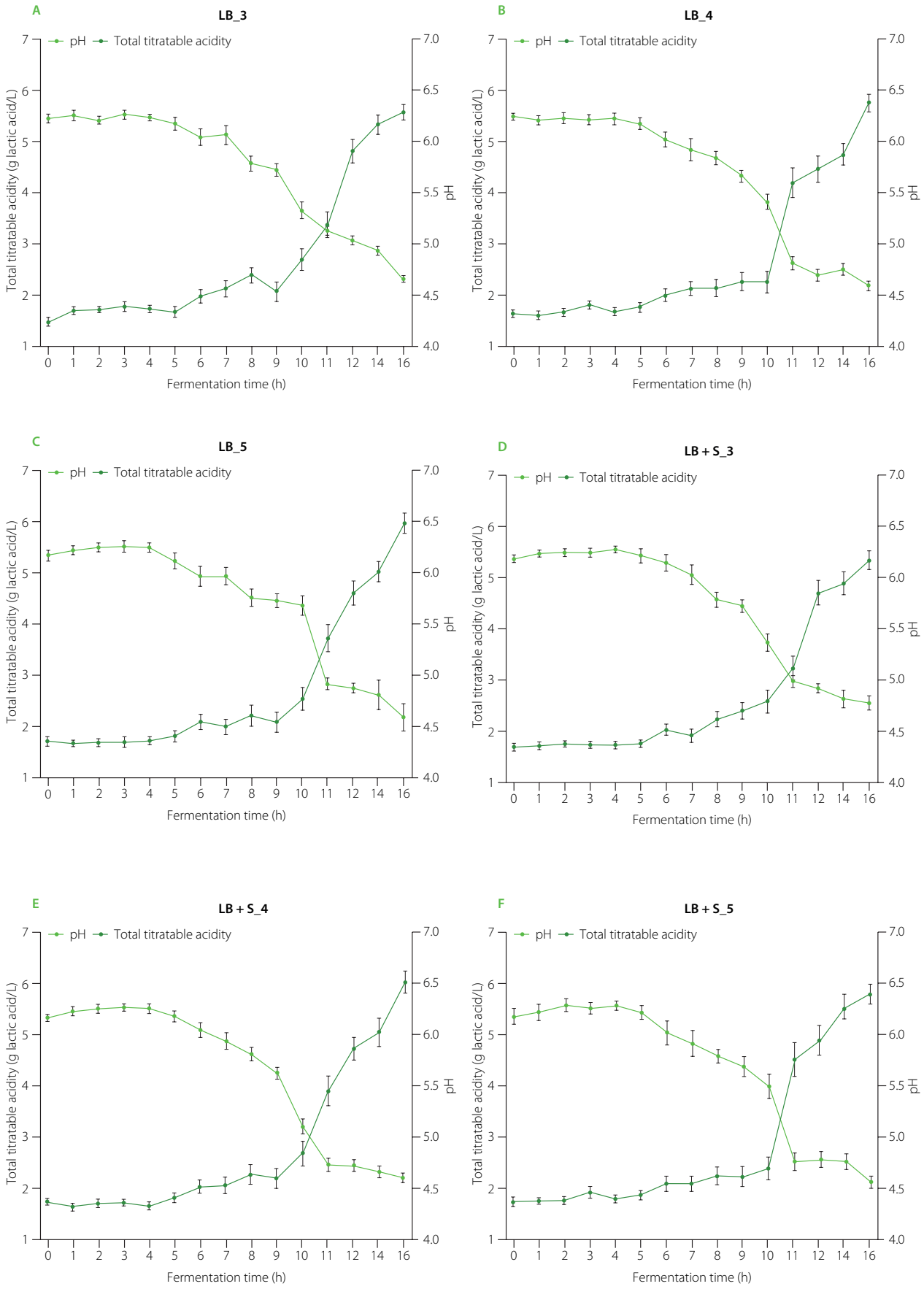

Figure 1. Changes in pH and total titratable acidity during soybean yoghurt alternative production by fermentation at 37°C using different cultures. LB_3, LB_4, LB_5: fermentation with *Levilactobacillus brevis* QD-1 with densities of 10^3, 10^4, 10^5 CFU/mL, respectively (**A–C**). LB+S_3, LB+S_4, LB+S_5: fermentation with a mixed culture of *L. brevis* and *Saccharomyces cerevisiae* (1:1, based on CFU counts) with densities of 10^3, 10^4, 10^5 CFU/mL, respectively (**D–F**).

6th and 10th h, a pronounced decline in pH was observed as a result of lactic acid accumulation (increase in total titratable acidity), with visible coagulation occurring at approximately 9 h, when pH reached 5.12–5.68. This observation is consistent with previous reports demonstrating that acidification reduces the net negative charge of soy proteins, thereby facilitating protein coagulation [Xu *et al*., 2019]. As pH decreases further, protein solubility diminishes, promoting the formation of larger aggregates and a denser gel network, which may lead to surface cracking [Rui *et al*., 2019]. In agreement with this mechanism, surface cracks were observed after 10–11 h of fermentation in all samples (**Figure 2**), suggesting that a fermentation duration of 9 h represents an optimal time for soybean yoghurt alternative production using *L. brevis* and *S. cerevisiae*.

It should be noted that the present study was primarily designed to provide an initial evaluation of the interactive effects between *L. brevis* and *S. cerevisiae* on soybean yoghurt alternative quality. Accordingly, the 1:1 inoculation ratio was employed as a balanced co-culture configuration to examine strain interactions under comparable initial cell densities. The incubation temperature of 37°C was selected based on the well-established performance of *L. brevis* in yoghurt-type fermentations [Nguyen *et al*., 2025]. However, both incubation temperature and inoculation ratio may influence co-fermentation dynamics between the two strains. Therefore, further studies are necessary to optimise temperature and inoculation ratio, combined with growth kinetic analysis, to gain deeper

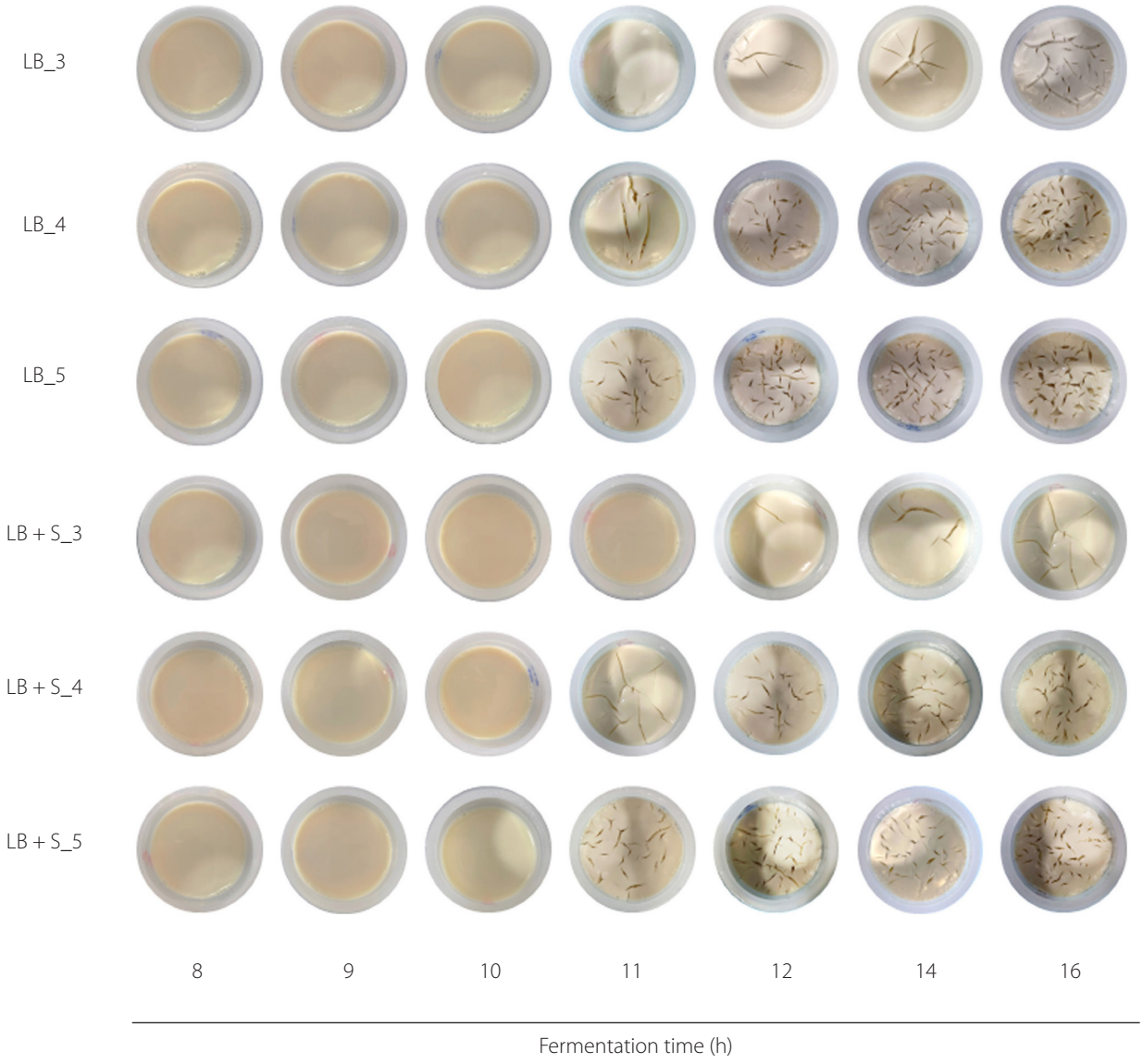

Figure 2. Surface morphology of the soybean yoghurt alternative during 16-h fermentation at 37°C using different cultures. LB_3, LB_4, LB_5: fermentation with *Levilactobacillus brevis* QD-1 with densities of 10^3, 10^4, 10^5 CFU/mL, respectively. LB+S_3, LB+S_4, LB+S_5: fermentation with a mixed culture of *L. brevis* and *Saccharomyces cerevisiae* (1:1, based on CFU counts) with densities of 10^3, 10^4, 10^5 CFU/mL, respectively.

Table 1. Microbial density, exopolysaccharide content, and texture parameters of the soybean yoghurt alternative after 9-h fermentation at 37 °C using different cultures.

Parameter	LB_3	LB_4	LB_5	LB+S_3	LB+S_4	LB+S_5
L. brevis count (log CFU/mL)	6.67±0.03^{c}	7.60±0.10^{b}	8.26±0.23^{a}	6.59±0.20^{c}	7.46±0.16^{b}	8.50±0.29^{a}
S. cerevisiae count (log CFU/mL)	–	–	–	5.78±0.09^{c}	6.76±0.24^{b}	7.75±0.16^{a}
Exopolysaccharide content (mg/L)	85±8^{c}	92±12^{c}	120±16^{c}	133±18^{b}	201±22^{a}	216±22^{a}
Hardness (N)	0.83±0.08^{c}	1.11±0.03^{b}	1.22±0.10^{b}	1.16±0.06^{b}	1.48±0.07^{a}	1.58±0.12^{a}
Cohesiveness	6.69±0.03^{c}	7.60±0.10^{b}	8.26±0.23^{a}	5.78±0.09^{d}	6.76±0.24^{c}	7.75±0.16^{b}
Springiness (mm)	3.88±0.13^{a}	3.61±0.10^{b}	3.52±0.08^{bc}	3.91±0.06^{a}	3.29±0.12^{cd}	3.26±0.06^{d}
Gumminess (N)	0.28±0.01^{c}	0.43±0.02^{b}	0.46±0.01^{b}	0.29±0.0^{c}	0.74±0.02^{a}	0.77±0.04^{a}
Adhesiveness (mJ)	2.12±0.10^{a}	1.83±0.06^{b}	1.57±0.06^{bc}	2.20±0.10^{a}	1.53±0.15^{c}	1.40±0.10^{c}
Water holding capacity (%)	16.0±2.3^{c}	18.7±1.5^{bc}	23.2± 3.8^{b}	23.4±3.5^{b}	33.8±3.9^{a}	34.4±4.5^{a}
Syneresis (%)	77.4±6.9^{a}	70.1±3.5^{a}	73.1±2.4^{a}	76.4±7.2^{a}	70.8±3.5^{a}	70.7±3.3^{a}

Data expressed as the mean ± standard deviation in the same row with different lowercase letters differs significantly at $p<0.05$. LB_3, LB_4, LB_5: fermentation with *Levilactobacillus brevis* QD-1 with densities of 10^3, 10^4, 10^5 CFU/mL, respectively. LB+S_3, LB+S_4, LB+S_5: fermentation with a mixed culture of *L. brevis* and *Saccharomyces cerevisiae* (1:1, based on CFU counts) with densities of 10^3, 10^4, 10^5 CFU/mL, respectively.

insight into each strain's contribution to fermentation performance and product quality.

Microbial density of the soybean yoghurt alternative

Yeasts can modulate LAB populations through both synergistic and antagonistic interactions. For example, *L. plantarum* and *S. cerevisiae* can physically attach to one another, which is known as co-aggregation which promotes the formation of mixed-species biofilms. This close physical association creates a stable microenvironment that supports higher bacterial density [Furukawa *et al*., 2011]. Conversely, competition for nutrients may suppress LAB growth, as demonstrated by reductions in *L. fermentum* populations and acid production in the presence of *S. cerevisiae* [Gu *et al*., 2022]. In addition, ethanol produced by yeasts may impose osmotic and environmental stress, leading to reduced growth of certain LAB strains [Tiukova *et al*., 2014]. In the present study, the densities of *L. brevis* and *S. cerevisiae* were assessed at the point of soybean yoghurt alternative coagulation and were found to depend on the initial inoculum size (**Table 1**). Notably, no significant differences were observed in *L. brevis* cell density between the LB and LB+S samples at equivalent inoculation levels, indicating that the presence of *S. cerevisiae* did not adversely affect the growth of *L. brevis* under the conditions tested.

Texture profile, water-holding capacity, and exopolysaccharide content of the soybean yoghurt alternative

The textural attributes of yoghurt are critical determinants of consumer acceptability, particularly for plant-based dairy alternatives. In the present study, results of texture profile analysis demonstrated that the soybean yoghurt alternative produced using a co-culture of *L. brevis* and *S. cerevisiae* exhibited significantly enhanced mechanical properties compared with the yoghurt soybean substrate fermented using *L. brevis* alone (**Table 1**). The LB+S_4 and LB+S_5 samples, inoculated at higher microbial densities (10^4 and 10^5 CFU/mL), recorded the highest values of selected textural parameters. These improvements were associated with elevated EPS content (201–216 mg/L), which corresponded to increased hardness (1.48–1.58 N) and gumminess (0.74–0.77 N) (**Table 1**). These findings are consistent with conclusions from previous studies indicating that EPS produced by lactic acid bacteria play an essential role in yoghurt structure by contributing to the formation of a dense protein-EPS network that enhances gel firmness and water retention [Akar, 2022; Brüls *et al*., 2024]. Notably, the co-cultivation with *S. cerevisiae* resulted in higher EPS levels at comparable *L. brevis* cell densities (**Table 1**). This observation aligns with the findings of Bertsch *et al*. [2019] who reported a 39–49% increase in EPS yield when *L. rhamnosus* strains (ATCC 9595, R0011, and RW-9595M) were co-cultured with *S. cerevisiae*. The higher gumminess of the co-cultured samples than of the monoculture treatments is consistent with the findings of Huang *et al*. [2020], who reported that the co-fermentation of LABs and *Kluyveromyces marxianus* improved gel integrity and functional textural properties of goat milk. However, springiness was slightly reduced in the high-density co-culture samples (LB+S_4 and LB+S_5), and similar decreasing trends were observed for cohesiveness and adhesiveness (**Table 1**), indicating that although the gel matrix became denser and mechanically stronger, its elastic recovery after deformation was partially diminished. In addition, cohesiveness in the co-culture

samples was not higher than in the corresponding monoculture samples at the same inoculation densities, suggesting that EPS enhancement may improve gel firmness and gumminess without necessarily increasing internal structural resilience. A similar phenomenon was described by Brüls *et al*. [2024], where elevated EPS levels contributed to the formation of a more compact and less elastic gel structure of yoghurt. Collectively, these findings suggest that EPS enhancement may strengthen gel structure but does not necessarily increase elasticity. Although previous studies have proposed that yeast may stimulate EPS production through interspecies metabolic interactions, such as growth factor provision or metabolite cross-feeding [Xu *et al*., 2025], these mechanisms were not directly examined in the present study. Therefore, further investigations incorporating quantitative analyses of yeast growth dynamics, metabolite exchange, and transcriptional regulation of EPS-related genes are necessary to elucidate the underlying mechanisms governing LAB-yeast interactions in fermentation during soybean yoghurt alternative production.

The enhanced WHC determined in the co-culture samples (**Table 1**) can be largely attributed to increased EPS production, which promotes the formation of a more robust gel matrix with a finer pore structure capable of retaining greater amounts of water. This interpretation is consistent with the findings of Li *et al*. [2014], who reported that EPS-producing *Lactobacillus* strains significantly improved the WHC of fermented soymilk. Similarly, Brüls *et al*. [2024] demonstrated that elevated EPS levels were associated with a reduced pore size and strengthened protein-EPS interactions, thereby enhancing water retention within the gel network. Despite the increase in WHC, syneresis values remained statistically comparable in all samples (70.1–77.4%), with no significant differences ($p \geq 0.05$) observed between mono-cultured and co-cultured samples (**Table 1**). This finding suggests that WHC and syneresis represent distinct aspects of gel behaviour: WHC reflects the capacity of the gel to retain water under applied force, whereas syneresis describes the gradual expulsion of whey under static conditions, which is more strongly influenced by gel elasticity and long-term structural stability. Moreover, although the co-cultured samples exhibited higher EPS levels, structural rearrangements within the protein matrix during storage may still have permitted water migration.

Overall, the co-fermentation of *L. brevis* and *S. cerevisiae* resulted in significant improvements in the textural quality of the soybean yoghurt alternative, which was largely attributable to enhanced EPS production. These findings indicate that co-cultivation may represent a promising approach for improving the structural integrity and sensory acceptability of plant-based yoghurt alternatives.

Protein profile of the soybean yoghurt alternative

Two major storage soybean proteins are glycinin and β-conglycinin. The β-conglycinin fraction comprises three subunits, namely: α (67 kDa), α′ (71 kDa), and β (45–50 kDa) [Picariello *et al*., 2013], whereas glycinin consists of acidic polypeptides (40–43 kDa) and basic polypeptides (~20 kDa) [Yaklich, 2001]. Both glycinin and β-conglycinin have been reported to activate the p38/JNK/NF-κB signalling pathway, which is associated with inflammatory responses [Peng *et al*., 2018]. These allergenic proteins may induce hypersensitivity reactions in the skin, gastrointestinal tract, and respiratory system [Pi *et al*., 2021]. Notably, the β subunit of β-conglycinin exhibits highly stable tertiary and secondary structures, even following heat treatment, and is therefore relatively resistant to degradation [Pi *et al*., 2021]. Previous studies have demonstrated that lactic acid bacteria can degrade the α′ subunit of β-conglycinin, although the extent of hydrolysis varies among *Lactobacillus* species, thereby potentially reducing the allergenicity of soymilk [Aguirre *et al*., 2014]. Accordingly, the present study examined whether fermentation with *L. brevis* in combination with *S. cerevisiae* could reduce the levels of these allergenic proteins.

As SDS-PAGE separations show (**Figure 3**), *L. brevis* effectively degraded proteins with molecular weights of 70, 50, and 20 kDa, corresponding to the α′ and β subunits of β-conglycinin and the acidic and basic fractions of glycinin, respectively. Notably, the soybean yoghurt substrate fermented with the co-culture of *L. brevis* and *S. cerevisiae* exhibited more pronounced degradation of these protein fractions than the samples fermented with *L. brevis* alone. Lactic acid bacteria have been shown to produce proteases that hydrolyse soybean proteins into smaller peptides and free amino acids. This enzymatic activity modifies protein structure and contributes to changes in soybean protein gel properties during fermentation [Kieliszek *et al*., 2021; Ren & Li, 2022]. In addition, *S. cerevisiae* has been reported to produce growth-promoting factors that stimulate enzyme activity, thereby enhancing the metabolic activity of lactic acid bacteria during fermentation [Sieuwerts *et al*., 2018]. Such interactions may generate a synergistic effect that facilitates more efficient degradation of soy proteins. Given that β-conglycinin is recognized as one of the principal allergenic storage proteins in soybean, its structural modification during fermentation may potentially contribute to a reduction in allergenic potential [Peng *et al*., 2018]. Further studies incorporating targeted immunoreactivity or epitope-specific analyses would help clarify whether these structural changes are associated with modified allergenic properties.

Changes in the protein secondary structure during soybean yoghurt alternative production

The FTIR spectra of soybean yoghurt alternative samples recorded over the wavenumber range of 400–4,000 cm^{-1} are presented in **Figure 4A**. Absorption bands observed in the regions of 3,200–3,600 cm^{-1} and 1,600–1,700 cm^{-1} correspond to the amide A and amide I bands of soy proteins, respectively, and were detected in all samples. In particular, the LB_3 sample exhibited a higher intensity of the amide A band compared to the other samples, together with the appearance of an amide IV band in the region of 530–610 cm^{-1}. During fermentation, pH changes are known to influence the hydrogen-bond strength and the

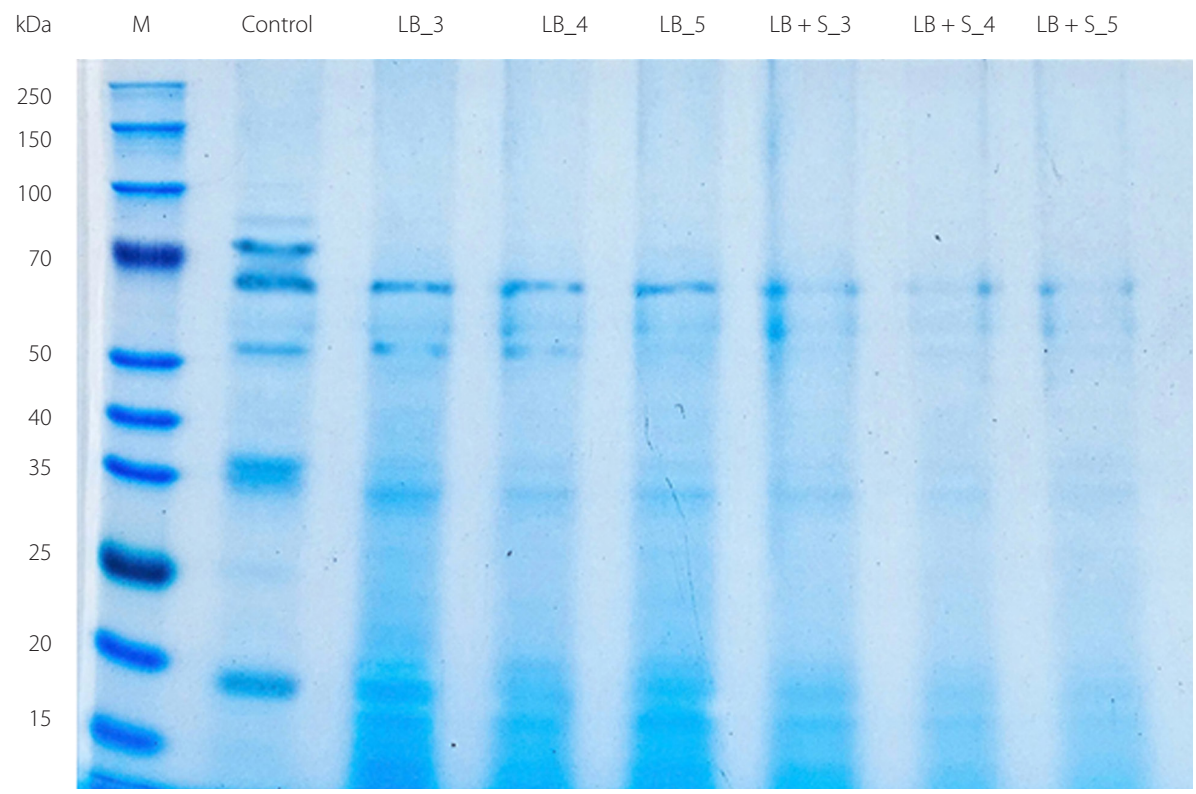

Figure 3. Sodium dodecyl sulfate–polyacrylamide gel electrophoresis (SDS-PAGE) separation of proteins of the soybean yoghurt alternative after 9 h of fermentation using different cultures. LB_3, LB_4, LB_5: fermentation with *Levilactobacillus brevis* QD-1 with densities of 10^3, 10^4, 10^5 CFU/mL, respectively. LB+S_3, LB+S_4, LB+S_5: fermentation with a mixed culture of *L. brevis* and *Saccharomyces cerevisiae* (1:1, based on CFU counts) with densities of 10^3, 10^4, 10^5 CFU/mL, respectively; M, standard proteins; Control, unfermented soybean substrate (prior to inoculation).

interaction patterns of amide groups within protein molecules [Liu *et al*., 2024]. Additionally, absorption peaks at 1,653 and 1,556 cm^{-1} were assigned to the stretching vibrations of carbonyl (C=O) and C–N groups, respectively, which is consistent with observations reported in recent studies on fermented soybean meal [Li *et al*., 2024].

Subsequently, deconvolution of the amide I band in the FTIR spectra of the soybean yoghurt alternative was performed to compare protein secondary structures based on structural components, including α-helix (1,650–1,658 cm^{-1}), β-sheet (1,620––1,640 cm^{-1} and 1,670–1,690 cm^{-1}), β-turn (1,660–1,680 cm^{-1}), and random coil (1,640–1,650 cm^{-1}) [Nguyen *et al*., 2026]. As revealed by FTIR deconvolution of the amide I band (**Figure 4B**), β-sheet was the dominant secondary structure in all soybean yoghurt alternative samples, ranging from 42.9% to 54.4%, which is consistent with the inherently β-sheet-rich conformation of major soy storage proteins, particularly glycinin and β-conglycinin [Yang *et al*., 2025]. In the *L. brevis* single-culture samples (LB), β-sheet content increased progressively with inoculation density, from 42.9% (LB_3) to 54.4% (LB_5), and was accompanied by a concurrent decrease in α-helix content from 25.3% to 12.3% (**Figure 4B**). This trend suggests that higher bacterial density promotes more extensive protein unfolding and intermolecular aggregation during fermentation, driven by accelerated acidification that destabilises native helical conformations and promotes the formation of ordered intermolecular hydrogen-bonded β-sheet networks [Liu *et al*., 2022a]. The reduction in α-helix content at higher inoculation densities is indicative of greater disruption of the compact globular structure of soy proteins [Ai *et al*., 2019], which is consistent with enhanced proteolytic activity and lower pH environments produced by denser *L. brevis* populations.

In the mixed-culture samples (LB+S), the overall structural profile was broadly similar to the single-culture counterparts, with β-sheet remaining the predominant structure (43.3–47.8%). However, α-helix content was generally higher in LB+S samples compared to their LB equivalents at the same inoculation density, most notably at the 10^4 CFU/mL level (LB+S_4: 28.3% vs. LB_4: 22.6%) (**Figure 4B**), suggesting that the co-fermentation with *S. cerevisiae* partially moderates protein denaturation. This may be attributed to the metabolic activity of *S. cerevisiae*, which produces CO_2 and ethanol alongside organic acids, potentially creating a different physicochemical environment that slows the complete unfolding of helical domains. Furthermore, random coil content tended to be lower in LB+S samples than in the LB samples, implying that the mixed fermentation system maintains a more ordered protein conformation, possibly through the combined effect of moderate acidification and yeast-derived compounds that interact with the protein matrix [Liu *et al*., 2022b]. In turn, β-turn content remained relatively stable (17.3–23.1%) in both fermentation systems (**Figure 4B**), indicating that these structural elements, which serve as flexible connectors between β-strands, are less sensitive to fermentation conditions than the

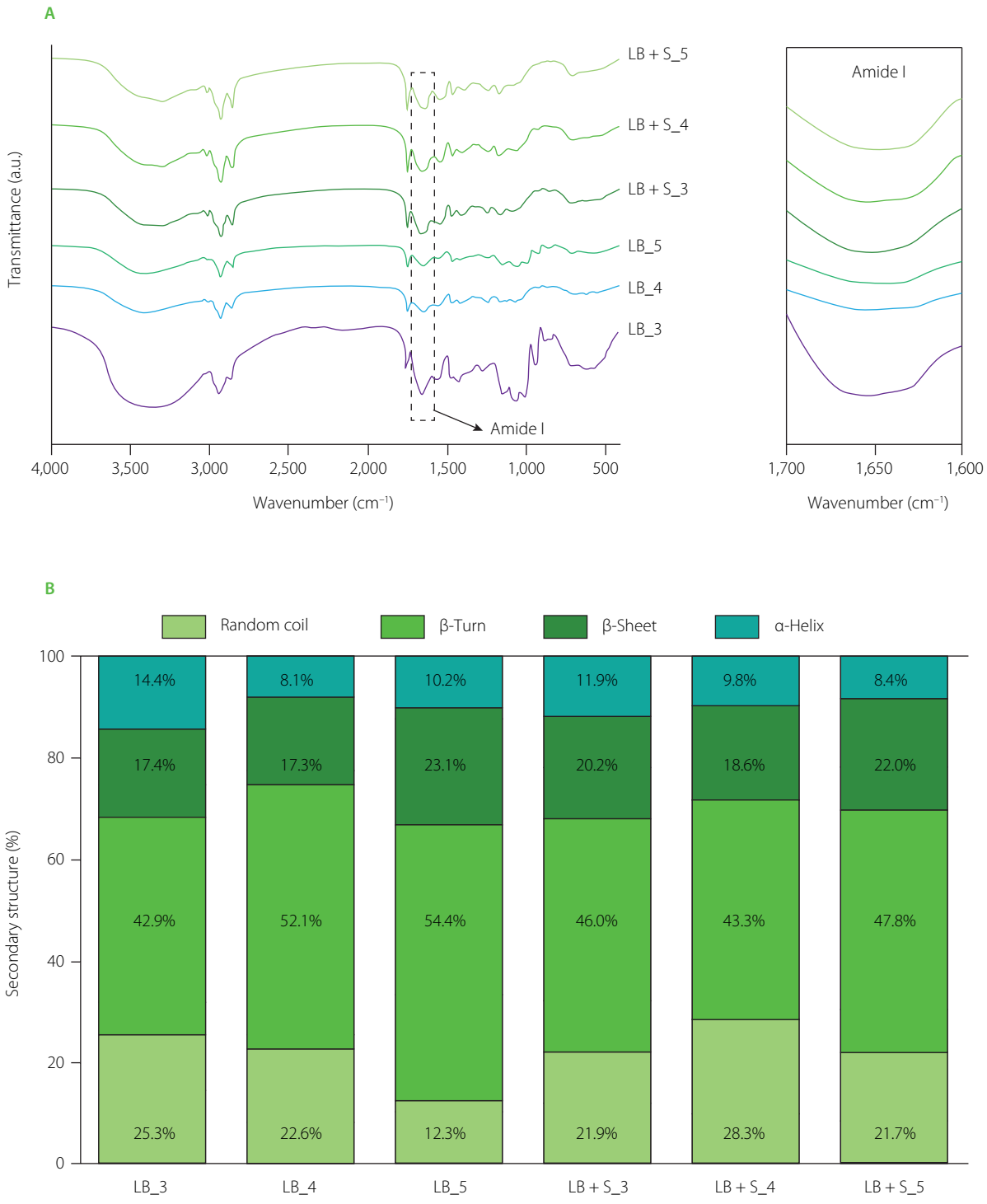

Figure 4. (**A**) Fourier transform infrared (FTIR) spectra with focused bands of amide I and (**B**) secondary structure contents of protein in the soybean yoghurt alternative after 9 h of fermentation using different cultures: LB_3, LB_4, LB_5: fermentation with *Levilactobacillus brevis* QD-1 with densities of 10^3, 10^4, 10^5 CFU/mL, respectively. LB+S_3, LB+S_4, LB+S_5: fermentation with a mixed culture of *L. brevis* and *Saccharomyces cerevisiae* (1:1, based on CFU counts) with densities of 10^3, 10^4, 10^5 CFU/mL, respectively.

α-helix or random coil fractions. These findings demonstrate that both inoculation density and culture composition significantly modulate the protein conformational changes during soybean yoghurtsubstrate fermentation, with implications for gel texture, water-holding capacity, and digestibility of the final product. The representative deconvoluted spectra and corresponding quantitative data are provided in **Figure S1** and **Table S1** (Supplementary Materials), respectively.

Volatile organic compounds of the soybean yoghurt alternative

The volatile organic compound profiles of the soybean yoghurt produced with *L. brevis* QD-1 at different inoculation densities, with and without co-cultivation with *S. cerevisiae*, are summarised in **Table 2**. Ethanol was the predominant volatile organic compound detected in all six samples, accounting for 91.02–92.83% of the total volatile organic compounds in the LB sample and 86.87–93.51% in the LB+S sample, followed by acetic acid (4.30––4.65% in the LB sample and 4.76–5.42% in the LB+S samples) and 2,3-butanediol (0.95–2.35% in the LB samples and 0.37––9.46% in the LB+S samples). *L. brevis*, as a heterofermentative lactic acid bacterium, possesses a metabolic framework that markedly influences the production of ethanol and acetic acid during fermentation. Its metabolic versatility enables the utilisation of various carbohydrates, including glucose and fructose, primarily *via* the phosphoketolase pathway, which underpins its heterofermentative metabolism. This pathway yields lactic acid alongside ethanol and acetic acid as major by-products, the latter two potentially constraining the efficiency of lactic acid production [Guo *et al*., 2014].

However, co-cultivation with *S. cerevisiae*, particularly at an inoculation density of 10^5 CFU/mL, markedly altered the volatile organic compound profile of the soybean yoghurt alternative. This shift was characterised by a smaller relative proportion of ethanol (69.55%) alongside increased relative levels of acetic acid (15.42%), 2,3-butanediol (9.46%), and phenethyl alcohol (1.87%). Elevated levels of polyols and aldehydes were recorder during high-density co-fermentation, which has been attributed to the upregulation of genes involved in carbohydrate and amino acid metabolism [Zhu *et al*., 2023]. *Saccharomyces* species primarily ferment sugars into ethanol and carbon dioxide and, while they can contribute to flavour development and textural modification, they do not substantially enhance isoflavone bioavailability nor generate the same diversity of bioactive compounds as LAB [Sharma *et al*., 2023]. The aroma profile generated during fermentation is strongly influenced by both the amino acid composition of the substrate and the yeast strain employed, as distinct strains exhibit unique metabolic capacities that govern the synthesis of volatile organic compounds [Scott *et al*., 2021]. In particular, the availability of specific amino acids can direct aroma formation, with methionine metabolism yielding methionol and its acetate ester, compounds that contribute to savoury flavour notes [Etschmann *et al*., 2008]. In contrast, LAB, including *L. plantarum* and *L. rhamnosus*, are well recognised for their capacity to biotransform isoflavones into more bioavailable aglycones, such as daidzein, genistein, glycitein, and further into metabolites with enhanced biological activity, including equol, dihydrodaidzein, and dihydrogenistein [Langa *et al*., 2023]. These transformations are mediated by LAB-derived β-glucosidase activity, which promotes the release of bound phenolic compounds including isoflavones, thereby increasing the bioactivity of the fermented product [Zhang *et al*., 2023]. In addition, LAB contributes to the generation of bioactive peptides with antioxidant properties through the proteolysis of soybean proteins, such as glycinin and β-conglycinin, which are abundant in germinated soymilk [Fadlillah *et al*., 2025]. Comparable effects have also been reported in kombucha fermentation systems, where the incorporation of LAB enhanced flavour complexity through increased production of alcohols and esters [Wang *et al*., 2024]. Overall, these findings indicate that the metabolic interactions between LAB and yeast can promote the formation of a broader and more balanced volatile organic compound profile, which is critical for improving the sensory quality of fermented foods and beverages. However, volatile organic compounds were analysed semi-quantitatively and expressed as relative percentages rather than absolute concentrations; therefore, the data reflect shifts in aroma composition rather than definitive differences in ethanol yield. A smaller relative ethanol proportion does not necessarily indicate reduced absolute production but may instead result from increased synthesis of other volatiles that affect proportional distribution. Further investigation incorporating absolute ethanol quantification, residual sugar analysis, and CO_2 measurement is required to clarify the metabolic contribution of *S. cerevisiae* to ethanol dynamics in yoghurt fermentation during soybean yoghurt alternative production.

CONCLUSIONS

In summary, this study demonstrates that the co-inoculation of *L. brevis* QD-1 with *S. cerevisiae* produced a soybean-based yoghurt alternative with improved textural properties associated with higher EPS levels, more extensive degradation of major soy storage proteins (β-conglycinin and glycinin), and favourable modifications in protein secondary structure compared with the *L. brevis* monoculture. Volatile profiles also showed shifts in the relative abundances of key compounds. The viability of *L. brevis* was not negatively affected by the presence of the yeast. These outcomes indicate that *S. cerevisiae* can serve as a supportive co-starter culture capable of modulating selected quality attributes of the soy yoghurt alternative produced by *L. brevis*-fermentation, where acidification and primary gel formation are driven by the lactic acid bacterium. The study results support the potential of this co-culture strategy for the development of high-quality vegan yoghurt alternatives. However, further studies are needed to clarify the respective contributions of each strain, optimise fermentation conditions, and evaluate sensory properties and consumer acceptability. Such work will help to better define the potential of LAB–yeast co-fermentation for developing plant-based yoghurt alternatives.

SUPPLEMENTARY MATERIALS

The following are available online at **https://journal.pan.olsztyn.pl/Development-of-a-Vegan-Soybean-Based-Yoghurt-Alternative-Using-Levilactobacillus,220155,0,2.html**; **Table S1**. Relative content of secondary structures of protein in soybean yoghurt alternative after 9-h fermentation at 37°C by using different cultures. **Figure S1**. Deconvolutionized spectra of soybean yoghurt alternative after 9 h of fermentation using various starter

Table 2. Volatile organic compound profile of the soybean yoghurt alternative after 9-h fermentation at 37°C using different cultures.

Compound	RT (min)	RI	MW	Formula	Content (%)					
					LB_3	LB_4	LB_5	LB+S_3	LB+S_4	LB+S_5
Acetaldehyde	1.10	408	44	C_2H_4O	0.07±0.02^{c}	0.13±0.03^{bc}	0.29±0.05^{b}	0.33±0.04^{a}	0.47±0.06^{a}	nd
Ethanol	1.17	463	46	C_2H_6O	92.79±1.75^{a}	91.02±2.07^{a}	92.83±1.41^{a}	93.51±2.52^{a}	86.87±3.08^{b}	69.55±5.45^{c}
Methyl isocyanide	1.25	465	41	C_2H_3N	0.16±0.03^{a}	0.22±0.09^{a}	0.15±0.05^{a}	nd	Nd	nd
1-Propanol	1.45	1052	60	C_3H_8O	nd	0.11±0.02^{a}	nd	0.18±0.03^{a}	nd	nd
Isobutyl alcohol	1.84	597	74	$C_4H_{10}O$	0.17±0.03^{b}	0.22±0.04^{ab}	0.17±0.05^{b}	0.27±0.05^{a}	nd	nd
3-Methylbutanal	2.06	643	86	$C_5H_{10}O$	nd	nd	nd	0.48±0.07^{b}	0.72±0.09^{a}	nd
Acetic acid	3.18	576	60	$C_2H_4O_2$	4.30±0.48^{c}	4.65±1.55^{c}	4.34±0.51^{c}	4.76±1.63^{c}	7.89±2.29^{b}	15.42±3.18^{a}
3-Methyl-1-butanol	3.01	697	88	$C_5H_{12}O$	nd	0.57±0.08^{a}	0.50±0.07^{a}	0.30±0.05^{b}	nd	nd
2,3-Butanediol	3.90	743	90	$C_4H_{10}O_2$	1.24±0.21^{b}	2.35±0.32^{a}	0.95±0.17^{b}	1.19±0.23^{b}	0.37±0.09^{c}	9.46±0.95^{a}
Phenethyl alcohol	10.42	1,136	122	$C_8H_{10}O$	0.55±0.08^{b}	0.67±0.10^{b}	0.76±0.12^{b}	0.54±0.07^{b}	0.34±0.06^{c}	1.87±0.19^{a}

Data are mean ± standard deviation (n=3). Means in the same row with different lowercase letters differ significantly (p<0.05). LB_3, LB_4, LB_5: fermentation with *Levilactobacillus brevis* QD-1 with densities of 10^3, 10^4, 10^5 CFU/mL, respectively. LB+S_3, LB+S_4, LB+S_5: fermentation with a mixed culture of *L. brevis* and *Saccharomyces cerevisiae* (1:1, based on CFU counts) with densities of 10^3, 10^4, 10^5 CFU/mL, respectively. RT, retention time; RI, retention index; MW, molecular weight; nd, not detected.

cultures. LB_3, LB_4, LB_5: fermentation with *Levilactobacillus brevis* QD-1 with densities of 10^3, 10^4, 10^5 CFU/mL, respectively (A–C). LB+S_3, LB+S_4, LB+S_5: fermentation with a mixed culture of *L. brevis* and *Saccharomyces cerevisiae* (1:1, based on CFU counts) with densities of 10^3, 10^4, 10^5 CFU/mL, respectively (D–E). Red and purple curves represent β-sheet (1,620–1,640 cm^{-1} and 1,670–1,695 cm^{-1}), green curve represents random coil (1,640–1,650 cm^{-1}), blue curve represents α-helix (1,650–1,658 cm^{-1}), and cyan curve represents β-turn (1,660–1,680 cm^{-1}); black and yellow curves represent the original and fitted ones obtained from FTIR data of Amide I region, respectively.

ACKNOWLEDGEMENTS

The authors gratefully acknowledge HUTECH University for granting permission and providing research facilities. The authors sincerely thank Saigon Technology University for providing the necessary research facilities. We acknowledge Nguyen Tat Thanh University, Ho Chi Minh City, Vietnam for supporting this study. We also thank VINACROP Company Limited, Ho Chi Minh City, Vietnam, for their permission and provision of facilities during the research period.

RESEARCH FUNDING

This research did not receive any specific grant from funding agencies in the public, commercial, or not-for-profit sectors.

CONFLICT OF INTERESTS

The authors declare that they have no conflict of interest to influence the work reported in this paper.

ADDITIONAL INFORMATION

The authors declare that generative AI tools (ChatGPT, version 5.2; OpenAI, San Francisco, CA, USA) were used to assist in language editing and improving the clarity of the manuscript. No AI tools were used for data analysis, interpretation, or generation of scientific content. All scientific conclusions and interpretations are the responsibility of the authors.

ORCID IDs

A.D. Do **https://orcid.org/0000-0002-3198-3383**
Q.D. Nguyen **https://orcid.org/0000-0001-9097-4471**
T.S. Nguyen **https://orcid.org/0000-0002-6816-2407**
H.T. Truong-Thi **https://orcid.org/0009-0005-7739-329X**
H. Vu-Quang **https://orcid.org/0000-0002-3468-5816**

REFERENCES

1. Agarbati, A., Ciani, M., Canonico, L., Comitini, F. (2023). Consortium of selected yeasts to produce healthy soy fermented beverage: Evaluation of microbial evolution, analytical, sensorial, and functional features. *Heliyon*, *9*(10), art. no. e20979. **https://doi.org/10.1016/j.heliyon.2023.e20979**
2. Aguirre, L., Hebert, E.M., Garro, M.S., Savoy de Giori, G. (2014). Proteolytic activity of *Lactobacillus* strains on soybean proteins. *LWT – Food Science and Technology*, *59*(2P1), 780-785. **https://doi.org/10.1016/j.lwt.2014.06.061**
3. Ai, M., Tang, T., Zhou, L., Ling, Z., Guo, S., Jiang, A. (2019). Effects of different proteases on the emulsifying capacity, rheological and structure characteristics of preserved egg white hydrolysates. *Food Hydrocolloids*, *87*, 933-942. **https://doi.org/10.1016/j.foodhyd.2018.09.023**
4. Akar, N.Z. (2022). Exopolysaccharides from lactic acid bacteria: Functional properties and effects on yogurt texture. *Osmaniye Korkut Ata Üniversitesi Fen Bilimleri Enstitüsü Dergisi*, *5*(2), 1053-1068. **https://doi.org/10.47495/okufbed.1016079**
5. Bertsch, A., Roy, D., LaPointe, G. (2019). Enhanced exopolysaccharide production by *Lactobacillus rhamnosus* in co-culture with *Saccharomyces cerevisiae*. *Applied Sciences*, *9*(19), art. no. 4026. **https://doi.org/10.3390/app9194026**
6. Brüls, M., Foroutanparsa, S., Maljaars, C.E.P., Olsthoorn, M., Tas, R.P., Voets, I.K. (2024). Investigating the impact of exopolysaccharides on yogurt network mechanics and syneresis through quantitative microstructural analysis. *Food Hydrocolloids*, *150*, art. no. 109629. **https://doi.org/10.1016/j.foodhyd.2023.109629**
7. Canon, F., Nidelet, T., Guédon, E., Thierry, A., Gagnaire, V. (2020). Understanding the mechanisms of positive microbial interactions that benefit lactic acid bacteria co-cultures. *Frontiers in Microbiology*, *11*, art. no. 2088. **https://doi.org/10.3389/fmicb.2020.02088**
8. Craig, W.J., Messina, V., Rowland, I., Frankowska, A., Bradbury, J., Smetana, S., Medici, E. (2023). Plant-based dairy alternatives contribute to a healthy and sustainable diet. *Nutrients*, *15*(15), art. no. 3393. **https://doi.org/10.3390/nu15153393**
9. do Amaral Santos, C.C.A., da Silva Libeck, B., Schwan, R.F. (2014). Co-culture fermentation of peanut-soy milk for the development of a novel functional beverage. *International Journal of Food Microbiology*, *186*, 32–41. **https://doi.org/10.1016/j.ijfoodmicro.2014.06.011**
10. Dönmez, Ö., Mogol, B.A., Gökmen, V. (2017). Syneresis and rheological behaviors of set yogurt containing green tea and green coffee powders. *Journal of Dairy Science*, *100*(2), 901–907. **https://doi.org/10.3168/jds.2016-11262**
11. Etschmann, M.M.W., Kötter, P., Hauf, J., Bluemke, W., Entian, K.D., Schrader, J. (2008). Production of the aroma chemicals 3-(methylthio)-1-propanol and 3-(methylthio)-propylacetate with yeasts. *Applied Microbiology and Biotechnology*, *80*(4), 579-587. **https://doi.org/10.1007/s00253-008-1573-4**
12. Fadlillah, H.N., Nuraida, L., Sitanggang, A.B., Palupi, N.S. (2025). Antioxidant peptides produced by *Pediococcus acidilactici* YKP4 and *Lacticaseibacillus rhamnosus* BD2 in fermented soymilk made from germinated soybeans. *International Journal of Food Science and Technology*, *60*(1), art. no. vvae002. **https://doi.org/10.1093/ijfood/vvae002**
13. Furukawa, S., Nojima, N., Yoshida, K., Hirayama, S., Ogihara, H., Morinaga, Y. (2011). The importance of inter-species cell-cell co-aggregation between *Lactobacillus plantarum* ML11-11 and *Saccharomyces cerevisiae* BY4741 in mixed-species biofilm formation. *Bioscience, Biotechnology and Biochemistry*, *75*(8), 1430-1434. **https://doi.org/10.1271/bbb.100817**
14. Gan, J., Kong, X., Wang, K., Chen, Y., Du, M., Xu, B., Xu, J., Wang, Z., Cheng, Y., Yu, T. (2023). Effect of fermentation using different lactic acid bacteria strains on the nutrient components and mineral bioavailability of soybean yogurt alternative. *Frontiers in Nutrition*, *10*, art. no. 1198456. **https://doi.org/10.3389/fnut.2023.1198456**
15. Gu, Y., Tian, J., Zhang, Y., Wu, J., He, Y. (2022). Effect of *Saccharomyces cerevisiae* cell-free supernatant on the physiology, quorum sensing, and protein synthesis of lactic acid bacteria. *LWT – Food Science and Technology*, *165*, art. no. 113732. **https://doi.org/10.1016/j.lwt.2022.113732**
16. Guo, W., He, R., Ma, L., Jia, W., Li, D., Chen, S. (2014). Construction of a constitutively expressed homo-fermentative pathway in *Lactobacillus brevis*. *Applied Microbiology and Biotechnology*, *98*(15), 6641-6650. **https://doi.org/10.1007/s00253-014-5703-x**
17. Huang, Z., Huang, L., Xing, G., Xu, X., Tu, C., Dong, M. (2020). Effect of co-fermentation with lactic acid bacteria and *K. marxianus* on physicochemical and sensory properties of goat milk. *Foods*, *9*(3), art. no. 299. **https://doi.org/10.3390/foods9030299**
18. Kieliszek, M., Pobiega, K., Piwowarek, K., Kot, A.M. (2021). Characteristics of the proteolytic enzymes produced by lactic acid bacteria. *Molecules*, *26*(7), art. no. 1858. **https://doi.org/10.3390/molecules26071858**
19. Laemmli, U.K. (1970). Cleavage of structural proteins during the assembly of the head of bacteriophage T4. *Nature*, *227*(5259), 680–685. **https://doi.org/10.1038/227680a0**
20. Langa, S., Peirotén, Á., Curiel, J.A., de la Bastida, A.R., Landete, J.M. (2023). Isoflavone metabolism by lactic acid bacteria and its application in the development of fermented soy food with beneficial effects on human health. *Foods*, *12*(6), art. no. 1293. **https://doi.org/10.3390/foods12061293**
21. Lee, D.H., Lee, W., Shin, D., Im, H., Jung, G., Lee, Y.-B., Choi, J. (2024). Genomic and metabolomic analysis of *Latilactobacillus sakei* DCF0720 for black soybean yogurt fermentation. *International Journal of Food Microbiology*, *425*, art. no. 110897. **https://doi.org/10.1016/j.ijfoodmicro.2024.110897**

22. Li, C., Li, W., Chen, X., Feng, M., Rui, X., Jiang, M., Dong, M. (2014). Microbiological, physicochemical and rheological properties of fermented soymilk produced with exopolysaccharide (EPS) producing lactic acid bacteria strains. *LWT – Food Science and Technology*, *57*(2), 477-485. **https://doi.org/10.1016/j.lwt.2014.02.025**
23. Li, L., Zhang, Q., Yuan, X., Yang, H., Qin, S., Hong, L., Pu, L., Li, L., Zhang, P., Zhang, J. (2024). Study of the molecular structure of proteins in fermented maize-soybean meal-based rations based on FTIR spectroscopy. *Food Chemistry*, *441*, art. no. 138310. **https://doi.org/10.1016/j.foodchem.2023.138310**
24. Lin, T.Y., Chien, M.F.C. (2007). Exopolysaccharides production as affected by lactic acid bacteria and fermentation time. *Food Chemistry*, *100*(4), 1419-1423. **https://doi.org/10.1016/j.foodchem.2005.11.033**
25. Liu, C., Wang, N., Wu, D., Wang, L., Zhang, N., Yu, D. (2024). Rapid quantitative analysis of soybean protein isolates secondary structure by two-dimensional correlation infrared spectroscopy through pH perturbation. *Food Chemistry*, *448*, art. no. 139074. **https://doi.org/10.1016/j.foodchem.2024.139074**
26. Liu, F.F., Li, Y. Q., Sun, G.J., Wang, C.Y., Liang, Y., Zhao, X.Z., He, J.X., Mo, H.Z. (2022a). Influence of ultrasound treatment on the physicochemical and antioxidant properties of mung bean protein hydrolysate. *Ultrasonics Sonochemistry*, *84*, art. no. 105964. **https://doi.org/10.1016/j.ultsonch.2022.105964**
27. Liu, F.F., Li, Y.Q., Wang, C.Y., Liang, Y., Zhao, X.Z., He, J.X., Mo, H.Z. (2022b). Physicochemical, functional and antioxidant properties of mung bean protein enzymatic hydrolysates. *Food Chemistry*, *393*, art. no. 133397. **https://doi.org/10.1016/j.foodchem.2022.133397**
28. Marchese, L.E., McNaughton, S.A., Hendrie, G.A., van der Pols, J.C., Tran, N.R., Lanham, A., Dickinson, K.M., Livingstone, K.M. (2024). Modelling the impact of substituting meat and dairy products with plant-based alternatives on nutrient adequacy and diet quality. *The Journal of Nutrition*, *154*(8), 2411-2421. **https://doi.org/10.1016/j.tjnut.2024.05.029**
29. Medici, E., Craig, W.J., Rowland, I. (2023). A comprehensive analysis of the nutritional composition of plant-based drinks and yogurt alternatives in Europe. *Nutrients*, *15*(15), art. no. 3415. **https://doi.org/10.3390/nu15153415**
30. Mehaya, F.M., El-Shazly, A.I., El-Dein, A.N., Farid, M.A. (2023). Evaluation of nutritional and physicochemical characteristics of soy yogurt by *Lactobacillus plantarum* KU985432 and *Saccharomyces boulardii* CNCMI-745. *Scientific Reports*, *13*(1), art. no. 13026. **https://doi.org/10.1038/s41598-023-40207-4**
31. Moshtaghian, H., Hallström, E., Bianchi, M., Bryngelsson, S. (2024). Nutritional profile of plant-based dairy alternatives in the Swedish market. *Current Research in Food Science*, *8*, art. no. 100712. **https://doi.org/10.1016/j.crfs.2024.100712**
32. Nguyen, N.N., Nguyen, Q.D. (2024). Evolution of kombucha tea from isolated acetic acid bacteria, lactic acid bacteria and yeast in single- and mixed-cultures: characteristics, bioactivities, fermentation performance and kinetics. *Food Biotechnology*, *38*(1), 86-117. **https://doi.org/10.1080/08905436.2024.2306505**
33. Nguyen, N.N., Do, A.D., Phan Van, T., Nguyen, V.L., Tran, M.T., Nguyen, Q.D. (2024). Development of dairy-free soybean-based yoghurt by active dry starter culture from kombucha: an investigation into microencapsulation, curd formation, protein and texture profiles during storage. *International Journal of Food Science and Technology*, *59*(4), 2383–2399. **https://doi.org/10.1111/IJFS.16966**
34. Nguyen, Q.D., Truong Thi, H.T., Ngo Thi, N.H., Nguyen, V.L., Nguyen, M.A., Do, A.D. (2025). Whole-genome sequencing, probiotic characterization, and safety evaluation of *Levilactobacillus brevis* QD-1 and its application in soy yogurt production. *Food Biotechnology*, *39*(4), 388–413. **https://doi.org/10.1080/08905436.2025.2581877**
35. Nguyen, T.-V.-L., Tran, T.T.V., Huynh, Q.-T., Dang, T.-T., Nguyen, T.-T.-D., Nguyen, P.-B.-D., Do, A.D., Nguyen, Q.-D. (2026). Accelerating the coagulation of germinated soymilk by glucono-δ-lactone using different physical treatments and quality assessment of separated soybean whey. *Food Chemistry: X*, *35*, art. no. 103724. **https://doi.org/10.1016/j.fochx.2026.103724**
36. Nielsen, S.S. (2017). *Food Analysis Laboratory Manual*, 3rd Edition, Springer Cham. **https://doi.org/10.1007/978-3-319-44127-6**
37. Otolowo, D.T., Omosebi, O.M., Araoye, K.T., Ernest, T.E., Osundahunsi, O.F. (2022). Effects of the substitution of cow's milk with soymilk on the micronutrients, microbial, and sensory qualities of yoghurt. *Food Production, Processing and Nutrition*, *4*(1), art. no. 15. **https://doi.org/10.1186/s43014-022-00093-1**
38. Park, I., Mannaa, M. (2025). Fermented foods as functional systems: microbial communities and metabolites influencing gut health and systemic outcomes. *Foods*, *14*(13), art. no. 2292. **https://doi.org/10.3390/foods14132292**
39. Peng, C., Cao, C., He, M., Shu, Y., Tang, X., Wang, Y., Zhang, Y., Xia, X., Li, Y., Wu, J. (2018). Soybean glycinin- and β-conglycinin-induced intestinal damage in piglets *via* the p38/JNK/NF-κB signaling pathway. *Journal of Agricultural and Food Chemistry*, *66*(36), 9534-9541. **https://doi.org/10.1021/acs.jafc.8b03641**
40. Pi, X., Sun, Y., Fu, G., Wu, Z., Cheng, J. (2021). Effect of processing on soybean allergens and their allergenicity. *Trends in Food Science and Technology, 118*(Part A), 316-327. **https://doi.org/10.1016/j.tifs.2021.10.006**
41. Picariello, G., Amigo-Benavent, M., del Castillo, M.D., Ferranti, P. (2013). Structural characterization of the N-glycosylation of individual soybean β-conglycinin subunits. *Journal of Chromatography A*, *1313*, 96–102. **https://doi.org/10.1016/j.chroma.2013.09.014**
42. Ren, Y., Li, L. (2022). The influence of protease hydrolysis of lactic acid bacteria on the fermentation induced soybean protein gel: Protein molecule, peptides and amino acids. *Food Research International*, *156*, art. no. 111284. **https://doi.org/10.1016/j.foodres.2022.111284**
43. Rui, X., Zhang, Q., Huang, J., Li, W., Chen, X., Jiang, M., Dong, M. (2019). Does lactic fermentation influence soy yogurt protein digestibility: a comparative study between soymilk and soy yogurt at different pH. *Journal of the Science of Food and Agriculture*, *99*(2), 861-867. **https://doi.org/10.1002/jsfa.9256**
44. Scott, W.T., van Mastrigt, O., Block, D.E., Notebaart, R.A., Smid, E.J. (2021). Nitrogenous compound utilization and production of volatile organic compounds among commercial wine yeasts highlight strain-specific metabolic diversity. *Microbiology Spectrum*, *9*(1), art. no. e00485-21. **https://doi.org/10.1128/spectrum.00485-21**
45. Sharma, H., Ozogul, F., Bartkiene, E., Rocha, J.M. (2023). Impact of lactic acid bacteria and their metabolites on the techno-functional properties and health benefits of fermented dairy products. *Critical Reviews in Food Science and Nutrition*, *63*(21), 4819-4841. **https://doi.org/10.1080/10408398.2021.2007844**
46. Sieuwerts, S., Bron, P.A., Smid, E.J. (2018). Mutually stimulating interactions between lactic acid bacteria and *Saccharomyces cerevisiae* in sourdough fermentation. *LWT – Food Science and Technology*, *90*, 201-206. **https://doi.org/10.1016/j.lwt.2017.12.022**
47. Tiukova, I., Eberhard, T., Passoth, V. (2014). Interaction of *Lactobacillus vini* with the ethanol-producing yeasts *Dekkera bruxellensis* and *Saccharomyces cerevisiae*. *Biotechnology and Applied Biochemistry*, *61*(1SI), 40-44. **https://doi.org/10.1002/bab.1135**
48. Urshev, Z.L., Dimitrov, Z.P., Fatchikova, N.S., Petrova, I.G., Ishlimova, D.I. (2007). Partial characterization and dynamics of synthesis of high molecular mass exopolysaccharides from *Lactobacillus delbrueckii* ssp. *bulgaricus* and *Streptococcus thermophilus*. *World Journal of Microbiology and Biotechnology, 24*(2), 171–179. **https://doi.org/10.1007/s11274-007-9453-0**
49. Van, T.P., Phan, Q.K., Quang, H.P., Pham, G.B., Thi, N.H.N., Thi, H.T.T., Do, A.D. (2023). Multi-strain probiotics enhance the bioactivity of cascara kombucha during microbial composition-controlled fermentation. *Preventive Nutrition and Food Science*, *28*(4), 502-513. **https://doi.org/10.3746/pnf.2023.28.4.502**
50. Wang, S., Li, C., Xu, Q., Wang, Y., Wang, S., Zou, Y., Yang, Z., Yuan, L. (2024). Addition of lactic acid bacteria modulates microbial community and promotes the flavor profiles of Kombucha. *Food Bioscience*, *60*, art. no. 104340. **https://doi.org/10.1016/j.fbio.2024.104340**
51. Weng, B.B.-C., Yuan, H.-D., Chen, L.-G., Chu, C., Hsieh, C.-W. (2023). Soy yoghurts produced with efficient GABA (γ-aminobutyric acid)-producing *Lactiplantibacillus plantarum* ameliorate hyperglycaemia and re-establish gut microbiota in streptozotocin (STZ)-induced diabetic mice. *Food & Function*, *14*(3), 1699–1709. **https://doi.org/10.1039/D2FO02708A**
52. Xu, Y., Ye, Q., Zhang, H., Yu, Y., Li, X., Zhang, Z., Zhang, L. (2019). Naturally fermented acid slurry of soy whey: High-throughput sequencing-based characterization of microbial flora and mechanism of tofu coagulation. *Frontiers in Microbiology*, *10*, art. no. 1088. **https://doi.org/10.3389/fmicb.2019.01088**
53. Xu, Z., Premarathna, M., Li, Y., Yin, X., Soteyome, T., Liu, J., Seneviratne, G. (2025). Current knowledge on the polymicrobial interaction and biofilm between *Saccharomyces* and *Lactobacillaceae*: regulatory mechanisms and applications. *Biofilm*, *10*(12), art. no. 100336. **https://doi.org/10.1016/j.bioflm.2025.100336**
54. Yaklich, R.W. (2001). β-Conglycinin and glycinin in high-protein soybean seeds. *Journal of Agricultural and Food Chemistry*, *49*(2), 729-735. **https://doi.org/10.1021/jf001110s**
55. Yang, H., Yang, S., Kong, J., Dong, A., Yu, S. (2015). Obtaining information about protein secondary structures in aqueous solution using Fourier transform IR spectroscopy. *Nature Protocols, 10*(3), 382–396. **https://doi.org/10.1038/nprot.2015.024**

56. Yang, Z., Li, D., Chen, L., Zhang, W., Jiang, L., Huang, Z., Tian, T. (2025). Structural characteristics, techno-functionalities, innovation applications and future prospects of soybean β-conglycinin/glycinin: a comprehensive review. *Critical Reviews in Food Science and Nutrition*, *65*(29), 6410–6427. **https://doi.org/10.1080/10408398.2024.2440601**
57. Zhang, J., Xia, N., Teng, J., Wei, B., Huang, L. (2023). Effect of lactic acid bacteria fermentation on extractable and non-extractable polyphenols of soybean milk: Influence of β-glucosidase and okara. *Food Bioscience*, *56*, art. no. 103326. **https://doi.org/10.1016/j.fbio.2023.103326**
58. Zhu, P., Yang, K., Shen, J., Lu, Z., Lv, F., Wang, P. (2023). Comparative transcriptome analysis revealing the enhanced volatiles of cofermentation of yeast and lactic acid bacteria on whole wheat steamed bread dough. *Journal of Agricultural and Food Chemistry*, *71*(48), 19129-19141. **https://doi.org/10.1021/acs.jafc.3c01650**

ORIGINAL ARTICLE
http://journal.pan.olsztyn.pl

Polish Journal of Food and Nutrition Sciences
2026, Vol. 76, No. 2, 135–148
DOI: 10.31883/pjfns/220797
ISSN 1230-0322, e-ISSN 2083-6007

Harnessing Vegetable Oils for β-Carotene Extraction from *Moringa oleifera* Lam. Leaves and Feasibility of Their Microencapsulation

Sandra E. García-Solís[1], Viridiana Pérez-Pérez[2]*, Luis C. Boyano Orozco[3], Jorge L. Gonzalez-Escobar[4], Carla P. Plazola-Jacinto[1], Raúl E. López-Hernández[1]

[1]Departamento de Ingeniería Bioquímica, Escuela Nacional de Ciencias Biológicas, Instituto Politécnico Nacional, Ciudad de México, México
[2]Departamento de Bioprocesos, Unidad Profesional Interdisciplinaria de Biotecnología, Instituto Politécnico Nacional, Ciudad de México, México
[3]Facultad de Ingeniería, Universidad del Atlántico, Barranquilla, Colombia
[4]Instituto Tecnológico de Ciudad Valles, Tecnológico Nacional de México, San Luis Potosí, México

Moringa oleifera Lam. leaves are known for their high carotenoid content; however, these bioactive compounds are highly susceptible to degradation under conditions of light exposure, oxygen contact, or high temperatures, resulting in a reduction in their functional effectiveness. Microencapsulation offers a promising method to protect these sensitive molecules. This study investigated the potential of edible vegetable oils as sustainable solvents for β-carotene extraction from *M. oleifera* leaves and evaluated the efficiency of their encapsulation. The extraction process was optimized using a D-optimal experimental design, focusing on variables such as oil ratio, temperature, and duration, with sunflower and corn oils as solvents. Optimal extraction was achieved using sunflower oil at 70°C for 10 min, yielding 51.92 mg of β-carotene/100 g oil, closely matching the predicted value (52.96 mg/100 g). The extract with the highest β-carotene content was microencapsulated through spray-drying, using maltodextrin and gum Arabic as wall materials. A 1:1 (*w/w*) wall material ratio resulted in microcapsules with the highest encapsulation efficiency (0.74), average particle size of 7.98 µm, low moisture content (3.02 g/100 g), and water activity values of 0.11, indicating enhanced stability. These findings highlight sunflower oil as an effective and sustainable solvent for carotenoid extraction, while spray-drying with optimized wall material ratios improves the physicochemical stability and handling properties of β-carotene microcapsules.

Keywords: emulsion, encapsulation efficiency, particle morphology, spray-drying

ABBREVIATIONS

ANOVA, analysis of variance; CLSM, confocal laser scanning microscopy; CO, corn oil; DE, dextrose equivalent; EE, encapsulation efficiency; ESI, emulsion stability index; GU, gum Arabic; MD, maltodextrin; PDI, polydispersity index; SEM, scanning electron microscopy; SFO, sunflower oil; T_g, glass transition temperature.

INTRODUCTION

Moringa oleifera Lam. is an indigenous plant of Indian origin, widely recognized for its nutritional richness and medicinal applications in traditional healthcare systems [Sonewane *et al*., 2022]. Its foliage is particularly abundant in β-carotene and vitamin C, being key contributors to its antioxidant capacity, as well as in B-group vitamins, minerals (calcium, potassium, and iron),

***Corresponding Author:**
E-mail: **perezperezviridiana88@gmail.com** (Dr. V. Pérez-Pérez)

Submitted: 5 January 2026
Accepted: 20 April 2026
Published on-line: 11 May 2026

and proteins [Islam *et al*., 2021]. The health-promoting properties of *M. oleifera* leaves, due to the bioactive compounds they contain, have recently gained attention, and their potential applications include the prevention of chronic diseases such as cancer, hypertension, cardiovascular dysfunctions, vision-related problems, and tissue repair [Jikah & Edo, 2023].

In food systems, β-carotene plays a dual role, acting both as a coloring agent and as an antioxidant. Its intake has been associated with positive health effects, mainly due to its provitamin A activity and its recognized antioxidative properties [Rodriguez-Amaya, 2016]. *M. oleifera* leaves have been reported to contain significant level of carotenoids, including β-carotene, lutein, zeaxanthin, and luteoxanthin with β-carotene being one of the major compounds [Saini *et al*., 2014], with contents ranging from approximately 11.86 to 23.15 mg/100 g, depending on plant cultivar.

Plant-derived bioactive compounds are generally extracted using solvents of varying polarities. Common polar solvents include ethanol, methanol, and isopropanol, while non-polar alternatives, such as acetone and hexane, are also employed [Tak *et al*., 2022]. However, many of these solvents are toxic and must be completely removed from the extract, which increases process complexity and generates additional costs. In contrast, food-grade vegetable oils present a safer and more sustainable extraction option, especially for non-polar compounds like carotenoids [Baria *et al*., 2019; Chutia & Mahanta, 2021]. These oils are not only safe for consumption but also do not require removal, streamlining the process, offering an alternative to conventional organic solvents while facilitating direct incorporation into food formulations. Vegetable oils, such as sunflower and corn oils, have demonstrated potential for carotenoid extraction Their compositional differences influence their capacity to solubilize lipophilic compounds, such as carotenoids [Plazola-Jacinto *et al*., 2019]. Corn oil contains a higher percentage of saturated fatty acids (~12% of total fatty acids) than sunflower oil (~10%) [Cherif & Slama, 2022]; and this difference may affect β-carotene extraction efficiency. However, the overall extraction efficiency also depends on processing conditions [Portillo-López *et al*., 2021]. Nevertheless, carotenoids are highly susceptible to degradation caused by exposure to heat, light, and oxygen, which can significantly reduce their functional efficacy [Rodriguez-Amaya, 2016]. To mitigate these effects, microencapsulation has been widely applied as an effective strategy to improve the stability and bioavailability of carotenoids [Drosou & Krokida, 2024; Lavelli & Sereikaitė, 2022; Menegazzi *et al*., 2020].

Spray-drying is widely regarded as a reliable technique for microencapsulating heat-sensitive bioactive compounds [Gharsallaoui *et al*., 2007]. It typically involves the creation of an emulsion by mixing the bioactive extract with wall materials, followed by atomization into fine droplets, drying *via* hot air exposure, and collection of the resulting powder. The final product is usually characterized by low moisture, high stability, and ease of handling and storage. Spray-drying is widely used to produce powdered β-carotene with enhanced stability [Drosou & Krokida, 2024; Gharsallaoui *et al*., 2007; Meng *et al*., 2024]. Compared with other drying methods, such as freeze-drying and hot air drying, spray-drying has been reported to provide improved resistance to photooxidative degradation, highlighting its industrial relevance for functional foods and supplements [Drosou & Krokida, 2024]. Maltodextrin (MD) and gum Arabic (GU) matrices have demonstrated good performance as carrier materials to enhance the stability of oils and their bioactive compounds during storage due to their emulsifying capacity [Comunian & Favaro-Trindade, 2016]. Composite wall materials, such as pullulan and whey protein isolate, are also used, which improve encapsulation efficiency compared to single-component wall materials and enhance the protection of β-carotene against oxidation and degradation during storage [Drosou & Krokida, 2024].

Previous studies have largely addressed oil-based extraction and spray-drying encapsulation as independent processes, with limited attention given to their integration within a single food-grade processing strategy. In particular, the combined influence of extraction conditions, emulsion properties, and wall-material composition on the physicochemical and functional performance of oil-based carotenoid microcapsules remains insufficiently explored. Therefore, this study proposes an integrated extraction–encapsulation approach using sunflower and corn oils as edible extraction media together with tailored MD–GU formulations as wall material. By linking extraction optimization, emulsion stability characterization, and multiscale evaluation of microcapsule structure and functionality, the present work aims to clarify how formulation and processing parameters collectively influence the stability and performance of oil-based β-carotenoid microcapsules.

MATERIALS AND METHODS

Raw materials

M. oleifera leaves were obtained from the research facility CEPROBI-IPN located in Yautepec, Mexico. The dried leaves were ground to a fine powder and passed through a 0.425 mm sieve to ensure uniformity. Although the leaves were dried, the powder was stored under freezing conditions to minimize potential degradation of carotenoids and other heat- and light-sensitive bioactive compounds, ensuring sample stability until experimentation. Commercial sunflower oil (Abreiko brand) and corn oil (Mazola brand) were purchased in the State of Mexico. Maltodextrin (MD) with a dextrose equivalent (DE) of 20 was sourced from Grain Processing Corporation (Muscatine, IA, USA), and gum Arabic (GU) was obtained from Sigma-Aldrich (Darmstadt, Germany).

β-Carotene extraction

β-Carotene was extracted from powdered *M. oleifera* leaves using corn and sunflower oils as solvents, following previously reported green extraction method [Sachindra & Mahendrakar, 2005] with slight modifications. For each extraction, 15 g of powdered *M. oleifera* leaves were mixed with 30 mL of the corn oil (CO) and sunflower oil (SFO) blend as a solvent, corresponding to a leaf-to-solvent ratio of 1:2 (*w/v*). Blends with different oil

proportions were used. The mixture was agitated at 100 rpm under different temperature and time conditions according to the experimental design.

β-Carotene was quantified using the spectrophotometric method developed by Nagata & Yamashita [1992] with some modifications. Oil samples (0.1 mL) were dissolved in 10 mL of hexane, and absorbance was measured at 663 nm (A_{663}), 505 nm (A_{505}), and 453 nm (A_{453}) using a spectrophotometer (Thermo Electron BioMate 3, Thermo Electron Corporation, Waltham, MA, USA). The β-carotene content was calculated according to Equation (1), and results were expressed as mg of β-carotene *per* 100 g of oil:

$$\beta\text{-Carotene} = 0.216\ A_{663} - 0.304\ A_{505} + 0.452\ A_{453} \quad (1)$$

D-optimal experimental design was employed to evaluate the combined effects of extraction time, temperature, and oil blend formulation on β-carotene content using Design-Expert software (version 11, Stat-Ease Inc., Minneapolis, MN, USA). Time (5, 10, and 30 min) and temperature (30, 60, and 70°C) were treated as numeric process factors, whereas oil proportion (CO to SFO ratios of 1:0, 0:1, 1:1, 1:2, and 2:1 *w/w*) was considered a formulation (mixture) variable. The levels of the variables, time and temperature, were selected based on previously reported conditions for carotenoid extraction using vegetable oils [Baria *et al*., 2019; Sachindra & Mahendrakar, 2005]. Experimental runs were selected according to the D-optimality criterion to efficiently explore the experimental space while reducing the total number of experiments. A total of 34 extraction runs were performed (**Table 1**).

Formulation of emulsion systems

Emulsions were formulated according to the procedure described by Plazola-Jacinto *et al*. [2019]. MD and GU blends (10 g of total solids) were dispersed in 100 mL of distilled water at MD to GU ratios of 2:1, 1:1, and 1:2 (*w/w*), and the mixtures were stored at 4°C overnight to ensure complete hydration. Subsequently, the oil extract obtained from *M. oleifera* leaf powder under optimized conditions (sunflower oil as a solvent, 70°C, 10 min) was incorporated at a 1:4 (*w/w*, oil extract to wall materials) proportion and homogenized at 11,000 rpm for 5 min using a homogenizer (Ultra-Turrax M45, IKA-Werke GmbH & Co. KG, Baden-Württemberg, Germany).

Emulsion stability assessment

Emulsion stability was assessed using a Turbiscan Lab Expert (Microtrac Formulaction SAS, Toulouse, France) within 4 h at 25°C. Emulsion samples (40 mm in height) were scanned using an 850 nm infrared source. Backscattering and transmission profiles were recorded at 45° and 180°, respectively, to monitor spatial and temporal variations in the dispersion [López-Hernández *et al*., 2022].

Table 1. Experimental design employed for β-carotene extraction from *Moringa oleifera* Lam. leaf powder using the blends of corn oil (CO) and sunflower oil (SFO).

Run	Time (min)	Temperature (°C)	CO to SFO proportion (*w/w*)
1	5	30	1:2
2	10	60	2:1
3	10	60	1:1
4	5	70	2:1
5	5	60	2:1
6	30	60	1:0
7	10	30	2:1
8	30	70	2:1
9	10	70	1:0
10	30	30	1:1
11	10	70	0:1
12	30	70	1:0
13	10	70	1:2
14	5	30	0:1
15	30	70	0:1
16	10	30	1:1
17	10	30	1:0
18	30	30	2:1
19	5	70	1:0
20	5	30	1:1
21	5	60	1:0
22	5	60	0:1
23	30	60	2:1
24	5	60	1:1
25	10	70	1:1
26	10	60	0:1
27	30	30	0:1
28	30	30	1:2
29	30	60	1:2
30	5	70	0:1
31	10	70	1:1
32	5	70	1:1
33	5	30	1:0
34	10	60	1:2

Droplet size and zeta potential analysis

Emulsions were diluted at 1:1,000 (*v/v*) with deionized water and analyzed for droplet size, polydispersity index (PDI), and zeta potential (ζ-potential) using a Zetasizer NANO-S90 analyzer (Malvern Panalytical Instruments Ltd., Malvern, UK). Measurements were performed by dynamic light scattering for particle size and PDI, and by laser Doppler electrophoresis for ζ-potential. The PDI was obtained from the cumulant analysis of the intensity autocorrelation function generated by the instrument software.

Apparent viscosity measurement

Apparent viscosity was measured at room temperature using an RST CC rheometer (Brookfield Engineering Labs Inc., Middleboro, MA, USA) equipped with a coaxial cylinder geometry. A shear rate range from 1 to 1,000 s^{-1} was used to evaluate the flow behavior of the emulsions.

Spray-drying process

Spray-drying of the emulsions was carried out in a Mobile Minor 2000 pilot-scale unit (GEA Niro, Søborg, Denmark). The emulsions were fed at 7.0 mL/min using a Watson-Marlow 520S pump (Watson-Marlow Fluid Technology Solutions, Falmouth, UK) and dried under co-current airflow with inlet and outlet temperatures of 180°C and 80°C, respectively. The atomization pressure was set at 100 kPa. The powders produced were transferred into sealed plastic bags and stored until further evaluation.

Encapsulation efficiency

Encapsulation efficiency (EE) was calculated with Equation (2), as the proportion of surface oil (S_o) to total oil (T_o) present in the microcapsules. Total oil was extracted using the Soxhlet method with *n*-hexane, whereas surface oil was determined by mixing 2 g of microcapsules with 10 mL of acetone for 5 min, centrifuging at 1,600×*g* for 15 min, and evaporating the solvent to measure the oil content [Di Giorgio *et al*., 2019]:

$$EE = (T_o - S_o)/T_o \quad (2)$$

Particle morphology

Approximately 1,500 microcapsules *per* sample were analyzed using a CILAS 1090 particle size and shape analyzer (CILAS, Orléans, France) equipped with an integrated optical imaging system. For the analysis, a small amount of microcapsule powder was gently dispersed onto a glass slide and spread using a fine brush to ensure adequate separation of individual particles and to minimize aggregation. Images were acquired at 20× magnification and analyzed using Expert Shape software (CILAS). The evaluated morphological parameters included particle size (µm), circularity, aspect ratio, sphericity, and kurtosis, as defined by the software.

Analysis of surface microstructure *via* scanning electron microscopy

Scanning electron microscopy (SEM) imaging was performed using a Carl Zeiss EVO LS 10 microscope (Carl Zeiss Microscopy GmbH, Jena, Germany) equipped with a backscattered electron detector. Prior to observation, the microcapsule samples were sputter-coated with a thin layer of gold to improve surface conductivity and image resolution. Microcapsules were examined at magnifications of 500× and 1,000× using accelerating voltages of 15 and 25 kV.

Component localization *via* confocal laser scanning microscopy

The internal distribution of core and wall components was analyzed by means of a Zeiss LSM 800 confocal laser scanning microscope (Carl Zeiss Microscopy GmbH, Jena, Germany). A 375 nm diode laser was used for excitation, and emissions were detected at 488 nm (green) and 640 nm (red). The resulting images were processed and reconstructed in 3D using ZEN software (Carl Zeiss Microscopy GmbH).

Determination of physicochemical and functional characteristics

Gravimetric analysis at 105°C (1-g sample) was used to determine moisture content of microcapsule powders [AOAC, 1995], while water activity (a_w) was measured at 25°C with an Aqualab 4TE device (Addium, Inc., Pullman, WA, USA). Hygroscopicity was evaluated by storing 1 g of the powder in a 75% relative humidity (RH) NaCl-saturated chamber at 25°C for one week. The results were expressed as g of adsorbed water *per* 100 g of dry sample (g H_2O/100 g) and calculated from the weight gain of the powder after storage. Bulk and tapped densities were determined using 2 g of the powder before and after 100 tapping cycles, respectively, and were calculated as the ratio between the sample mass and the corresponding bulk or tapped volume (g/mL). The Hausner ratio (tapped/bulk density) was used to assess powder flowability. Solubility and dissolution behavior were evaluated by monitoring absorbance changes over time using a Thermo Electron BioMate 3 spectrophotometer (Thermo Electron Corporation) at 620 nm. Briefly, 30 mg of the powder were dispersed in 3 mL of distilled water, and absorbance was recorded at predetermined time intervals. Dissolution profiles were constructed by plotting absorbance at 620 nm (A_{620}) as a function of time, following the methodology described by Plazola-Jacinto *et al.* [2019].

Glass transition temperature

A DSC Q-2000 differential scanning calorimeter (TA Instruments-Waters LLC, New Castle, Delaware, USA) was used to measure glass transition temperature (T_g). Approximately 10 mg of the microcapsule sample were sealed in aluminum pans and scanned between −20°C and 150°C at 10°C/min. Data analysis was performed using Orchestrator v.7.2.0.4 software (TA Instruments, New Castle, DE, USA).

Statistical analysis

Experimental data obtained from the extraction design were analyzed using Design-Expert version 11 (Stat-Ease Inc.) *via*

regression modelling and multifactor analysis of variance (ANOVA) to assess the significance of the process variables within the D-optimal experimental design. Model adequacy was assessed using F-values, *p*-values, coefficients of determination (R^2 and adjusted R^2), and adequate precision. Experiments were performed in triplicate, and results were expressed as mean and standard deviation (SD). One-way ANOVA followed by Tukey's test (95% confidence level) was applied only for comparison of physicochemical properties of the selected microcapsule formulations using GraphPad Prism v.5.0 (GraphPad Software Inc., San Diego, CA, USA).

RESULTS AND DISCUSSION

β-Carotene extraction

The β-carotene content in the blends of corn and sunflower oils used as solvents for its extraction from powdered *M. oleifera* leaves varied depending on the ratios of oils in the blend (**Figure 1**). A higher content of sunflower oil in the mixture corresponded to greater β-carotene yields. This finding may be attributed to the fatty acid composition, particularly the content of unsaturated fatty acids in the oils. According to the United States Department of Agriculture (USDA) data, the content of polyunsaturated fatty acids in sunflower oil is higher (about 65.78 g/100 g) than in corn oil (60 g/100 g) [USDA, 2019]. In turn, Baria *et al.* [2019] reported that a higher lipid unsaturation enhances the solubility of carotenoids. Solvent viscosity also plays a key role in the extraction process. Lower viscosity promotes better penetration of the solvent into the plant tissue, improving the release of target compounds [Silva *et al.*, 2021]. In this study, sunflower oil exhibited a lower viscosity (26.3±0.8 mPa×s) than corn oil (33.2±1.2 mPa×s), which likely contributed to its superior extraction performance.

Temperature and time were also critical factors in β-carotene extraction from *M. oleifera* leaf powder using oil blends (**Figure 1**). Higher extraction temperatures led to increased β-carotene recovery in all oil combinations. This can be explained by improved solute-solvent interaction due to reduced oil viscosity and enhanced diffusion rates at elevated temperatures [Chutia & Mahanta, 2021]. In turn, increasing the extraction time from 5 to 10 min significantly boosted β-carotene content in the oils, likely due to extended contact time between the solvent and plant matrix. However, extending extraction beyond 10 min did not lead to further improvements, which suggests that a short extraction time is sufficient and potentially advantageous in maintaining compound stability and simplifying the process.

The experimental data were modelled using a two-factor interaction (2FI) model to evaluate the effects of extraction time (A), temperature (B), and oil ratio (C) on carotenoid recovery. The model included the main effects of all factors and their two-way interactions and was fitted using the least squares method. No transformation of the response variable was required. Several mathematical models were evaluated to describe the experimental responses, and the inverse square root model provided the best fit according to ANOVA (**Table 2**). The selected model was statistically significant ($p<0.05$) and exhibited a coefficient of determination (R^2) of 0.8973, indicating good agreement between predicted and experimental values. The results of the lack-of-fit test were non-significant ($p>0.05$), confirming the adequacy of the model. The ANOVA results showed that all three factors, including oil ratio (C), had a significant effect on β-carotene extraction ($p<0.05$). However, a simplified regression equation including only the most influential continuous variables is presented for clarity and visualization purposes (Equation 3):

$$Y = 34.0556 - 11.702\ A + 6.1678\ B \quad (3)$$

where: A corresponds to extraction time and B to temperature.

The model predicted optimal extraction conditions of 70°C, 10 min, and sunflower oil. Under these conditions, the predicted carotenoid content (52.96 mg/100 g oil) was in close agreement with the experimental value (51.92±1.3 mg/100 g oil), confirming the reliability and predictive capability of the proposed model. These findings demonstrate that the inverse square root model effectively describes the kinetics of carotenoid extraction under the evaluated parameters.

Comparable studies on the optimization of carotenoid extraction using multifactor experimental designs have reported similar time and temperature ranges as critical variables influencing yield [Chutia & Mahanta, 2021; Rodriguez-Amaya, 2016]. For example, optimization studies on carotenoid extraction using edible oils as solvents have identified moderate temperatures and extraction times as key factors influencing extraction efficiency [Sachindra & Mahendrakar, 2005], showing trends comparable to those observed in the present study.

Emulsion characteristics

Maintaining emulsion stability is essential for efficient encapsulation, particularly when using spray-drying. Fine and uniformly distributed droplets help minimize coalescence and aggregation, thus preserving the structural integrity of the emulsion [Guo *et al.*, 2024]. In our study, an increase in GU content in the emulsion led to smaller droplet sizes (**Table 3**). This reduction in droplet size can be attributed to the good emulsifying properties of GU, which enhanced interfacial adsorption and reduced interfacial tension during homogenization, facilitating the formation of smaller droplets. The smallest average droplet size (1.07 µm) was observed at a 1:1 (*w/w*) ratio of MD to GU. This behavior suggests a balance between the emulsifying capacity of GU and the viscosity contribution of MD, which together promoted efficient droplet disruption during homogenization. At higher GU proportion, changes in the continuous phase properties, including viscosity and interfacial dynamics, may diminish the efficiency of droplet breakup, resulting in slightly larger droplet sizes.

The polydispersity index (PDI) and zeta potential (ζ-potential) values are presented in **Table 3**. A decrease in PDI was observed with an increasing GU content, indicating improved droplet size

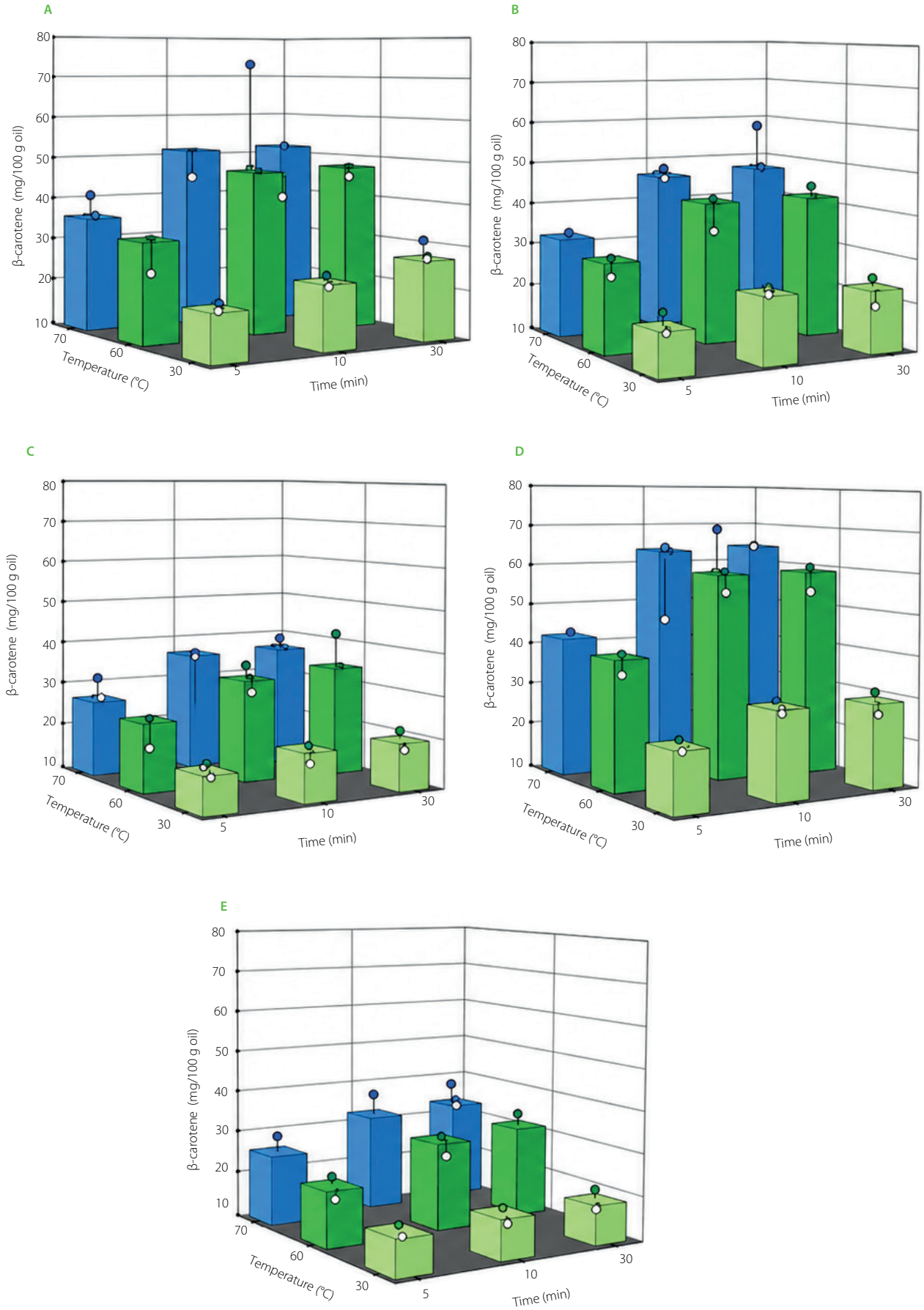

Figure 1. Effect of extraction time and temperature on β-carotene extraction from *Moringa oleifera* Lam. leaf powder using blends with different proportions of corn oil (CO) to sunflower oil (SFO) (*w/w*): (**A**) 0:1, (**B**) 1:1, (**C**) 2:1, (**D**) 1:2, and (**E**) 1:0. Experimental values are shown as lines, and model-predicted values are shown as bars.

Table 2. Results of the analysis of variance for regression modelling of β-carotene extraction from *Moringa oleifera* Lam. leaf powder using the blends of corn oil and sunflower oil.

Source	dF	Mean square	F-value	*p*-Value
Model	8	0.0045	12.29	0.0001
A	2	0.0031	8.43	0.0016
B	2	0.0099	27.21	0.0001
C	4	0.0024	6.76	0.0008
Residual	25			
Corrected total	33			
R^2	0.8973			
Adjusted R^2	0.8324			
CV (%)	9.49			
Standard deviation	0.0198			
Adequate accuracy	13.2			

dF, Degrees of freedom; CV, coefficient of variation; A, time; B, temperature; C, proportion of corn and sunflower oils in the blend.

uniformity. At the same time, the ζ-potential values became more negative, suggesting enhanced electrostatic repulsion between droplets. These results indicate that increasing GU content improved emulsion stability by reducing droplet aggregation through electrostatic stabilization. The PDI reflected improved uniformity with increasing GU content, because the addition of this wall material enhanced the negative surface charge, further preventing droplet aggregation [Jayme *et al.*, 1999]. These observations are consistent with findings by Premi & Sharma [2017], who reported more negative ζ-potential values with an increasing gum Arabic (GU) content in emulsions. Additionally, all samples in the present study exhibited ζ-potential values lower than −30 mV (**Table 3**), indicating sufficient electrostatic repulsion to ensure physical stability of the emulsions [McClements, 2005].

A significant ($p<0.05$) increase in apparent viscosity was observed with increasing GU content in the emulsion (**Table 3**), which can be attributed to its high molecular weight and the resulting enhancement of the continuous phase viscosity. Higher viscosity may reduce droplet mobility and collision frequency, thereby contributing to improved physical stability of the emulsion. This effect has been widely reported in food emulsions, where increased viscosity of the continuous phase limited flocculation and coalescence [McClements, 2005].

The physical stability of the emulsions was evaluated using backscattering profiles (**Figure 2**). Higher proportions of GU in the emulsions led to minimal temporal changes in backscattering, suggesting a reduced tendency toward creaming (*i.e.*, the upward migration of oil droplets due to density differences) or phase separation. Thus, increasing GU content appeared to enhance emulsion stability, likely due to better steric and electrostatic stabilization. However, a balance between MD and GU was critical for emulsion properties and encapsulation performance. A 1:1 (*w/w*) ratio produced the smallest droplet size and improved size distribution (**Table 3**), indicating more efficient droplet disruption during homogenization. This formulation also showed the highest encapsulation efficiency (0.74) (discussed in the subsection below), meaning better retention of β-carotene in final microcapsules. These findings underscore the importance of optimizing wall material composition to achieve favorable emulsion properties and enhance encapsulation efficiency.

Based on the results, the MD to GU ratio of 1:1 (*w/w*) yielded the most stable emulsion under the studied conditions. This formulation may be particularly relevant for the encapsulation of sensitive bioactive compounds, such as β-carotene. Previous studies have reported that carbohydrate-based wall materials can improve the protection of bioactive compounds against oxidation and enhance their stability in food systems [Drosou & Krokida, 2024; Lavelli & Sereikaitė, 2022]. Therefore, the optimization of wall material composition plays an important role in improving the functional performance of emulsions.

For comparison, other wall material strategies have been reported to improve emulsion stability and β-carotene protection. For instance, chitosan-stabilized Pickering emulsions have been shown to produce smaller droplet sizes and enhanced

Table 3. Physicochemical parameters of emulsions of *Moringa oleifera* Lam. leaf oil extract with β-carotene, containing blends of maltodextrin (MD) and gum Arabic (GU).

Parameter	MD to GU ratio		
	2:1 (*w/w*)	1:1 (*w/w*)	1:2 (*w/w*)
Emulsion droplet size (μm)	1.36±0.02^a	1.07±0.02^c	1.14±0.01^b
Polydispersity index	0.79±0.01^b	0.76±0.01^b	0.83±0.02^a
Zeta potential (mV)	−30.81±0.15^a	−31.53±0.55^a	−37.47±0.49^b
Apparent viscosity (mPa×s)	606.71±1.02^c	627.42± 0.20^b	670.91± 0.36^a

Different letters within a row denote significant differences among means ($p<0.05$).

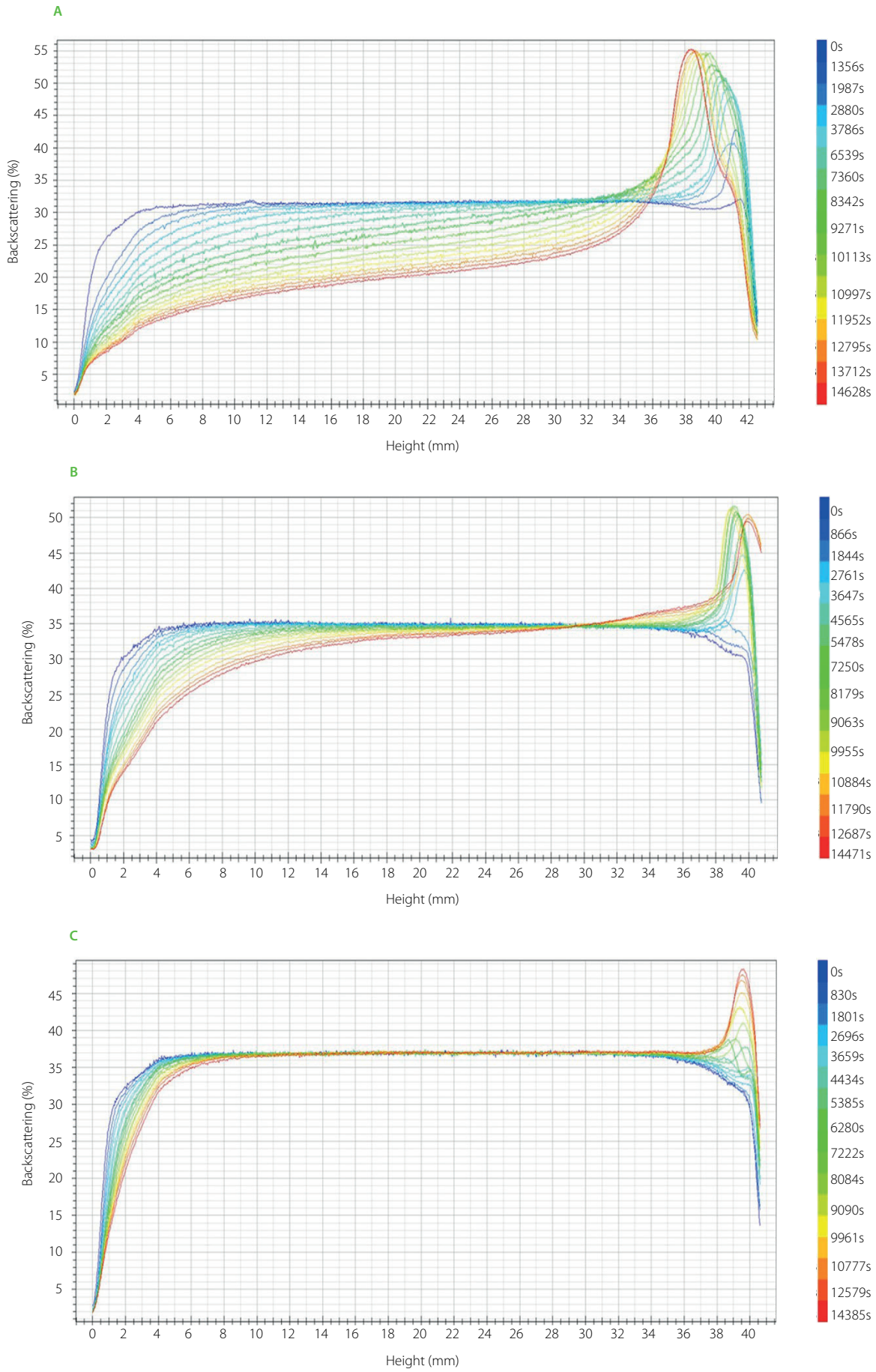

Figure 2. Backscattering profiles of emulsions of *Moringa oleifera* Lam. leaf oil extract with β-carotene, containing blends of maltodextrin (MD) and gum Arabic (GU) during 4 h at 25°C. (**A**) 2:1 MD to GU ratio (*w/w*); (**B**) 1:1 MD to GU ratio (*w/w*); and (**C**) 1:2 MD to GU ratio (*w/w*).

stability, which has been attributed to the formation of strong interfacial barriers [Yin *et al*., 2024]. In their review article, also Lavelli & Sereikaitė [2022] indicate that composite wall materials or coencapsulation strategies significantly reduce β-carotene oxidative degradation compared with single-component systems. These results suggest that while GU effectively stabilizes emulsions, alternative or combined wall materials may provide additional protection and improved performance.

Encapsulation efficiency

Encapsulation performance was strongly influenced by the ratio of wall materials used in the emulsion formulations. The combination of MD and GU at a 1:1 (*w/w*) ratio produced the highest encapsulation efficiency (0.74±0.02), whereas MD to GU ratios of 2:1 and 1:2 (*w/w*) resulted in lower efficiencies of 0.43±0.02 and 0.67±0.02, respectively. This behavior can be attributed to the complementary functional properties of both wall materials, since maltodextrin contributes to film formation and reduced viscosity, while gum Arabic provides emulsifying capacity that enhances interfacial stability of emulsion [Gupta *et al*., 2015].

The superior encapsulation efficiency observed for the formulation with MD to GU of 1:1 (*w/w*) is likely related to favorable emulsion characteristics, particularly smaller droplet size, lower polydispersity, and appropriate viscosity. These parameters play a key role in improving encapsulation efficiency, as smaller and more uniformly distributed droplets are more easily embedded within the wall matrix, reducing oil migration to the particle surface and minimizing surface oil formation during spray-drying [Salimi *et al*., 2018].

The 0.74 encapsulation efficiency obtained in this study is similar to that reported by Menegazzi *et al*. [2020] (~0.70), and De Souza *et al*. [2024] (~0.88) for carotenoid encapsulation by spray-drying. Higher β-carotene encapsulation efficiencies have been reported when alternative wall materials or optimized emulsification techniques were used; for instance, the use of the polysaccharide fraction obtained from yeast cell walls, consisting mainly of β-glucans and mannans (including mannoproteins) matrices, allowed achieving efficiency close to 0.90 under optimized spray-drying conditions [Do *et al*., 2019].

Overall, the results confirm that spray-drying remains a robust technique for encapsulating thermolabile compounds such as β-carotene, as it enables the formation of stable microcapsules while protecting sensitive bioactive compounds from oxidation, temperature, and light exposure [Meng *et al*., 2024].

Morphometry and structural features of microcapsules

The physical properties of the resulting microcapsules, such as size, shape, and surface characteristics, are critical for determining their performance in storage and application. **Table 4** shows that the MD to GU ratio of the wall material significantly affected particle morphology. Increasing GU content led to smaller microcapsule sizes, possibly due to GU's ability to lower surface tension and promote finer droplet formation during spray-drying [Mahdi *et al*., 2020]. Conversely, higher levels of MD may have reduced emulsion stability, contributing to the formation of larger particles upon drying. In this study, the microcapsules formed with the MD to GU of 1:1 (*w/w*) ratio had an average diameter of 7.98 µm, being smaller than those reported by Guadarrama-Lezama *et al*. [2012], *i.e.*, from 11.1 to 12.7 µm, who used similar materials. One of the contributing factors was the atomization pressure, namely 1.0 bar used in the present study and 0.4 bar in the cited work. Higher atomization pressure typically produces smaller particles due to greater droplet break-up energy.

Shape descriptors, such as circularity, sphericity, and aspect ratio, indicate how spherical the particles are; with values close to 1 indicating more spherical particles [Rosal, 2021]. Such particles are typically associated with greater mechanical and storage stability of the microcapsules [Gharsallaoui *et al*., 2007]. The microcapsules obtained with MD to GU ratios of 2:1 (*w/w*) and 1:1 (*w/w*) had sphericity values closer to 1 compared to those obtained with a 1:2 (*w/w*) ratio (**Table 4**). This may be related to the emulsion's high viscosity, which leads to irregular droplet formation. Irregular shapes can compromise the capsule wall structure, increasing the risk of rupture and the early release of encapsulated compounds. Kurtosis values were positive for all treatments (**Table 4**),

Table 4. Particle size and morphology characteristics of microcapsules of *Moringa oleifera* Lam. leaf oil extract with β-carotene, encapsulated using blends of maltodextrin (DM) and gum Arabic (GU) as wall material.

Characteristic	MD to GU ratio		
	2:1 (*w/w*)	1:1 (*w/w*)	1:2 (*w/w*)
Particle size (µm)	16.11±0.96^a	7.98±1.5^b	6.54±0.23^c
Circularity	0.81±0.02^a	0.85±0.06^a	0.74±0.06^b
Aspect ratio	1.43±0.02^a	1.45±0.02^a	1.37±0.03^b
Sphericity	0.66±0.03^a	0.67±0.04^a	0.50±0.06^b
Kurtosis	4.56	7.88	8.34

MD, maltodextrin; GU, gum Arabic. Different letters within a row denote significant differences among means ($p<0.05$).

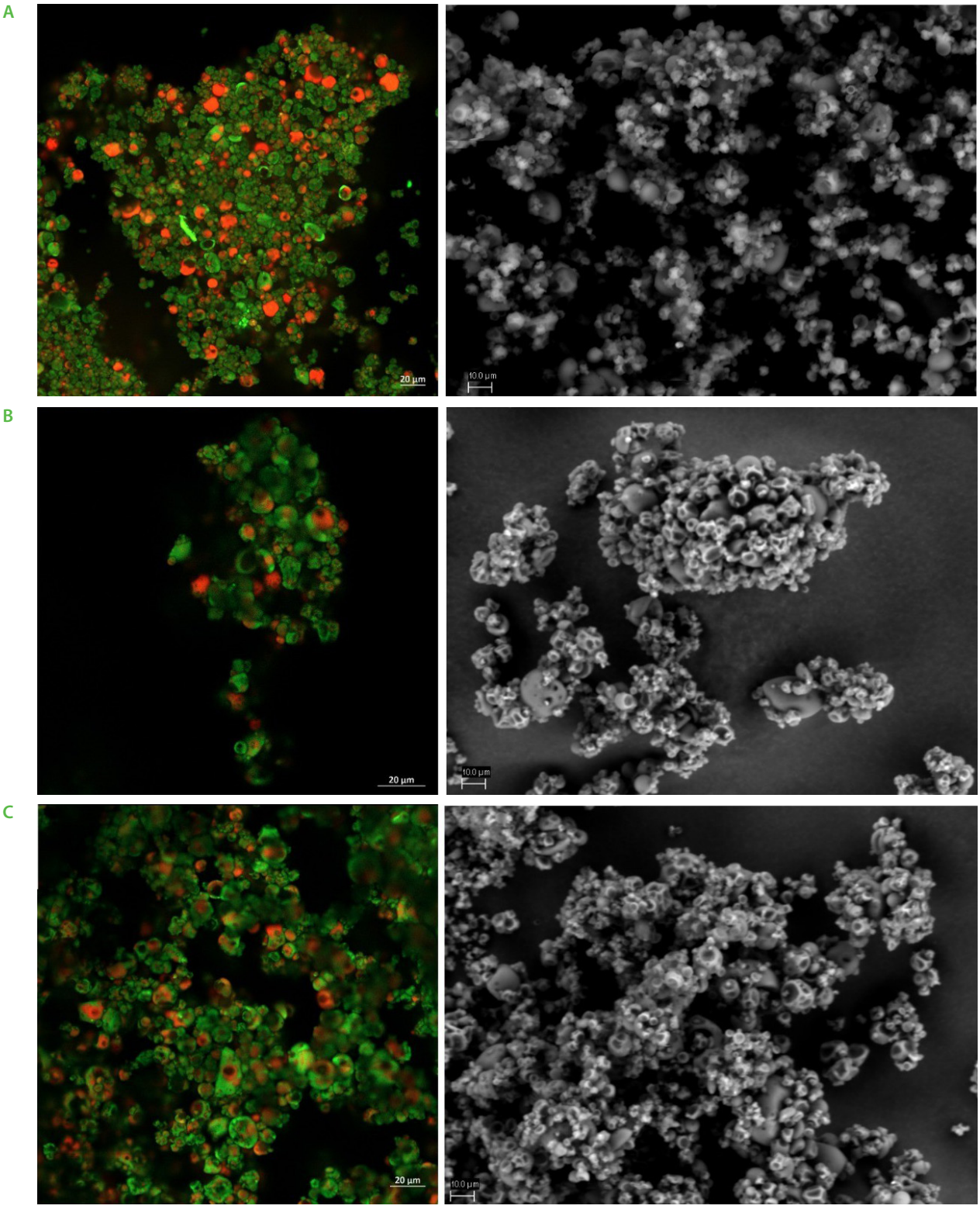

Figure 3. Morphology of microcapsules of *Moringa oleifera* Lim. leaf oil extract with β-carotene, encapsulated using blends of maltodextrin (DM) and gum Arabic (GU) as wall material observed by confocal laser scanning microscopy (left) and scanning electron microscopy (right). (**A**) 2:1 MD to GU ratio (*w/w*); (**B**) 1:1 MD to GU ratio (*w/w*); and (**C**) 1:2 MD to GU ratio (*w/w*).

indicating a leptokurtic (narrow and peaked) distribution of particle sizes [Garcia-Solis *et al*., 2022]. Kurtosis increased with a higher GU content in the wall material, suggesting that GU supports the formation of more uniform microcapsules.

Distribution of components in the microcapsule determined by confocal laser scanning microscopy

CLSM proved to be an effective tool for visualizing the spatial distribution of core and wall materials within microcapsules.

Table 5. Physicochemical and functional properties of microcapsules of *Moringa oleifera* Lam. leaf oil extract with β-carotene, encapsulated using blends of maltodextrin (DM) and gum Arabic (GU) as wall material.

Parameter	MD to GU ratio		
	2:1 (*w/w*)	1:1 (*w/w*)	1:2 (*w/w*)
Moisture (g H_2O/100 g)	3.09±0.05^b	3.02±0.08^b	4.59±0.19^a
Water activity	0.11±0.01^b	0.11±0.01^b	0.16±0.01^a
Hygroscopicity (g H_2O/100 g)	11.52±0.22^c	12.14±0.23^b	12.95±0.17^a
Bulk density (g/mL)	0.33±0.11^b	0.30±0.11^b	0.63±0.15^a
Tapped density (g/mL)	0.51±0.11^b	0.46±0.11^b	0.95±0.10^a
Hausner ratio	1.50±0.12^a	1.49±0.11^a	1.51±0.11^a

Different letters within a row denote significant differences among means ($p<0.05$).

As shown in **Figure 3**, the encapsulating agents (green) and the β-carotene extract (orange) were clearly distinguishable. The MD to GU ratio influenced the observed internal structure and surface characteristics of the microcapsules. The formulations with a higher GU content (**Figures 3B** and **3C**) appeared to differ in the distribution of the core material compared to those with a higher MD content (**Figure 3A**), which was qualitatively consistent with the encapsulation efficiency results. Notably, the 1:1 MD to GU (*w/w*) formulation displayed the most uniform distribution, and clear separation between core and wall materials. Similar microstructural organization has been reported in carotenoid-loaded microencapsulation systems, where confocal microscopy has been used to evaluate the spatial distribution of lipid cores within spray-dried matrices, depending on processing conditions and wall material composition [Zhu *et al*., 2021]. These findings highlight the importance of optimizing wall material ratios to enhance core retention and maintain the structural integrity of spray-dried microcapsules.

Microstructure of microcapsules determined by scanning electronic microscopy

SEM images of microcapsules produced with varying MD to GU ratios are shown in **Figure 3**. The results confirm that increasing the GU content led to smaller particle sizes, supporting earlier observations made *via* droplet size analysis. Regardless of the formulation, all microcapsule samples displayed signs of agglomeration, which suggests that the formation of aggregates was not directly related to the MD to GU ratio. A similar behavior has been reported by other authors working with spray-dried systems [Garcia-Solis *et al*., 2022]. The tendency for agglomerate formation could be influenced by high inlet temperatures used during spray-drying and the inherent hygroscopic nature of wall materials, which may absorb moisture post-process. These factors collectively contribute to particle adhesion and clustering during storage [Wang *et al*., 2015].

Physicochemical and functional properties of microcapsules

As summarized in **Table 5**, the microcapsules produced in this study exhibited moisture contents between 3.02 and 4.59 g H_2O/100 g of microcapsule powders, and a_w values ranging from 0.11 to 0.16. Such low values are favorable for preserving the bioactivity of β-carotene, as excess moisture can trigger enzymatic reactions that promote oxidation and compromise functional stability of this compound. Additionally, low a_w suppresses microbial growth, enhancing both shelf-life and safety of the powder. These characteristics were primarily achieved due to the spray-drying conditions employed, namely a high inlet temperature (180°C) and a moderate outlet temperature (80°C), which likely accelerated solvent evaporation and resulted in a reduced powder moisture content [Zhang *et al*., 2021].

The bulk and tapped densities of the microcapsules, shown in **Table 5**, varied significantly with the ratio of wall materials used. A higher GU content yielded powders with greater density, likely due to the smaller and more uniform particle size of those formulations. When particles are smaller and evenly distributed, they pack more efficiently, improving density parameters. High packing density in encapsulated powders has practical advantages. It reduces interstitial air between particles, which in turn minimizes exposure to oxygen and slows down the oxidation of encapsulated oils. The Hausner ratio, which is an indicator of powder flowability and cohesion [Garcia-Solis *et al*., 2022], was between 1.49 and 1.51 for all samples. Since values below 1.6 suggest an acceptable flow behavior [Guo *et al*., 2024], all formulations in this study were deemed to have good handling properties.

As shown in **Table 5**, the GU-rich microcapsules exhibited significantly ($p<0.05$) higher hygroscopicity (12.95 g H_2O/100 g) compared with the MD-rich formulations (11.52 g H_2O/100 g). A similar behavior has been reported in spray-dried microencapsulation systems using maltodextrin and gum Arabic, where higher gum

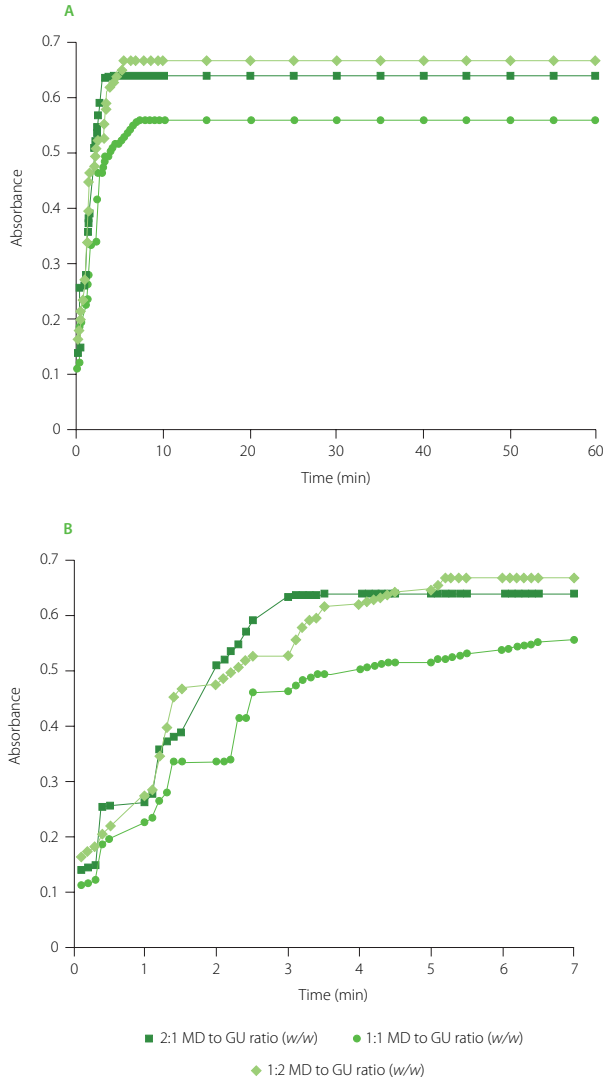

Figure 4. Dissolution profile of microcapsules of *Moringa oleifera* Lim. leaf oil extract with β-carotene, encapsulated using blends of maltodextrin (DM) and gum Arabic (GU) as wall material. (**A**) Absorbance at 620 nm over 60 min; and (**B**) enlargement of the first 7 min showing the initial stage of the dissolution.

Arabic content has been associated with increased hygroscopicity due to its higher affinity for water, while maltodextrin contributed to a lower moisture uptake and improved powder stability [Karaca *et al*., 2020]. Although beneficial for emulsion stabilization and encapsulation efficiency, excessive hygroscopicity may compromise storage stability of microcapsules by accelerating degradation of structural and bioactive compounds.

Figure 4 shows the dissolution profiles of microcapsules formulated with different MD to GU ratios, plotted as absorbance *vs*. time. The sample is considered dissolved when its absorbance remains constant over time. The sample that dissolved most rapidly was the one containing the highest proportion of MD, which dispersed in water within 3 min. The GU-rich formulation dissolved in approximately 5 min, whereas the sample with a 1:1 MD

Table 6. Glass transition temperature of wall materials and microcapsules of *Moringa oleifera* Lam. leaf oil extract with β-carotene, encapsulated using blends of maltodextrin (DM) and gum Arabic (GU).

Wall material/microcapsules	T_g (°C)
MD	189.98±0.54[a]
GU	147.17±0.58[b]
Microcapsules (2:1 MD to GU, *w/w*)	56.94±0.75[c]
Microcapsules (1:1 MD to GU, *w/w*)	58.87±1.22[c]
Microcapsules (1:2 MD to GU, *w/w*)	47.32±1.33[d]

Different letters within a column denote significant differences among means ($p<0.05$). T_g, glass transition temperature.

to GU (*w/w*) ratio needed about 6 min to disperse completely. These differences are attributed primarily to the water solubility of the wall materials. Maltodextrin, known for its high water solubility, serves as an effective carrier in spray-drying encapsulation systems and enables rapid dissolution in aqueous media. In contrast, gum Arabic is a complex polysaccharide–protein hydrocolloid that provides interfacial activity and forms more structured hydrated solutions, potentially affecting the release behavior of encapsulated compounds [Dickinson, 2003].

All microcapsule formulations exhibited lower T_g values than the pure wall materials (**Table 6**), likely due to the plasticizing effect of saturated fatty acids in the β-carotene extract [Guadarrama-Lezama *et al*., 2012]. The GU-rich formulations showed the lowest glass transition temperature (T_g), while the formulations that included MD exhibited the highest T_g. This behavior suggests that the balance between maltodextrin and gum Arabic influences molecular mobility within the matrix, affecting the thermal properties of the microcapsules.

The observed T_g values reflect differences in the molecular mobility of the microcapsule matrix. In general, higher T_g values are associated with reduced molecular mobility, which can contribute to improved retention of encapsulated compounds, such as β-carotene, during storage. Based on these properties, spray-dried microcapsules have been widely applied in food systems for the protection and delivery of bioactive compounds in various matrices [Gharsallaoui *et al*., 2007]. The enhanced structural stability of the microcapsules from the 1:1 MD to GU (*w/w*) formulation, in particular, indicates its suitability for applications that demand prolonged shelf-life and resistance to processing stresses.

CONCLUSIONS

This study demonstrated that both sunflower and corn oils as well as their blends could effectively serve as carriers for extracting β-carotene from *M. oleifera* leaves, with sunflower oil used at 70°C for 10 min yielding the highest extraction efficiency. β-Carotene-rich extracts were successfully microencapsulated by spray-drying

using MD and GU, with the MD to GU ratio of 1:1 (*w/w*) yielding the highest encapsulation efficiency, flowability, and glass transition temperature. These findings indicate that optimizing wall material composition can improve the structural stability of microcapsules and retention of the core material under the tested conditions. However, the study was limited to laboratory-scale experiments, and the stability of β-carotene microcapsules during storage or incorporation into real food matrices was not assessed. Future work should, therefore, evaluate long-term bioactive retention, performance in different food systems, and process scalability to better support potential industrial applications.

ACKNOWLEDGEMENTS

This work was supported by the Consejo Mexiquense de Ciencia y Tecnologia (COMECYT), through support for Postdoctoral stays to Sandra Elizabeth García Solís.

CONFLICT OF INTERESTS

The authors declare no conflicts of interest.

ORCID IDs

L.C. Boyano Orozco https://orcid.org/0000-0001-7147-6370
S.E. García-Solís https://orcid.org/0000-0002-9136-1607
J.L. Gonzalez-Escobar https://orcid.org/0000-0002-6548-5913
R.E. López-Hernández https://orcid.org/0000-0001-9738-7026
C.P. Plazola-Jacinto https://orcid.org/0000-0003-4615-8164
V. Pérez-Pérez https://orcid.org/0000-0003-3442-6969

REFERENCES

1. AOAC (1995). *Official Methods of Analysis* (15th ed.). The Association of Official Analytical Chemists International, Washington DC, USA, p. 1094.
2. Baria, B., Upadhyay, N., Singh, A.K., Malhotra, R.K. (2019). Optimization of 'green' extraction of carotenoids from mango pulp using split plot design and its characterization. *LWT – Food Science and Technology*, *104*, 186–194. https://doi.org/10.1016/j.lwt.2019.01.044
3. Cherif, A., Slama, A. (2022). Stability and change in fatty acids composition of soybean, corn, and sunflower oils during the heating process. *Journal of Food Quality*, *2022*, art. no. 6761029. https://doi.org/10.1155/2022/6761029
4. Chutia, H., Mahanta, C.L. (2021). Green ultrasound and microwave extraction of carotenoids from passion fruit peel using vegetable oils as a solvent: Optimization, comparison, kinetics, and thermodynamic studies. *Innovative Food Science & Emerging Technologies, 67*, art. no. 102547. https://doi.org/10.1016/j.ifset.2020.102547
5. Comunian, T.A., Favaro-Trindade, C.S. (2016). Microencapsulation using biopolymers as an alternative to produce food enhanced with phytosterols and omega-3 fatty acids: A review. *Food Hydrocolloids*, *61*, 442-457. https://doi.org/10.1016/j.foodhyd.2016.06.003
6. De Souza, L.R., Santos, I.A., Machado, G.G.L., Pereira, E.P., De Barros Vilas Boas, E.V., Botrel, D.A., De Carvalho, E.E.N., Damiani, C. (2024). Microencapsulation of carotenoids from tucumã (*Astrocaryum aculeatum*) peel by spray drying: Physicochemical properties, antioxidant activity and application in yogurt. *Food and Humanity*, *3*, art. no. 100454. https://doi.org/10.1016/j.foohum.2024.100454
7. Dickinson, E. (2003). Hydrocolloids at interfaces and the influence on the properties of dispersed systems. *Food Hydrocolloids*, *17*(1), 25-39. https://doi.org/10.1016/S0268-005X(01)00120-5
8. Di Giorgio, L., Salgado, P.R., Mauri, A.N. (2019). Encapsulation of fish oil in soybean protein particles by emulsification and spray drying. *Food Hydrocolloids*, *87*, 891-901. https://doi.org/10.1016/j.foodhyd.2018.09.024
9. Do, H.T., Kha, C.T., Huynh, P.P.T. (2019). Spray-drying microencapsulation of β-carotene by polysaccharide from yeast cell walls. *The Journal of Agriculture and Development*, *18*(06), 49-57. https://doi.org/10.52997/jad.7.06.2019
10. Drosou, C., Krokida, M. (2024). A comparative study of encapsulation of β-carotene via spray-drying and freeze-drying techniques using pullulan and whey protein isolate as wall material. *Foods*, *13*(12), art. no. 1933. https://doi.org/10.3390/foods13121933
11. Garcia-Solis, S.E., Perez-Perez, V., Tapia-Maruri, D., Villalobos-Castillejos, F., Arenas-Ocampo, M.L., Camacho-Diaz, B.H., Alamilla-Beltran, L. (2022). Microencapsulation of the green coffee waste extract with high antioxidant activity by spray-drying. *Journal of Food Processing and Preservation*, *46*(10), art. no. e16864. https://doi.org/10.1111/jfpp.16864
12. Gharsallaoui, A., Roudaut, G., Chambin, O., Voilley, A., Saurel, R. (2007). Applications of spray-drying in microencapsulation of food ingredients: An overview. *Food Research International*, *40*(9), 1107-1121. https://doi.org/10.1016/j.foodres.2007.07.004
13. Guadarrama-Lezama, A.Y., Dorantes-Alvarez, L., Jaramillo-Flores, M.E., Pérez-Alonso, C., Niranjan, K., Gutiérrez-López, G.F., Alamilla-Beltrán, L. (2012). Preparation and characterization of non-aqueous extracts from chilli (*Capsicum annuum* L.) and their microencapsulates obtained by spray-drying. *Journal of Food Engineering*, *112*(1–2), 29–37. https://doi.org/10.1016/j.jfoodeng.2012.03.032
14. Guo, L., Fan, L., Liu, Y., Li, J. (2024). Strategies for improving loading of emulsion-based functional oil powder. *Critical Reviews in Food Science and Nutrition*, *64*(33), 12780-12799. https://doi.org/10.1080/10408398.2023.2257325
15. Gupta, C., Chawla, P., Arora, S., Tomar, S., Singh, A. (2015). Iron microencapsulation with blend of gum arabic, maltodextrin and modified starch using modified solvent evaporation method – Milk fortification. *Food Hydrocolloids*, *43*, 622-628. https://doi.org/10.1016/j.foodhyd.2014.07.021
16. Islam, Z., Islam, S.R., Hossen, F., Mahtab-ul-Islam, K., Hasan, M.R., Karim, R. (2021). *Moringa oleifera* is a prominent source of nutrients with potential health benefits. *International Journal of Food Science*, *2021*(1), art. no. 6627265. https://doi.org/10.1155/2021/6627265
17. Jayme, M., Dunstan, D., Gee, M. (1999). Zeta potentials of gum arabic stabilised oil in water emulsions. *Food Hydrocolloids*, *13*(6), 459-465. https://doi.org/10.1016/S0268-005X(99)00029-6
18. Jikah, A.N., Edo, G.I. (2023). *Moringa oleifera*: a valuable insight into recent advances in medicinal uses and pharmacological activities. *Journal of the Science of Food and Agriculture*, *103*(15), 7343-7361. https://doi.org/10.1002/jsfa.12892
19. Karaca, A.C. (2020). Encapsulation of black pepper seed oil using maltodextrin and pea protein. *Food Science and Technology International*, *26*(5), 369-378. https://doi.org/10.1177/1082013219896429
20. Lavelli, V., Sereikaitė, J. (2022). Kinetic study of encapsulated β-carotene degradation in dried systems: A review. *Foods*, *11*(3), art. no. 437. https://doi.org/10.3390/foods11030437
21. López-Hernández, R.E., García-Solís, S.E., Monroy-Rodríguez, I., Cornejo-Mazón, M., Calderón-Domínguez, G., Alamilla-Beltrán, L., Hernández-Sánchez, H., Gutiérrez-López, G.F. (2022). Preparation and characterization of canola oil-in-water Pickering emulsions stabilized by barley starch nanocrystals. *Journal of Food Engineering*, *326*, art. no. 111037. https://doi.org/10.1016/j.jfoodeng.2022.111037
22. Mahdi, A.A., Mohammed, J.K., Al-Ansi, W., Ghaleb, A.D., Al-Maqtari, Q.A., Ma, M., Ahmed, M.I., Wang, H. (2020). Microencapsulation of fingered citron extract with gum arabic, modified starch, whey protein, and maltodextrin using spray drying. *International Journal of Biological Macromolecules*, *152*, 1125-1134. https://doi.org/10.1016/j.ijbiomac.2019.10.201
23. McClements, D.J. (2005). Characterization of emulsion properties. In: D.J. McClements (Ed.), *Food Emulsions: Principles, Practices, and Techniques* (2nd ed.), Boca Raton: CRC Press, pp. 475–485. https://doi.org/10.1201/9781420039436
24. Menegazzi, G.D.S., Teixeira, E.C., Pinto, L.A.D.A., Burkert, J.F.D.M. (2020). Spray-drying microencapsulation of carotenoids produced by *Phaffia rhodozyma*. *Industrial Biotechnology*, *16*(5), 300-308. https://doi.org/10.1089/ind.2020.0025
25. Meng, W., Sun, H., Mu, T., Garcia-Vaquero, M. (2024). Spray-drying and rehydration on β-carotene encapsulated Pickering emulsion with chitosan and seaweed polyphenol. *International Journal of Biological Macromolecules*, *268*(Pt 1), art. no. 131654. https://doi.org/10.1016/j.ijbiomac.2024.131654
26. Nagata, M., Yamashita, I. (1992). Simple method for simultaneous determination of chlorophyll and carotenoids in tomato fruit. *NIPPON SHOKUHIN KOGYO GAKKAISHI*, *39*(10), 925-928. https://doi.org/10.3136/nskkk1962.39.925
27. Plazola-Jacinto, C.P., Pérez-Pérez, V., Pereyra-Castro, S.C., Alamilla-Beltrán, L., Ortiz-Moreno, A. (2019). Microencapsulation of biocompounds from avocado leaves oily extracts. *Revista Mexicana de Ingeniería Química 18*(3), 1261-1276. https://doi.org/10.24275/uam/izt/dcbi/revmexingquim/2019v18n3/Plazola
28. Portillo-López, R., Morales-Contreras, B.E., Lozano-Guzmán, E., Basilio-Heredia, J., Muy-Rangel, M.D., Ochoa-Martínez, L.A., Rosas-Flores, W., Morales-Castro, J. (2021). Vegetable oils as green solvents for carotenoid extraction from pump-

kin (*Cucurbita argyrosperma Huber*) byproducts: Optimization of extraction parameters. *Journal of Food Science*, *86*(7), 3122-3136. **https://doi.org/10.1111/1750-3841.15815**

29. Premi, M., Sharma, H.K. (2017). Effect of different combinations of maltodextrin, gum arabic and whey protein concentrate on the encapsulation behavior and oxidative stability of spray dried drumstick (*Moringa oleifera*) oil. *International Journal of Biological Macromolecules, 105*(Pt 1), 1232–1240. **https://doi.org/10.1016/j.ijbiomac.2017.07.160**
30. Rodriguez-Amaya, D.B. (2016). Natural food pigments and colorants. *Current Opinion in Food Science*, *7*, 20-26. **https://doi.org/10.1016/j.cofs.2015.08.004**
31. Rosal, R. (2021). Morphological description of microplastic particles for environmental fate studies. *Marine Pollution Bulletin*, *171*, art. no. 112716. **https://doi.org/10.1016/j.marpolbul.2021.112716**
32. Sachindra, N.M., Mahendrakar, N.S. (2005) Process optimization for extraction of carotenoids from shrimp waste with vegetable oils. *Bioresource Technology*, *96*(10), 1195–1200. **https://doi.org/10.1016/j.biortech.2004.09.018**
33. Saini, R.K., Shetty, N.P., Giridhar, P. (2014). Carotenoid content in vegetative and reproductive parts of commercially grown *Moringa oleifera* Lam. cultivars from India by LC–APCI–MS. *European Food Research and Technology, 238*, 971–978. **https://doi.org/10.1007/s00217-014-2174-3**
34. Salimi, A., Maghsoudlou, Y., Jafari, S.M. (2018). Effect of emulsion stability and spray drying conditions on physicochemical characteristics of encapsulated powders. *Latin American Applied Research – An International Journal*, *48*(2), 95-100. **https://doi.org/10.52292/j.laar.2018.265**
35. Silva, S.S., Gomes, J.M., Reis, R.L., Kundu, S.C. (2021). Green solvents combined with bioactive compounds as delivery systems: present status and future trends. *ACS Applied Bio Materials*, *4*(5), 4000-4013. **https://doi.org/10.1021/acsabm.1c00013**
36. Sonewane, K., Chouhan, S.S., Rajan, M., Chauhan, N.S., Rout, O.P., Kumar, A., Baghle, G.S., Gupta, P.K. (2022). Pharmacological, ethnomedicinal, and evidence-based comparative review of *Moringa oleifera* Lam. (Shigru) and its potential role in the management of malnutrition in Tribal Regions of India, especially Chhattisgarh. *World Journal of Traditional Chinese Medicine*, *8*(3), 314-338. **https://doi.org/10.4103/wjtcm.wjtcm_69_21**
37. Tak, Y., Kaur, M., Jain, M.C., Samota, M.K., Meena, N.K., Kaur, G., Kumar, R., Sharma, D., Lorenzo, J.M., Amarowicz, R. (2022). Jamun seed: A review on bioactive constituents, nutritional value and health benefits. *Polish Journal of Food and Nutrition Sciences*, *72*(3), 211-228. **https://doi.org/10.31883/pjfns/152568**
38. USDA (2019). United States Department of Agriculture FoodData *Central*. **https://fdc.nal.usda.gov/**
39. Wang, W., Dufour, C., Zhou, W. (2015). Impacts of spray-drying conditions on the physicochemical properties of soy sauce powders using maltodextrin as auxiliary drying carrier. *CYTA – Journal of Food, 13*(4), 548–555. **https://doi.org/10.1080/19476337.2015.1014430**
40. Yin, X., Lu, J., Du, W., Wu, Q., Han, L., Su, S. (2024). Encapsulation of β-carotene in Pickering emulsions stabilized by self-aggregated chitosan nanoparticles: Factors affecting β-carotene stability. *International Journal of Biological Macromolecules*, *277*(Pt 1), art. no. 133696. **https://doi.org/10.1016/j.ijbiomac.2024.133696**
41. Zhang, L., Liao, W., Wei, Y., Tong, Z., Wang, Y., Gao, Y. (2021). Fabrication, characterization and *in vitro* digestion of food-grade β-carotene high loaded microcapsules: A wet-milling and spray drying coupling approach. *LWT – Food Science and Technology*, *151*, art. no. 112176. **https://doi.org/10.1016/j.lwt.2021.112176**
42. Zhu, Y., Peng, Y., Wen, J., Quek, S.Y. (2021). A comparison of microfluidic-jet spray drying, two-fluid nozzle spray drying, and freeze-drying for co-encapsulating β-carotene, lutein, zeaxanthin, and fish oil. *Foods*, *10*(7), art. no. 1522. **https://doi.org/10.3390/foods10071522**

ORIGINAL ARTICLE
http://journal.pan.olsztyn.pl

Polish Journal of Food and Nutrition Sciences
2026, Vol. 76, No. 2, 149–161
DOI: 10.31883/pjfns/221424
ISSN 1230-0322, e-ISSN 2083-6007

Functional Whipped Cream Based on Duck Fat and Inulin: A Study on Rheological, Microstructural, and Whipping Properties

Muhammad U. Amjad[1], Saman Azeem[1], Baocheng Xu[1, 2, 3*], Enguo Lyu[4], Yiming Sun[1], Xinjing Dou[1, 2, 3]

[1]College of Food and Bioengineering, Henan University of Science and Technology, Luoyang, 471023, China
[2]Henan International Joint Laboratory of Food Green Processing and Safety Control, Luoyang, 471023, China
[3]National Experimental Teaching Demonstration Center of Food Processing and Safety, Henan University of Science and Technology, Luoyang, 471023, China
[4]Henan Huaying Cherry Valley Food Co., Ltd., Huangchuan, 465150, China

This study investigates natural inulin as a stabilizer in a novel whipped cream formulated with duck fat fraction rich in unsaturated fatty acids. The objective was to develop a functional whipped cream with favorable structural, rheological, and sensory properties using a non-traditional fat source. Increasing inulin content (0–14.7%, *w/w*) significantly modified emulsion microstructure and viscoelastic behavior. Rheological measurements showed a concentration-dependent increase in viscosity and storage modulus, indicating progressive strengthening of the continuous phase. Whipping performance was strongly influenced by inulin content. Although overrun decreased at higher inulin levels, the 12.1% (*w/w*) formulation achieved an optimal balance, maintaining a desirable overrun of 214% while completely eliminating serum loss (0%) after 3 h at 22°C. Higher inulin levels (≥12.1%, *w/w*) significantly improved shaping ability, air cell uniformity, and structural retention. Sensory evaluation demonstrated that formulations containing ≥12.1% (*w/w*) inulin exhibited a smooth texture and improved smoothness approaching that of the commercial whipped cream reference sample. Overall, 12.1% (*w/w*) inulin was identified as the optimal content, offering excellent physicochemical stability, balanced whipping behavior, enhanced structural integrity, and favorable sensory characteristics. These findings establish inulin as an effective stabilizer for producing duck-fat-based whipped cream with promising functional quality and potential nutritional benefits.

Keywords: emulsions, foam stability, overrun, rheology, sensory quality

INTRODUCTION

Whipped cream is an aerated oil-in-water (O/W) emulsion system composed of lipids, proteins, stabilizers, surfactants, and sweeteners [Zeng *et al*., 2022b]. The structural integrity of this foam is primarily attributed to the immobilization of air bubbles by a network of partially coalesced fat globules at the air-water interface [Goff, 1997; Turner *et al*., 1999]. It is widely used in bakeries as a topping for desserts, such as cakes and pies, or for hot beverages like coffee. Moreover, it also serves as a filling in pastries and imparts creaminess to parfaits and trifles [Wu *et al*., 2023].

Currently, the primary lipid sources for whipped cream are milk fat and hydrogenated vegetable oils. While milk fat contributes to desirable textural characteristics and structural integrity of whipped cream [Cui *et al*., 2025; Nguyen *et al*., 2015; Rybak,

***Corresponding Author:**
E-mail address: **xbc76@163.com** (Prof. B. Xu)

Submitted: 25 February 2026
Accepted: 4 May 2026
Published on-line: 12 May 2026

2016], its high saturated fatty acid content is increasingly linked to adverse effects on cardiovascular health [Günç Ergönül & Ergönül, 2023]. Plant-based alternatives offer little improvement, as they typically rely on palm stearin or hydrogenated palm kernel oil, both of which are rich in saturated fats [Nesaretnam *et al*., 1993]. Furthermore, the hydrogenation process generates trans-fatty acids, a known contributor to coronary heart disease [Motamedzadegan *et al*., 2020]. Consequently, there is a need for alternative lipid sources that maintain the solid fat content required for partial coalescence while offering a better nutritional profile. To address this concern, the present study utilized a duck fat fraction, which was richer in unsaturated fatty acids than the fats typically used in whipped cream.

The stabilization of whipped cream rich in unsaturated fatty acids poses a significant challenge that can be overcome by using stabilizers. Inulin, the natural β (2⟶1) linear fructan, has gained prominence as this type of a food additive. Due to its ability to modify texture, extend shelf-life, and enhance organoleptic properties, inulin is widely utilized in products such as yogurt, ice cream, and spreads [Shoaib *et al*., 2016]. Its functionality is largely governed by its chain length, with shorter chains exhibiting higher water solubility than longer ones. Because of its structure, inulin easily forms hydrogen bonds and immobilizes water, which, at contents between 13% and 50%, allows the formation of a microcrystalline gel network upon shearing and cooling [Desu *et al*., 2025]. We hypothesize that this inulin-templated network may contribute to whipped cream stability through a dual mechanism: first, by increasing the viscosity of the aqueous phase to reduce serum drainage; and second, by forming a cohesive, three-dimensional microstructure that physically entraps and stabilizes air bubbles and fat globules. This structural reinforcement may help reduce fat globule coalescence and delay foam collapse [Athari *et al*., 2021; Kim *et al*., 2001].

Previous studies have reported that inulin can enhance the emulsification performance of protein-stabilized emulsion systems [Liu *et al*., 2016]. This effect has been primarily attributed to inulin's strong water-absorbing capacity and its ability to maintain a stable hydrated network structure, which modifies water distribution in the continuous phase and modulates hydrogen bonding and van der Waals interactions among casein molecules [Nieto-Nieto *et al*., 2015; Xu *et al*., 2021]. Such interactions may induce partial unfolding of sodium caseinate structures, increasing the exposure of hydrophilic groups and thereby improving protein solubility and interfacial activity. These physicochemical modifications have been associated with improved emulsion stability in protein-polysaccharide systems, without inulin acting as a classical surface-active emulsifier [Liu *et al*., 2016]. Although inulin does not possess the characteristics of a conventional surfactant, it functions as an important structuring agent in the aqueous phase.

Beyond its structural contributions, inulin may provide additional nutritional value as dietary fiber with recognized prebiotic functionality. Because it resists hydrolysis in the small intestine, it is fermented by beneficial gut microbiota, such as *Bifidobacterium* and *Lactobacillus*, thereby promoting gastrointestinal health [Shoaib *et al*., 2016].

Although inulin has been investigated in several emulsion and dairy systems, its application in whipped cream formulated with a duck fat fraction has not been reported so far. Duck fat differs from conventional cream fats in fatty acid composition, solid fat content, and crystallization characteristics, which may pose challenges in terms of aeration, partial coalescence, and foam stability. Therefore, evaluating inulin as a stabilizer in this alternative lipid matrix represents an important research gap. The primary novelty of this study is the development of a non-dairy whipped cream formulated using an unsaturated duck fat fraction. The secondary novelty is the use of natural inulin as a stabilizer to improve rheological properties and foam stability, while also serving as a potential source of dietary fiber. Given the above, this study investigated the effects of inulin content (0–14.7% of emulsion, *w/w*) on physicochemical properties, rheology, overrun, foam stability, microstructure, and sensory attributes. This content range was selected based on preliminary experiments, where low levels (3.3–6.5%, *w/w*) showed limited viscosity enhancement, while higher levels (≈12.1%, *w/w*) significantly increased viscosity and structural stability. Therefore, a broad range was selected to evaluate concentration-dependent effects and identify the optimal formulation. We hypothesized that increasing inulin content would enhance structural stability and viscoelastic properties, with a critical content required to form a self-supporting network that optimizes overall product quality.

MATERIALS AND METHODS

Materials

The duck fat fraction, consisting of 47.01% of saturated fatty acids (mainly palmitic and stearic acids), 31.34% of monounsaturated fatty acids (mainly oleic acid), and 21.65% of polyunsaturated fatty acids (mainly linoleic acid), was graciously donated by Henan Huaying Cherry Valley Co., Ltd. (Xinyang, China). Mono- and diglycerides were purchased from Jialishi Additives (Hai'an) Co., Ltd. (Jiangsu, China). Natural inulin, extracted from chicory root, with a degree of polymerization ranging from 2 to 60 and purity ≥86% was provided by Cosucra (Warcoing, Belgium). Sodium caseinate (protein content ≥90%) was purchased from Huaan Group (Gansu, China). Guar gum was sourced from Henan Anrui Biotechnology Co., Ltd. (Zhengzhou, China). Polyglycerol fatty acid ester (hydrophilic-lipophilic balance, HLB 13) was supplied by Zhengzhou Dahe Food Technology Co., Ltd. (Zhengzhou, China). Disodium hydrogen phosphate and potassium dihydrogen phosphate were purchased from Tianjin De'en Chemical Reagent Co., Ltd. (Tianjin, China). The fluorescent dyes Nile red, Nile blue, and calcofluor white were provided by Shanghai Yuanleaf Biological Technology Co., Ltd. (Shanghai, China) and Sigma-Aldrich Shanghai Trading Co., Ltd. (Shanghai, China), respectively. A commercial milk fat-based whipped cream was purchased from Fonterra Commercial Trading Co., Ltd. (Shanghai, China). All other chemicals used were of analytical grade. Deionized water was produced using a Milli-Q water filtration system (Millipore Corporation, Milford, MA, USA).

Preparation of emulsions

Whipping cream emulsions were prepared by mixing aqueous and oil phases. To obtain aqueous mixtures, 0.5 g of sodium caseinate, 0.1 g of polyglycerol fatty acid ester with an HLB value of 13, as well as 0, 3, 6, 9, 12, or 15 g of inulin were added to 56.17 g of distilled water adjusted to pH=7.0 with potassium dihydrogen phosphate and disodium hydrogen phosphate. These amounts of inulin constituted 0%, 3.3%, 6.5%, 9.4%, 12.1%, and 14.7% of the total emulsion (*w/w*), respectively, and the corresponding emulsions were named IN-0, IN-3.3, IN-6.5, IN-9.4, IN-12.1, and IN-14.7, respectively. Aqueous mixtures were stirred at 60°C until complete dissolution and hydration had been achieved. The oil phase consisted of a duck fat fraction (29.5 g), which was heated to 70°C for 30 min. Mono- and diglycerides (0.5 g) were then added and allowed to dissolve completely before emulsification. A guar gum reference sample was prepared under identical processing conditions, in which inulin was replaced with guar gum (0.23 g; 0.26% of total emulsion, *w/w*). This level was selected based on preliminary trials, as a higher guar gum content produced excessive viscosity and impaired whipping performance. The oil phase was slowly added to the water phase and then pre-emulsified at 10,000 rpm for 3 min using a high-speed shear mixer. These emulsions were then homogenized using a high-pressure homogenizer (GJJ-0.02/60, Shanghai Noni Light Industry Machinery Co., Ltd., Shanghai, China) at 20 MPa for 3 min to obtain a fine and uniform oil-in-water emulsion. Emulsions were cooled immediately and allowed to age at 4°C for 24 h to promote fat crystallization and to stabilize prior to analysis.

Analysis of emulsion properties

Determination of particle size distribution

The particle size distributions of the emulsions were characterized by a dynamic light scattering (DLS) instrument (BeNano 90 Zeta, Bettersize Instruments Ltd., Dandong, China). Each sample was diluted 1,000-fold with deionized water prior to measurement. The optical parameters were defined with a refractive index of 1.33 for the continuous phase (water) and 1.451 for the dispersed phase, using an absorption index of 0.001. All measurements were conducted at a constant temperature of 25°C [Chen *et al.*, 2025]. The mean particle size expressed on a volume-weighted basis ($d_{4,3}$), was recorded, with all measurements conducted in triplicate.

Confocal laser scanning microscopy analysis

Microstructure analysis of emulsions and whipped foams was performed using confocal laser scanning microscopy (CLSM, Olympus FV3000, Tokyo, Japan) to observe fat globule size and network formation. The lipid phase, protein phase, and polysaccharides (inulin and guar gum) were specifically stained with Nile red (0.1%, *w/w*), Nile blue (0.5%, *w/w*), and calcofluor white, respectively. Images were captured using a 63× oil immersion objective with an additional 3× digital zoom**.** The excitation wavelengths were set at 635 nm for Nile red, 488 nm for Nile blue, and 432 nm for calcofluor white.

Determination of zeta potential

The surface charge of the emulsion droplets was determined by zeta potential analysis using a BeNano 90 Zeta DLS instrument (Bettersize Instruments Ltd.). To prevent multiple scattering effects, samples were diluted 1,000-fold with deionized water before measurement [Wang *et al.*, 2023]. Data were collected in triplicate and reported as the mean values.

Determination of rheological properties

The rheological properties of the emulsions were characterized using a TA DHR-2 rheometer (TA DHR-2, Waters Corporation, Milford, MA, USA) equipped with a 40-mm parallel steel plate. All measurements were conducted at 4°C with a geometry gap of 1,000 µm. Steady-state flow tests were performed by applying a logarithmic shear rate ramp from 0.1 to 100 s^{-1}. At each shear rate, data were recorded after a 5-s equilibrium time, followed by a 30-s averaging period. To determine the linear viscoelastic region (LVR), dynamic strain sweep measurements were conducted between 0.01% and 100% strain at a constant frequency of 1 Hz. This allowed for the characterization of the storage (G′) and loss (G″) moduli as functions of the applied deformation [Zhang *et al.*, 2024].

Whipped cream preparation

The aged emulsion samples were whipped using a planetary mixer (KitchenAid 5KSM3311, St. Joseph, MI, USA). Prior to whipping, both the mixing bowl and the whisk attachment were pre-cooled at 4°C for 30 min. Subsequently, 150 g of the emulsion, also pre-cooled to 4°C, was whipped at a constant speed of 1,000 rpm. The whipping process was stopped upon the formation of a smooth texture and the appearance of soft peaks on the whisk, indicating the optimal whipping time [Fredrick *et al.*, 2013]. To minimize variability, three experimental replicates were performed by the same operator and the results were averaged.

Characterization of whipped cream

Whipping time determination

The whipping time was defined as the duration (in seconds) from the initiation of whipping at 1,000 rpm until the emulsion reached the predetermined whipping endpoint, as described in whipping cream preparation procedure.

Determination of overrun

Following the procedure established by Zeng *et al.* [2022a], overrun was determined by measuring the mass difference of a constant volume of the sample in its liquid and aerated states according to Equation (1):

$$\text{Overrun (\%)} = \frac{w_1 - w_2}{w_2} \times 100 \quad (1)$$

where: w_1 indicates the mass of unwhipped emulsion, while w_2 represents the mass of whipped cream.

Foam stability determination

The foam stability of the whipped foams was measured over time, with minimal serum drainage correlating with higher stability in the aerated system [Liu *et al*., 2024]. The procedure was adapted from Zeng *et al*. [2022b]. To this end, 20 g of freshly whipped cream were transferred to a mesh funnel and incubated at 22°C for 3 h. The percentage serum loss was calculated using Equation (2):

$$\text{Serum loss (\%)} = \frac{m_{serum}}{m_{whipped\ cream}} \times 100 \quad (2)$$

where: m_{serum} represents the serum mass (g) separated from the whipped cream after 3 h, and $m_{whipped\ cream}$ refers to the initial mass (g) of the whipped cream.

Analysis of microstructure of whipped cream

The whipped foam microstructure was examined using a polarized light microscope (PLM, XPV-203, Changfang Optical Instrument Co., Ltd., Shanghai, China). Samples obtained at the optimal whipping time were placed on a glass slide with a coverslip and visualized at 40× magnification to analyze the size and distribution of air bubbles.

Visualization of whipped cream decorative appearance imaging

The retention of decorative shape was assessed using a standard piping method. Freshly whipped samples were piped into uniform rosettes on a flat surface using a pastry bag equipped with a closed-star tip. The rosettes were then subjected to a stability test in an environmental chamber set at 22°C. To observe shape change over time, digital images were captured immediately after piping and following a 3-h holding period.

The internal stability of the whipped cream was evaluated by examining the surface topography of a cut section. Freshly whipped samples were first shaped into a mound and equilibrated at 25°C for 1 h. Subsequently, the mound was sectioned with a metal scraper. The resulting cross-section was immediately photographed under standardized lighting conditions to capture its texture.

Sensory evaluation

Sensory evaluation was conducted using a descriptive analysis approach from Ma *et al*. [2025] with minor modifications. Twenty trained panellists (10 men and 10 women, aged 22–40 years) were recruited from postgraduate students and staff members of the College of Food and Bioengineering, Henan University of Science and Technology, China. All panellists were regular consumers of dairy or whipped cream products and had previous experience in sensory evaluation. Prior to the test, the panellists had two orientation sessions to familiarize themselves with the evaluation attributes, scoring criteria, and reference standards. Individuals with known dairy allergies, impaired taste or smell perception, smoking habits, or recent illness affecting sensory perception were excluded. Freshly prepared whipped cream samples were labeled with random three-digit codes and presented to the panellists in randomized order to minimize bias. Approximately 10 g of each sample were served at 8±1°C in identical odorless cups. Sensory evaluations were conducted in individual booths under standardized white lighting at 22±2°C. Panellists were provided with drinking water to cleanse their palates between successive samples. They rated each sample on a 10-point intensity scale for four key sensory attributes: (a) smoothness (extremely smooth, 10–8; a little coarseness, 7–5; much harshness, 4–1); (b) texture (melts in the mouth, 10–8; weak and fluffy, 7–5; grainy, 4–1); (c) greasiness (no greasiness, 10–7; heavy greasiness, 6–1); (d) flavor and taste (no criticism, 10; delicate flavor, 9–7; lack of flavor, 6–4; other defects, 3–1). These attributes were selected based on the key quality characteristics of whipped cream and preliminary screening trials.

Statistical analysis

Experiments were performed in triplicate, and data are reported as mean and standard deviation. One-way analysis of variance (ANOVA) and Tukey's post hoc tests were applied to determine significant differences between samples using IBM SPSS Statistics for Windows, Version 27.0 (IBM Corp., Armonk, NY, USA). Differences were considered significant at $p<0.05$.

RESULTS AND DISCUSSION

Emulsion properties

Particle size distribution of emulsions

The stability of cream emulsions is significantly affected by particle size distribution, which is also an important parameter influencing the whipping properties of cream [Wang *et al*., 2023]. The particle size distribution and volume weighted mean diameters ($d_{4,3}$) of duck fat-based emulsions stabilized by varying inulin contents, guar gum, and commercial whipped cream (CWC) are presented in **Figure 1**. As the inulin content increased from 0% to 12.1% (*w/w*), the mean particle size increased significantly from 0.761 µm (IN-0) to 1.106 µm (IN-12.1), before decreasing to 0.855 µm at 14.7% (*w/w*) inulin (IN-14.7). Guar gum reference sample (GG-0.26) showed an intermediate $d_{4,3}$ value of 0.943 µm, while the CWC sample exhibited the finest dispersion, with a mean diameter of 0.739 µm.

The increase in particle size up to 12.1% (*w/w*) inulin suggests enhanced droplet-droplet interactions and partial aggregation. This phenomenon may be explained by a bridging flocculation mechanism, where chains in the continuous phase associate with the surfaces of fat droplets, promoting the formation of flocs and increasing the effective droplet size. Bridging phenomena of this type are well-described for protein-stabilized emulsions in the presence of non-adsorbing or partially adsorbing polysaccharides [Dickinson, 2003]. Analogous concentration-dependent effects have been reported in protein-stabilized Pickering emulsions and inulin-containing salad dressings, where moderate polysaccharide levels promote droplet association once the protein surface coverage becomes incomplete [Li *et al*., 2024; Sinsuwan, 2024].

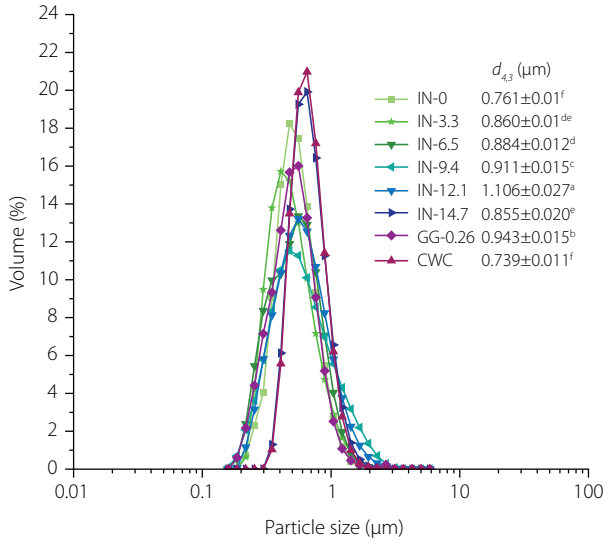

Figure 1. Particle size distribution and volume-weighted mean particle diameter ($d_{4,3}$) of duck fat-based cream emulsions formulated without inulin (IN-0), with inulin content ranging from 3.3% to 14.7%, *w/w*, (IN-3.3–IN-14.7), and with guar gum (GG-0.26), as well as a commercial whipping cream emulsion (CWC). Results of $d_{4,3}$ are shown as mean ± standard deviation. Different superscript letters (a–f) indicate significant differences among emulsions ($p<0.05$).

At the higher inulin content (14.7%, *w/w*), the decrease in $d_{4,3}$ indicates a transition from bridging to steric stabilization. The high content of inulin likely promoted the formation of a dense, viscoelastic microgel network in the continuous phase [Kim *et al*., 2001; Shoaib *et al*., 2016] as corroborated by the sharp increase in viscosity and moduli. This network impedes droplet movement and coalescence through a combination of steric hindrance and increased continuous phase viscosity leading to a finer and more stable dispersion [Ai, 2023]. The corresponding shift in particle size distribution supports the formation of a structured, immobilized system. The guar gum reference sample exhibited a relatively narrow particle size distribution, reflecting the strong thickening efficiency of guar gum even at a low content. In contrast, the fine and uniform droplets observed in CWC likely reflect optimized industrial homogenization and formulation conditions.

Overall, inulin levels play a part in governing the microstructure of duck fat-based emulsions. Moderate inulin levels promote bridging flocculation, while higher levels (>14.7%, *w/w*) stabilize the emulsion through bulk network formation.

Microstructure of emulsions determined by confocal laser scanning microscopy

Distribution of fat droplets (red) and proteins (green) in an emulsion under CLSM can be observed in **Figure 2**. Under consistent magnification, fat droplets were observed to be encapsulated by a protein-rich interface (green), forming a protective barrier essential for preventing coalescence and ensuring emulsion stability. While the fat globules exhibited spherical morphologies of varying sizes across all samples, their spatial distribution remained relatively uniform. The high protein density at the interface may provide robust stabilization against droplet aggregation. Additionally, the presence of some irregularly shaped globules in all emulsions may be attributed to pressure fluctuations during high-pressure homogenization. Inadequate pressure may lead to incomplete fragmentation of fat globules, whereas excessive pressure may result in irregularly shaped globules [Dhungana *et al*., 2020; Panchal *et al*., 2017].

With an increase in inulin content until reaching 12.1% of emulsion (*w/w*), the fat globule size continued to increase. However, the fat globule size observed in IN-14.7 was smaller than that of IN-12.1. As discussed in the particle size distribution

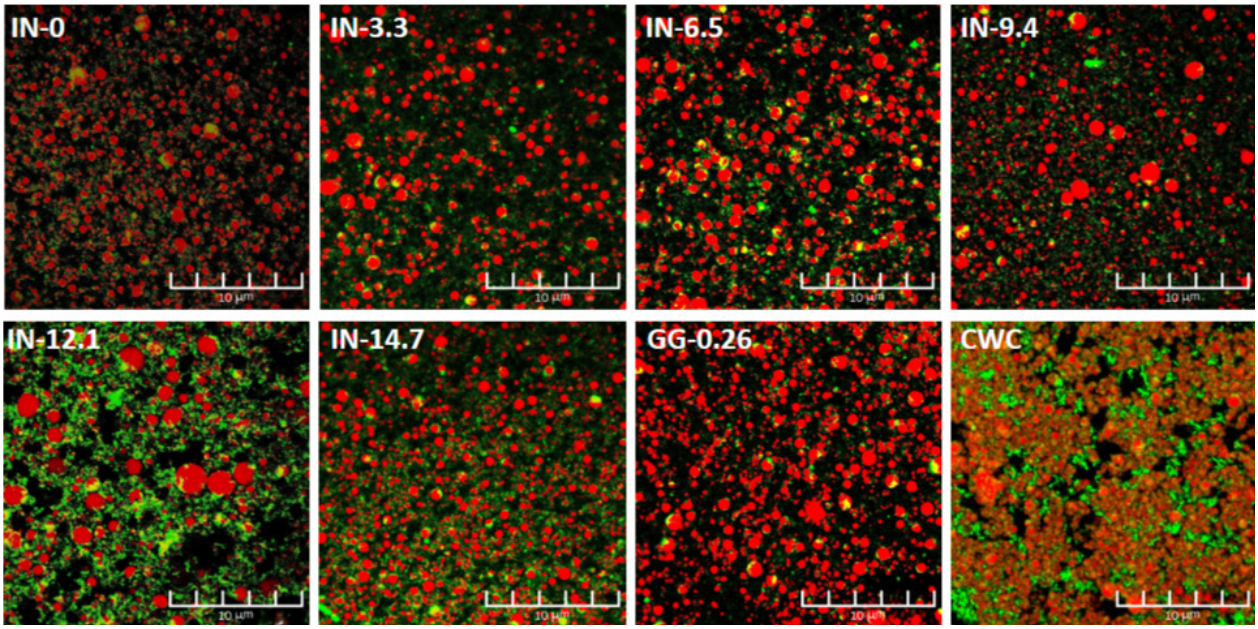

Figure 2. Confocal laser scanning microscopy (CLSM) images of duck fat-based cream emulsions formulated without inulin (IN-0), with inulin content ranging from 3.3% to 14.7%, *w/w*, (IN-3.3–IN-14.7), and with guar gum (GG-0.26), as well as commercial whipping cream (CWC). Fat and protein phases are stained in red and green, respectively, illustrating the microstructural organization of the emulsions. Scale bar is 10 μm.

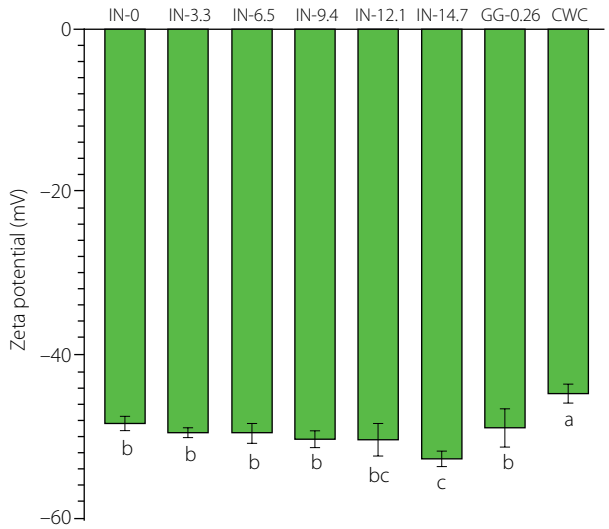

Figure 3. Zeta potential of duck fat-based cream emulsions formulated without inulin (IN-0), with inulin content ranging from 3.3% to 14.7%, *w/w*, (IN-3.3–IN-14.7), and with guar gum (GG-0.26), as well as a commercial whipped cream (CWC). Different lowercase letters (a–c) indicate significant differences among emulsions ($p<0.05$).

section, steric hindrance may have occurred in sample IN-14.7; therefore, the decrease in fat globule size could be attributed to this effect. Specifically, the reduction in fat globule size in sample IN-14.7 can be attributed to the enhanced steric repulsion provided by the inulin-rich continuous phase. At this concentration, inulin may form a dense network that effectively isolates fat droplets, preventing coalescence [Torres *et al*., 2010]. As a result, the IN-14.7 sample exhibited a homogeneous dispersion of discrete, spherical droplets with clear boundaries and no visible aggregates. This microstructure is characteristic of systems stabilized by a structured continuous phase [Franck, 2002]. In contrast, sample GG-0.26 exhibited relatively larger globules, which may reflect the strong water-binding and thickening properties of guar gum that modify droplet organization within the matrix.

Zeta potential

The zeta potential reflects the surface charge of the droplets and influences the electrostatic interactions contributing to emulsion stability [Cai *et al*., 2022]. As shown in **Figure 3**, all samples demonstrated strongly negative zeta potential ranging from −44 mV to −53 mV, with the absolute values generally increasing with an increasing inulin content in the duck fat-based emulsions. Sample IN-14.7 exhibited the highest absolute zeta potential, suggesting improved colloidal stability, which is consistent with the particle size results. Sample GG-0.26 showed a zeta potential of approximately −49 mV, which was statistically comparable to that of several inulin-containing samples, indicating that both hydrocolloids maintained a stable dispersed system under the tested conditions. However, as a neutral, non-ionic polysaccharide, inulin lacks a surface charge and is generally considered non-surface-active [Kim *et al*., 2001]. Therefore, the observed increase in the negative charge magnitude is likely an indirect effect rather than a result of inulin adsorption. It is hypothesized that inulin modulates the molecular environment and hydration of the sodium caseinate layer at the oil-water interface. This interaction may induce partial unfolding of the protein chains, exposing more negatively charged amino acid residues and thus increasing the measured surface potential [Nieto-Nieto *et al*., 2015; Xu *et al*., 2021]. Similarly, guar gum is also a non-surface-active polysaccharide, and its stabilizing effect is unlikely to arise primarily from direct interfacial charging.

The enhanced stability may be partly due to steric stabilization and aqueous-phase structuring. Inulin may provide stability through steric hindrance, where its hydrated polymer chains form a physical barrier that prevents fat globule proximity and coalescence [Clements, 2005]. This mechanical stabilization, combined with the microcrystalline gel network formed in the continuous phase, effectively preserves the structural integrity of the system irrespective of the direct interfacial charge.

Rheological properties

Rheological behavior of an emulsion is an important factor that determines product stability and final texture [Zhang *et al*., 2024; Zhao *et al*., 2009]. An optimal viscosity range is critical; excessive viscosity impedes air incorporation and fat globule movement during whipping, while low viscosity promotes bubble coalescence and reduces structural integrity under stress [Rezvani *et al*., 2020]. As shown in **Figure 4**, all emulsions exhibited shear-thinning behavior, where viscosity decreased with increasing shear rate. This characteristic is typical of structured fluids, where applied shear disrupts intermolecular interactions and aligns particles, thereby reducing flow resistance [Ningtyas *et al*., 2021]. The zero-shear viscosity (η_0), indicative of the emulsion's structure at rest, increased markedly with inulin content (**Figure 4**). A significant increase was observed from 10.9 Pa×s for IN-0 to 23.1 Pa×s for IN-12.1 at 0.1 s^{-1}, suggesting that inulin reinforced the emulsion network, enhancing its resistance to serum

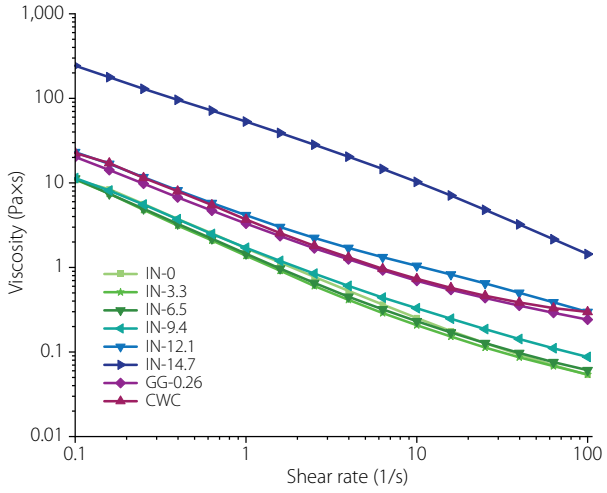

Figure 4. Viscosity as a function of shear rate for duck fat-based whipping emulsions formulated without inulin (IN-0), with inulin content ranging from 3.3% to 14.7%, *w/w*, (IN-3.3–IN-14.7), and with guar gum (GG-0.26), as well as a commercial whipping cream emulsion (CWC).

separation under quiescent conditions [Dabo *et al.*, 2024]. This trend aligns with reports of inulin's concentration-dependent thickening effect in protein-stabilized emulsions [López-Castejón *et al.*, 2019]. At intermediate inulin levels (3.3–9.4%, *w/w*), the increase in viscosity was less pronounced, suggesting that lower inulin levels had a limited impact on rheological behavior [Franck, 2002]. A substantial change occurred at 14.7% (*w/w*) inulin content (IN-14.7), where η_0 increased to 243.3 Pa×s. This sharp increase in viscosity may indicate the formation of a continuous gel-like network [Kim *et al.*, 2001]. The guar gum-stabilized sample displayed a viscosity profile between IN-9.4 and IN-12.1, confirming its efficacy as a thickener at low usage levels. Notably, the CWC sample exhibited a viscosity similar to IN-12.1, suggesting that moderate inulin levels may effectively replicate the rheological properties of commercial stabilizer blends.

Oscillatory strain sweep tests were performed to determine the linear viscoelastic region (LVR) of the emulsions. As shown in **Figures 5A** and **5B**, the storage modulus (G') remained higher than the loss modulus (G") across the tested strain range for all samples, indicating predominantly elastic (solid-like) behavior. Both G' and G" increased with an increasing inulin content, suggesting enhanced structural integrity and viscoelastic properties of the emulsions. This trend supports the role of inulin in reinforcing the emulsion network and increasing resistance to deformation under oscillatory stress, which is consistent with previous reports describing the thickening effect of inulin on viscoelastic moduli [López-Castejón *et al.*, 2019]. Sample IN-14.7 exhibited the highest G' value, indicating the formation of a highly rigid network, which is consistent with the gelation behavior of inulin at elevated concentrations [Kim *et al.*, 2001]. In contrast, samples IN-0, IN-3.3, and IN-6.5 exhibited low critical strain values, indicating weak structures that may break down under minimal deformation. On the other hand, samples IN-9.4, IN-12.1, GG-0.26, and CWC showed a significantly wider LVR, withstanding strains above 10–20% before yielding. This indicates the presence of cohesive and deformation-tolerant networks capable of maintaining structural integrity under greater strain. The rheological behavior of GG-0.26 and CWC showed similar trends to that of IN-12.1, suggesting that a moderate level of inulin can provide favorable viscoelastic properties within the range observed for the guar gum reference and the commercial whipped cream sample. However, this comparison is limited to the rheological parameters evaluated in the present study and does not imply full equivalence in overall product performance or composition.

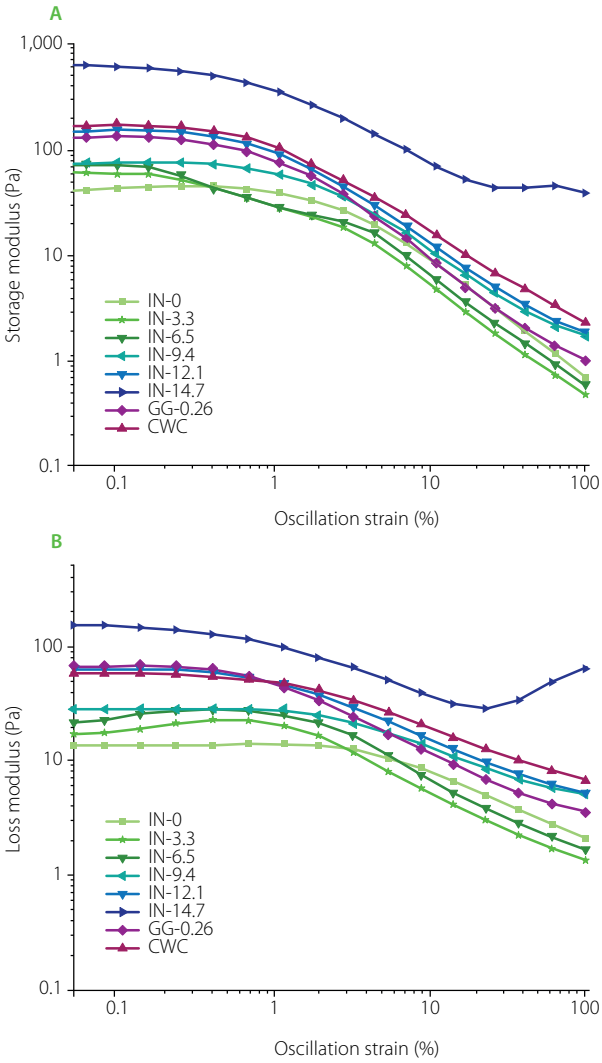

Figure 5. (**A**) Storage modulus (G') and (**B**) loss modulus (G") as a function of strain for duck fat-based cream emulsions formulated without inulin (IN-0), with inulin content ranging from 3.3% to 14.7%, *w/w*, (IN-3.3–IN-14.7), and with guar gum (GG-0.26), as well as commercial whipping cream sample (CWC).

Whipped cream properties

Whipping time and overrun

Whipping time plays a significant role in determining the partial coalescence of whipped cream [Nguyen *et al.*, 2015]. A clear concentration-dependent increase in whipping time was observed, as shown in **Table 1**. Increasing inulin content from 0% to 14.7% (*w/w*) lengthened the time required to achieve stiff peaks from 106 s to 316 s. This trend can be attributed to inulin-induced rheological modifications, as discussed in the rheological properties section. The higher viscosities observed in inulin-added samples prevent the partial coalescence of fat globules and thus increase the whipping time [Wang *et al.*, 2023]. Sample GG-0.26 showed similar effects by increasing viscosity and delaying coalescence, but primarily through phase thickening rather than network formation. The continuous increase in viscosity and stronger gel network with increasing inulin content physically resists air incorporation during whipping. In addition, a more viscous and structured continuous phase can slow whisk movement, restrict droplet interactions, and hinder liquid drainage from lamellae surrounding air bubbles, all of which may contribute to longer whipping times [Liu *et al.*, 2024; Rezvani *et al.*, 2020].

Overrun is a key indicator of whipping performance, reflecting the extent of air incorporation and the resulting increase in volume [Liu *et al.*, 2024]. In this study, overrun was significantly influenced by inulin content, showing a clear inverse

Table 1. Optimum whipping time, overrun, and serum loss for duck fat-based whipped cream samples formulated without inulin (IN-0), with inulin content ranging from 3.3% to 14.7%, *w/w*, (IN-3.3–IN-14.7), and with guar gum (GG-0.26), as well as a commercial whipped cream (CWC).

Whipped cream	Optimum whipping time (s)	Overrun (%)	Serum loss (%)
IN-0	106 ± 3^{f}	330 ± 6^{a}	6.92 ± 0.44^{b}
IN-3.3	116 ± 3^{e}	320 ± 3^{b}	6.26 ± 0.15^{bc}
IN-6.5	118 ± 7^{de}	311 ± 5^{c}	5.84 ± 0.95^{cd}
IN-9.4	125 ± 8^{d}	274 ± 5^{d}	5.19 ± 0.57^{de}
IN-12.1	220 ± 5^{b}	214 ± 4^{e}	0 ± 00^{f}
IN-14.7	316 ± 3^{a}	169 ± 5^{f}	0 ± 00^{f}
GG-0.26	215 ± 5^{b}	209 ± 6^{e}	4.53 ± 0.75^{e}
CWC	182 ± 2^{c}	211 ± 5^{e}	12.43 ± 0.85^{a}

Values are expressed as mean ± standard deviation. Different letters in the same column indicate significant differences among whipped cream samples ($p<0.05$).

relationship. As inulin content increased from 0% to 14.7% (*w/w*), overrun decreased significantly from 330% to 169% (**Table 1**). At lower contents (0–6.5%, *w/w*), inulin had a minimal impact on overrun; however, at higher contents (9.4–14.7%, *w/w*), it significantly reduced the overrun. This can be attributed to the formation of a highly viscous network at a higher inulin content, which restricts air incorporation. In samples IN-12.1 and IN-14.7, the strengthened network limited air entrapment during whipping. Additionally, inulin at higher levels may compete with surface-active components at the fat droplet interface, reducing interfacial stabilization and promoting coalescence, thereby hindering air incorporation [Liu *et al*., 2024]. Interestingly, sample IN-12.1 exhibited overrun values statistically comparable to GG-0.26 and commercial whipped cream, indicating an optimal balance between structure formation and air incorporation. This suggests that both inulin (at optimal content) and guar gum can enhance structural stability without excessively compromising air incorporation, although their mechanisms differ. Guar gum primarily increases viscosity through hydrocolloid thickening, whereas inulin contributes to network formation and fat structuring. At the 12.1% (*w/w*) inulin level, the network provided sufficient rigidity to stabilize air cells without excessively limiting their formation, as also supported by rheological and microstructural observations. In contrast, sample IN-14.7 presented an over-stabilized system, characterized by prolonged whipping time and reduced overrun.

The whipping properties of duck fat-based cream were negatively impacted by the higher inulin levels, resulting in extended whipping time and decreased overrun. This inverse correlation is consistent with the findings of Camacho *et al*. [1998], who showed that the addition of hydrocolloids to whipped cream increased the cream's elastic properties during whipping, which resulted in lesser air incorporation, longer whipping time, and reduced overrun [Camacho *et al*., 2001]. It should be noted that when no inulin was added or when the added level was low, although the foaming rate during whipping was high and the whipping time was short, the bubbles in the system were large, uneven, and had defects such as easy collapse.

Serum loss

Foam stability depends on the physical and rheological properties of the interface and the continuous phase. Factors such as air bubble size distribution, interface thickness, surface tension, and interface permeability all have an obvious impact on foam stability [Kováčová *et al*., 2010], which can be additionally determined by the level of serum loss. A lower level of serum loss indicates high foam stability [Liu *et al*., 2024]. An increase in inulin content significantly reduced the serum loss after 3 h of storage at 22°C, as demonstrated in **Table 1**. Samples with inulin contents up to 9.4%, *w/w*, (IN-0 to IN-9.4) showed considerable serum loss, ranging from 6.92% to 5.19%. This could be attributed to the lower viscosities of these samples which allow a large number of air bubbles to be incorporated during whipping, resulting in sample instability [Ma *et al*., 2025]. At higher inulin contents (IN-12.1 and IN-14.7), excellent stabilization was achieved, as these samples exhibited complete stability with no measurable serum loss (0.00%) under the tested conditions. This improvement may be associated with the formation of a stronger continuous network with enhanced water-immobilization capacity. The higher viscosities observed for samples IN-12.1 and IN-14.7, together with the solid-like behavior (G'>G''), confirm the formation of a gel structure characterized by high water-holding capacity [Kim *et al*., 2001; Shoaib *et al*., 2016]. The inulin gel forms a physical barrier that immobilizes the aqueous phase, consequently inhibiting drainage and syneresis under the influence of gravity [Bot *et al*., 2004; Desu et *al*., 2025]. When compared with control samples GG-0.26 and CWC, IN-12.1 and IN-14.7 exhibited better foam stability. The serum loss observed in GG-0.26 and CWC was 4.53% and 12.43%, respectively, whereas samples IN-12.1 and IN-14.7 showed no serum loss under the same tested conditions. This highlights the efficiency of inulin as a stabilizer in duck fat-based whipped cream system. These findings enable concluding that inulin, like other polysaccharides, stabilizes the three-phase system, which is consistent with other polysaccharide applications in whipped cream [Farahmandfar *et al*., 2017; Kováčová *et al*., 2010]. The use of polysaccharides as stabilizers in whipped creams enhances the viscosity of the continuous phase and forms a network structure. This network ensures foam stability by reducing bubble coalescence and disproportionation, thereby reinforcing the interfacial walls and preventing serum drainage.

Microstructure of whipped cream by optical microscope

The stability of whipped cream is strongly influenced by the size and distribution of air bubbles [Liu *et al*., 2022]. Microstructure analysis using an optical microscope revealed that increasing the inulin content resulted in a more uniform distribution of air

bubbles (**Figure 6**). The negative control sample (IN-0) showed the largest foam size and the loosest bubble distribution. Sample GG-0.26 showed a heterogeneous bubble-size distribution, containing both large and small air bubbles. Similarly, the whipped cream samples IN-3.3, IN-6.5, and IN-9.4 exhibited larger and unevenly distributed air bubbles, indicating the formation of a weak interfacial film and insufficient stabilization of the incorporated air. Larger bubbles generate higher internal pressure, making them more prone to coalescence, which may explain the greater serum loss observed in these samples. With an increase in inulin content, a corresponding decrease in bubble size was observed, accompanied by a more uniform distribution of air bubbles. It is worth noting that samples IN-12.1 and IN-14.7 showed the smallest bubble sizes, with a close and even distribution. Small bubble size has been associated with improved long-term foam stability in hydrophilic colloid systems [Zhan *et al*., 2020]. At higher inulin contents, the formation of a continuous and flexible inulin network within the aqueous phase likely increased viscosity, thereby providing a structural framework that stabilized air bubbles and reduced coalescence and drainage. Overall, the microstructure analysis suggests that an adequate inulin level (≥12.1%, *w/w*) is required to produce a fine and uniform air-cell structure.

Confocal laser scanning microscopy images of whipped cream

As shown in **Figure 7**, the negative control sample (IN-0) exhibited irregular air bubbles stabilized by a protein layer at the interface, with several fat globules forming clumps. This underdeveloped structure accounts for its poor stability. While intermediate inulin contents (IN-3.3, IN-6.5, and IN-9.4) exhibited a gradual structural transition (images not shown), the IN-12.1 sample was selected as the representative stabilized model, as it showed the most distinct shift toward uniform, spherical air bubbles. This phenomenon could be attributed to the enhanced structuring effects of inulin within the continuous phase. Notably, sample IN-12.1 exhibited a prominent interfacial film stabilized by sodium caseinate alongside a three-dimensional network of inulin aggregates within the continuous phase. These structural features suggest that IN-12.1 possesses superior mechanical strength and enhanced foam stability, as corroborated by its rheological properties and favorable decoration performance. Furthermore, un-adsorbed proteins observed in the continuous phase may aggregate, further strengthening the network structure [Xu *et al*., 2021]. In contrast, the guar gum reference sample did not exhibit the same degree of integrated interfacial and continuous-phase structuring under the observed conditions.

Decoration appearance and cross section

The ability of whipped cream to maintain its decorative shape over time is a critical quality attribute for applications in cakes and pastries. As illustrated in **Figure 8**, sample IN-0 exhibited the poorest shaping ability, indicating that the internal network structure was inadequate to withstand gravitational stress. The shaping performance of samples IN-3.3, IN-6.5, and IN-9.4 improved progressively. Although only slight differences were observed in viscosity among these samples, a clear improvement in shape retention from IN-0 to IN-9.4 was evident, suggesting that inulin contributed to a more cohesive structure even at relatively low levels. The shaping ability was enhanced, and the structural definition improved as the inulin content increased from 0 to 14.7% (*w/w*). The enhanced shaping feature can be attributed to the ability of inulin to form a three-dimensional gel network, which provides the structural support and textural stability to whipped cream [Kim *et al*., 2001]. Samples IN-12.1 and IN-14.7 had sharp edges that were well-defined and remained in a rosette-like structure immediately upon piping, and retained their structural integrity without any slumping or serum loss after 3 h at 22°C. These observations are consistent with the results of rheological and microstructural analyses, which indicated increased continuous-phase structuring at higher inulin contents, contributing to a self-supporting matrix. Samples IN-6.5 to IN-14.7

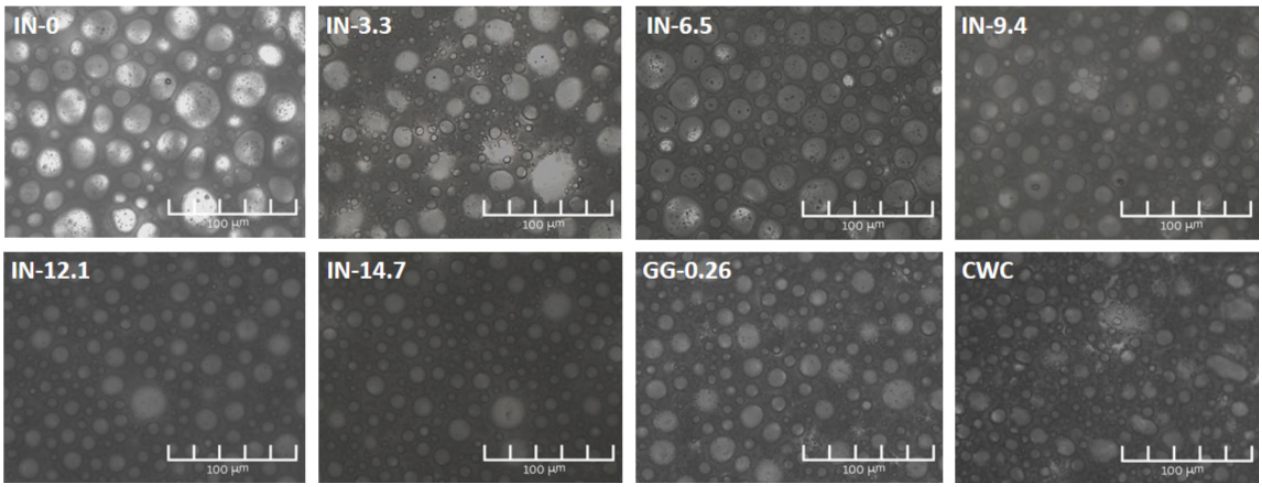

Figure 6. Optical microscopy images (40× magnification) of duck fat-based whipped cream samples prepared without inulin (IN-0), with inulin content ranging from 3.3% to 14.7%, *w/w*, (IN-3.3–IN-14.7), and with guar gum (GG-0.26), as well as a commercial whipped cream (CWC), showing the distribution and size of air bubbles within the foam structure. The scale bar is 100 µm.

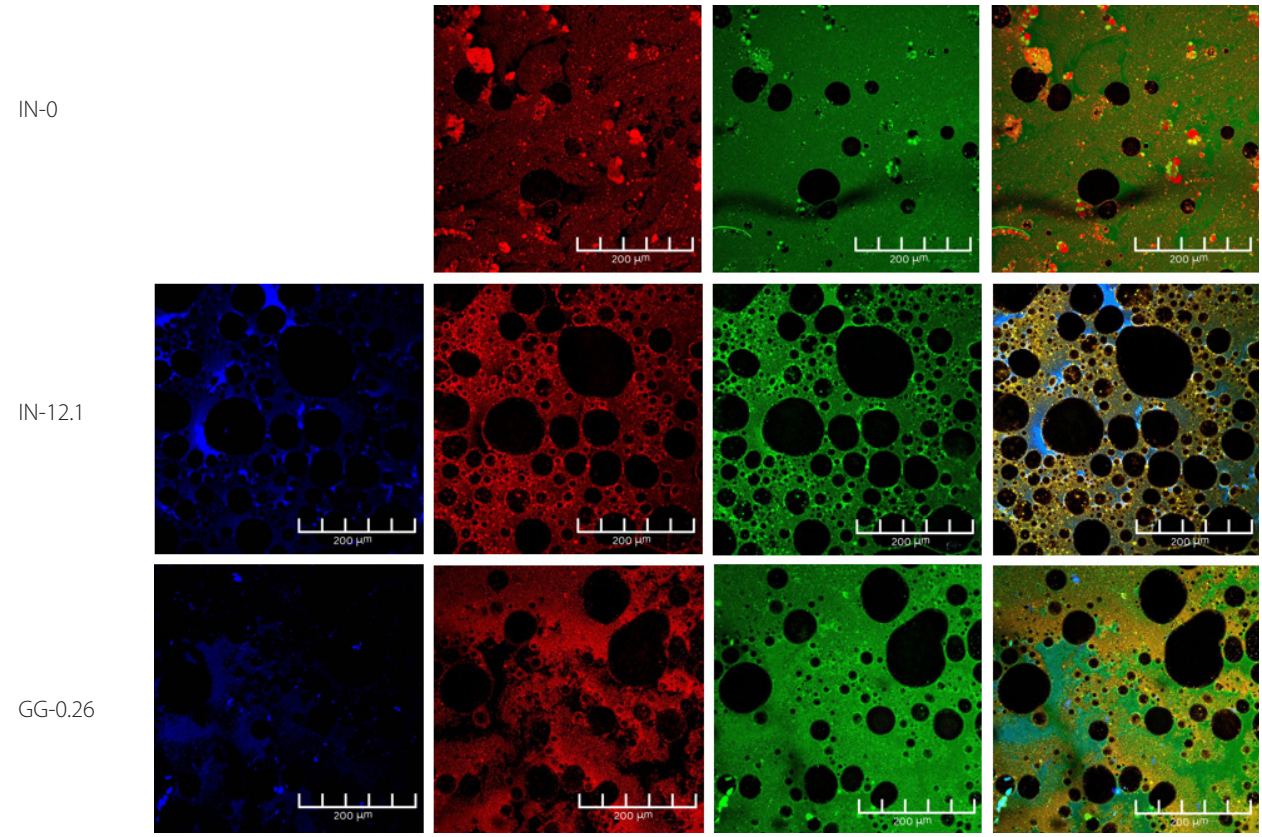

Figure 7. Confocal laser scanning microscopy (CLSM) images of duck fat-based whipped cream sample without inulin (IN-0), with inulin content of 12.1%, *w/w*, (IN-12), and with guar gum (GG-0.26). Fat, protein, and polysaccharides are labeled in red, green, and blue, respectively. Scale bar is 200 µm.

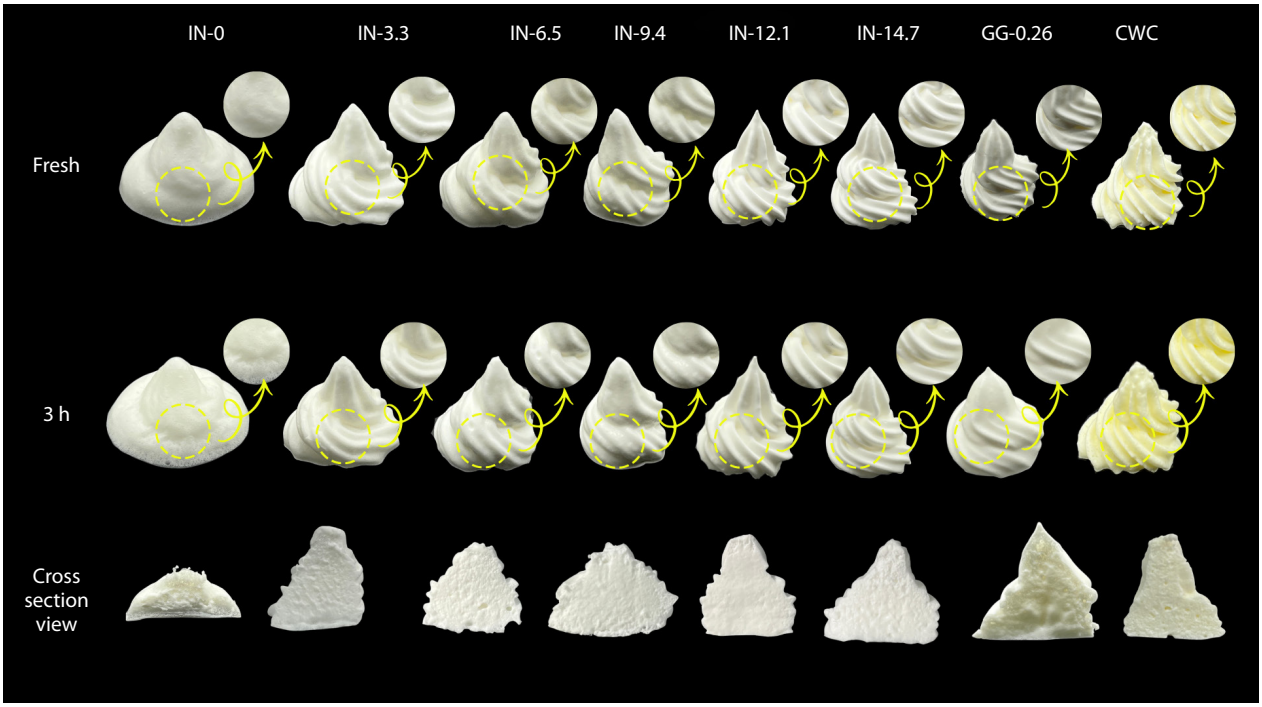

Figure 8. Decorative appearance of duck fat-based whipped cream samples prepared without inulin (IN-0), with inulin content ranging from 3.3% to 14.7%, *w/w*, (IN-3.3–IN-14.7), and with guar gum (GG-0.26), as well as commercial whipped cream (CWC), evaluated immediately after whipping (fresh) and after 3 h of storage at 22°C. Cross-sectional images illustrate structural integrity and internal texture as influenced by stabilizer type and inulin content.

showed no collapse after 3 h at 22°C. A higher inulin content likely increased viscosity and strengthened the network, improving foam stability and resistance to collapse [Farahmandfar *et al*., 2017]. Although the guar gum reference sample and commercial whipped cream initially formed rosettes with well-defined spikes, both exhibited noticeable structural deterioration after 3 h. The GG-0.26 sample lost much of its spike definition, whereas the CWC sample showed pronounced slumping and a visible reduction in height.

As shown in **Figure 8**, the cross-sectional analysis of the whipped cream samples further supports the role of inulin as a potential stabilizing and structuring ingredient. Sample IN-0 exhibited a rough, irregular surface, indicating the formation of weak internal networks and large, unstable air cells. In contrast, an increase in inulin content from 0% to 14.7% (*w/w*) resulted in a uniform, smooth, and delicate cross-sectional view, which was even better than that of the control samples (GG-0.26 and CWC). The appearance of the cross-section can indicate the stability of whipped cream, with smoother and more uniform surfaces often correlating with greater structural integrity [Li *et al*., 2023; Zeng *et al*., 2022b].

Sensory evaluation

Sensory scores were significantly ($p<0.05$) affected by inulin content in the duck fat-based whipped cream (**Table 2**). All evaluated attributes, including flavor and taste, texture, smoothness, and greasiness, improved progressively as the inulin level increased from 0% to 14.7% (*w/w*). Sample IN-0 received the lowest scores across all attributes, consistent with its weak rheological structure, poor foam stability, and coarse microstructure. These properties likely resulted in a rough mouthfeel and lower overall acceptability. Samples containing moderate to high inulin levels (IN-9.4 to IN-14.7) showed significantly higher scores, particularly for texture and smoothness. This trend was consistent with increased viscosity, stronger viscoelastic behavior, reduced serum loss, and finer air-bubble distribution, indicating that improved structural stability enhanced sensory perception. Among the experimental samples, IN-12.1 and IN-14.7 achieved the highest sensory ratings, with no significant differences between them ($p\geq0.05$). Their superior performance was likely associated with the formation of a stronger inulin-stabilized network, which provided a creamier texture, smoother mouthfeel, and lower greasy sensation. The guar gum sample (GG-0.26) showed intermediate scores, lower than IN-12.1 and IN-14.7, suggesting that inulin was more effective than guar gum in enhancing sensory quality under the tested conditions. Although the commercial whipped cream (CWC) obtained the highest scores overall, the addition of 12.1–14.7% (*w/w*) inulin significantly improved the sensory quality of the duck-fat-based whipped cream relative to the lower-inulin formulations. Overall, the sensory assessment results were consistent with the instrumental findings, confirming that improvements in rheological and microstructural properties contributed to enhanced product acceptability. It should be noted that the experimental samples were formulated without added flavoring agents. Future research should investigate appropriate flavor optimization strategies to further enhance sensory acceptability.

CONCLUSIONS

This study demonstrates that natural inulin can effectively serve as a structuring stabilizer in duck-fat-based whipped cream, enabling the development of a functional product with quality characteristics approaching those of commercial cream. The whipping performance, rheology, decoration appearance, shape retention ability, microstructure, and sensory qualities of whipped cream were systematically evaluated. As the inulin content increased, more non-adsorbed inulin was present in the liquid phase of the whipped foams, which aggregated and cross-linked,

Table 2. Sensory evaluation scores of duck fat-based whipped cream samples prepared without inulin (IN-0), with inulin content ranging from 3.3% to 14.7%, *w/w*, (IN-3.3–IN-14.7), and with guar gum (GG-0.26), as well as commercial whipping cream sample (CWC).

Whipped cream	Flavor and taste	Texture	Smoothness	Greasiness
IN-0	2.10 ± 0.36^{f}	3.50 ± 0.50^{f}	2.50 ± 0.50^{f}	3.80 ± 0.36^{f}
IN-3.3	4.46 ± 0.55^{e}	4.10 ± 0.36^{e}	4.00 ± 0.50^{e}	4.53 ± 0.30^{e}
IN-6.5	5.63 ± 0.32^{d}	5.36 ± 0.61^{d}	5.36 ± 0.40^{d}	5.20 ± 0.30^{d}
IN-9.4	6.53 ± 0.47^{c}	7.00 ± 0.20^{c}	7.20 ± 0.43^{c}	5.86 ± 0.20^{c}
IN-12.1	7.56 ± 0.30^{b}	8.20 ± 0.26^{b}	8.23 ± 0.15^{b}	7.46 ± 0.15^{b}
IN-14.7	8.16 ± 0.30^{b}	8.73 ± 0.37^{b}	8.33 ± 0.30^{b}	7.50 ± 0.40^{b}
GG-0.26	5.53 ± 0.45^{d}	5.50 ± 0.45^{d}	5.46 ± 0.40^{d}	5.80 ± 0.20^{c}
CWC	9.43 ± 0.40^{a}	9.76 ± 0.25^{a}	9.90 ± 0.17^{a}	9.53 ± 0.25^{a}

Values are expressed as mean ± standard deviation. Different letters in the same column indicate significant differences among whipped cream samples ($p<0.05$).

resulting in enhanced rigidity of the continuous phase. As a result, the cross-section's smoothness and the whipped cream's shaping ability improved. Higher inulin contents (≥12.1%, *w/w*) resulted in a more rigid structure, increased viscosity, longer whipping times, and reduced overrun. These changes contributed to greater foam stability, as shown by samples IN-12.1 and IN-14.7. Samples with high inulin levels (≥12.1%, *w/w*) exhibited more favourable sensory qualities than those with lower levels. Overall, this paper highlights the importance of inulin as a potential stabilizer in duck-fat whipped cream. The addition of inulin to whipped cream not only improved texture and stability but may also provide added functional value through its recognized prebiotic benefits.

RESEARCH FUNDING

This research was financially supported by the National Natural Science Foundation of China (31772094), the Special Project of key Research and Promotion of Henan Province of China (222102110033), the Natural Science Foundation of Henan Province – China (162300410076), and the Doctoral Scientific Research Start–up Foundation of Henan University of Science and Technology – China (13480057).

CONFLICT OF INTERESTS

The authors declare that they have no known competing financial interests or personal relationships that could have appeared to influence the work reported in this paper.

ORCID IDs

M.U. Amjad https://orcid.org/0009-0008-5724-7609
B. Xu https://orcid.org/0000-0001-6394-8235

REFERENCES

1. Ai, C. (2023). Recent advances on the emulsifying properties of dietary polysaccharides. *eFood*, *4*(4), art. no. e106. https://doi.org/10.1002/efd2.106
2. Athari, B., Nasirpour, A., Saeidy, S., Esehaghbeygi, A. (2021). Physicochemical properties of whipped cream stabilized with electrohydrodynamic (EHD) modified cellulose. *Journal of Food Processing and Preservation*, *45*, art. no. e15688. https://doi.org/10.1111/jfpp.15688
3. Bot, A., Erle, U., Vreeker, R., Agterof, W. (2004). Influence of crystallisation conditions on the large deformation rheology of inulin gels. *Food Hydrocolloids*, *18*(4), 547-556. https://doi.org/10.1016/j.foodhyd.2003.09.003
4. Cai, Y., Zeng, D., Huang, L., Zhao, M., Zhao, Q., Van der Meeren, P. (2022). Emulsifying and whipping properties of mixing polysaccharide dispersions: effect of ratio between insoluble soybean fiber and hydroxypropyl methylcellulose. *Journal of the Science of Food and Agriculture*, *102*(14), 6707-6717. https://doi.org/10.1002/jsfa.12038
5. Camacho, M.M., Martınez-Navarrete, N., Chiralt, A. (1998). Influence of locust bean gum/λ-carrageenan mixtures on whipping and mechanical properties and stability of dairy creams. *Food Research International*, *31*(9), 653-658. https://doi.org/10.1016/S0963-9969(99)00041-1
6. Camacho, M., Martınez-Navarrete, N., Chiralt, A. (2001). Stability of whipped dairy creams containing locust bean gum/λ-carrageenan mixtures during freezing–thawing processes. *Food Research International*, *34*(10), 887-894. https://doi.org/10.1016/S0963-9969(01)00113-2
7. Chen, W., Deng, Z., Shen, Q., Ye, S., An, D., Li, J., Li, B., Liang, H. (2025). Fabrication and characterization of a novel non-dairy whipping cream formed by only gliadin colloidal particles and shea butter. *Food Hydrocolloids*, *163*, art. no. 111091. https://doi.org/10.1016/j.foodhyd.2025.111091
8. Clements, D. (2005). Colloidal interactions. In D. Clements (Ed.), *Food Emulsions: Principles, Practices and Techniques* (2nd edition), CRC Press, Boca Raton, USA, pp. 53-93. https://doi.org/10.1201/9781420039436
9. Cui, G., Liu, Q., Li, F., Pang, X., Xie, N., Geng, X., Li, H., Wang, Y., Lv, J., Zhang, S. (2025). Exploring the role of milk fat structure and crystallization in enhancing whipped cream properties and stability. *LWT – Food Science and Technology*, *228*, art. no. 118054. https://doi.org/10.1016/j.lwt.2025.118054
10. Dabo, K.F., Chèné, C., Fame, A.L., Karoui, R. (2024). Whipping creams: Advances in molecular composition and nutritional chemistry. *Molecules*, *29*(24), art. no. 5933. https://doi.org/10.3390/molecules29245933
11. Desu, B.S.R., Biradar, R.M., Vijaykanth, M.S., Sethi, P., Krishnan, K., Prema, S., Kallur, H.J., Senthamaraikannan, A. (2025). Inulin as stabilizer. In W. Akram, N. Mishra, T. Haider (Eds.), *Inulin for Pharmaceutical Applications: A Versatile Biopolymer*, Springer Nature Singapore, pp. 73-90. https://doi.org/10.1007/978-981-97-9056-2_4
12. Dhungana, P., Truong, T., Bansal, N., Bhandari, B. (2020). Effect of fat globule size and addition of surfactants on whippability of native and homogenised dairy creams. *International Dairy Journal*, *105*, art. no. 104671. https://doi.org/10.1016/j.idairyj.2020.104671
13. Dickinson, E. (2003). Hydrocolloids at interface and the influence on the properties of dispersed systems. *Food Hydrocolloids*, *17*(1), 25-39. https://doi.org/10.1016/S0268-005X(01)00120-5
14. Farahmandfar, R., Asnaashari, M., Salahi, M.R., Khosravi Rad, T. (2017). Effects of basil seed gum, Cress seed gum and Quince seed gum on the physical, textural and rheological properties of whipped cream. *International Journal of Biological Macromolecules*, *98*, 820-828. https://doi.org/10.1016/j.ijbiomac.2017.02.046
15. Franck, A. (2002). Technological functionality of inulin and oligofructose. *British Journal of Nutrition*, *87*(S2), S287-S291. https://doi.org/10.1079/BJN/2002550
16. Fredrick, E., Heyman, B., Moens, K., Fischer, S., Verwijlen, T., Moldenaers, P., Van der Meeren, P., Dewettinck, K. (2013). Monoacylglycerols in dairy recombined cream: II. The effect on partial coalescence and whipping properties. *Food Research International*, *51*(2), 936-945. https://doi.org/10.1016/j.foodres.2013.02.006
17. Goff, H.D. (1997). Instability and partial coalescence in whippable dairy emulsions. *Journal of Dairy Science*, *80*(10), 2620-2630. https://doi.org/10.3168/jds.S0022-0302(97)76219-2
18. Günç Ergönül, P., Ergönül, B. (2023). How healthy are commercial cream and butter-creams? Assessment according to their fatty acid composition, cholesterol contents, atherogenic and thrombogenic indices. *Novel Techniques in Nutrition & Food Science*, *6*(5), art. no. 648. https://doi.org/10.31031/NTNF.2023.06.000648
19. Kim, Y., Faqih, M.N., Wang, S.S. (2001). Factors affecting gel formation of inulin. *Carbohydrate Polymers*, *46*(2), 135-145. https://doi.org/10.1016/S0144-8617(00)00296-4
20. Kováčová, R., Štětina, J., Curda, L. (2010). Influence of processing and κ-carrageenan on properties of whipping cream. *Journal of Food Engineering*, *99*(4), 471-478. https://doi.org/10.1016/j.jfoodeng.2010.02.010
21. Li, Y., Liao, T., Liu, T., Yan, R., Sun, Z., Zhao, M., Deng, X. Zhao, Q. (2023). The quality of whipped cream: Effect of polyglycerol ester on the crystallization of fat blend and the properties of interface. *Food Hydrocolloids*, *145*, art. no. 109145. https://doi.org/10.1016/j.foodhyd.2023.109145
22. Li, Y., Wang, J., Ying, R., Huang, M., Hayat, K. (2024). Protein-stabilized Pickering emulsion interacting with inulin, xanthan gum and chitosan: Rheological behavior and 3D printing. *Carbohydrate Polymers*, *326*, art. no. 121658. https://doi.org/10.1016/j.carbpol.2023.121658
23. Liu, J., Luo, D., Li, X., Xu, B., Zhang, X., Liu, J. (2016). Effects of inulin on the structure and emulsifying properties of protein components in dough. *Food Chemistry*, *210*, 235-241. https://doi.org/10.1016/j.foodchem.2016.04.001
24. Liu, R., Wang, X., Goff, H., Cui, S. (2024). Application of yellow mustard gum-fenugreek mixed gum in preparation of non-dairy fat whipping cream. *International Journal of Food Science & Technology*, *59*(12), 8998-9008. https://doi.org/10.1111/ijfs.17375
25. Liu, Z., Cao, Z., Zhao, M., Zhang, H., Wang, J., Sun, B. (2022). Synergistic influence of protein particles and low-molecular-weight emulsifiers on the stability

of a milk fat-based whippable oil-in-water emulsion. *Food Hydrocolloids*, *127*, art. no. 107520.
https://doi.org/10.1016/j.foodhyd.2022.107520

26. López-Castejón, M., Bengoechea, C., Espinosa, S., Carrera, C. (2019). Characterization of prebiotic emulsions stabilized by inulin and β-lactoglobulin. *Food Hydrocolloids*, *87*, 382-393 .
https://doi.org/10.1016/j.foodhyd.2018.08.024
27. Ma, Q., Sun, Y., Wang, L., Lyu, E., Li, J., Zhao, D., Amjad, U., Xu, B., Dou, X., Liu, L. (2025). Strategic design of interesterified lipid phases: Developing an α-linolenic enriched whipping cream using perilla-palm stearin composite fat. *Innovative Food Science & Emerging Technologies*, *106*, art. no. 104275.
https://doi.org/10.1016/j.ifset.2025.104275
28. Motamedzadegan, A., Dehghan, B., Nemati, A., Tirgarian, B., Safarpour, B. (2020). Functionality improvement of virgin coconut oil through physical blending and chemical interesterification. *SN Applied Sciences*, *2*, art. no. 1513.
https://doi.org/10.1007/s42452-020-03309-6
29. Nesaretnam, K., Robertson, N., Basiron, Y., Macphie, C.S. (1993). Application of hydrogenated palm kernel oil and palm stearin in whipping cream. *Journal of the Science of Food and Agriculture*, *61*(4), 401-407.
https://doi.org/10.1002/jsfa.2740610405
30. Nguyen, V., Duong, C., Vu, V. (2015). Effect of thermal treatment on physical properties and stability of whipping and whipped cream. *Journal of Food Engineering*, *163*, 32-36.
https://doi.org/10.1016/j.jfoodeng.2015.04.026
31. Nieto-Nieto, T., Wang, Y., Ozimek, L., Chen, L. (2015). Inulin at low concentrations significantly improves the gelling properties of oat protein – A molecular mechanism study. *Food Hydrocolloids*, *50*, 116-127.
https://doi.org/10.1016/j.foodhyd.2015.03.031
32. Ningtyas, D., Bhandari, B., Prakash, S. (2021). Modulation fat globules of the plant-based cream emulsion: Influence of the source of plant proteins. *Innovative Food Science & Emerging Technologies*, *74*, art. no. 102852.
https://doi.org/10.1016/j.ifset.2021.102852
33. Panchal, B.R., Truong, T., Prakash, S., Bansal, N., Bhandari, B. (2017). Effect of fat globule size on the churnability of dairy cream. *Food Research International*, *99*(Part 1), 229-238.
https://doi.org/10.1016/j.foodres.2017.05.027
34. Rezvani, F., Abbasi, H., Nourani, M. (2020). Effects of protein–polysaccharide interactions on the physical and textural characteristics of low-fat whipped cream. *Journal of Food Processing and Preservation*, *44*(10), art. no. 14743.
https://doi.org/10.1111/jfpp.14743
35. Rybak, O. (2016). Milk fat in structure formation of dairy products: a review. *Ukrainian Food Journal*, *5*(3), 499-514.
https://doi.org/10.24263/2304-974X-2016-5-3-9
36. Shoaib, M., Shehzad, A., Omar, M., Rakha, A., Raza, H., Sharif, H.R., Shakeel, A., Ansari, A., Niazi, S. (2016). Inulin: Properties, health benefits and food applications. *Carbohydrate Polymers*, *147*, 444-454.
https://doi.org/10.1016/j.carbpol.2016.04.020
37. Sinsuwan, S. (2024). Effect of inulin on rheological properties and emulsion stability of a reduced-fat salad dressing. *International Journal of Food Science*, *2024*, art. no. 4229514.
https://doi.org/10.1155/2024/4229514
38. Torres, J.D., Tárrega, A., Costell, E. (2010). Storage stability of starch-based dairy desserts containing long-chain inulin: Rheology and particle size distribution. *International Dairy Journal*, *20*(1), 46-52.
https://doi.org/10.1016/j.idairyj.2009.08.001
39. Turner, D., Dlugogorski, B., Palmer, T. (1999). Factors affecting the stability of foamed concentrated emulsions. *Colloids and Surfaces A: Physicochemical and Engineering Aspects*, *150*(1-3), 171-184.
https://doi.org/10.1016/S0927-7757(98)00814-0
40. Wang, J., Liu, Z., Zheng, Y., Hong, Q., Wang, Q., Xu, X. (2023). Synergistic effects of microcrystalline cellulose and xanthan gum on the stability of milk fat-based UHT whipping cream. *LWT – Food Science and Technology*, *184*, art. no. 114966.
https://doi.org/10.1016/j.lwt.2023.114966
41. Wu, C., Liu, Z., Zhi, L., Jiao, B., Hu, H., Ma, X., Zhu, J., Pignitter, M., Wang, Q., Shi, A. (2023). Effect of oil content and protein particles concentration on non-dairy whip topping based on Pickering emulsion system and their 3D printing properties. *Food Hydrocolloids*, *144*, art. no. 109012.
https://doi.org/10.1016/j.foodhyd.2023.109012
42. Xu, Q., Qi, B., Han, L., Wang, D., Zhang, S., Jiang, L., Xie, F., Li, Y. (2021). Study on the gel properties, interactions, and pH stability of pea protein isolate emulsion gels as influenced by inulin. *LWT – Food Science and Technology*, *137*, art. no. 110421.
https://doi.org/10.1016/j.lwt.2020.110421
43. Zeng, D., Cai, Y., Liu, T., Huang, L., Zeng, Y., Zhao, Q., Zhao, M. (2022a). The effect of sucrose esters S1570 on partial coalescence and whipping properties. *Food Hydrocolloids*, *125*, 107429.
https://doi.org/10.1016/j.foodhyd.2021.107429
44. Zeng, Y., Zeng, D., Liu, T., Cai, Y., Li, Y., Zhao, M., Zhao, Q. (2022b). Effects of glucose and corn syrup on the physical characteristics and whipping properties of vegetable-fat based whipped creams. *Foods*, *11*(9), art. no. 1195.
https://doi.org/10.3390/foods11091195
45. Zhan, F., Chen, Y., Hu, J., Youssef, M., Korin, A., Li, J., Li, B. (2020). Combining surface dilatational rheology and quantitative proteomics as a tool for understanding microstructures of air/water interfaces stabilized by sodium caseinate/tannic acid complex. *Food Hydrocolloids*, *102*, art. no. 105627.
https://doi.org/10.1016/j.foodhyd.2019.105627
46. Zhang, J., Zhu, R., Meng, Z. (2024). Whipped cream stabilized by faba bean protein isolate microgel particles substituted for sodium caseinate: Whipping performance and foam stabilization analysis. *Food Hydrocolloids*, *157*, art. no. 110388.
https://doi.org/10.1016/j.foodhyd.2024.110388
47. Zhao, Q., Zhao, M., Li, J., Yang, B., Su, G., Cui, C., Jiang, Y. (2009). Effect of hydroxypropyl methylcellulose on the textural and whipping properties of whipped cream. *Food Hydrocolloids*, *23*(8), 2168-2173.
https://doi.org/10.1016/j.foodhyd.2009.04.007

ORIGINAL ARTICLE
http://journal.pan.olsztyn.pl

Polish Journal of Food and Nutrition Sciences
2026, Vol. 76, No. 2, 162–172
DOI: 10.31883/pjfns/221193
ISSN 1230-0322, e-ISSN 2083-6007

Instant Noodles from Climate-Resilient Crops: Nutritional Quality, Sensory Acceptance, and Satiety of Sago–Bambara Groundnut Noodles Compared with Conventional Wheat Noodles

Yoanita R. Indrining Tyas[1]†, Eny Palupi[1]*†, Zuraidah Nasution[1], Desy R. Tarigan[1], Alit Pangestu[2], Norhaizan M. Esa[3]

[1]Department of Nutrition Science, Faculty of Medicine and Nutrition, Bogor Agricultural University, Bogor 16680, Indonesia
[2]Research Center for Food Technology and Processing, National Research and Innovation Agency, Yogyakarta 55861 Indonesia
[3]Department of Nutrition and Dietetics, Faculty of Medicine and Health Sciences, Universiti Putra Malaysia, 43400 Serdang, Selangor, Malaysia

Climate-resilient crops, such as sago (*Metroxylon sagu* Rottb.) and Bambara groundnut (*Vigna subterranea* (L.) Verdc.), offer promising solutions to enhance food security, nutritional quality, and sustainability under climate change. This study aimed to develop instant noodles based on sago starch enriched with Bambara groundnut flour and to evaluate their physicochemical properties, nutritional composition, sensory acceptability, and satiety response in comparison with conventional wheat-based instant noodles. Four different ratios of sago starch to Bambara groundnut flour were used 100:0 (F0), 70:30 (F1), 60:40 (F2), and 50:50 (F3) (*w/w*). The results demonstrated that sago-Bambara groundnut noodles exhibited a significantly higher total dietary fiber content (9.4–12.2 g/100 g dry matter basis, db) than sago noodles (4.5 g/100 g db) and wheat noodles (2.5 g/100 g db). However, sensory evaluation in the hedonic test showed that increasing the ratio of Bambara groundnut flour in the formula decreased noodle sensory acceptability. Therefore, formula F2 (60:40, *w/w*) was selected as the optimal. The quantitative descriptive sensory analysis (QDA) demonstrated that the noodles made according to this formula exhibited stronger off-beany and beany aroma, savory and starchy taste, off-beany and beany aftertaste, hardness and graininess mouthfeel compared to the sago noodles. Notably, the satiety index measurement using the visual analogue scale (VAS) questionnaire showed that the sago–Bambara groundnut noodles sustained a 50% fullness level for a significantly longer time (135 min) than wheat noodles (77 min) and demonstrated a higher satiety index (122% *vs*. 90%). These findings demonstrate that instant noodles formulated entirely from climate-resilient crops can enhance nutritional quality and satiety compared to the conventional wheat-based instant noodles, while remaining sensorially acceptable.

Keywords: cereal products, high-fiber food, *Metroxylon sagu*, satiety index, *Vigna subterranea*

INTRODUCTION

Obesity, as a multifactorial metabolic disorder characterized by excess fat accumulation due to an energy imbalance, has become a global nutritional problem, which according to the World Health Organization (WHO), afflicts one in eight people in the world [WHO, 2024]. One primary contributing factor to obesity is the frequent consumption of ultra-processed food, such as instant noodles [Septiani & Sugiatmi, 2026]. Instant noodles are processed foods that contain high calories, saturated fats, and sodium but are generally low in essential nutrients, such as fiber, vitamins, and minerals and are often associated with a high glycemic response and low satiety response [Huh *et al.*, 2017; Salihu *et al.*, 2025]. Conventional instant noodles are predominantly produced using refined wheat flour. The increasing reliance on wheat, particularly in regions

***Corresponding Author:**
E-mail: **enypalupi@apps.ipb.ac.id** (Dr. E. Palupi)
†These authors had equal contribution to this work

Submitted: 22 January 2026
Accepted: 28 April 2026
Published on-line: 25 May 2026

where it is not locally produced, raises concerns regarding food system vulnerability [Farhan *et al.*, 2025]. This vulnerability is exacerbated as climate change poses additional challenges to global food security [Begna & Wakweya, 2026], emphasizing the urgent need to diversify staple food sources with climate-resilient crops [Benitez-Alfonso *et al.*, 2023].

Sago (*Metroxylon sagu* Rottb.) and Bambara groundnut (*Vigna subterranea* (L.) Verdc.) are underutilized crops that exhibit strong adaptability to marginal environments, drought tolerance, and stable yields under adverse climatic conditions [Bintoro *et al.*, 2018; Tan *et al.*, 2020]. Sago is a traditional source of starch in some tropical regions that contains high levels of carbohydrates, approximately 84.7 g *per* 100 g of starch [Moshawih *et al.*, 2025], but has a low protein content (0.9 g/100 g starch) [Ministry of Health, 2018]. Consequently, food products developed primarily from sago tend to have a limited protein content; for instance, previous studies have reported that sago-based noodles contain only 3.07 g protein/100 g [Dewita *et al.*, 2019]. In contrast, Bambara groundnut is a legume rich in protein (17–25 g/100 g), with a relatively balanced amino acid profile [Maphosa *et al.*, 2022]. Therefore, the partial substitution of sago starch with Bambara groundnut flour is expected to significantly improve the nutritional quality of sago-based products, particularly by increasing their protein content. The complementary nutritional characteristics of these two climate-resilient crops suggest their potential for the development of nutritionally-enhanced staple foods.

Previous research has demonstrated the effectiveness of legume substitutions in noodle formulations; for instance, substituting wheat flour with 25% chickpea flour increased the protein content of noodles from 12.79 to 15.31 g/100 g [Bayomy & Alamri, 2022]. However, research on the integration of fully climate-resilient crops into instant noodle formulations remains limited. In particular, the combined use of sago starch and Bambara groundnut flour in instant noodles has not been extensively investigated, especially regarding the enhancement of protein and dietary fiber levels and satiety-related outcomes. Given the growing interest in functional convenience foods that support appetite regulation and metabolic health, the evaluation of satiety responses alongside nutritional composition is becoming increasingly relevant.

Therefore, this study aimed to develop instant noodles based on sago starch enriched with Bambara groundnut flour and compare their nutritional quality and satiety properties with those of conventional wheat-based instant noodles. By linking climate resilience, nutritional improvement, and consumer-relevant functional outcomes, this study contributes to the development of sustainable and healthier instant noodle alternatives.

To achieve these objectives, this study was conducted in several stages, including (1) formulation of sago noodles with Bambara groundnut flour, (2) assessment of their physical characteristics and nutritional content, (3) their sensory evaluation, and (4) their satiety index measurement.

MATERIALS AND METHODS

Materials

There were two main materials that have been used in this research, *i.e.*, sago (*M. sagu*) starch and Bambara groundnut (*V. subterranea*) beans. The Bambara groundnut was purchased from the traditional market in Bogor, Indonesia. As many as 40 kg of beans have been used in a single run of Bambara groundnut flour. The sago starch (20 kg) was procured from the local farmer in Banggai, Central Sulawesi, Indonesia. Commercial all-salt (Refina, UnichemCandi Indonesia, Sidoarjo, Indonesia), sodium tripolyphosphate (Sodium tripolyphosphate, Aditya Birla Chemicals, Samut Prakan, Thailand), and wheat-based instant noodles (Indomie, Indofood, Jakarta, Indonesia) were purchased at a local market in Bogor, Indonesia.

Production of sago and Bambara groundnut noodles

The production of the sago and Bambara groundnut noodles consisted of two main stages, *i.e.*, sago flour and Bambara groundnut flour preparation, and noodle preparation. To produce sago flour, sago starch was sun-dried for 18 h. Dried sago starch was ground and sieved using an 80-mesh screen to obtain sago flour. To produce Bambara groundnut flour, the beans were soaked for 12 h. Then, they were boiled at 90°C for 10 min to inactivate lipoxygenase and eliminate the beany flavor [Chong *et al.*, 2019]. The beans were dried using a cabinet dryer (CTM SRL Manufacture, Milan, Italy) at 90°C at 10 rpm. Dried beans were milled using a pin disc mill and sieved using an 80-mesh screen to obtain Bambara groundnut flour.

The development of the sago and Bambara groundnut noodle formulations was conducted as a trial-and-error process based on the Agustia *et al.* [2016] recipe before producing the final noodle product. Formulas of noodles with different flour composition used in this study have been adjusted to the Indonesian National Standard to meet the requirements of instant noodle quality standards [BSN, 2018] and the high-fiber claims for processed food products [Indonesian Food and Drug Authority, 2022]. The formulas contained different ratios of sago flour (SF) and Bambara groundnut flour (BGF): F0 (100% SF), F1 (70% SF:30% BGF, *w/w*), F2 (60% SF:40% BGF, *w/w*), and F3 (50% SF:50% BGF, *w/w*) (**Table 1**).

Sago flour was mixed into 100 mL of water and cooked at 90°C for 1 min until it thickened to produce a gelatinized sago starch. Then, it was mixed with Bambara groundnut flour and other ingredients, including sodium tripolyphosphate (0.5% of recipe ingredients, *w/w*) and salt (0.5% of recipe ingredients, *w/w*) using a mixer (Miyako HM-620, Jakarta, Indonesia) until a smooth dough was formed. A dough made from wheat flour, instead of SF and BGF, was also prepared. The noodles were formed using a roll press (Ardin CM2020, Jakarta, Indonesia) with a length of ±15 cm and dried at 105°C for 60 min in an oven (Kirin KBO 190RA, Jakarta, Indonesia). The dried noodles were boiled at 100°C for 7–9 min and allowed to cool to room temperature prior to analysis.

Table 1. Formulas of noodles with different ratios of sago flour (SF) and Bambara groundnut flour (BGF).

Ingredient	Unit	F0 (100:0)	F1 (70:30)	F2 (60:40)	F3 (50:50)
Sago flour	g (%)	100 (49.5)	70 (34.7)	60 (29.7)	50 (24.8)
Bambara groundnut flour	g (%)	0 (0)	30 (14.9)	40 (19.8)	50 (24.8)
Salt (NaCl)	g (%)	1 (0.5)	1 (0.5)	1 (0.5)	1 (0.5)
Sodium tripolyphosphate	g (%)	1 (0.5)	1 (0.5)	1 (0.5)	1 (0.5)
Water	mL	100 (49.5)	100 (49.5)	100 (49.5)	100 (49.5)

F0, formula of noodles made from SF; F1, formula of noodles made from SF and BGF in a 70:30 (*w/w*) ratio; F2, formula of noodles made from SF and BGF in a 60:40 (*w/w*) ratio; and F3, formula of noodles made from SF and BGF in a 50:50 (*w/w*) ratio.

Analysis of physical characteristics

The physical characteristics of the noodles were assessed by evaluating their color and texture. The color was measured using a chromameter (AMT511, Amtast, Lakeland, FL, USA), calibrated with a provided set of black and white plates. The CIELab color space was defined by *L**, *a**, and *b** values, which represent lightness (dark–bright), redness (green–red), and yellowness (blue–yellow), respectively.

The firmness was measured using a texture analyzer (TA. XT Plus, Stable Micro Systems, Godalming, UK). Three strands of cooked noodles were placed parallel to each other on the platform and positioned perpendicular to the Asian Noodle Rig (HDP/ANR) probe. Compression was initiated at a pre-test speed of 1 mm/s, a test speed of 2 mm/s, and a post-test speed of 10 mm/s with a compression distance of 9.9 mm and a strain level of 10%. The test was activated by a trigger force of 0.049 N and trigger distance of 2 mm until the sample was compressed with a force of 0.981 N and break sensitivity of 0.098 N. The firmness value was obtained from the maximum force required to compress the noodle strands, expressed in Newton (N).

Nutrient content determination

The nutrient content determination of sago and Bambara groundnut noodles included determining the moisture content using the gravimetric method (AOAC International method no. 2005:925.10), ash content using the gravimetric method (AOAC 2005:923.03), protein content using the Kjeldahl method (AOAC 2005:955.04), lipid content using the Soxhlet method (AOAC 2005:920.39c), carbohydrate content using the by-difference method, and dietary fiber content (total, soluble and insoluble) using the enzymatic gravimetric method [AOAC, 2005]. The available carbohydrate content was calculated as the difference between the carbohydrate content and the dietary fiber content. The results of nutrient content were expressed on a dry matter basis (db) of noodles.

Sensory evaluation

The research protocol of sensory evaluation has been reviewed and approved by the Human Research Ethics Committee of Bogor Agricultural University in Bogor, Indonesia, with the approval number 1633/IT3.KEPMSM IPB/SK/2025. The sensory evaluation consisted of two tests: a hedonic acceptance test and a quantitative descriptive analysis.

The sensory attributes assessed in the acceptance test included appearance, aroma, taste, mouthfeel, aftertaste, and overall acceptability of noodles. Sensory attributes were assessed using a 9-point hedonic scale ranging from 1 (dislike extremely) to 9 (like extremely), based on the level of preference for each sensory attribute assessed. Thirty semi-trained panelists (23 women and 7 men) aged 18–40 years participated in the study. The inclusion criteria for panelists in the sensory evaluation were as follows: willingness to participate in the sensory evaluation; consistency in decision-making; absence of ear, nose, and throat disorders; normal color vision; no allergies to ingredients contained in the noodle formulations; required to fast for 1 h prior to the sensory evaluation; avoid consuming pungent foods before sensory evaluation; and prohibited using strongly scented cosmetics such as perfumes during the sensory evaluation [ISO 8586:2014].

The quantitative descriptive sensory analysis (QDA) was carried out only on the sago flour noodles (F0; as control) and optimal noodle formula made from SF and BGF in ratio 40:60, *w/w* (F2). The selection of noodle formula for QDA and satiety index measurement was made by considering the most relevant results from the nutritional composition analysis and hedonic sensory evaluation.

The QDA involved 11 trained panelists who were selected using the Ishihara test, matching test, triangle test, and ranking test. The QDA procedure was carried out in two main stages: a focus group discussion (FGD) to identify sensory attributes, followed by an assessment of the intensity of each attribute. The sensory attributes assessed included aroma, taste, mouthfeel, and aftertaste. The sensory attributes were assessed using an intensity scale ranging from 0 (very weak) to 10 (very strong) [ISO 8586:2014].

Satiety index measurement

The research protocol of satiety index measurement has been reviewed and approved by the Human Research Ethics Committee of Bogor Agricultural University in Bogor, Indonesia, with the approval number 1633/IT3.KEPMSM IPB/SK/2025.

Table 2. Subject characteristics for satiety index assessment.

Subject code	Sex	Age (years)	BMI (kg/m^2)	FBS (mg/dL)
01	Female	25	21.3	85
02	Female	22	21.4	89
03	Female	24	21.9	79
04	Female	23	23.3	88
05	Female	24	19.1	90
06	Female	23	19	91
07	Female	21	21.6	96
08	Female	20	20.9	88
09	Female	24	22.9	94
10	Female	19	22.3	94
11	Male	24	21.7	97
12	Male	24	20.9	99
13	Male	22	21.7	92
14	Male	21	22.1	79
15	Male	21	22.8	83
16	Male	25	22.5	86
17	Male	24	21	93
Mean		22.71	21.55	89.59
SD		1.79	1.18	5.86
%CV		7.8	5.4	6.5

BMI, body mass index; FBS, fasting blood sugar; SD, standard deviation; %CV, coefficient of variation.

Seventeen subjects participated in this study, including ten women (58.8%) and seven men (41.2%) with an average age of 22.91±1.30 years (**Table 2**), who were selected using a purposive sampling method. The inclusion criteria for the subjects of this study were as follows: (1) man or woman aged between 20 and 25 years, (2) a normal body mass index (BMI) (18.5–22.9 kg/m^2), (3) a normal fasting blood sugar level (<100 mg/dL), (4) no allergies or food intolerance, (5) engaged in light to moderate physical activity, and (6) normal dietary behavior. The exclusion criteria for the subjects of this study were (1) pregnancy or breastfeeding (for female subjects), (2) active smokers, (3) consuming alcohol, (4) experiencing digestive disorders and/or eating disorders, and (5) undergoing medications that can affect eating habits. One subject was excluded due to human error in completing the questionnaire. The satiety scores of the excluded subject exhibited abnormal fluctuations that deviated significantly from those of the other subjects, resulting in outlier data for the satiety index measurement. A sample size of 17 was considered acceptable for a satiety index study [Forde, 2018]. The homogeneity of subject characteristics was determined using the coefficient of variation percentage (%CV). If the %CV ≤5% for body mass index and %CV <33% for fasting blood sugar, then the subject characteristics were considered homogenous [Jamaiyah *et al*., 2010; Mo *et al*., 2021]. The %CV was calculated using Equation (1) [Ulijaszek & Kerr, 1999]:

$$\%CV = \frac{\text{Standard deviation}}{\text{Mean}} \times 100\% \quad (1)$$

The satiety index measurement was conducted on four different days with a 6-day washout period between the tested foods to ensure that the physiological condition had returned to normal [Nolan *et al*., 2016]. Subjects were required to fast for 8–10 h before the test. After fasting, they consumed isocaloric food (240 kcal) and one cup of water (220 mL) within a maximum of 15 min. The isocaloric foods given to the subjects consisted of standard and test foods. White bread was used as a standard food, according to Holt *et al*. [1995]. The tested foods were F0 (100% SF), F2 (60% SF:40% BGF, *w/w*), and wheat noodles. According to their energy content, the portion of F0 was 55.9 g, that of F2 was 55.1 g, that of wheat noodles was 37.4 g, and that of white bread was 100.0 g. The tested foods were served with 250 mL of broth and seasonings. Then, the four parameters of the satiety index: (1) hunger score, (2) fullness score, (3) desire to eat score, and (4) food quantity score, were measured using the 100-mm visual analogue scale (VAS) questionnaire at 0, 30, 60, 90, 120, 150, and 180 min after consumption of the tested foods.

The scores of hunger, fullness, desire to eat, and food quantity were plotted on a graph to calculate the area under the curve (AUC). The curve was scaled in units of sampling time (counted in hours) and fullness index, which was expressed as a ruler scale in mm. The AUC was calculated using the trapezoid method and expressed as mm×h. The satiety index was calculated by comparing the AUC of the tested food with that of the standard food for each subject. Then, the satiety index was calculated using Equation (2) based on Holt *et al*. [1995]:

$$\text{Satiety index} = \frac{\text{AUC of tested food}}{\text{AUC of standard food}} \times 100\% \quad (2)$$

Statistical analysis

The data for each parameter were presented as mean and standard deviation of triplicated measurements/determinations. Statistical analysis was performed using Excel 2016 for Windows (Microsoft, Redmond, WA, USA) and IBM SPSS Statistics (version 26.0; IBM Corp., Armonk, NY, USA). The results of the determination of the physical characteristics, nutritional composition, hedonic sensory evaluation, and satiety index were analyzed using the one-way analysis of variance (ANOVA), followed by the Duncan's multiple range test. However, the results of the quantitative descriptive analysis were analyzed using the independent *t*-test. The differences were considered significant at $p<0.05$.

RESULTS AND DISCUSSION

Physical characteristics

The firmness values of noodles made from sago and Bambara groundnut flours are shown in **Table 3**. The incorporation of Bambara groundnut flour into the recipe significantly ($p<0.05$) decreased the firmness of the noodles compared to those made from sago flour. However, the firmness exhibited no significant difference ($p\geq0.05$) among the F1, F2, and F3 samples. Similar results were reported by Singthong *et al*. [2026], according to whom the noodles substituted with 50% kidney bean flour had significantly decreased firmness compared to the rice and tapioca flour noodles. The incorporation of legume flour can disrupt the starch structure, which causes firmness reduction [Singthong *et al*., 2026]. The protein and fiber in legume flour form physical barriers around starch granules and aggressively compete for available water. These macromolecules restrict the swelling required for starch gelatinization, disrupting the formation of the starch gel network. This process may weaken the structural integrity of the noodle matrix, resulting in softer noodles [Singthong *et al*., 2026].

The color coordinate values of the noodles made from sago and Bambara groundnut flours are shown in **Table 3**. Additionally, the appearance of cooked noodles is presented in **Figure 1**. The substitution of the Bambara groundnut flour significantly ($p<0.05$) decreased the lightness (L^*), redness (a^*), and yellowness (b^*) values of noodle color compared to those made from sago flour (**Table 3**). Similar findings were reported by Mashau *et al.* [2022], who showed that the crust and crumb of steamed breads fortified with Bambara groundnut flour had significantly lower L^* and a^* values compared to the steamed wheat bread, although an increase in b^* value was noted, in contrast to the noodles in our study. The darker color of the noodles might be due to the presence of color flavonoids and tannins in the Bambara groundnut seeds, especially in the seed coat [Palamae *et al*., 2024; Pretorius *et al*., 2023].

Nutritional composition

The nutritional composition of the sago and Bambara groundnut flours as well as noodles made from these flours is presented in **Table 4**. Data on wheat noodles is also shown in **Table 4**. The energy value and nutrient content of the noodles made from sago and Bambara groundnut flour were significantly different ($p<0.05$) from those of wheat noodles. The contents of carbohydrates, available carbohydrates, and total dietary fiber of the noodles made from sago and Bambara groundnut flour were significantly higher ($p<0.05$) compared to wheat noodles. However, the energy value and contents of protein and lipids of the noodles made from sago and Bambara groundnut flour were significantly lower ($p<0.05$) than those of the wheat noodles. The use of Bambara groundnut flour in the noodle formula significantly ($p<0.05$) increased the energy value and contents of protein, lipids, total dietary fiber, soluble dietary fiber, insoluble

Table 3. Physical characteristics of noodles made from sago flour (SF) and Bambara groundnut flour (BGF) used in different ratios.

Physical characteristic	F0 (100:0)	F1 (70:30)	F2 (60:40)	F3 (50:50)
L^*	80.8 ± 0.7^{a}	77.3 ± 0.5^{b}	76.2 ± 0.7^{c}	74.9 ± 0.4^{d}
a^*	10.0 ± 0.4^{a}	6.3 ± 0.2^{b}	6.0 ± 0.3^{bc}	5.7 ± 0.2^{c}
b^*	15.0 ± 1.1^{a}	9.1 ± 0.3^{b}	8.6 ± 0.6^{b}	7.9 ± 0.5^{b}
Firmness (N)	53.0 ± 1.2^{a}	33.9 ± 4.7^{b}	28.5 ± 1.2^{b}	27.4 ± 0.0^{b}

Results are shown mean ± standard deviation. Different superscript letters in each row indicate significant differences at $p<0.05$, analyzed using Duncan's multiple range test. F0, noodles made from SF; F1, noodles made from SF and BGF in a 70:30 (*w/w*) ratio; F2, noodles made from SF and BGF in a 60:40 (*w/w*) ratio; and F3, noodles made from SF and BGF in a 50:50 (*w/w*) ratio; L^*, lightness; a^*, redness; b^*, yellowness.

F0 F1 F2 F3

Figure 1. Appearance of noodles made from sago flour (SF) and Bambara groundnut flour (BGF) used in different ratios. F0, noodles made from SF; F1, noodles made from SF and BGF in a 70:30 (*w/w*) ratio; F2, noodles made from SF and BGF in a 60:40 (*w/w*) ratio; and F3, noodles made from SF and BGF in a 50:50 (*w/w*) ratio.

Table 4. Nutritional composition of wheat noodles and noodles made from sago flour (SF) and Bambara groundnut flour (BGF) used in different ratios.

Nutritional composition	SF	BGF	F0 (100:0)	F1 (70:30)	F2 (60:40)	F3 (50:50)	Wheat noodles
Energy (g/100 g db)	401±0.0^{f}	424±0.3^{b}	393±0.3^{g}	403±0.3^{e}	406±0.2^{d}	409±0.7^{c}	481±0.1^{a}
Protein (g/100 g db)	0.4±0.0^{g}	18.7±0.0^{a}	2.1±0.1^{f}	6.5±0.0^{e}	8.6±0.0^{d}	10.6±0.2^{c}	12.0±0.1^{b}
Lipid (g/100 g db)	0.5±0.0^{f}	7.6±0.0^{b}	0.0±0.0^{g}	2.9±0.0^{e}	3.6±0.1^{d}	4.5±0.1^{c}	17.3±0.0^{a}
Carbohydrate (g/100 g db)	98.6±0.0^{a}	70.2±0.0^{f}	96.0±0.2^{b}	87.9±0.1^{c}	84.7±0.2^{d}	81.8±0.3^{e}	69.4±0.1^{g}
Available carbohydrate (g/100 g db)	–	–	91.7±0.3^{a}	78.5±0.1^{b}	73.6±0.1^{c}	69.7±0.1^{d}	66.9±0.1^{e}
Total dietary fiber (g/100 g db)	–	–	4.5±0.2^{d}	9.4±0.1^{c}	11.1±0.3^{b}	12.2±0.1^{a}	2.5±0.0^{e}
Soluble dietary fiber (g/100 g db)	–	–	1.1±0.2^{d}	2.1±0.0^{c}	2.5±0.1^{b}	2.8±0.1^{a}	–
Insoluble dietary fiber (g/100 g db)	–	–	3.4±0.0^{d}	7.3±0.1^{c}	8.5±0.4^{b}	9.4±0.2^{a}	–
Moisture (g/100 g wb)	14.5±0.1^{a}	9.7±0.0^{b}	5.5±0.3^{e}	7.3±0.3^{c}	6.7±0.3^{d}	4.6±0.2^{f}	6.6±0.0^{d}
Ash (g/100 g db)	0.5±0.0^{f}	3.5±0.0^{a}	1.9±0.1^{d}	2.8±0.8^{c}	3.1±0.7^{b}	3.2±0.2^{b}	1.3±0.0^{e}

Results are shown mean ± standard deviation. Different superscript letters in each row indicate significant differences at $p<0.05$, analyzed using Duncan's multiple range test. F0, noodles made from SF; F1, noodles made from SF and BGF in a 70:30 (*w/w*) ratio; F2, noodles made from SF and BGF in a 60:40 (*w/w*) ratio; and F3, noodles made from SF and BGF in a 50:50 (*w/w*) ratio; db, dry basis; wb, wet basis.

dietary fiber, and ash of the noodles compared to the control sample made from sago flour. Meanwhile, the substitution of sago starch with Bambara groundnut flour significantly ($p<0.05$) decreased the carbohydrate and available carbohydrate contents of the noodles compared to the control sample made from sago flour. Similar results were reported by Makhuvha *et al*. [2024], who found that substituting wheat flour with 25% Bambara groundnut flour in pasta significantly increased the protein, lipid, fiber, and ash contents, while decreasing the carbohydrate content compared to wheat flour pasta. Based on the Indonesian Food and Drug Authority regulation [2022] regarding the supervision of food labeling and advertisements, the developed noodle formulas demonstrate significant potential for nutritional claims. The F0 noodle formula meets the claim criteria for a 'source of fiber' food product (≥3 g/100 g), while F1, F2, and F3 formulas for a 'high-fiber' food product (≥6 g/100 g). High-fiber foods are associated with higher satiety index scores, leading to a more sustained feeling of fullness [Gerstein *et al*., 2004]. Consequently, enhancing satiety through fiber intake serves as a strategic approach to mitigating the risk of excess energy intake and subsequent weight gain [Hervik & Svihus, 2019; Savastano *et al*., 2014].

Sensory characteristics

The results of the sensory characteristics assessment in the hedonic acceptance test of the noodles made from sago flour and Bambara groundnut flour are presented in **Table 5**. The scoring of the hedonic attributes of F1 and F2 did not differ significantly ($p\geq0.05$). However, the higher proportion of Bambara groundnut flour in the noodle formula resulted in the taste, mouthfeel, aftertaste, and overall acceptance of F3 being significantly ($p<0.05$) lower rated by panelists than F2. These noodles did not differ significantly ($p\geq0.05$) only in the appearance and aroma. The overall result of the sensory hedonic acceptance test indicates that the noodles made from sago flour and Bambara groundnut flour received hedonic scores between 5 and 6, indicating they fell within the 'like moderately' category and were generally accepted by the panelists.

Since noodles F1 and F2 received higher scores in the hedonic acceptance test than F3 and, at the same time, F2 had a more favorable nutrient composition than F1 (especially a higher dietary fiber content), the F2 noodles were selected for QDA and satiety index measurement.

Table 5. Sensory characteristics in the hedonic acceptance test of noodles made from sago flour (SF) and Bambara groundnut flour (BGF) used in different ratios.

Sensory attribute	F1 (70:30)	F2 (60:40)	F3 (50:50)
Appearance	5.9±1.7^{a}	6.1±1.4^{a}	5.2±1.5^{a}
Aroma	6.0±1.1^{a}	6.3±1.1^{a}	5.7±1.3^{a}
Taste	5.6±1.7^{ab}	6.0±1.3^{a}	5.1±1.4^{b}
Mouthfeel	5.1±1.8^{ab}	5.6±1.4^{a}	4.5±1.4^{b}
Aftertaste	5.4±1.4^{ab}	5.8±1.1^{a}	5.0±1.3^{b}
Overall acceptance	5.9±1.4^{ab}	6.2±1.2^{a}	5.2±1.5^{b}

Results are shown mean ± standard deviation. Different superscript letters in each row indicate significant differences at $p<0.05$, analyzed using Duncan's multiple range test. F1, noodles made from SF and BGF in a 70:30 (*w/w*) ratio; F2, noodles made from SF and BGF in a 60:40 (*w/w*) ratio; and F3, noodles made from SF and BGF in a 50:50 (*w/w*) ratio.

Table 6. Sensory attributes and intensity standards used in the quantitative descriptive analysis of noodles.

Attribute		Definition	Standards	Intensity
Aroma	Off-beany	The aroma associated with uncooked or raw beans	Bambara groundnut flour	10
	Onion	The aroma associated with fried onions	Onion oil	10
	Beany	The aroma associated with cooked or boiled beans	Boiled Bambara groundnut	10
Taste	Salty	The salt taste on the tongue associated with sodium chloride	0.2% NaCl solution 0.8% NaCl solution	2 8
	Savory	The savory taste on the tongue associated with monosodium glutamate	0.18% MSG solution 0.72% MSG solution	2 8
	Starchy	The starch taste on the tongue associated with sago flour	Sago flour	10
	Onion	The fried onion taste on the tongue	Onion oil	10
Aftertaste	Off-beany	The intensity of taste lingering in the mouth for 15 s after swallowing associated with uncooked or raw beans	Bambara groundnut flour	10
	Beany	The intensity of taste lingering in the mouth for 15 s after swallowing associated with cooked or boiled beans	Boiled Bambara groundnut	10
	Starchy	The intensity of taste lingering in the mouth for 15 s after swallowing associated with starch or flour	Sago flour	10
Mouthfeel	Springiness	The rate of return of the sample to its original shape after chewing	Wheat noodle	10
	Hardness	The force required to bite the sample completely with the molars	Wheat noodle	10
	Graininess	Degree to which grains are perceived in the mouth	Bambara groundnut flour	10

Thirteen sensory attributes were selected by the panel in QDA of the sago flour noodles and noodles made from sago flour and Bambara groundnut flour. These sensory attributes and intensity standards used are listed in **Table 6**. Scores of eight attributes exhibited significant differences ($p<0.05$) between F0 and F2, comprising two aroma, two taste, two aftertaste, and two mouthfeel attributes (**Figure 2**). The substitution of sago starch with 40% (*w/w*) Bambara groundnut flour resulted in a stronger off-beany aroma, beany aroma, savory taste, starchy taste, off-beany aftertaste, beany aftertaste, hardness mouthfeel, and graininess mouthfeel of the noodles compared to the sago noodles. The stronger beany aroma of noodles made from both flours compared to the sample without Bambara groundnut flour may be due to activity of lipoxygenase of Bambara groundnut [Kudre & Benjakul, 2013]. Lipoxygenase catalyzes the oxidation of polyunsaturated fatty acids, such as linoleic acid, resulting in aldehyde compounds that produce a beany aroma [Kudre & Benjakul, 2013]. Although blanching can inactivate the lipoxygenase [Chong *et al*., 2019], the decrease in enzyme activity depends on the temperature and time [Estiasih *et al*. 2025]. According to Nguyen *et al*. [2025], lipoxygenase activity remains at 32–63% after heating at 80–90°C for 25 min. Consequently, the sub-optimal heating temperatures and times lead to the incomplete inactivation of the lipoxygenase enzyme. Furthermore, the substitution of Bambara groundnut flour significantly enhances the savory taste of the noodles, due to its high glutamic acid content (18.31 g/100 g) [Aremu *et al*., 2025]. This amino acid is present naturally in protein-rich foods that produce a savory taste [Jahanshiri *et al*., 2022]. Moreover, it also enhances the graininess of the noodles, because the insoluble fiber content exceeding 2% is known to induce a gritty texture in the mouth [Aussanasuwannakul *et al*., 2022; Chakraborty *et al*., 2019], which is further exacerbated by insufficiently fine flour sieving during the processing [Iju *et al*., 2025].

Satiety index

The satiety index is a measure that evaluates the level of satiety produced by a test food compared to that produced by a standard food, and is expressed as a percentage [Forde, 2018]. The nutrient content of the tested noodles and wheat bread used as a standard food *per* 240 kcal, satiety scores, and satiety indices are shown in **Table 7**. A significant difference ($p<0.05$) was found in the satiety index between sago noodles (F0), noodles made from sago and Bambara groundnut flours (F2) and wheat noodles. The satiety index values of the tested foods, in the order of wheat noodles, sago noodles as control sample, and sago noodles with Bambara groundnut flour, were 90%, 113%, and 122%, respectively. The satiety index of the noodles made from sago and Bambara groundnut flours was significantly higher than that of the wheat noodles, indicating that the substitution of sago starch with 40% (*w/w*) Bambara groundnut flour resulted in a greater sense of fullness. As shown in **Table 7**, the sago noodles with and without Bambara groundnut flour

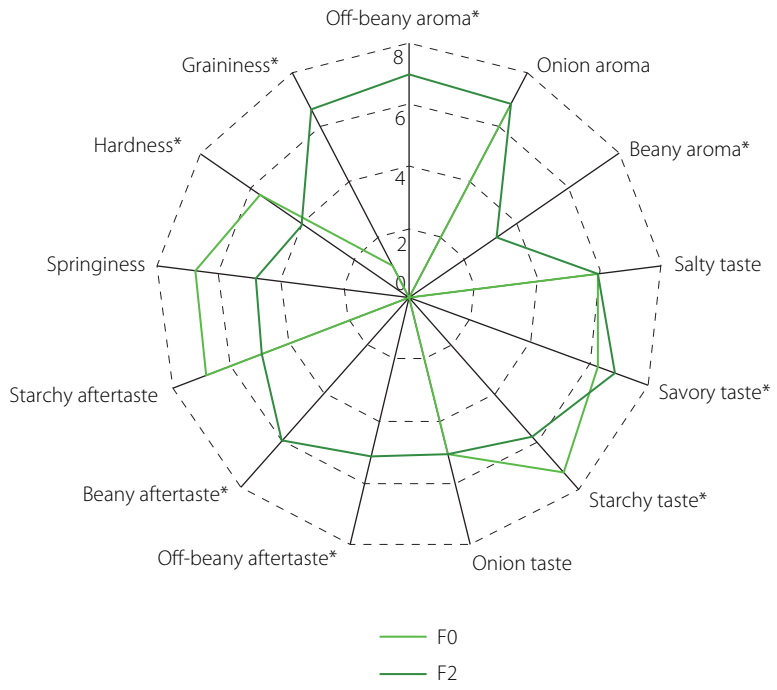

Figure 2. Results of quantitative descriptive sensory analysis (QDA) of noodles made from sago flour (F0) and sago and Bambara groundnut flours used in a 60:40 (*w/w*) ratio (F2). Asterisks indicate significant differences at $p<0.05$, analyzed using independent *t*-test.

Table 7. Nutrient composition of a portion (240 kcal) of white bread, wheat noodles, and noodles made from sago flour (F0), and from sago and Bambara groundnut flours in a ratio of 60:40, *w/w* (F2), as well as satiety scores and satiety index for these food products.

Parameter	White bread	F0 (100:0)	F2 (60:40)	Wheat noodles
Nutrient content				
Protein (g)	9.9±0.0[a]	1.1±0.1[d]	4.4±0.0[c]	5.3±0.1[b]
Lipid (g)	4.7±0.0[b]	0.0±0.0[d]	1.9±0.1[c]	7.7±0.0[a]
Carbohydrate (g)	48.4±3.6[a]	48.0±0.2[b]	40.5±0.2[c]	30.8±0.1[d]
Available carbohydrate (g)	45.4±0.1[a]	45.8±0.4[a]	35.2±0.1[b]	29.7±0.1[c]
Total dietary fiber (g)	3.0±0.1[b]	2.4±0.1[c]	5.7±0.2[a]	1.1±0.0[d]
Soluble dietary fiber (g)	0.7±0.0[b]	0.6±0.1[c]	1.3±0.0[a]	–
Insoluble dietary fiber (g)	2.3±0.1[b]	1.8±0.0[c]	4.4±0.2[a]	–
Moisture (mL)	35.4±0.4[a]	34.6±0.0[b]	36±0.0[a]	25.4±0.0[c]
Weight *per* 240 kcal (g)	100	55.9	55.1	37.4
Satiety score				
Hunger (mm×h)	44.6±6.9[b]	38.6±7.9[c]	36.4±8.9[c]	51.4±17.9[a]
Fullness (mm×h)	54.8±7.1[b]	61.6±8.2[a]	65.8±8.2[a]	46.6±17.3[b]
Desire to eat (mm×h)	45.9±5.9[b]	38.5±8.7[c]	36.9±8.0[c]	55.5±16.7[a]
Food quantity (mm×h)	45.5±7.4[b]	37.9±8.9[c]	37.3±11.0[c]	54.2±15.2[a]
Satiety index (%)	Reference	113±15[b]	122±17[a]	90±31[c]

Results are shown mean ± standard deviation. Different superscript letters in each row indicate significant differences at $p<0.05$, analyzed using Duncan's multiple range test.

significantly ($p<0.05$) reduced hunger, increased fullness, decreased desire to eat, and decreased food quantity compared to wheat noodles.

Figure 3 shows that the curve of the fullness index of the sago noodles with Bambara groundnut flour exceeds the standard white bread food curve, indicating that it can provide a longer feeling of fullness than white bread. The regression equations showed that sago noodles with Bambara groundnut flour (y= –0.344x + 96.354) reached a 50% level of fullness at 135 min. In comparison, white bread (y= –0.384x + 89.361) and wheat noodles (y= –0.296x + 72.911) reached the same level of fullness significantly faster, *i.e.*, at 102 min and 77 min, respectively. Therefore, it can be concluded that the consumption of noodles made from sago and Bambara groundnut flours in a 60:40 (*w/w*) ratio can prolong the feeling of fullness for up to 45 min longer than white bread, and even further up to 58 min longer than wheat noodles. These findings are consistent with observations made by Ridwan *et al*. [2024], who reported that tuber-bread with 60% Bambara groundnut flour could prolong the feeling of fullness up to 95 min longer than white bread. The increased feeling of fullness was due to the fact that F2 portion served had the highest content of total fiber (5.7 g) compared to F0 portion (2.4 g) and wheat noodle portion (1.1 g) (**Table 7**). According to Palupi *et al*. [2024], the consumption of foods high in fiber can increase the feeling of fullness or satiety. Dietary fiber, particularly soluble fiber, plays a significant role in increasing satiety through several physiological mechanisms throughout the digestive tract [Hervik & Svihus, 2019]. Due to its water solubility and gel-forming ability, soluble dietary fiber may increase the viscosity of gastrointestinal digesta. Higher viscosity can slow down gastrointestinal transit, delay gastric emptying, and increase gastric distension [Ariyarathna *et al*., 2025]. Increasing the gastric distention can inhibit the secretion of the ghrelin hormone, which sends signals to the hypothalamus to suppress hunger and stimulate satiety [Hervik & Svihus, 2019]. In addition, dietary fiber can increase oral processing time and effort needed for mastication. A longer oral processing time seems to stimulate cephalic phase responses, and these are deemed to contribute to satiety [Hervik & Svihus, 2019]. Thus, the sago with Bambara groundnut noodles can be used as an alternative high-fiber staple food that can increase the feeling of fullness and reduce the consumption of additional foods, which often contribute to excess calorie intake.

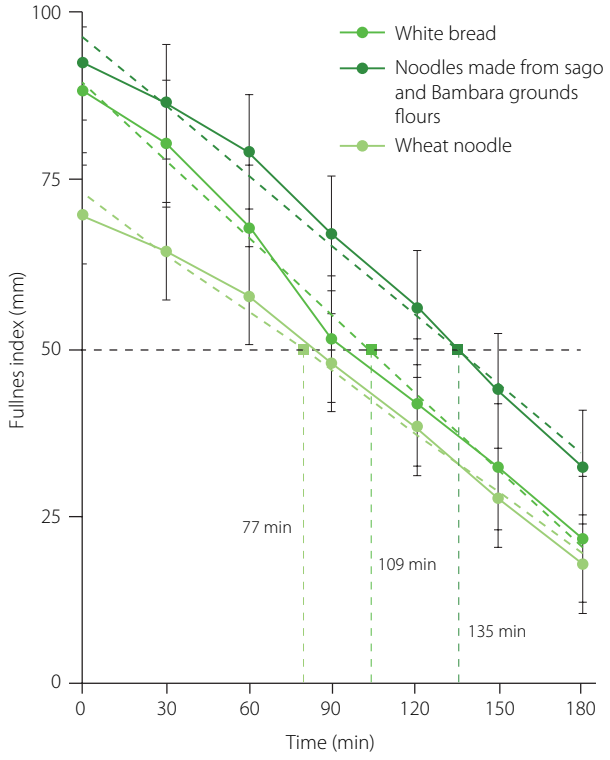

Figure 3. Visual analogue scale for the fullness index at fasting intervals of 30, 60, 90, 120, 150, and 180 min after the consumption of white bread, wheat noodles and noodles made from sago and Bambara groundnut flours used in a 60:40 (*w/w*) ratio.

CONCLUSIONS

Instant noodles developed from sago starch enriched with Bambara groundnut flour exhibited superior nutritional quality and satiety effects compared with conventional wheat-based instant noodles. Their higher protein and dietary fiber contents contributed to enhanced fullness, highlighting the potential role of these noodles in promoting appetite control. Beyond their nutritional advantages, the use of sago and Bambara groundnut – both climate-resilient and locally available crops – supports diversification of raw materials and reduces dependence on imported wheat. Overall, this study provides evidence that climate-resilient crops can be successfully transformed into acceptable, nutrient-dense, and highly satiating instant foods. The sago–Bambara groundnut noodle represents a promising functional and sustainable alternative for future food innovation, particularly in regions vulnerable to climate change and food insecurity. Furthermore, future research is needed to optimize the physicochemical properties of the resulting flour, thereby improving the sensory and textural quality of the noodles.

RESEARCH FUNDING

The authors would like to express their sincere gratitude to the Directorate of Research, Technology, and Community Service (DRTPM), Ministry of Higher Education, Science, and Technology of the Republic of Indonesia (Kementerian Pendidikan Tinggi, Sains, dan Teknologi Republik Indonesia) for the financial support provided through the "Penelitian Tesis Magister (PTM)" or Master's Thesis Research scheme for the project entitled 'Development of Sago and Bambara Groundnut Noodles as a High-Fiber, Low Glycemic Index Alternative Food for Obesity and Diabetes' (Contract No. 006/C3/DT.05.00/PL/2025). The authors would also like to gratefully acknowledge IPB University for covering the Article Processing Charge.

CONFLICT OF INTERESTS

The authors declare no conflict of interests.

INFORMED CONSENT

This research has obtained permission from the Commission on Research Ethics Involving Human Subjects, IPB University Number: 1633/IT3.KEPMSM-IPB/SK/2025.

ORCID IDs

N.M. Esa https://orcid.org/0000-0003-1545-0306
Y.R. Indrining Tyas https://orcid.org/0009-0007-7142-8142
Z. Nasution https://orcid.org/0000-0001-8307-1012
E. Palupi https://orcid.org/0000-0003-2029-3106
A. Pangestu https://orcid.org/0000-0002-6965-3988
D.R. Tarigan https://orcid.org/0009-0009-5878-2387

REFERENCES

1. Agustia, F.C., Subardjo, Y.P., Sitasari, A. (2016). Formulation and characterization of free gluten high protein sago starch noodle substituted with beans flour. *Jurnal Gizi dan Pangan*, *11*(3), 183–190 (in Indonesian, English abstract). https://doi.org/10.25182/jgp.2016.11.3.183-190
2. Aremu, M.O., Aremu, S.O., Aliyu, I., Passali, D.B., Hussaini, M., Musa, B.Z., Salau, R.B. (2025). Amino acids profile and health attributes of Bambara groundnut (*Vigna subteranea L.*) and sesame (*Sesamum indicum L.*): a comparative study. *African Scientific Reports*, *4*(1), art. no. 233. https://doi.org/10.46481/asr.2025.4.1.233
3. Ariyarathna, P., Mizera, P., Walkowiak, J., Dziedzic, K. (2025). Physicochemical and functional properties of soluble and insoluble dietary fibers in whole grains and their health benefits. *Foods*, *14*, art. no. 2447. https://doi.org/10.3390/foods14142447
4. Aussanasuwannakul, A., Teangpook, C., Treesuwan, W., Puntaburt, K., Butsuwan, P. (2022). Effect of the addition of soybean residue (okara) on the physicochemical, tribological, instrumental, and sensory texture properties of extruded snacks. *Foods*, *11*(19), art. no. 2967. https://doi.org/10.3390/foods11192967
5. AOAC (2005). *Official Methods of Analysis* (18th ed Association of Official Analytical Chemists International, Gaithersburg, MD, USA.
6. Bayomy, H., Alamri, E. (2022). Technological and nutritional properties of instant noodles enriched with chickpea or lentil flour. *Journal of King Saud University Science*, *34*(3), art. no. 101833. https://doi.org/10.1016/j.jksus.2022.101833
7. Begna, T., Wakweya, R.B. (2026). Mitigating climate change impacts on food security *via* climate-smart agriculture. *Plant Stress*, *19*, art. no. 101152. https://doi.org/10.1016/j.stress.2025.101152
8. Benitez-Alfonso, Y., Soanes, B.K., Zimba, S., Sinanaj, B., German, L., Sharma, V., Bohra, A., Kolesnikova, A., Dunn, J.A., Martin, A.C., Rahman, M.K.u., Saati-Santamaría, Z., García-Fraile, P., Ferreira, E.A., Frazão, L.A., Cowling, W.A., Siddique, K.H.M., Pandey, M.K., Farooq, M., Varshney, R.K., Chapman, M.A., Boesch, C., Daszkowska-Golec, A., Foyer, C.H. (2023). Enhancing climate change resilience in agricultural crops. *Current Biology*, *33*(23), R1246–R1261. https://doi.org/10.1016/j.cub.2023.10.028
9. Bintoro, M.H., Nurulhaq, M.I., Pratama, A.J., Ahmad, F., Ayulia, L. (2018). Growing area of sago palm and its environment. In: H. Ehara, Y. Toyoda, D.V. Johnson (Eds.). *Sago Palm Multiple Contributions to Food Security and Sustainable Livelihoods*, Springer, Singapore, pp. 17–29. https://doi.org/10.1007/978-981-10-5269-9_2
10. BSN (2018). SNI 3551:2018 Mi instan (Instant Noodle). Badan Standardisasi Nasional.
11. Chakraborty, P., Witt, T., Harris, D., Ashton, J., Stokes, J.R., Smyth, H.E. (2019). Texture and mouthfeel perceptions of a model beverage system containing soluble and insoluble oat bran fibres. *Food Research International*, *120*, 62–72. https://doi.org/10.1016/j.foodres.2019.01.070
12. Chong, W.K., Mah, S.Y., Easa, A.M., Tan, T.C. (2019). Thermal inactivation of lipoxygenase in soya bean using superheated steam to produce low beany flavour soya milk. *Journal of Food Science and Technology*, *56*(9), 4371–4379. https://doi.org/10.1007/s13197-019-03905-4
13. Dewita, Desmelati, Edison, Syahrul (2019). The development of instant (dried) sago noodles fortified with functional components. *IOP Conference Series: Earth and Environmental Science*, *253*, art. no. 012018. https://doi.org/10.1088/1755-1315/253/1/012018
14. Estiasih, T., Hidayat, R., Putri, R.N., Ahmadi, K.A., Ali, D.Y., Laeliocattleya, R.A. (2025). *Moringa oleifera* leaf powder colour improvement and lipoxygenase inactivation by different pHs and water-blanching times. *CyTA – Journal of Food*, *23*(1), art. no. 2586311. https://doi.org/10.1080/19476337.2025.2586311
15. Farhan, I., Sarayrah, H., Hayek, W., Alkhasoneh, H., Almayouf, F. (2025). Analyzing wheat production in Jordan: The role of population dynamics, climate variability, and GIS-based projections. *Sustainability*, *17*(8), art. no. 3493. https://doi.org/10.3390/su17083493
16. Forde, C.G. (2018). Chapter 7: Measuring satiation and satiety. In: G. Ares, P. Varela (Eds.). *Methods in Consumer Research*, Volume 2, Woodhead Publishing, pp. 151–182. https://doi.org/10.1016/B978-0-08-101743-2.00007-8
17. Gerstein, D.E., Woodward-Lopez, G., Evans, A.E., Kelsey, K., Drewnowski, A. (2004). Clarifying concepts about macronutrients' effects on satiation and satiety. *Journal of the American Dietetic Association*, *104*(7), 1151–1153. https://doi.org/10.1016/j.jada.2004.04.027
18. Hervik, A.K., Svihus, B. (2019). The role of fiber in energy balance. *Journal of Nutrition and Metabolism*, *2019*, art. no. 4983657. https://doi.org/10.1155/2019/4983657
19. Holt, S.H.A., Miller, J.C.B., Petocz, P., Farmakalidis, E. (1995). A satiety index of common foods. *European Journal of Clinical Nutrition*, *49*(9), 675–690.
20. Huh, I.S., Kim, H., Jo, H.K., Lim, C.S., Kim, J.S., Kim, S.J., Kwon, O., Oh, B., Chang, N. (2017). Instant noodle consumption is associated with cardiometabolic risk factors among college students in Seoul. *Nutrition Research and Practice*, *11*(3), 232–239. https://doi.org/10.4162/nrp.2017.11.3.232
21. Iju, S., Sarinah, Rejeki, S. (2025). Formulation of instant baby porridge from red rice flour substituted with moringa (*Moringa oleifera*) leaf flour and natural banana (*Musa paradisiaca*) flavor as an alternative complementary food to breast milk. *Jurnal Gizi dan Pangan*, *3*(2), 241–260 (in Indonesian, English abstract).
22. Indonesian Food and Drug Authority (2022). Regulation of Indonesian Food and Drug Authority Number 1 of 2022 About Monitoring Claims on Processed Food Label and Food Advertisement. Jakarta: Indonesian Food and Drug Authority.
23. ISO 8586 (2014). Sensory analysis – General guidelines for the selection, training and monitoring of selected assessors and expert sensory assessors.
24. Jahanshiri, E., Goh, E.V., Wimalasiri, E.M., Azam-Ali, S., Mayes, S., Suhairi, T.A.S.T.M., Nizar, N.M.M., Sinin, S.S.M. (2022). The potential of bambara groundnut: an analysis for the People's Republic of China. *Food and Energy Security*, *11*(2), art. no. e358. https://doi.org/10.1002/fes3.358
25. Jamaiyah, H., Geeta, A., Safiza, M.N., Khor, G.L., Wong, N.F., Kee, C.C., Rahmah, R., Ahmad, A.Z., Suzana, S., Chen, W.S., Rajaah, M., Adam, B. (2010). Reliability, technical error of measurements and validity of length and weight measurements for children under two years old in Malaysia. *Medical Journal of Malaysia*, *65*(Suppl. A), 131–137.
26. Kudre, T.G., Benjakul, S. (2013). Effects of binary organic solvents and heating on lipid removal and the reduction of beany odour in Bambara groundnut *(Vigna subterranean)* flour. *Food Chemistry*, *141*(2), 1390–1397. https://doi.org/10.1016/j.foodchem.2013.04.047
27. Makhuvha, M.C., Laurie, S., Mosala, M. (2024). Effect of orange-fleshed sweet potato (*Ipomoea batatas*)–Bambara groundnut (*Vigna subterranea*) composite flour on quality properties of pasta. *Journal of Food Science*, *89*(11), 7348–7359. https://doi.org/10.1111/1750-3841.17432
28. Maphosa, Y., Jideani, V. A., Maphosa, L. (2022). Bambara groundnut production, grain composition and nutritional value: Opportunities for improvements. *Journal of Agricultural Science*, *160*(6), 448–458. https://doi.org/10.1017/S0021859622000521
29. Mashau, M.E., Mukwevho, T.A., Ramashia, S.E., Siwela, M. (2022). The influence of Bambara groundnut (*Vigna subterranean*) flour on the nutritional, physical and antioxidant properties of steamed bread. *CyTA – Journal of Food*, *20*(1), 259–270. https://doi.org/10.1080/19476337.2022.2130435
30. Ministry of Health Indonesia (2019). National Basic Health Research Report 2018. Jakarta: Ministry of Health Indonesia. https://repository.kemkes.go.id/book/1323
31. Mo, Y., Ma, X., Lu, J., Shen, Y., Wang, Y., Zhang, L., Lu, W., Zhu, W., Bao, Y., Zhou, J. (2021). Defining the target value of the coefficient of variation by continuous glucose monitoring in Chinese people with diabetes. *Journal of Diabetes Investigation*, *12*(6), 1025–1034. https://doi.org/10.1111/jdi.13453
32. Moshawih, S., Kong, J.P.T., Goh, B.H., Renganathan, E., Goh, H.P., Goh, K.W., Ming, L.C. (2025). Exploring the nutritional, cultural, and industrial significance of *Metroxylon sagu*. *Discovery Food*, *5*, art. no. 337. https://doi.org/10.1007/s44187-025-00638-6

33. Nguyen, T.N., Tran, T.T.T., Le, V.V.M. (2025). Effects of blanching conditions on the enzyme inhibition and antioxidant loss in rambutan (*Nephelium lappaceum* L.) seeds. *Polish Journal of Food and Nutrition Sciences*, *75*(1), 49–59. **https://doi.org/10.31883/pjfns/200589**
34. Nolan, S.J., Hambleton, I., Dwan, K. (2016). The use and reporting of the cross--over study design in clinical trials and systematic reviews: a systematic assessment. *PLoS One*, *11*(7), art. no. e0159014. **https://doi.org/10.1371/journal.pone.0159014**
35. Palamae, S., Suyapoh, W., Boonrat, O., Zhang, B., Amin, M., Buatong, J., Benjakul, S. (2024). Activity of bambara groundnut seed coat extract against *Shewanella* species: efficacy and mechanisms of action. *Foods*, *13*(21), art. no. 3516. **https://doi.org/10.3390/foods13213516**
36. Palupi, E., Nurdin, N.M., Mufida, G., Valentine, F.N., Pangestika, R., Rimbawan, Sulaeman, A., Briawan, D., Filianty, F. (2024). High-fiber extruded purple sweet potato (*Ipomoea batatas*) and kidney bean (*Phaseolus vulgaris*) extends the feeling of fullness. *Polish Journal Food and Nutrition Sciences*, *74*(1), 82–91. **https://doi.org/10.31883/pjfns/183995**
37. Pretorius, B., Otto, M., Schönfeldt, H.C. (2023). Antinutrients and metabolomic compounds of Bambara groundnut (*Vigna subterranean*) as affected by traditional processing by smallholder farmers. *Journal of Food Science*, *88*(8), 3435–3444. **https://doi.org/10.1111/1750-3841.16698**
38. Ridwan, M., Palupi, E., Setiawan, B., Heksana, R.A.R. (2024). Bambara bean substitution improves the nutritional content and increases the satiety index of purple sweet potato bread. *Preventive Nutrition and Food Science*, *29*(4), 512–521. **https://doi.org/10.3746/pnf.2024.29.4.512**
39. Salihu, S., Elezaj, B., Qorri, D., Gashi, N. (2025). Exploring instant noodle consumption patterns and consumer awareness in Kosovo. *Foods*, *14*(24), art. no. 4245. **https://doi.org/10.3390/foods14244245**
40. Savastano, D.M., Hodge, R.J., Nunez, D.J., Walker, A., Kapikian, R. (2014). Effect of two dietary fibers on satiety and glycemic parameters: a randomized, double--blind, placebo-controlled, exploratory study. *Nutrition Journal*, *13*, art. no. 45. **https://doi.org/10.1186/1475-2891-13-45**
41. Septiani, M., Sugiatmi, S. (2026). Relationship between ultra-processed food consumption patterns and physical activity with overnutrition in adolescents of SMK Kesehatan YHB Sukabumi. *Jurnal Imu Gizi dan Dietetik*, 5(1), 423–430 (in Indonesian, English abstract). **https://doi.org/10.25182/jigd.2026.5.1.423-430**
42. Singthong, J., Oonmetta-aree, J., Oonsivilai, R. (2026). Impact of red kidney bean flour substitution on the nutritional, physicochemical, and functional properties of gluten-free noodles. *Food Chemistry Advances*, *11*, art. no. 101279. **https://doi.org/10.1016/j.focha.2026.101279**
43. Tan, X.L., Azam-Ali, S., Goh, E.V., Mustafa, M., Chai, H.H., Ho, W.K., Mayes, S., Mabhaudhi, T., Azam-Ali, S., Massawe, F. (2020). Bambara groundnut: An underutilized leguminous crop for global food security and nutrition. *Frontiers in Nutrition*, *7*, art. no. 601496. **https://doi.org/10.3389/fnut.2020.601496**
44. Ulijaszek, S.J., Kerr, D.A. (1999). Anthropometric measurement error and the assessment of nutritional status. *British Journal of Nutrition*, *82*(3), 165–177. **https://doi.org/10.1017/S0007114599001348**
45. WHO (2024). World Health Organization. Overweight and Obesity. UK. **https://www.who.int/news-room/fact-sheets/detail/obesity-and--overweight**

ORIGINAL ARTICLE
http://journal.pan.olsztyn.pl

Polish Journal of Food and Nutrition Sciences
2026, Vol. 76, No. 2, 173–188
DOI: 10.31883/pjfns/220853
ISSN 1230-0322, e-ISSN 2083-6007

Comparative Effects of *Origanum onites* L. Extract and Carvacrol on the Metabolic Syndrome and Hepatic/Pancreatic Inflammatory Markers in Rats

Kübra Öztürk[1], Seda Koçak[2]*, Emine Bilginoğlu[3], Halime Tozak-Yıldız[4], Ali Güneş[5]

[1]Department of Genetics and Bioengineering, Faculty of Engineering and Architecture, Kırşehir Ahi Evran University, 40100 Kırşehir, Türkiye
[2]Department of Physiology, Faculty of Medicine, Kırşehir Ahi Evran University, 40100 Kırşehir, Türkiye
[3]Department of Field Corps, Medicinal and Aromatic Plants, Faculty of Agriculture, Kırşehir Ahi Evran University, 40100 Kırşehir, Türkiye
[4]Department of Histology and Embryology, Faculty of Medicine, Kırşehir Ahi Evran University, 40100 Kırşehir, Türkiye
[5]Department of Pediatrics, Faculty of Medicine, Kırşehir Ahi Evran University, 40100 Kırşehir, Türkiye

This study investigated the effects of an *Origanum onites* L. extract, carvacrol, and metformin on the metabolic syndrome (MetS) induced by a high-fat, high-fructose diet (HFFD) in rats. Oregano was extracted using supercritical CO_2, and profiles of phenolics and volatile organic compounds were analyzed *via* high-performance liquid chromatography and gas chromatography–mass spectrometry methods, respectively. Rats with MetS were treated with carvacrol (MetS +CRV group), the oregano extract (MetS+OREG group), and metformin (MetS+METF group). In the two remaining groups, rats were fed only HFFD (MetS group) and a standard diet (control group). Treatments were administered daily during the final 4 weeks of a 10-week MetS induction period. Evaluations included body weight, blood pressure, blood glucose, serum lipid profile and liver function parameters, selenoprotein P (SeP), TNF-α, and histopathology of the liver and pancreas. The Lee index was significantly higher in the METS group (0.30) than in the control group (0.27), indicating greater metabolic disturbance. Liver SeP level increased in the MetS group (227.1 ng/mL) *vs*. control (144.3 ng/mL). The oregano extract and carvacrol did not significantly affect SeP levels. However, they both reduced systolic blood pressure and improved blood glucose level in the oral glucose tolerance test. Serum aspartate aminotransferase (AST) and alanine aminotransferase (ALT) levels were elevated in the MetS group but decreased with the oregano extract and carvacrol treatment. Histopathology showed that the MetS+CRV group had hepatocyte architecture resembling the control, with slight sinusoidal dilation and minimal necrosis. The MetS+OREG group also showed reduced degeneration. Overall, the oregano extract and carvacrol improved metabolic parameters and hepatic function. Further research is needed, however, to elucidate their long-term impact on selenium metabolism and tissue-specific SeP regulation in MetS.

Keywords: bioactive phytochemicals, high-fat high-fructose diet, histopathology, selenoprotein P, TNF-α

ABBREVIATIONS

ALT, alanine aminotransferase; AMPK, AMP-activated protein kinase; HFFD, high-fat and fructose diet; AST, aminotransferase; AUC, area under the curve; SC-CO2, supercritical CO_2; CRV, carvacrol; OREG, oregano; METF, metformin; HDL, high-density lipoprotein; LDL, low-density lipoprotein; MetS, metabolic syndrome;

***Corresponding Author:**
E-mail: **seda.kocak@ahievran.edu.tr** (Dr. S. Kocak)

Submitted: 16 October 2025
Accepted: 21 April 2026
Published on-line: 1 June 2026

OGTT, oral glucose tolerance test; SeP, selenoprotein P; T2DM, type 2 diabetes mellitus; TG, triglycerides; TNF-α, tumor necrosis factor.

INTRODUCTION

Metabolic syndrome (MetS) encompasses multiple metabolic disorders including abdominal obesity, insulin resistance, glucose intolerance, inflammation, low high-density lipoprotein (HDL) cholesterol levels, high triglyceride (TG) levels, and hypertension [Gunawan *et al.*, 2021]. It is also associated with chronic conditions, such as type 2 diabetes mellitus (T2DM), dyslipidemia, cardiovascular disease, and non-alcoholic fatty liver disease. Its incidence increases with obesity epidemics, affecting about a quarter of the world population and increasing the risk of chronic diseases and creating a serious burden on the health system [Saklayen, 2018]. Although the etiopathogenesis of MetS is not fully understood due to its heterogeneous nature, its short- and long-term complications are important.

Although lifestyle changes and pharmaceutical interventions are generally preferred in MetS treatment, the long-term side effects and high costs of these methods make traditional herbal approaches a complementary alternative important to investigate. Moreover, pharmaceutical interventions are mono-therapeutic and usually target several health outcomes associated with metabolic dysfunction. In this context, medicinal plants containing synergistic and pharmacodynamic bioactive compounds draw attention as therapeutic or preventive agents to manage metabolic disorders [Rodriguez-Casado, 2016].

Carvacrol, one of the main compounds of oregano essential oil, has the potential to be used as a valuable food additive [Ayres Cacciatore *et al.*, 2020; Elbouny *et al.*, 2025]. It exhibits a wide range of biological activities, including anti-inflammatory, immunomodulatory, antioxidative, antitumor, antibacterial, anti-apoptotic, and neuroprotective ones [Sharifi-Rad *et al.*, 2018]. Current research also suggests that it is a compound with therapeutic potential in MetS management [Khalil *et al.*, 2022; Khazdair *et al.*, 2024]. However, although studies on the effects of carvacrol in isolation are increasing, studies examining the effects of an oregano extract as a whole on MetS are limited, and thus more comprehensive evaluations are needed. In this context, some *in vivo* studies investigating the effects of *Origanum* species on MetS-related parameters have revealed that oregano extracts may show ameliorative effects on glucose homeostasis, lipid metabolism, and hepatic functions [Abou-Seif & Hozayen, 2023; Elbouny *et al.*, 2025; Lieshchova & Brygadyrenko, 2022]. For example, in rats with obesity and liver damage induced by high-fat diet, *Origanum vulgare* L. extract decreased body weight, serum aspartate aminotransferase (AST) and alanine aminotransferase (ALT), total cholesterol, TG and low-density lipoprotein (LDL) cholesterol levels, while increasing HDL cholesterol levels [Lee *et al.*, 2024]. In addition, it contributed to the improvement of steatosis by suppressing the expression of genes involved in hepatic lipogenesis. Similarly, in diabetic and hyperlipidemic rats treated with *Origanum majorana* L. extract, hyperglycemia, hyperinsulinemia, and hepatic adiposity were reported to be markedly reduced [Pasavei *et al.*, 2020]. Although the effects of *Origanum onites* L. on MetS have not yet been sufficiently studied, a clinical study in individuals with mild hyperlipidemia reported that regular consumption of the aqueous distillate obtained from this species exerted positive effects on the lipid profile, inflammatory markers, and antioxidant enzyme activities [Özdemir *et al.*, 2008]. These data indicates that *O. onites* extract, which carries the pharmacological effects of carvacrol, is a promising natural agent for the prevention or management of MetS and scientifically supports its investigation in experimental models.

Most previous studies have utilized oregano extracts obtained through conventional extraction techniques, such as hydrodistillation or solvent extraction [Gheitasi *et al.*, 2021; Pasavei *et al.*, 2020], which may involve high solvent consumption, prolonged extraction times, and potential thermal degradation of bioactive compounds [Bitwell *et al.*, 2023]. Additionally, the incomplete removal of organic solvents (such as methanol or hexane) commonly used in traditional extraction can affect the purity of the extract and raise safety concerns. In recent years, green extraction technologies have attracted increasing attention as safer and more sustainable alternatives. Among these, supercritical fluid extraction (SFE) using carbon dioxide (CO_2) has emerged as a particularly advantageous method for natural product extraction. SFE exploits the unique properties of supercritical fluids – high density, high diffusivity, low viscosity, and the absence of surface tension – resulting in efficient mass transfer and selective extraction of bioactive compounds. CO_2 is the most widely used supercritical fluid due to its non-toxic, non-flammable, and chemically inert nature, wide availability, and relatively mild critical conditions (critical temperature, Tc=31.1°C; critical pressure, Pc=73.8 bar) [Roko *et al.*, 2024]. The extraction process is conducted in a closed system, isolated from air and light, thereby minimizing degradation of sensitive compounds. In addition, CO_2 is generally recognized as safe (GRAS), and supercritical CO_2 extraction (SC-CO_2) yields solvent-free, highly concentrated extracts suitable for applications relevant to both the food and pharmaceutical industries. Although SC-CO_2 is inherently non-polar, its solvating power and selectivity can be modulated through the use of co-solvents, enabling efficient extraction of a broad range of phytochemicals [Gregorius *et al.*, 2019; Uwineza & Waśkiewicz, 2020]. Despite these well-documented advantages, the application of SC-CO_2 in studies evaluating oregano extracts within the context of the metabolic syndrome remains limited.

Given the above, the present study aimed to investigate the biochemical, physiopathological, and histopathological effects of administering an oregano plant extract obtained through a green extraction method, along with its active compound – carvacrol, in a rat model of metabolic syndrome. Additionally, its strived to elucidate how oregano and carvacrol influence selenoprotein P (SeP) levels in pancreatic and liver tissues and to identify their role in the pathophysiology of MetS.

MATERIALS AND METHODS

Source of plant material

Oregano (*O. onites*) plant, which was cultivated at the Kırşehir Ahi Evran University, AHIGETAM (Kırşehir Ahi Evran University Traditional and Complementary Medicine Application and Research Centre) Medicinal and Aromatic Plants Application and Research Area (39.137684 N and 34.155483 W, altitude 982), was harvested in its 3rd year on 20 July 2023. The aired parts of *O. onites* were dried in the shade at ambient temperature and packed in kraft paper to be prepared for analysis.

Extraction of plant material

The dried oregano was ground, and its 150-g portion was placed in a stainless-steel vessel of a supercritical fluid extraction device (F-500, Superex, Konya, Turkey). The sample was fixed between layers of glass wool at the top and bottom of the vessel. The extraction process was carried out fully automatically under 20 MP pressure, 40°C for 3 h, and the CO_2 flow rate kept constant at 5 g/min throughout the time. The extract obtained was stored at −20°C to be used in experimental studies. The total extract amount obtained from a single extraction batch was 6.82 g, corresponding to an extraction yield of 4.55 g/100 g dried oregano (*w/w*). In total, eight extraction batches were prepared for the *in vivo* experiments, and the extracts were pooled prior to use.

Analysis of phenolic and volatile organic compound profiles

The phenolic compounds of the oregano extract were analyzed using a reverse phase high performance liquid chromatography (RP-HPLC) method reported by Caponio *et al.* [1999] with modification. Analysis was performed using a system consisting of a 20ACBM system control unit, an SPD-M20A diode array detector, a CTO-10ASVp column oven, an SIL-20ACHT autosampler, and an LC-20AT pump (Shimadzu, Kyoto, Japan). Data were analyzed using LC Solution software (Shimadzu). Chromatographic separations were achieved using a Zorbax C18 column (250×4.6 mm, 5 µm particle size; Agilent Technologies, Santa Clara, CA, USA), and signals from the eluate were monitored at wavelengths of 280 nm and 320 nm. The column temperature was fixed at 30°C. Solvent A (water containing 3% (*v/v*) formic acid) and solvent B (methanol) were used as a mobile phase by gradient elution. The following elution program was applied at a flow rate of 0.8 mL/min: 93% A + 7% B for 3 min, 72% A + 28% B in 28 min, 67% A + 33% B in 60 min, 58% A + 42% B in 62 min, 50% A + 50% B in 70 min, 30% A + 70% B in 75 min, and 93% A + 7% B in 90 min. The extract was dissolved in the mobile phase and after passing through a 0.45 µm polytetrafluoroethylene filter, 20 µL of a sample solution were injected into the HPLC system. Phenolic compounds were identified by comparing their retention times with those of authentic reference standards. All analytical standards were purchased from Sigma-Aldrich (St. Louis, MO, USA). Quantification was performed using external standard calibration curves constructed at multiple concentration levels. Results were expressed as mg/kg of dry extract.

Volatile organic compounds of the oregano extract administered to the animals were analyzed using a 7890 A gas chromatograph connected to an MSD 5975 C series mass spectrometer (Agilent Technologies) and resolved on a CP WAX 52 CB capillary column (50 m × 0.32 mm ID, 1.2 µm, Agilent Technologies). Helium was used as carrier gas at a flow rate of 1.2 mL/min. Temperature conditions for gas chromatography (GC) were: 60°C initial temperature, 2 min at 60°C, then increasing to 220°C at 2°C/min, after which the temperature was kept constant for 20 min. A 1-µL aliquot was injected in a split mode (20:1). The mass spectrometry (MS) ion source temperature was set at 230°C, and the MS-quadrupole temperature at 150°C. Mass spectra were recorded in the range of 30–500 atomic mass units (amu) and under electron pulse ionization at an electron energy of 70 eV. The identification of the compounds was made by comparing their mass spectra with the Wiley Registry of mass spectral data, 11th edition (John Wiley & Sons, Inc., Hoboken, NJ, USA). Spectrum integrations were performed using MSDCHEM software (Agilent Technologies). Quantification was performed by peak area normalization, and the results were expressed as relative percentages of the total ion chromatogram (TIC).

Animals and experimental design

Wistar albino rats (≈130 g average body weight) were obtained from the Kırşehir Ahi Evran University Experimental Research Centre in Turkey. Before and during the experiment, all animals were housed in rooms with 12 h light and 12 h dark photoperiod and a constant temperature of 22–24°C. The experimental protocol was approved by the Experimental Animals Ethics Committee of Kırşehir Ahi Evran University (Ethics No: 2023/23/4). Prior to the treatment period, animals were gently handled and accustomed to the gavage procedure through a short acclimatization period to minimize stress.

During the experimental period, animals had access to water and feed *ad libitum*. To induce MetS, the rats were fed a high-fat, high-fructose diet (HFFD). This type of diet was chosen because MetS induced by high-carbohydrate and high-fat dietary mixtures has been shown to better mimic the disease state in humans compared to other methods of inducing the syndrome [Gunawan *et al.*, 2021]. HFFD was formulated based on previously published high-fat diet models, with modifications [Gunawan *et al.*, 2021; Wang *et al.*, 2015]. The diet composition (g/kg diet) was as follows: casein (177 g), L-cystine/DL-methionine (3 g), corn starch (100 g), fructose (262 g), maltodextrin (30 g), cellulose (50 g), butter as a fat source (310 g), corn oil (10 g), mineral mix (10 g), dicalcium phosphate (13 g), calcium carbonate (5.5 g), potassium citrate (16.5 g), vitamin mix (10 g), choline bitartrate (2 g), and food colorant (1 g).

The animals were divided into five groups. In the control group (n=8), the rats were provided with standard rat chow

and tap water throughout the experiment. Rats of the MetS group (n=8) were fed a HFFD, which was provided *ad libitum* as free feeding every day for 10 weeks. Rats of the MetS+CRV group (n=8) were administered HFFD for 6 weeks and at the beginning of the 7th week, 75 mg of carvacrol *per* kg of body weight was administered by oral gavage every day for 4 more weeks along with HFFD. The dose of carvacrol was determined based on findings from a previous study [Shoorei *et al.*, 2019]. Pure carvacrol (≥98% purity) was purchased from Sigma-Aldrich (St. Louis, MO, USA). The next MetS+OREG group (n=8), was treated with HFFD for 6 weeks, and at the beginning of the 7th week, an oregano extract was administered by oral gavage every day for 4 more weeks at a dose of 500 mg/kg body weight [Raeeszadeh *et al.*, 2024] along with HFFD. In the MetS+METF group (n=8), the rats were fed HFFD for 6 weeks and at the beginning of the 7th week, metformin (Glukofen, Sandoz, Basel, Switzerland) was administered by oral gavage every day for 4 more weeks at a dose of 300 mg/kg body weight [Ajiboye *et al.*, 2016] along with HFFD.

Morphometric analysis of obesity induction

Body weight gain and Lee index were calculated as indicators of obesity. Body weight was measured weekly using an electronic weighing scale. The length of the rats was measured between the nasal and anal region. The recorded measurements were used to calculate the Lee index according to Equation (1):

$$\text{Lee index} = \frac{\sqrt[3]{\text{Body weight (g)}}}{\text{Nasal–anal length (cm)}} \quad (1)$$

Blood pressure measurement

Non-invasive tail-cuff blood pressure measurements were performed in rats using a MAY-NIBP250 system (MAY Biotechnology, Ankara, Turkey). Cuffs were routinely checked for patency before experiments. All measurements were conducted in a designated quiet area (22±2°C), and rats were acclimatized for 1 h prior to recording. Animals were gently guided into restraint tubes to minimize movement, with the occlusion cuff placed at the base of the tail and the sensor cuff positioned adjacent to it. A heating chamber maintained at 32°C was used, and rats were warmed for 5 min before and during recordings. Blood pressure was measured by inflating the occlusion cuff to 250 mmHg and deflating over 15 s, while the sensor cuff detected volume changes in the tail. Rats were habituated for at least 7 consecutive days before baseline measurements. For each animal, a total of five measurements were taken at 1-min intervals. The highest and lowest values were excluded, and the mean of the remaining three measurements was used to obtain systolic pressure (SP), diastolic pressure (DP), heart rate, and mean arterial pressure (AP) data. Mean AP was calculated using Equation (2):

$$\text{Mean AP} = \text{DP} + \frac{\text{SP} - \text{DP}}{3} \quad (2)$$

Oral glucose tolerance test

Oral glucose tolerance test (OGTT) was performed in rats fasted for 12 h at the end of the experiment. Blood glucose levels of the rats before glucose loading (minute 0) were measured by an ACCU-Check device (Roche Diagnostics, Mannheim, Germany) from blood taken from tail veins. Then, a 50% (*w/v*) glucose solution was administered to the rats at a dose of 2 g/kg body weight by oral gavage, and blood glucose levels were measured at 30, 60, 90, and 120 min after glucose loading. The area under the curve (AUC) of the OGTT was calculated.

Tissue collection

At the end of the experiment, the animals were fasted overnight, and then the rats from all groups were decapitated under anesthesia with ketamine 75 mg/kg + xylazine 10 mg/kg intraperitoneally. Blood samples collected after decapitation were placed into gold top tubes without ethylenediaminetetraacetic acid (EDTA), and then centrifuged at 5,700×*g* for 15 min at 4°C to separate the serum. The liver and pancreas were excised, weighed, and then cut into pieces for storage at −80°C. Liver and pancreas tissue samples were also placed in a 10% formaldehyde solution for histological analysis.

Evaluation of gross changes in the liver and adipose tissue

At the end of the experiment, after decapitation, the organs of the rats were excised, excess blood was removed, and weighed on a precision balance and recorded. Additionally, the accumulation of abdominal adipose tissue, including omental, retroperitoneal, and epididymal fat, was observed *in situ*, and the weighing results were recorded. Results were expressed as absolute organ weights (g).

Biochemical analysis of rat serum and tissue samples

Rat serum TG, LDL, HDL, ALT, and AST were analyzed by an autoanalyzer (Mindray-BS400, Mindray Bio-Medical Electronics Co., Ltd., Shenzhen, China) using commercial kits Ottobc155, Ottobc145, Ottobc144, Ottobc128, and Ottobc127 (Otto Scientific, Otto Scientific, Miami, FL, USA), respectively. SeP and tumor necrosis factor-α (TNF-α) levels in the liver and pancreas of rats were evaluated using enzyme-linked immunosorbent assay (ELISA) kits (Cat. No: 201-11-0765 and 201-11-1158, respectively; SunredBio, Shanghai, China).

Histopathological analysis

Liver and pancreas tissue samples obtained from all rats were initially fixed in a 10% formaldehyde solution for at least 72 h for light microscopic examination. After fixation, the tissue samples were placed in cassettes and washed under running water for 24 h. To remove water, the tissues were dehydrated through a graded ethanol series (50%, 70%, 80%, 90%, 100%). Subsequently, they were cleared in xylene and then embedded in molten paraffin. Sections of 4–5 µm thickness obtained from the prepared paraffin blocks were stained with hematoxylin-eosin

(H&E) (Bio-Optica, Milan, Italy; 05-06004/L Harris' hematoxylin and 05-10002/L eosin Y 1%). The stained sections of liver were assessed for hydropic degeneration and coagulative necrosis in hepatocytes, dilatation in sinusoids, and hyperemia in blood vessels. The pancreatic islets were additionally evaluated for islet histomorphology, cellular changes, and degenerations. In each liver and pancreas section, 10 different areas were scored for each damage parameter, and the average percentage values within the group were calculated. Histopathological changes were graded for liver as follows: 1 (mild) when observed in less than 25% of the tubular epithelium and islet architecture, 2 (moderate) when observed in 25-50%, 3 (severe) when observed in more than 50–75%, and 4 (very severe) when observed in 75–100% (none = 0, mild = 1, moderate = 2, severe = 3, very severe = 4).

Statistical analysis

Statistical analyses were performed using GraphPad Prism version 9.0 (GraphPad Software, San Diego, CA, USA). Data distribution was assessed for normality prior to statistical analysis. Normally distributed data are presented as the mean and standard deviation (SD), whereas non-normally distributed data are presented as the median. For normally distributed data, differences between groups were evaluated using one-way analysis of variance (one-way ANOVA), followed by Tukey's post hoc test for multiple comparisons. Non-parametric tests, such as the Kruskal–Wallis and Mann–Whitney U tests, were used when the assumption of normality was not satisfied. Differences were considered statistically significant at $p<0.05$.

RESULTS AND DISCUSSION

Chemical profile of the *Origanum onites* L. extract

The phenolic compounds of the *O. onites* extract obtained with the SC-CO_2 method were quantitatively determined by HPLC analysis (**Table 1**). The phenolic acid detected in the highest content was gallic acid (66.01 mg/kg dry extract). This compound is well known as an antioxidant and can significantly contribute to the antioxidant capacity of the extract. Compounds such as caffeic acid and rosmarinic acid were also found at high contents (25.49 and 24.79 mg/kg, respectively). Their anti-inflammatory and antioxidative effects have been widely reported in the literature [Kassa *et al.*, 2021; Xiang *et al.*, 2022]. Rutin (43.09 mg/kg), luteolin (21.28 mg/kg), and apigenin (26.44 mg/kg) were the major flavonoids. These phenolic compounds increase the cell-protective, vascular health-promoting, and antioxidative potential of the extract [Li *et al.*, 2024]. Compounds, such as quercetin, cinnamic acid, vanillic acid, *p*-coumaric acid, and hesperidin, which were detected in low contents, may act synergistically and enhance biological activity.

The volatile organic compound profile of the oregano extract, revealed 59 compounds (**Table S1** in Supplementary Materials). They accounted for 9.74% of TIC peak area. The most dominant compound was carvacrol, which accounted for 64.65% of the total volatile organic compounds. This monoterpenic phenolic compound plays an important role in the therapeutic effects of *O. onites*, including its anti-inflammatory, antioxidative, and metabolic regulatory activities, which have been associated with improvements in metabolic disturbances, such as dyslipidemia, oxidative stress, and inflammation [Khazdair *et al.*, 2024]. Other important volatile compounds of the extract were linalool (10.22%), thymol (4.12%), β-caryophyllene (1.30%), and β-bisabolene (1.36%), *i.e.*, molecules with known anti-inflammatory, antioxidative, and metabolic regulatory effects [Jugreet & Mahomoodally, 2020; Stojanović *et al.*, 2024].

Table 1. Content of phenolic compounds in the *Origanum onites* L. extract obtained by supercritical CO_2 extraction.

Compound	R.T. (min)	Content (mg/kg dry extract)	LOD (ppm)
Gallic acid	6.8	66.01±3.30	0.01
Chlorogenic acid	18.2	0.56±0.03	0.01
Vanillic acid	19.2	0.04± 0.00	0.11
Caffeic acid	22.7	25.49±1.53	0.01
p-Coumaric acid	26.1	0.35± 0.03	0.01
Ferulic acid	30.1	2.74±0.16	0.01
Rutin	45.6	43.10±2.12	0.57
Naringin	49.7	7.56±0.45	0.40
Hesperidin	51.1	0.51±0.04	0.80
Rosmarinic acid	61.9	24.79±1.24	0.68
Luteolin	65.3	21.29±1.06	0.05
Apigenin	67.0	26.44±1.32	0.04
Quercetin	67.2	0.22±0.02	0.60
Cinnamic acid	71.1	0.04±0.00	0.01

Results are shown as mean ± standard deviation. R.T., retention time; LOD, limit of detection.

The chromatographic data obtained reveal that SC-CO_2 extraction yielded high contents of phenolic, volatile and semi-volatile compounds, and that the extract obtained presents a complex compound profile with potential for therapeutic use.

Weight of body, liver, and intra-abdominal adipose tissue in rats

There was no significant difference in the body weight of rats between the groups at the beginning of the experiment ($p\geq0.05$) (**Figure 1**). At the end of the study (week 10), the body weight of MetS group rats fed the HFFD diet was 375.1 g and was significantly higher ($p=0.014$) compared to the control group (236.4 g). When the MetS group animals were compared with those of the MetS+METF group, they had a significantly higher body weight ($p=0.012$). No significant difference was observed in the groups administered the oregano extract and carvacrol compared to the other groups ($p\geq0.05$). The Lee index of the MetS group was significantly higher ($p<0.01$) compared to the control group (0.30 *vs.* 0.27) (**Figure 2**). Moreover, a lower

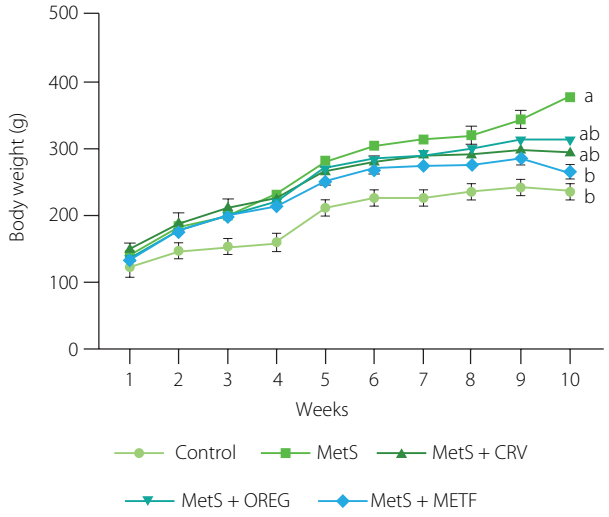

Figure 1. Body weights of rats with induced metabolic syndrome (MetS) and treated with carvacrol (MetS+CRV), oregano extract (MetS+OREG) or metformin (MetS+METF), as well as rats without induced MetS (control) over a 10-week period. Data are represented as mean and standard derivation. Different letters indicate significant differences between the groups in week 10 ($p<0.05$).

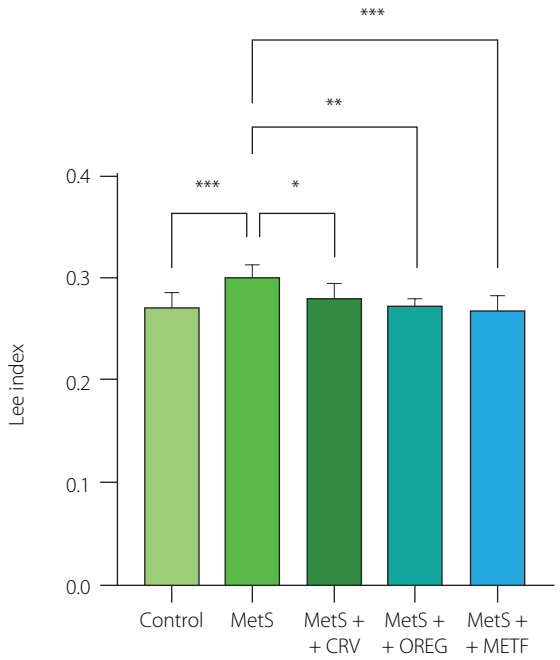

Figure 2. Lee index of rats with induced metabolic syndrome (MetS) and treated with carvacrol (MetS+CRV), oregano extract (MetS+OREG) or metformin (MetS+METF), as well as rats without induced MetS (control) at the end of the 10-week period. Data are represented as mean and standard derivation. Significant differences between groups are indicated with asterisks (*$p<0.05$, **$p<0.01$, ***$p<0.001$).

Lee index was computed for the MetS+CRV (0.28), MetS+OREG (0.27), and MetS+METF (0.27) groups compared to the MetS group at *p*-values of 0.033, 0.020, and <0.01, respectively.

Rat liver and intra-abdominal adipose tissue (including omentum, retroperitoneal, and epididymal adipose tissues) weights are presented in **Figure 3**. Liver weights were higher in the MetS+CRV group (11.00 g) and the MetS+METF group (11.07 g) compared with the control group (8.17 g) at $p=0.045$ and $p=0.038$, respectively. Intra-abdominal adipose tissue analysis also showed that the rats from the MetS group and the MetS+CRV group had significantly higher weights of this tissue when compared to the control animals (9.33 and 7.71 *vs*. 2.65 g, respectively; $p<0.001$) Oregano extract treatment significantly lowered the weight of intra-abdominal adipose tissue to 5.86 g compared to the MetS group ($p=0.011$). Intra-abdominal adipose tissue level in the MetS+METF group was also significantly lower (5.86 g) compared to that determined in the MetS group ($p=0.022$).

To sum up, the results of this study showed that HFFD administered for 10 weeks promoted obesity parameters that are effective in MetS formation by increasing body weight, liver size, Lee index as well as omental, retroperitoneal, and epididymal fat content. However, oregano extract and carvacrol administration significantly decreased the Lee index of obese rats. Moreover, carvacrol supplementation reduced omental, retroperitoneal, and epididymal fat levels, while oregano extract also led to a significant reduction in these fat depots. Another study demonstrated that oregano seed extract administration reduced weight gain in rats administered a high-fat diet [Lee *et al.*, 2023]. This effect may be due to the presence of phytochemicals that inhibit the pancreatic lipase enzyme by preventing the absorption of dietary fat, thereby increasing fecal excretion of fats and reducing the energy intake of animals. Previous reports have shown that plants rich in phytochemicals, such as saponins, flavonoids, alkaloids and terpenoids, exhibit anti-obesity activity [Rajan *et al.*, 2020]. In the present study, although no significant decrease in body weight was observed among the treatment groups (MetS, MetS+CRV and MetS+OREG), a significant reduction in the Lee index was detected. Since the Lee index is a parameter that takes into account not only body weight but also body length, this finding suggests a favorable change in body composition. The decrease in the Lee index, despite the unchanged body weight, may be attributed to the suppression of visceral adiposity. This suggests the potential of oregano extract and carvacrol to improve body composition without weight loss. Thus, the anti-obesity effects of these compounds may extend beyond weight reduction and involve changes in fat distribution and metabolic profile.

The results indicate that the metabolic syndrome increased liver and intra-abdominal fat accumulation, whereas both oregano extract and metformin treatments mitigated this adverse effect. The observation that oregano extract's effect was comparable to that of metformin suggests that this herbal treatment may exert potential anti-metabolic or lipid-regulating effects.

Hemodynamic parameters

Analysis of systolic and diastolic blood pressure in rats indicated that values of the MetS group were higher compared to those noted in the control group (**Table 2**). However, the treatments with oregano extract, carvacrol, and metformin reduced the systolic blood pressure. More precisely, its values were significantly lower in the MetS+CRV, MetS+OREG, and MetS+METF groups

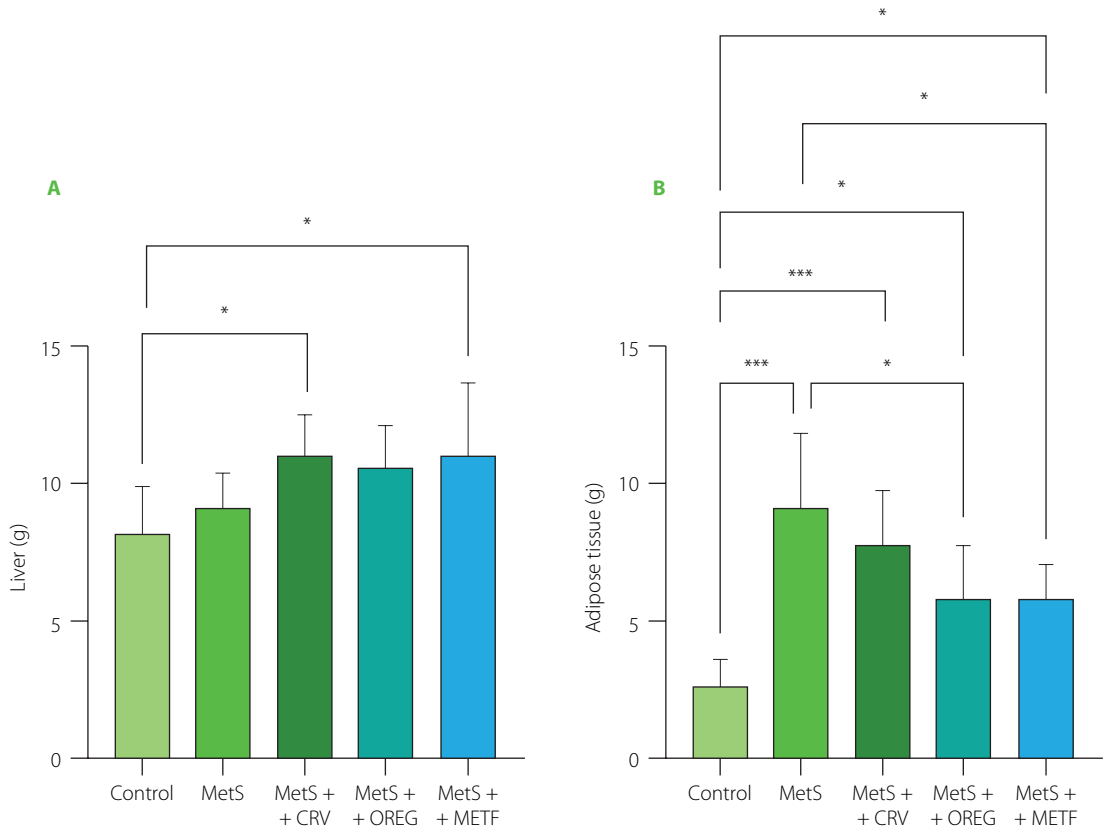

Figure 3. Weights of liver (**A**) and adipose tissue (**B**) of rats with induced metabolic syndrome (MetS) and treated with carvacrol (MetS+CRV), oregano extract (MetS+OREG) or metformin (MetS+METF), as well as rats without induced MetS (control). Data are represented as mean and standard derivation. Significant differences between groups are indicated with asterisks (*p<0.05, ***p<0.001).

Table 2. Blood pressure of rats with induced metabolic syndrome (MetS) and treated with carvacrol (MetS+CRV), oregano extract (MetS+OREG) or metformin (MetS+METF), as well as rats without induced MetS (control).

Parameter	Control	MetS	MetS+CRV	MetS+OREG	MetS+METF
Systolic blood pressure	111±9^{b}	174±42^{a}	115±17^{b}	120±27^{b}	125±15^{b}
Diastolic blood pressure	58±8^{b}	95±34^{a}	66±14^{ab}	66±15^{ab}	77±13^{ab}
Mean arterial pressure	76±8^{b}	121±29^{a}	82±8^{b}	84±13^{b}	93±13^{b}
Heart rate	317±38^{b}	374±37^{a}	206±16^{c}	285±42^{b}	270±29^{b}

Results are shown as mean ± standard deviation. Different letters in a row indicate significant differences between groups (p<0.05).

when compared to the MetS group. On the contrary, there was no significant effect of oregano extract and carvacrol administrations on diastolic blood pressure in rats. Additionally, heart rate in the rats from the METS group was significantly higher compared to the animals from control group. However, both oregano extract and carvacrol treatments resulted in a reduction of heart rate values.

Hypertension is another leading risk factor for morbidity and mortality in MetS. In the case of a high-sugar and high-fat diet, fat cells produce angiotensinogen, which causes an increase in blood pressure [Athyros *et al.*, 2010]. The antihypertensive effects of the oregano extract and carvacrol supplementation observed in this study are in agreement with earlier research findings indicating their potential to decrease blood pressure and support cardiovascular protection by enhancing endothelial function and promoting the synthesis of nitric oxide (NO), a well-known vasodilator [Khazdair *et al.*, 2024; Merimi *et al.*, 2025]. The effects observed in rats with the metabolic syndrome may be partially attributed to free radical scavenging and antihyperglycemic properties of an oregano extract and carvacrol [Cicalău *et al.*, 2021; Radünz *et al.*, 2021].

Blood glucose levels in the oral glucose tolerance test

The OGTT results measured at the end of 10 weeks are shown in **Figure 4**. At minute 0, the fasting blood glucose level in the rats from the MetS group was significantly higher than that of the control group (p=0.046). Thirty minutes after the administration of a glucose solution at a dose of 2 g/kg body

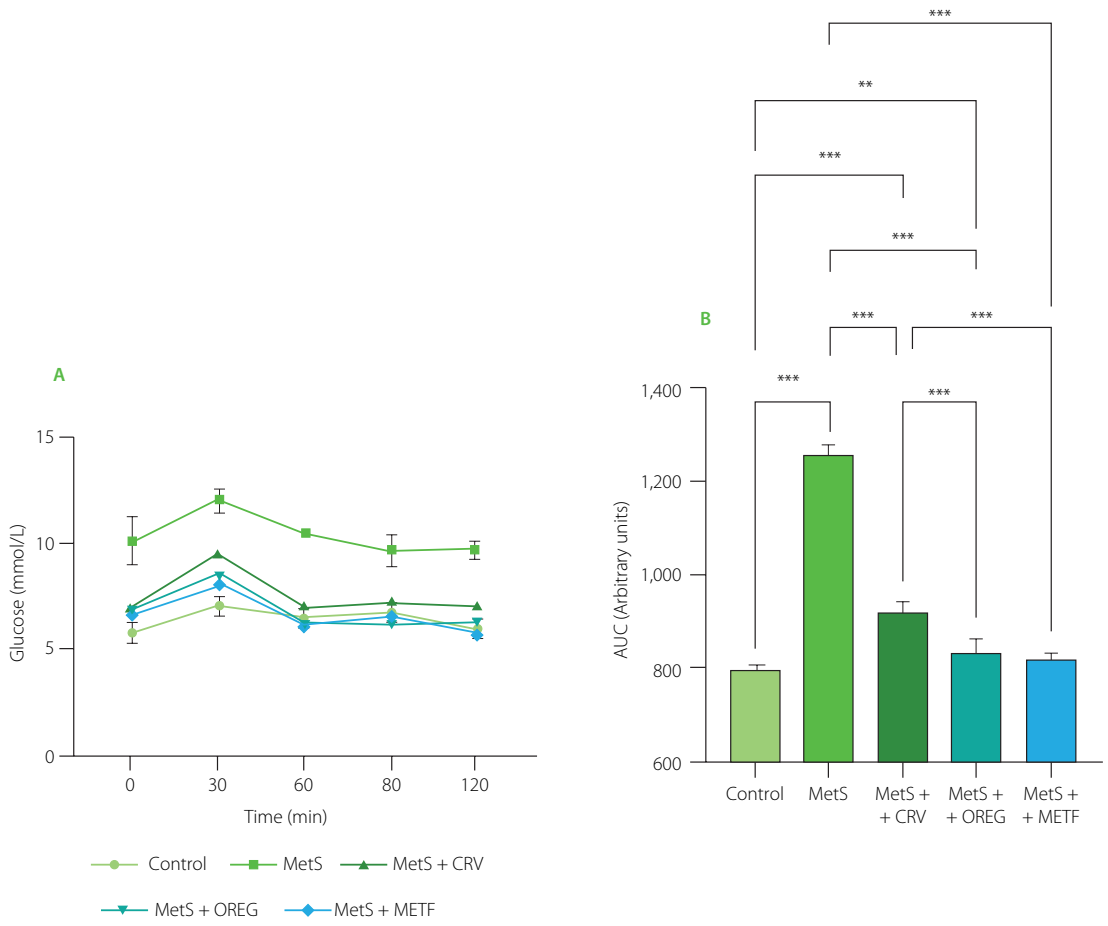

Figure 4. Blood glucose level (**A**) and area under the curve (AUC) (**B**) in oral glucose tolerance test of rats with induced metabolic syndrome (MetS) and treated with carvacrol (MetS+CRV), oregano extract (MetS+OREG) or metformin (MetS+METF), as well as rats without induced MetS (control). Data are represented as mean and standar deviation. In graph **B**, significant differences between groups are indicated with asterisks (**p<0.01, ***p<0.001).

weight, the rats administered the oregano extract (p=0.009), carvacrol (p=0.022), and metformin (p=0.008) showed significantly decreased blood glucose levels compared to the MetS rats. The MetS group had the highest fasting blood glucose value among all groups 120 min after glucose administration. Oregano extract (p=0.002) and carvacrol (p=0.001) supplementation significantly reduced glucose levels at this time point, whereas the reduction observed in the metformin group was not significantly greater (p≥0.05) than that achieved in the MetS+CRV and MetS+OREG groups, despite a lower mean value.

Considering AUC of OGTT, the value for the control group was 789.3, whereas the highest value (1257) was determined for the MetS group (**Figure 4**). The AUC determined for the combined treatment groups showed lower values, including 919.8 (MetS+CRV), 834.0 (MetS+OREG), and 816.9 (MetS+METF). The results of the Tukey's multiple comparison test indicated that the AUC of the MetS group was significantly higher than that of the control group (p<0.001). Similarly, AUC determined for MetS+CRV (p<0.001) and MetS+OREG (p=0.003) was significantly higher compared to the control group, whereas the difference between MetS+METF and control was not statistically significant (p=0.097). In turn, the diferences between the MetS group and all combination treatments (MetS+CRV, MetS+OREG, and MetS+METF) were significant at p<0.001. Furthermore, AUC values determined for MetS+OREG and MetS+METF were significantly lower compared to MetS+CRV at p<0.001, while no significant difference was observed between MetS+METF and MetS+OREG (p=0.486).

Another parameter that triggers symptoms in the occurrence of MetS is insulin resistance. Blood glucose levels and AUC values of OGTT performed during the study were significantly increased in the HFFD groups, indicating that feeding HFFD significantly impairs insulin-stimulated glucose uptake in peripheral tissues. This effect may be explained by the fact that a high fat intake reduces the ability of insulin to increase glucose uptake by increasing the release of free fatty acids and fructose that are rapidly metabolized in the liver, increasing TG production [Melo *et al.*, 2021]. Our study results showed that the rats fed a HFFD developed hyperglycemia, which was in agreement with the findings reported by Omidifar *et al.* [2021]. Furthermore, oregano extract and carvacrol administration decreased the glycemic levels of rats, showing a similar effect as metformin. This healing effect may be due to the presence of phytochemicals that inhibit the digestion of carbohydrates and, therefore, reduce glucose absorption and the postprandial blood sugar level.

Serum biochemical parameters

The findings regarding the effects of carvacrol and oregano extract treatments on serum biochemical parameters are presented in **Figure 5**. Serum AST levels were significantly (p<0.001) higher in the MetS group, with values of 177.1 U/L compared to 83.79 U/L determined in the control group. ALT values were similar for both groups. Oregano extract and carvacrol treatments reduced AST and ALT values in the metabolic syndrome groups. This was further supported by the significant reductions in AST levels in the MetS+CRV group (122.9 U/L) and MetS+OREG group (107.4 U/L), when compared to the MetS group (p=0.013 and p=0.002, respectively). Similarly, ALT values were significantly lower in the MetS+OREG (49.42 U/L) and MetS+CRV (50.03 U/L) as compared to the MetS group (68.40 U/L) (p=0.033 and p=0.039, respectively). Moreover, in the MetS+METF group, both AST and ALT levels (84.98 and 37.57 U/L, respectively) were significantly higher when compared to the MetS group (p<0.001 and p=0.001, respectively). Similarly, serum TG levels were significantly higher in the MetS group at 173.5 mg/dL compared to the control group at 28.37 mg/dL (p<0.001). At the same time, serum TG levels were significantly reduced in the MetS+CRV group at 30.87 mg/dL, MetS+OREG group at 45.04 mg/dL, and MetS+METF group at 50.24 mg/dL compared to the MetS group (p<0.001). In the evaluation of serum levels of HDL, it was observed that its value was significantly lower in the MetS group when compared with the control group (15.43 *vs*. 23.70 mg/dL, p=0.004). The values determined in the MetS+CRV (26.32 mg/dL), MetS+OREG (24.88 mg/dL), and MetS+METF (25.60 mg/dL) groups were significantly higher than those assayed in the MetS group (p<0.001, p=0.001, and p<0.001, respectively). Lastly, serum LDL levels were significantly higher in the MetS group (6.24 mg/dL) compared with the control group (3.21 mg/dL) (p=0.008). In the meantime, lower LDL levels were observed in the MetS+CRV (3.69 mg/dL) and MetS+OREG (3.87 mg/dL) groups when compared with MetS group (p<0.05). In this context, the effects of the oregano extract and carvacrol were comparable to those of metformin.

One of the abnormalities that define MetS is dyslipidemia [Gunawan *et al*., 2021]. In our study, the consumption of the HFFD caused an increase in serum LDL and TG levels, while decreased HDL levels, contributing to a dyslipidemia state. This may be explained by the fact that the high fat content of the diet induces hypercholesterolemia by causing the accumulation of cholesterol plaques in the vascular walls of rats with metabolic disorders [Kenné Toussé *et al*., 2024]. According to the present study results, oregano extract and carvacrol supplementation decreased TG and LDL levels, while significantly increasing HDL levels. Metformin was less effective than the oregano extract and carvacrol in lowering LDL levels. These effects may be due to the impaired cholesterol synthesis caused by the inhibition of 3-hydroxy-3-methylglutaryl coenzyme A (HMG-CoA) reductase by phytochemicals of the oregano extract. This enzyme is the main regulator of endogenous cholesterol production and its inhibitory effect leads to a decrease in LDL levels [Bampidis *et al*., 2005]. At the same time, the antioxidative properties of carvacrol prevent free radical damage by reducing lipid peroxidation, which promotes a decrease in TG levels. The increase in HDL level may be attributed to the acceleration of cholesterol transport by increasing apolipoprotein A1 synthesis [Haas *et al*., 2014]. Thus, oregano and carvacrol positively affect overall cardiovascular health by increasing HDL level while improving both cholesterol and TG levels. Furthermore, the lipid profile results in this study are in agreement with the findings of Özdemir *et al*. [2008] and Lee *et al*. [2024], who found that an aqueous distillate of *O. onites* and an ethyl acetate fraction of *O. vulgare* seed, respectively, have significant hypocholesterolemic and hypotriglyceridemic effects. Impaired glucose uptake in the liver and muscle tissues leads to insulin resistance and hyperglycemia, triggering hepatic steatosis and inflammatory processes in the liver. This leads to increased lipid peroxidation and oxidative stress in hepatocytes, resulting in elevated ALT and AST levels, which are liver enzymes. Elevated ALT and AST values have been reported in MetS [Nderitu *et al*., 2023]. This study showed that ALT and AST values were increased in HFFD-fed rats compared to the other treatment groups. Along with the increases in serum ALT and AST, liver histopathological findings from this study showed that HFFD administration caused liver damage. However, in the groups treated with the oregano extract and carvacrol, ALT and AST levels significantly decreased, approximating the control values, and also prevented liver damage. This shows that oregano and carvacrol consumption is safe. These findings are consistent with previous studies reporting hepatoprotective effects of *O. vulgare* extract, which significantly decreased serum AST and ALT levels in experimental models of liver injury [Habibi *et al*., 2015].

Liver and pancreas TNF-α levels

TNF-α levels of liver and pancreas tissues are presented in **Figure 6**. The MetS group had significantly higher hepatic TNF-α levels (119.0 ng/L) when compared to the control group (69.36 ng/L) (p<0.001). In a similar manner, pancreatic levels of TNF-α were significantly higher in the MetS group when compared to the control group; 34.32 *vs*. 12.29 ng/L, respectively (p<0.001). Carvacrol and oregano extract treatment reduced liver TNF-α level significantly in the MetS+CRV (69.07 ng/L) and MetS+OREG (82.22 ng/L) groups compared to the MetS group (p<0.001). Remarkably, carvacrol drastically decreased pancreatic TNF-α levels, and in the MetS+CRV group, the level reached 20.05 ng/L, which was lower than that in the MetS group (p=0.025). In turn, the oregano extract did not show this kind of activity in terms of pancreatic TNF-α levels. Furthermore, in the MetS+METF group, the liver TNF-α level was significantly lower, measured as 69.25 ng/L, compared to the MetS group. However, the pancreatic level of TNF-α in the MetS+MetF group was significantly raised as compared with the control group, indicating an interaction between metformin and TNF-α modulation in pancreatic tissues.

Increased adipose tissue in rats with MetS, correlated with increased macrophages, can trigger the release of various cytokines,

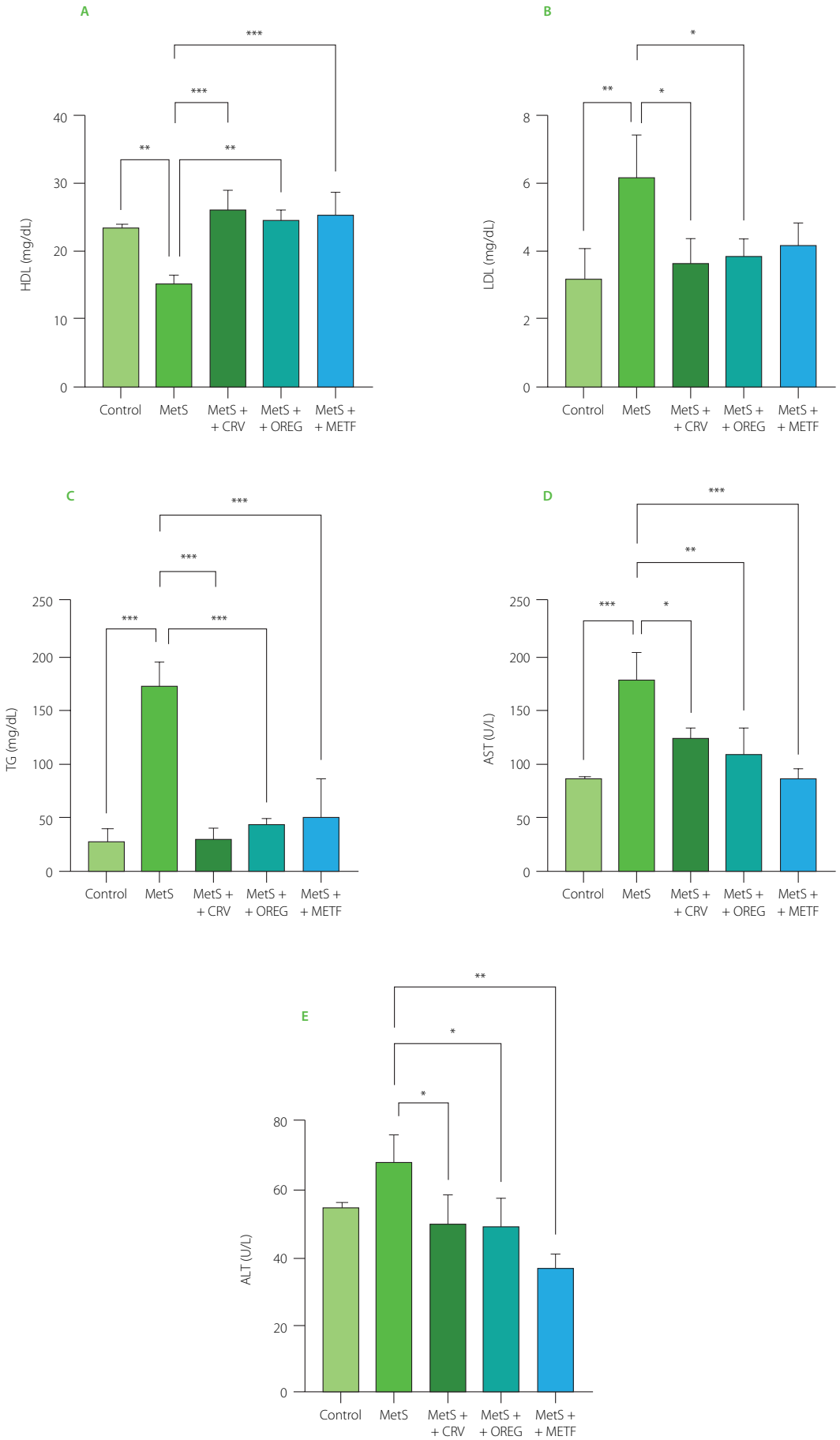

Figure 5. Serum biochemical parameters, including levels of high-density lipoprotein (HDL) cholesterol (**A**), low-density lipoprotein (LDL) cholesterol (**B**), triglycerides (TG) (**C**), aspartate aminotransferase (AST) (**D**), and alanine aminotransferase (ALT) (**E**), of rats with induced metabolic syndrome (MetS) and treated with carvacrol (MetS+CRV), oregano extract (MetS+OREG) or metformin (MetS+METF), as well as rats without induced MetS (control). Data are represented as mean and standard deviation. Significant differences between groups are indicated with asterisks (*p<0.05, **p<0.01, ***p<0.001).

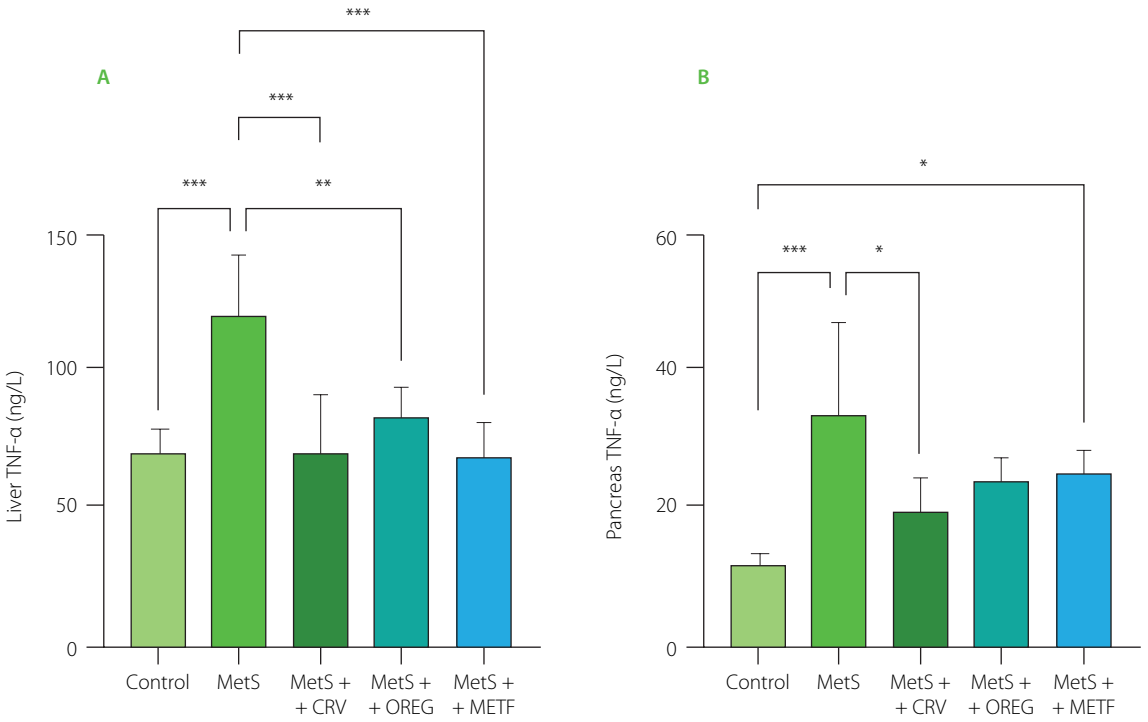

Figure 6. Tumor necrosis factor-α (TNF-α) levels in the liver (**A**) and pancreas (**B**) of rats with induced metabolic syndrome (MetS) and treated with carvacrol (MetS+CRV), oregano extract (MetS+OREG) or metformin (MetS+METF), as well as rats without induced MetS (control). Data expressed as mean and standard deviation. Significant differences between groups are indicated with asterisks (*p<0.05, **p<0.01, ***p<0.001).

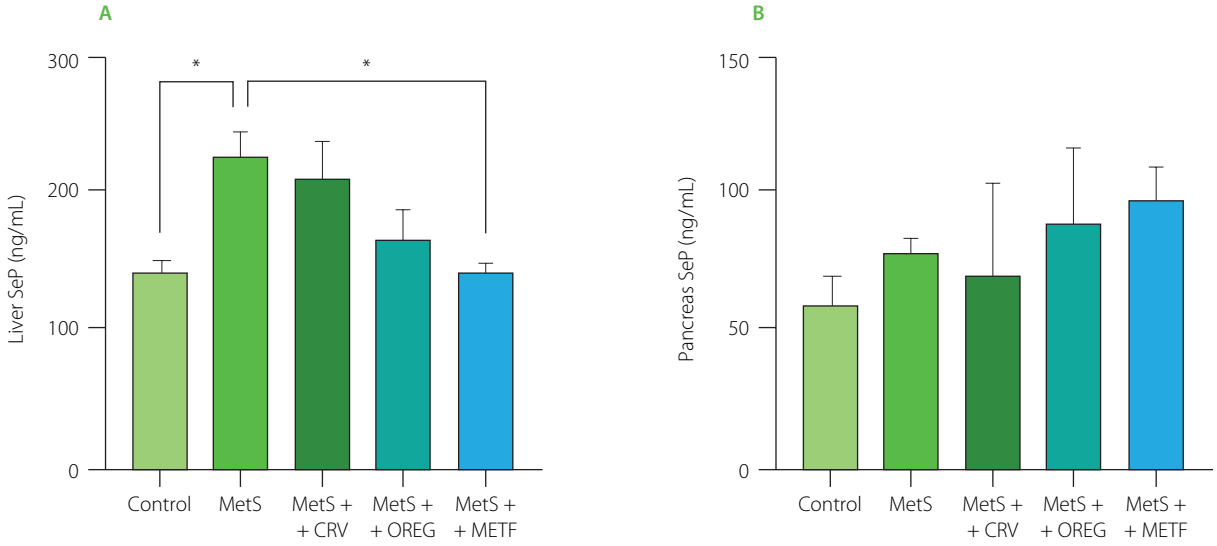

Figure 7. Selenoprotein P (SeP) levels in the liver (**A**) and pancreas (**B**) of rats with induced metabolic syndrome (MetS) and treated with carvacrol (MetS+CRV), oregano extract (MetS+OREG) or metformin (MetS+METF), as well as rats without induced MetS (control). Data expressed as mean and standard deviation. Significant differences between groups are indicated with asterisks (*p<0.05).

such as TNF-α, IL-6 and HMGB1, by switching from the anti-inflammatory 'M2' (alternatively activated) to the pro-inflammatory 'M1' (classical activation) state [Frisardi *et al.*, 2021]. Overexpression of TNF-α suggests that TNF-α may be a predictor for early diagnosis of MetS [Chen *et al.*, 2021]. In this study, an increase in TNF-α levels was observed in pancreatic and liver tissues of the rats fed a high fat and sugar diet. The oregano extract decreased liver TNF-α level, while carvacrol significantly decreased pancreatic TNF-α level (**Figure 6**). Phenolic compounds have been reported to exhibit different biological activities, such as antioxidant, anti-inflammatory, antitumoral, and antimicrobial ones [Zhang *et al.*, 2014]. Therefore, the anti-inflammatory effects obtained in this study may be related to the phenolic compounds of the oregano extract. These findings are consistent with the study reported by Sharifi-Rigi *et al.* [2019] indicating that the *O. vulgare* extract exerted inhibitory effects on paraquat-induced liver injury due to its antioxidative properties in a rat model of liver injury.

Liver and pancreas selenoprotein P levels

SeP levels of liver and pancreas tissues are presented in **Figure 7**. The hepatic SeP level in the MetS group was significantly increased to 227.1 ng/mL, compared to the control group

showing a value of 144.3 ng/mL (p=0.022). In addition, a significant difference (p=0.016) was observed between the MetS group (227.1 ng/mL) and the MetS+METF group (144.3 ng/mL). In contrast, no significant differences (p≥0.05) were noted in SeP levels among the groups in pancreatic tissue. Most notably, oregano extract and carvacrol had no significant impact on SeP levels in liver and pancreas, indicating that neither of these compounds affects selenium metabolism in MetS.

In the present study, SeP tissue levels in liver and pancreas were evaluated to examine the role of SeP in the development of MetS. SeP exhibits antioxidative properties in various tissues as well as acts as an Se transport protein that provides Se to tissues in the body and aids biosynthesis of intracellular selenoproteins [Jensen-Cody & Potthoff, 2021]. No study was found in which SeP levels were analyzed in liver and pancreatic tissues of MetS-induced experimental animals. It has been reported that hepatic expression of SeP and circulating selenium and SeP levels are decreased in rats with acute phase reaction; this impairs hepatic SeP expression during acute phase reaction and thus affects the transport of Se to peripheral tissues [Renko *et al.*, 2009]. In contrast, hepatic SeP levels have been reported to increase with hepatic steatosis and oxidative stress in rats fed a high-fat diet; this change may represent a mechanism against high-fat diet-induced steatosis, oxidative stress, and subsequent inflammation [Murano *et al.*, 2018].

The present study results further showed that there was a significant increase in SeP levels in the liver and no significant increase in pancreatic tissue of the MetS group rats fed a high-fat and high-sugar diet. This finding suggests that SeP may have a regulatory role in pathological processes associated with MetS and may lead to adverse physiopathological processes on liver functions. In our study, oregano extract and carvacrol supplements administered exogenously did not significantly alter SeP levels. However, these supplements have been found to cause a decrease in TG levels. A previous study reported that SeP was positively correlated with plasma TG levels, indicating its association with dyslipidemia [Chen *et al.*, 2017]. This finding suggests that these therapeutic approaches may be effective on lipid profile and inflammation rather than affect SeP metabolism. Moreover, the association of SeP with obesity is another important factor to be considered in the pathogenesis of MetS. In the present study, when body weight changes were analyzed between groups, insulin resistance occurred with increasing body weight in the MetS group and SeP levels increased significantly.

Misu *et al*. [2010] reported that SeP knockout mice fed a high fat/high sucrose diet were protected against the development of insulin resistance. In addition, SeP decreased AMP-activated protein kinase (AMPK) phosphorylation in the liver, resulting in enhanced fatty acid biosynthesis. This suggests that serum SeP level may exert autocrine effects in the liver. The authors also reported a high glucose-induced up-regulation of SeP in hepatocytes [Misu *et al.*, 2010]. Considering literature data, our study findings support the hypothesis that SeP plays a regulatory role in glucose homeostasis and is also involved in liver physiological processes. Speckmann *et al.* [2009] reported that treatment with metformin, a drug used in the treatment of diabetes, reduced hepatic SeP mRNA expression and secretion, but the dose of metformin administered was higher than the therapeutic dose in humans (2 mM). According to our study findings, metformin administration decreased the SeP level in the liver of rats with the metabolic syndrome, whereas there was no significant difference in pancreatic tissue. These findings suggest that metformin may exert an effect on liver function through the modulation of SeP levels. However, oregano extract and carvacrol treatments did not produce significant changes in SeP levels, suggesting that their effects may occur through mechanisms other than SeP regulation.

Histopathological assessments

The histopathological images of the liver and pancreas sections of rats from different groups are shown in **Figure 8**. Furthermore, the results of histopathological scoring of the liver and pancreas are presented in **Tables S2** and **S3** in the Supplementary Materials, respectively. In the liver sections of the control group, hepatocytes were regularly arranged around the central vein with distinct nuclei, forming orderly cords. The sinusoids between the cell cords exhibited a normal appearance. In the MetS group, where metabolic syndrome was induced by feeding with a specific diet, liver sections showed hydropic degeneration and coagulative necrosis in the parenchyma, particularly in the hepatocytes. There was also irregularity, dilation, and hyperemia in the sinusoids, with disruption of the integrity of the central vein when compared to the control group. In the MetS+CRV group, hepatocytes and cord formations were similar to those of the control group; however, sinusoids were slightly dilated, and there was less coagulative necrosis in the hepatocytes and increased hyperemia. In the MetS+OREG group, liver sections showed minimal hydropic degeneration and coagulative necrosis in hepatocytes in the periacinar region, and less dilation of the sinusoids. Pathological changes were less pronounced in these two groups. In the MetS+METF group, the histomorphology was similar to the control group, although prominent hydropic degeneration was observed in hepatocytes surrounding the central vein in the periacinar region. There was also minimal coagulative necrosis in hepatocytes and reduced sinusoidal dilation. Upon examining the pancreatic sections, the normal islet histomorphology in the control group was disrupted in the MetS groups, showing a scattered and irregular appearance. The cell boundaries became indistinct, and structural abnormalities due to vacuolization, along with hydropic degeneration, were observed. The islets had shrunk, and their boundaries were more blurred. Additionally, a reduction was noted in the number of islet cells. Among the treatment groups, the MetS+METF group showed the most similar appearance to the control group. In the MetS+CRV group, significant improvement was observed compared to the MetS group. The islet contours were distinct and regular, and the cells showed structural and numerical similarities to those in the control group. The MetS+OREG group's islet cells resembled those in the control

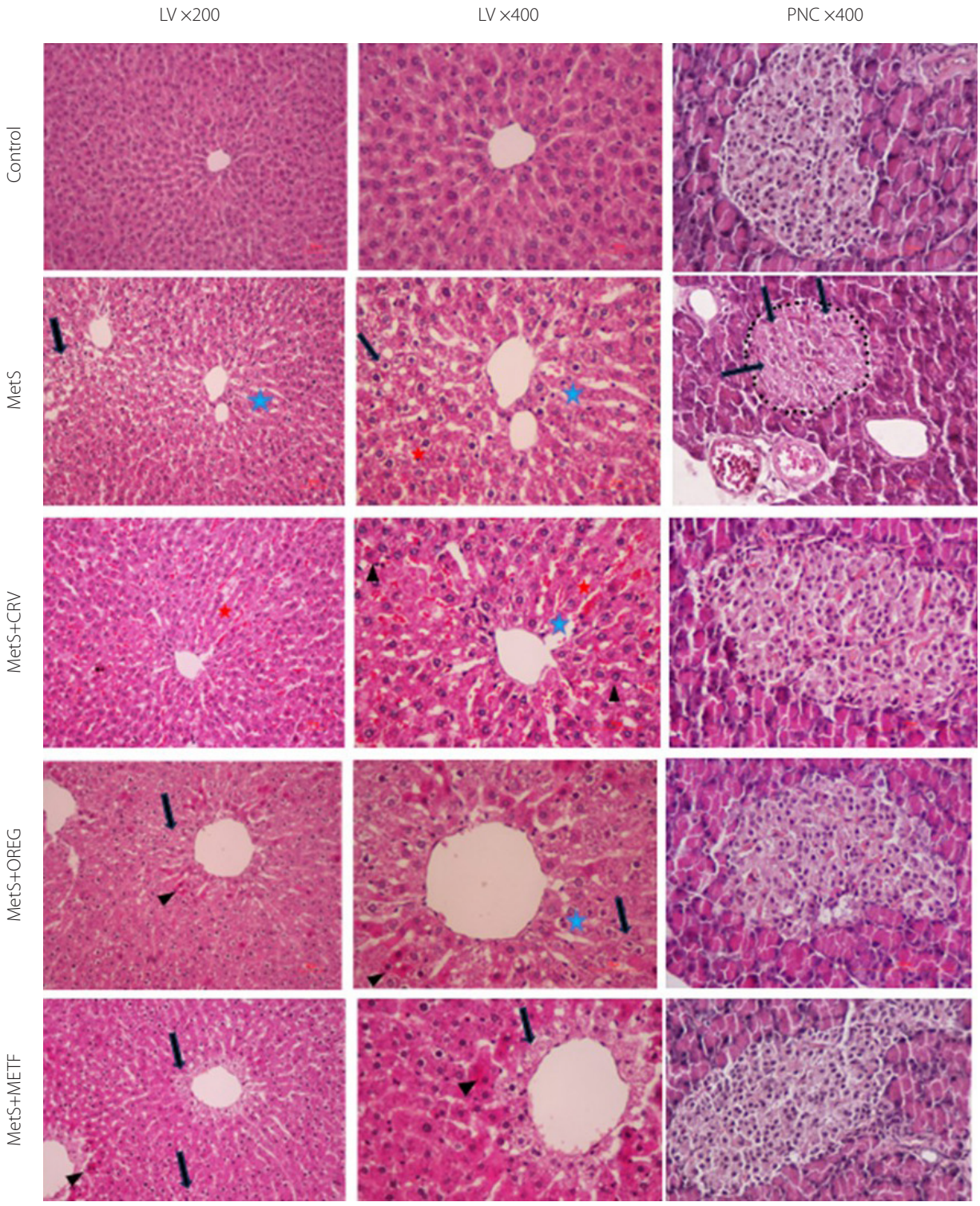

Figure 8. Sections of livers (LV) and pancreas (PNC) in different groups of rats. Control group; normal histology in control group. MetS group (LV); coagulation necrosis (arrowheads), severe hydropic degeneration of hepatocytes (black arrow) in the central region, sinusoidal dilatation (blue asterisks) and hyperemia (red asterisks). MetS+CRV group (LV); near-normal histology, comparable to control, but minimal coagulation necrosis, dilatation and hyperemia of the sinusoid. MetS+OREG group (LV); minimal hydropic degeneration and coagulation necrosis of hepatocytes in the periacinar region, mild dilatation of the sinusoids. MetS+METF group (LV); hydropic degeneration and coagulation necrosis in the periacinar region. MetS group (PNC); severe hydropic degeneration of islet cell (black arrow), shrunken and irregular islet borders (a dotted line). MetS+CRV group (PNC); near-normal histology, comparable to control. MetS+OREG group (PNC); near-normal histology, with minimal irregularities in islet borders. MetS+METF group (PNC); near-normal histology.

group. However, unlike the control group, the number of cells was low, and the islet boundaries were somewhat irregular (**Table S2** and **S3**). These results suggest that the metabolic syndrome induces significant histopathological damage in both hepatic and pancreatic tissues. However, treatments with the oregano extract and metformin alleviate these alterations to varying

extents, with metformin showing the strongest protective effect in the pancreas, and oregano extract demonstrating comparable hepatoprotective potential.

CONCLUSIONS

This study demonstrates that both SC-CO_2–derived *O. onites* extract and pure carvacrol exert beneficial effects on histological, biochemical, and metabolic alterations in a high-fat, high-fructose diet–induced rat model of MetS. Chemical characterization confirmed that the oregano extract was rich in carvacrol and other bioactive compounds. Treatment with the oregano extract and carvacrol was associated with improvements in lipid parameters, particularly triglyceride levels, and with amelioration of histopathological alterations observed in liver and pancreatic tissues. In addition, both treatments showed anti-inflammatory potential through modulation of TNF-α levels, while hepatic SeP alterations indicated a possible role in metabolic regulation during MetS development.

While the present results support the potential of the *O. onites* extract and carvacrol as candidates for further investigation in MetS, additional studies focusing on molecular mechanisms, as well as well-designed clinical trials, are required to confirm their translational relevance.

SUPPLEMENTARY MATERIALS

The following are available online at **https://journal.pan.olsztyn.pl/Comparative-Effects-of-Origanum-onites-L-Extract-and-Carvacrol-on-the-Metabolic-Syndrome,220853,0,2.html**; **Table S1**. Volatile compound composition of the *Origanum onites* L. extract obtained by supercritical CO_2 extraction. **Table S2**. Histopathological scoring of liver of rats with induced metabolic syndrome (MetS) and treated with carvacrol (MetS+CRV), oregano extract (MetS+OREG) or metformin (MetS+METF), as well as rats without induced MetS (control). **Table S3**. Histopathological scoring of pancreas of rats with induced metabolic syndrome (MetS) and treated with carvacrol (MetS+CRV), oregano extract (MetS+OREG) or metformin (MetS+METF), as well as rats without induced MetS (control).

ACKNOWLEDGEMENTS

The authors would like to thank Davut Yolcu for his technical support. In addition to, the authors thank the Scientific Research Projects Unit of Kırşehir Ahi Evran University for its support.

RESEARCH FUNDING

This work was supported by Kırşehir Ahi Evran University (Grant number MMF.A1.24.001).

CONFLICT OF INTERESTS

The authors have no relevant financial or non-financial interests to disclose.

ADDITIONAL INFORMATION

This study has been approved by the Kırşehir Ahi Evran University Local Ethics Committee for Experimental Animals (2023/23/4).

ORCID IDs

E. Bilginoğlu **https://orcid.org/0000-0001-5974-327X**
A. Güneş **https://orcid.org/0000-0001-6878-9325**
S. Koçak **https://orcid.org/0000-0003-1183-4847**
K. Öztürk **https://orcid.org/0000-0002-4488-0164**
H. Tozak-Yıldız **https://orcid.org/0000-0003-4310-6238**

REFERENCES

1. Abou-Seif, H.S., Hozayen, W.G. (2023). *Origanum majorana* L. extract alleviates dexamethasone-induced hepatotoxicity, oxidative stress and pathological alterations *in vivo*. *Bulletin of the National Research Centre*, *47*(1), art. no. 39. **https://doi.org/10.1186/s42269-023-01012-1**
2. Ajiboye, T., Aliyu, H., Tanimu, M., Muhammad, R., Ibitoye, O. (2016). *Dioscoreophyllum cumminsii* (Stapf) Diels leaves halt high-fructose induced metabolic syndrome: Hyperglycemia, insulin resistance, inflammation and oxidative stress. *Journal of Ethnopharmacology*, *192*, 471-479. **https://doi.org/10.1016/j.jep.2016.08.024**
3. Athyros, V.G., Tziomalos, K., Karagiannis, A., Anagnostis, P., Mikhailidis, D.P., Fiorino, G., Rovida, S., Correale, C., Malesci, A., Danese, S. (2010). Should adipokines be considered in the choice of the treatment of obesity-related health problems? *Current Drug Targets*, *11*(1), 122-135. **https://doi.org/10.2174/138945010790030992**
4. Ayres Cacciatore, F., Dalmás, M., Maders, C., Ataíde Isaía, H., Brandelli, A., da Silva Malheiros, P. (2020). Carvacrol encapsulation into nanostructures: Characterization and antimicrobial activity against foodborne pathogens adhered to stainless steel. *Food Research International*, *133*, art. no. 109143. **https://doi.org/10.1016/j.foodres.2020.109143**
5. Bampidis, V., Christodoulou, V., Florou-Paneri, P., Christaki, E., Chatzopoulou, P., Tsiligianni, T., Spais, A. (2005). Effect of dietary dried oregano leaves on growth performance, carcase characteristics and serum cholesterol of female early maturing turkeys. *British Poultry Science*, *46*(5), 595-601. **https://doi.org/10.1080/00071660500256057**
6. Bitwell, C., Indra, S.S., Luke, C., Kakoma, M.K. (2023). A review of modern and conventional extraction techniques and their applications for extracting phytochemicals from plants. *Scientific African*, *19*, art. no. e01585. **https://doi.org/10.1016/j.sciaf.2023.e01585**
7. Caponio, F., Alloggio, V., Gomes, T. (1999). Phenolic compounds of virgin olive oil: influence of paste preparation techniques. *Food Chemistry*, *64*(2), 203-209. **https://doi.org/10.1016/S0308-8146(98)00146-0**
8. Chen, M., Liu, B., Wilkinson, D., Hutchison, A.T., Thompson, C.H., Wittert, G.A., Heilbronn, L.K. (2017). Selenoprotein P is elevated in individuals with obesity, but is not independently associated with insulin resistance. *Obesity Research & Clinical Practice*, *11*(2), 227-232. **https://doi.org/10.1016/j.orcp.2016.07.004**
9. Chen, T.-H., Kung, W.-S., Sun, H.-Y., Huang, J.-J., Lu, J.-Y., Luo, K.-H., Chuang, H.-Y. (2021). The relationship between metabolic syndrome and plasma metals modified by EGFR and TNF-α gene polymorphisms. *Toxics*, *9*(9), art. no. 225. **https://doi.org/10.3390/toxics9090225**
10. Cicalău, G.I.P., Babes, P.A., Calniceanu, H., Popa, A., Ciavoi, G., Iova, G. M., Ganea, M., Scrobotă, I. (2021). Anti-inflammatory and antioxidant properties of carvacrol and magnolol, in periodontal disease and diabetes mellitus. *Molecules*, *26*(22), art. no. 6899. **https://doi.org/10.3390/molecules26226899**
11. Elbouny, H., Amssayef, A., Benjamaa, R., Ajebli, M., Ouahzizi, B., Bammou, M., Sellam, K., Alem, C. (2025). Thyme, oregano, and rosemary: herbs and food supplements for the management of metabolic associated fatty liver disease. *Nutrire*, *50*(1), art. no. 6. **https://doi.org/10.1186/s41110-024-00307-1**
12. Frisardi, V., Matrone, C., Street, M.E. (2021). Metabolic syndrome and autophagy: Focus on HMGB1 protein. *Frontiers in Cell and Developmental Biology*, *9*, art. no. 654913. **https://doi.org/10.3389/fcell.2021.654913**
13. Gheitasi, I., Motaghi, N., Sadeghi, H., Sadeghi, H., Moslemi, Z., Eftekhari, M., Shakerinasab, N., Doustimotlagh, A.H. (2021). Antioxidant and anti-inflammatory effects of *Origanum majorana* L. methanolic extract on bile duct ligation in male rats. *Evidence-Based Complementary and Alternative Medicine*, *2021*(1), art. no. 9927196. **https://doi.org/10.1155/2021/9927196**
14. Gregorius, A., Krzyczkowski, W., Wierucka, M., Kupińska, J., Dębczak, A., Łopatek, U., Tyśkiewicz, K., Wiejak, R., Wrona, O., Rój, E. (2019). Supercritical carbon dioxide *Cannabis sativa* L. and *Humulus lupulus* extracts and their influence on human macrophages inflammatory state. *Postępy Higieny i Medycyny Doświadczalnej, 73*, 782-790.
15. Gunawan, S., Aulia, A., Soetikno, V. (2021). Development of rat metabolic syndrome models: A review. *Veterinary World*, *14*(7), 1774-1783. **https://doi.org/10.14202/vetworld.2021.1774-1783**

16. Haas, M.J., Onstead-Haas, L.M., Naem, E., Wong, N.C., Mooradian, A.D. (2014). Induction of apolipoprotein A-I gene expression by black seed (*Nigella sativa*) extracts. *Pharmaceutical Biology*, *52*(9), 1119-1127. **https://doi.org/10.3109/13880209.2013.879187**
17. Habibi, E., Shokrzadeh, M., Chabra, A., Naghshvar, F., Keshavarz-Maleki, R., Ahmadi, A. (2015). Protective effects of *Origanum vulgare* ethanol extract against cyclophosphamide-induced liver toxicity in mice. *Pharmaceutical Biology*, *53*(1), 10-15. **https://doi.org/10.3109/13880209.2014.908399**
18. Jensen-Cody, S.O., Potthoff, M.J. (2021). Hepatokines and metabolism: Deciphering communication from the liver. *Molecular Metabolism*, *44*, art. no. 101138. **https://doi.org/10.1016/j.molmet.2020.101138**
19. Jugreet, B.S., Mahomoodally, M.F. (2020). Pharmacological properties of essential oil constituents and their mechanisms of action. In M.K. Swammy (Ed.), *Plant-derived Bioactives: Chemistry and Mode of Action*, Springer, Singapore, pp. 387-415. **https://doi.org/10.1007/978-981-15-2361-8_18**
20. Kassa, T., Whalin, J.G., Richards, M.P., Alayash, A.I. (2021). Caffeic acid: an antioxidant with novel antisickling properties. *FEBS Open Bio*, *11*(12), 3293-3303. **https://doi.org/10.1002/2211-5463.13295**
21. Kenné Toussé, R., Dangang Bossi, D.S., Dandji Saah, M.B., Foko Kouam, E.M., Njapndounke, B., Tambo Tene, S., Kaktcham, P.M., Zambou Ngoufack, F. (2024). Effect of *Curcuma longa* rhizome powder on metabolic parameters and oxidative stress markers in high-fructose and high-fat diet-fed rats. *Journal of Food Biochemistry*, *2024*(1), art. no. 1445355. **https://doi.org/10.1155/2024/1445355**
22. Khalil, M., Serale, N., Diab, F., Baldini, F., Portincasa, P., Lupidi, G., Vergani, L. (2022). Beneficial effects of carvacrol on *in vitro* models of metabolically-associated liver steatosis and endothelial dysfunction: A role for fatty acids in interfering with carvacrol binding to serum albumin. *Current Medicinal Chemistry*, *29*(30), 5113-5129. **https://doi.org/10.2174/0929867329666220401103643**
23. Khazdair, M.R., Moshtagh, M., Anaeigoudari, A., Jafari, S., Kazemi, T. (2024). Protective effects of carvacrol on lipid profiles, oxidative stress, hypertension, and cardiac dysfunction – A comprehensive review. *Food Science & Nutrition*, *12*(5), 3137-3149. **https://doi.org/10.1002/fsn3.4014**
24. Lee, H.J., Bae, J.Y., Park, K.W., Kim, M.J. (2024). Ethyl acetate fraction of oregano seed protects non-alcoholic fatty liver in high-fat diet-induced obese mice through modulation of Srebp-1c. *Food Science & Nutrition*, *12*(4), 2578-2587. **https://doi.org/10.1002/fsn3.3939**
25. Lee, Y. R., Lee, H.-B., Oh, M.-J., Kim, Y., Park, H.-Y. (2023). Thyme extract alleviates high-fat diet-induced obesity and gut dysfunction. *Nutrients*, *15*(23), art. no. 5007. **https://doi.org/10.3390/nu15235007**
26. Li, H., Zeng, Y., Zi, J., Hu, Y., Ma, G., Wang, X., Shan, S., Cheng, G., Xiong, J. (2024). Dietary flavonoids consumption and health: an umbrella review. *Molecular Nutrition & Food Research*, *68*(12), art. no. 2300727. **https://doi.org/10.1002/mnfr.202300727**
27. Lieshchova, M., Brygadyrenko, V. (2022). Effects of *Origanum vulgare* and *Scutellaria baicalensis* on the physiological activity and biochemical parameters of the blood in rats on a high-fat diet. *Scientia Pharmaceutica*, *90*(3), art. no. 49. **https://doi.org/10.3390/scipharm90030049**
28. Melo, B.P., Zacarias, A.C., Oliveira, J.C.C., de Souza, L.M.C., Sabino, J., Ferreira, A.V.M., Tonoli, C., dos Santos, M.L., de Avelar, G.F., Meeusen, R., Heyman, E., Soaers, D.D. (2021). Thirty days of combined consumption of a high-fat diet and fructose-rich beverages promotes insulin resistance and modulates inflammatory response and histomorphometry parameters of liver, pancreas, and adipose tissue in Wistar rats. *Nutrition*, *91-92*, art. no. 111403. **https://doi.org/10.1016/j.nut.2021.111403**
29. Merimi, C., Benabbou, A., Bourassi, L., Addous, A., Elhenawy, A. A., Touzani, R., Hammouti, B. (2025). *In silico* evaluation of bioactive compounds (flavonoids, rosmarinic acid) from five plants (rosemary, oregano, pink savory, lemon balm, and saffron) and their role in cardiovascular health and hypertension. *OBM Integrative and Complementary Medicine*, *10*(2), art. no. 027. **https://doi.org/10.21926/obm.icm.2502027**
30. Misu, H., Takamura, T., Takayama, H., Hayashi, H., Matsuzawa-Nagata, N., Kurita, S., Ishikura, K., Ando, H., Takeshita, Y., Ota, T., Sakurai, M., Yamashita, T., Mizukoshi, E., Yamashita, T., Honda, M., Miyamoto, K.I., Kubota, T., Kubota, N., Kadowaki, T., Kim, H.J., Lee, I.K., Minokoshi, Y., Saito, Y., Takahashi, K., Yamada, Y., Takakura, N., Kaneko, S. (2010). A liver-derived secretory protein, selenoprotein P, causes insulin resistance. *Cell Metabolism*, *12*(5), 483-495. **https://doi.org/10.1016/j.cmet.2010.09.015**
31. Murano, K., Ogino, H., Okuno, T., Arakawa, T., Ueno, H. (2018). Role of supplementary selenium on the induction of insulin resistance and oxidative stress in NSY mice fed a high fat diet. *Biological and Pharmaceutical Bulletin*, *41*(1), 92-98. **https://doi.org/10.1248/bpb.b17-00622**
32. Nderitu, K.W., Mecha, E., Nyachieo, A. (2023). *Solanum nigrum* show anti-obesity effects on high-fat diet-fed Sprague Dawley rats in a randomized study. *Scientific African*, *20*, art. no. e01713. **https://doi.org/10.1016/j.sciaf.2023.e01713**
33. Omidifar, A., Shirvani, H., Taheri, R.A., Gorgani-Firouzjae, S., Delfan, M., Kalaki-Jouybari, F., Khakdan, S. (2021). Protective effects of HIIT *vs*. CET exercise training on high-fat-high-fructose diet-induced hyperglycemia, hyperlipidemia, and histopathology of liver in rats: regulation of SIRT1/PGC-1α. *Sport Sciences for Health*, *17*, 707-715. **https://doi.org/10.1007/s11332-021-00736-9**
34. Özdemir, B., Ekbul, A., Topal, N., Sarandöl, E., Sağ, S., Başer, K., Cordan, J., Güllülü, S., Tuncel, E., Baran, I. (2008). Effects of *Origanum onites* on endothelial function and serum biochemical markers in hyperlipidaemic patients. *Journal of International Medical Research*, *36*(6), 1326-1334. **https://doi.org/10.1177/147323000803600621**
35. Pasavei, A.G., Mohebbati, R., Boroumand, N., Ghorbani, A., Hosseini, A., Jamshidi, S.T., Soukhtanloo, M. (2020). Anti-hypolipidemic and anti-oxidative effects of hydroalcoholic extract of *Origanum majorana* on the hepatosteatosis induced with high-fat diet in rats. *The Malaysian Journal of Medical Sciences: MJMS*, *27*(1), 57-69.
36. Radünz, M., Camargo, T.M., dos Santos Hackbart, H.C., Alves, P.I.C., Radünz, A.L., Gandra, E.A., da Rosa Zavareze, E. (2021). Chemical composition and *in vitro* antioxidant and antihyperglycemic activities of clove, thyme, oregano, and sweet orange essential oils. *LWT – Food Science and Technology*, *138*, art. no. 110632. **https://doi.org/10.1016/j.lwt.2020.110632**
37. Raeeszadeh, M., Shokrollahi, B., Akbari, A., Masumi, S., Amiri, A.A. (2024). Thyme extract could overcome diabetes-induced reproductive dysfunction by inhibiting oxidative damage and increasing the expression of insulin receptor substrate and pyruvate kinase in the rat sperm. *Journal of Pharmacy and Pharmacology*, *76*(5), 534-544. **https://doi.org/10.1093/jpp/rgad099**
38. Rajan, L., Palaniswamy, D., Mohankumar, S.K. (2020). Targeting obesity with plant-derived pancreatic lipase inhibitors: A comprehensive review. *Pharmacological Research*, *155*, art. no. 104681. **https://doi.org/10.1016/j.phrs.2020.104681**
39. Renko, K., Hofmann, P.J., Stoedter, M., Hollenbach, B., Behrends, T., Köhrle, J., Schweizer, U., Schomburg, L. (2009). Down-regulation of the hepatic selenoprotein biosynthesis machinery impairs selenium metabolism during the acute phase response in mice. *The FASEB Journal*, *23*(6), 1758-1765. **https://doi.org/10.1096/fj.08-119370**
40. Rodriguez-Casado, A. (2016). The health potential of fruits and vegetables phytochemicals: Notable examples. *Critical Reviews in Food Science and Nutrition*, *56*(7), 1097-1107. **https://doi.org/10.1080/10408398.2012.755149**
41. Roko, G., Porada, R., Gdula-Argasińska, J., Piekoszewski, W., Chabi-Sika, K., Krakowska-Sieprawska, A., Buszewski, B., Librowski, T., Baba-Moussa, L. (2024). Comparison of supercritical CO2 extraction and pressurized fluid extraction for isolation of alkaloids from *Anacardium occidentale* with the study of its anti-inflammatory activity. *Journal of Pharmaceutical and Biomedical Analysis*, *241*, art. no. 115982. **https://doi.org/10.1016/j.jpba.2024.115982**
42. Saklayen, M.G. (2018). The global epidemic of the metabolic syndrome. *Current Hypertension Reports*, *20*(2), art. no. 12. **https://doi.org/10.1007/s11906-018-0812-z**
43. Sharifi-Rad, M., Varoni, E. M., Iriti, M., Martorell, M., Setzer, W.N., del Mar Contreras, M., Salehi, B., Soltani-Nejad, A., Rajabi, S., Tajbakhsh, M., Sharifi-Rad, J. (2018). Carvacrol and human health: A comprehensive review. *Phytotherapy Research*, *32*(9), 1675-1687. **https://doi.org/10.1002/ptr.6103**
44. Sharifi-Rigi, A., Heidarian, E., Amini, S.A. (2019). Protective and anti-inflammatory effects of hydroalcoholic leaf extract of *Origanum vulgare* on oxidative stress, TNF-α gene expression and liver histological changes in paraquat-induced hepatotoxicity in rats. *Archives of Physiology and Biochemistry*, *125*(1), 56-63. **https://doi.org/10.1080/13813455.2018.1437186**
45. Shoorei, H., Khaki, A., Khaki, A.A., Hemmati, A.A., Moghimian, M., Shokoohi, M. (2019). The ameliorative effect of carvacrol on oxidative stress and germ cell apoptosis in testicular tissue of adult diabetic rats. *Biomedicine & Pharmacotherapy*, *111*, 568-578. **https://doi.org/10.1016/j.biopha.2018.12.054**
46. Speckmann, B., Sies, H., Steinbrenner, H. (2009). Attenuation of hepatic expression and secretion of selenoprotein P by metformin. *Biochemical and Biophysical Research Communications*, *387*(1), 158-163. **https://doi.org/10.1016/j.bbrc.2009.06.143**
47. Stojanović, N.M., Randelović, P.J., Simonović, M., Radić, M., Todorović, S., Corrigan, M., Harkin, A., Boylan, F. (2024). Essential oil constituents as an-

ti-inflammatory and neuroprotective agents: an insight through microglia modulation. *International Journal of Molecular Sciences*, *25*(10), art. no. 5168. **https://doi.org/10.3390/ijms25105168**

48. Uwineza, P.A., Waśkiewicz, A. (2020). Recent advances in supercritical fluid extraction of natural bioactive compounds from natural plant materials. *Molecules*, *25*(17), 3847. **https://doi.org/10.3390/molecules25173847**
49. Wang, O., Liu, J., Cheng, Q., Guo, X., Wang, Y., Zhao, L., Zhou, F., Ji, B. (2015). Effects of ferulic acid and γ-oryzanol on high-fat and high-fructose diet-induced metabolic syndrome in rats. *PLoS One*, *10*(2), art. no. e0118135. **https://doi.org/10.1371/journal.pone.0118135**
50. Xiang, Y., Ji, M., Wu, L., Lv, L., Liang, Q., Deng, R., Deng, Z., Liu, X., Ren, L., Feng, X., He, J. (2022). Rosmarinic acid prevents cisplatin-induced liver and kidney injury by inhibiting inflammatory responses and enhancing total antioxidant capacity, thereby activating the Nrf2 signaling pathway. *Molecules*, *27*(22), art. no. 7815. **https://doi.org/10.3390/molecules27227815**
51. Zhang, X.-L., Guo, Y.-S., Wang, C.-H., Li, G.-Q., Xu, J.-J., Chung, H.Y., Ye, W.-C., Li, Y.-L., Wang, G.-C. (2014). Phenolic compounds from *Origanum vulgare* and their antioxidant and antiviral activities. *Food Chemistry*, *152*, 300-306. **https://doi.org/10.1016/j.foodchem.2013.11.153**

ORIGINAL ARTICLE
http://journal.pan.olsztyn.pl

Polish Journal of Food and Nutrition Sciences
2026, Vol. 76, No. 2, 189–201
DOI: 10.31883/pjfns/221669
ISSN 1230-0322, e-ISSN 2083-6007

Impact of Extrusion Parameters on Textural and Sensory Characteristics of High-Moisture Meat Analogue from Mung Bean Protein and Wheat Gluten

Kantapit Mektun[1], Kongkarn Kijroongrojana[1]*

[1]Food Science and Technology Program, Faculty of Agro-Industry, Prince of Songkla University, Hat Yai, Songkhla, 90110, Thailand

A high-moisture extrusion process was used to produce plant-based meat analogues with fibrous structure. Mung bean protein isolate (MBP) and wheat gluten (WG) blend (70:30, *w/w*) were extruded using a co-rotating twin screw extruder. The optimization of extrusion parameters, including feed moisture content (55–65%, *w/w*) and barrel temperature (140–160°C), with respect to the textural properties and sensory characteristics of high-moisture meat analogue (HMMA) was investigated using central composite design. An increase in moisture content of the meat analogue led to a decrease in its firmness, hardness, and chewiness determined using instrumental analysis. These results were consistent with hardness, number of chews, and roughness scores evaluated by the trained panelists. Moreover, the microstructure and visual observations showed that fibrous alignment tended to become less compact and form finer strands with an increasing moisture content. However, the barrel temperature had no or slight impact on texture properties of the meat analogue. Acceptance test result revealed that the liking scores of all attributes tended to increase with an increasing extrudate moisture content. The optimized process conditions according to the maximized acceptance score included 65% feed moisture content and extrusion temperature of 140°C with 0.644 desirability. The acceptance scores of the resulting HMMA ranged from 6.4 to 6.7 on a 9-point hedonic scale.

Keywords: consumer acceptance, extrusion optimization, fibrous structure, plant-based protein, texture

ABBREVIATIONS

ANOVA, analysis of variance; BT, barrel temperature; HMMA, high-moisture meat analogue; MC, moisture content; MBP, mung bean protein isolate; WG, wheat gluten; DT, degree of texturization.

INTRODUCTION

The concern about health and sustainable foods has affected the development of the innovation of plant-based protein foods. It is anticipated that the global market of plant-based meat alternatives will grow consistently, reaching around 21.81 billion USD by 2030 [Arizton, 2024]. However, the quality, nutritive value (*i.e.*, insufficient contents of amino acids and some elements, such as iron), and sensory characteristics of these products are challenged as the first parameters of consumers' acceptability.

Soybeans are commonly used in the production of meat analogues due to their strong gel-forming properties, ability to develop a fibrous meat-like texture, and amino acid composition comparable to that of animal proteins [Zhang *et al.*, 2021]. The addition of wheat gluten into soy protein-based meat analogue resulted in enhanced fibrous structure development, *via* the formation of disulfide bonds, hydrophobic and hydrogen bonds, producing textural characteristics comparable to those of chicken meat [Chiang *et al.*, 2019; Samard *et al.*, 2019].

***Corresponding Author:**
tel.: 66-7428-6336; e-mail: **kongkarn.k@psu.ac.th** (K. Kijroongrojana)

Submitted: 3 November 2025
Accepted: 11 May 2026
Published on-line: 8 June 2026

Nevertheless, the use of soy-derived meat analogues is limited by their beany off-flavor and potential allergenicity as well as growing consumer concerns regarding genetically-modified soybean, which is increasingly being cultivated [Joshi & Kumar, 2015]. As a result, the use of soy protein in meat analogues has faced challenges. Recently, several researches have focused on the use of proteins from non-traditional sources, such as pea, fava bean, rice bran, and spirulina, for development meat analogues [Plattner *et al.,* 2024; Theng *et al*., 2025; Zhao *et al*., 2024]. Among these, mung bean (*Vigna radiata* (L.) R. Wilczek) is one of the nutrient-rich legumes with a high content of vitamins B and C, as well as essential minerals, like manganese, iron, and calcium [Anwar *et al.*, 2007; Dahiya *et al*., 2015]. In addition, mung beans are low in fat (~1–2%) and high in proteins (~21–31%) [Anwar *et al.*, 2007]. Their proteins exhibit high *in vitro* digestibility (~80%), which can be increased by 10% after heat treatment [Mubarak, 2005]. Additionally, the essential amino acid profile of mung bean protein is comparable with that of soy bean and FAO/WHO reference protein, with the exception of valine and sulfur-containing amino acids (methionine and cysteine) [Du *et al.*, 2018]. Despite its nutritional advantage, there has been limited research on using mung bean protein for meat analogue development. Hwang *et al*. [2024] revealed that mung bean protein has the potential to be a substitute for soy protein in the development of high-moisture meat analogue (HMMA). They reported that increasing mung bean protein content improved the gelling ability and formation of the fibrous structure, especially at 40–50% protein, where the most meat-like texture was observed. However, the springiness, chewiness, and cutting strength were decreased with an increasing proportion of mung bean protein in the formulation, resulting in a softer and juicier product. In turn, Seetapan *et al*. [2023] reported that increasing the mung bean flour content (10–30%, *w/w*) in blends with a mung bean protein isolate reduced the flow velocity and enhanced anisotropic layering, demonstrating its potential for customizable textures. However, no studies to date have explored the production of HMMA using mung bean depending on the process condition. Thus, this study aimed to determine the optimized conditions for producing mung bean protein and wheat gluten based-HMMA by investigating the effects of barrel temperature (140–160°C) and feed moisture content (55–65%, *w/w*) on its textural and sensory characteristics using response surface methodology.

MATERIALS AND METHODS

Material

Mung bean protein isolate (MBP) was obtained from AGT Food and Ingredients Inc., Tianjin, China. The proximate composition of 100 g of MBP (wet matter basis) was: 6.80 g of moisture, 0.28 g of fat, 72.74 g of protein, 3.12 g of ash, and 17.06 g of carbohydrates. Wheat gluten (WG) was obtained from Anhui Ante Food Co., Ltd., Suzhou, China, and 100 g of WG contained 7.32 g of moisture, 0.26 g of fat, 75.92 g of protein, 0.80 g of ash, and 15.7 g of carbohydrates.

Preparation of high-moisture meat analogues

The HMMAs were produced from the blend of 4.2 kg of MBP and 1.8 kg of WG (70:30, *w/w*) using a co-rotating twin screw extruder (ZSK 18MEGAlab, Coperion, Stuttgart, Germany). The length of the extruder barrel and the diameter of screws were 72 mm and 18 mm, respectively. The extruder barrel was divided into nine heating zones. For the temperature profile, zones 1, 2, 3, 4, 5, 8, and 9 were set and kept constantly at 25, 40, 60, 90, 120, 140, and 120°C, respectively. To investigate the effect of temperature, barrel zones 6 and 7 (X_1) were adjusted to temperatures ranging from 140 to 160°C for the trials. During the operation, the cooling die was kept at a steady temperature of 50°C. Dimensions of the cooling die were specified as 50×15×800 mm (width × height × length). Moisture levels (X_2) in the blends were modified to 55%–65% by adding a calculated amount of water followed by thorough mixing. A fixed screw speed of 400 rpm was applied throughout the experiment. The total feed rate of 6 kg/h was used to deliver the dry raw material mixture into the extruder. Each experimental run was carried out for 10 min before the extrudates were collected and cut into pieces (5×30 cm, thickness 15 mm). The samples were individually sealed in nylon/linear low-density polyethylene (LLDPE) bags (five samples *per* pack). All samples were stored at −20°C for no longer than 1 month.

Experimental design using central composite design (CCD) was employed to optimize extrusion conditions. The independent variables were: barrel temperature at zone 6 and 7 (X_1) and feed moisture (X_2). The coded and actual levels for the independent variables are listed in **Table 1**. The response variables for the predicted models included textural and sensory parameters. In addition, appearance and microstructure determinations were conducted.

Analysis of high-moisture meat analogues

The frozen meat analogue samples were defrosted at 4°C overnight, followed by equilibration at room temperature for a minimum of 2 h before analyses.

Appearance visualization

To evaluate the internal structure, HMMA samples were cut into pieces measuring 5×10 cm with a thickness of 15 mm, manually torn to half of their thickness, and photographed using an iPhone 12 Pro camera (Apple Inc., Cupertino, CA, USA).

Texture analysis

Texture profile analysis (TPA) of the meat analogue samples with the size of 2×2 cm and 1.5 cm thickness was performed according to Zahari *et al*. [2020] using a texture analyzer (TA-XT2i, Texture Technologies Corp., Scarsdale, NY, USA). A double-compression test was used to simulate chewing, and sensory-related parameters were calculated from the resulting force–time curves as described by Bourne [2002]. Hardness was defined as the maximum force during the first compression (N). Cohesiveness was calculated as the ratio of the area under the second

Table 1. Central composite design with coded and actual levels of extrusion parameters including barrel temperature (BT) and feed moisture content (MC).

Treatment	Actual level		Coded level	
	X_1 (Temperature, °C)	X_2 (Moisture, %, *w/w*)	X_1	X_2
140BT-55MC	140	55	−1	−1
160BT-55MC	160	55	1	−1
140BT-65MC	140	65	−1	1
160BT-65MC	160	65	1	1
135.86BT-60MC	135.86	60	−1.414	0
164.14BT-60MC	164.14	60	1.414	0
150BT-52.93MC	150	52.93	0	−1.414
150BT-67.07MC	150	67.07	0	1.414
150BT-60MC*	150	60	0	0

*Treatment was carried out in triplicate.

compression curve to that under the first compression curve. Springiness was defined as the distance the sample recovered after the first compression. Chewiness was defined as the energy required to chew the sample and was calculated as hardness × cohesiveness × springiness. Resilience was calculated as the ratio of the area during withdrawal to the area during compression in the first cycle. All parameters were determined at a minimum of ten measurements.

The degree of texturization (DT) was determined to evaluate the formation of a fibrous structure. The HMMA samples (2×2×1.5 cm) were cut to 75% of their original thickness using a Meullenet Owens razor shear blade at a speed of 2 mm/s in both vertical (lengthwise strength) and parallel (crosswise strength) direction. The razor blade shear force max (cutting force in N) was measured. A minimum of ten measurements were performed for each sample. DT was calculated according to Equation (1) [Chiang *et al*., 2019]:

$$DT = \text{Lengthwise strength}/\text{Crosswise strength} \quad (1)$$

A multiple puncture probe was used to penetrate into the HMMA sample (4×4 cm, 1.5 cm thickness) with 75% of its original thickness at a speed of 2 mm/s. The rupture force (firmness, N) was measured. A minimum of ten measurements were performed for each sample.

Determination of microstructure

Microstructure images of meat analogues were performed using a scanning electron microscope (SU3900, Hitachi, Japan). The samples taken from the center of HMMA were cut into small rectangular pieces (10×10×10 mm) and fixed in 2.5% glutaraldehyde in 0.2 M phosphate buffer, pH 7.2, for 2 h at room temperature [Chiang *et al*., 2019]. After that, the samples were dehydrated by immersion in a series of ethanol solutions of increasing concentrations (25%, 50%, 75%, 95%, and 100%) for 15 min each, and finally washed with 100% ethanol for 1 h. After drying and coating with gold particles, scanning electron micrographs were taken at 2,000× magnification. Analysis was done in triplicate for each HMMA.

Sensory evaluation

Two pieces of HMMA samples (5×10 cm, with a thickness of 15 mm) were packed in nylon/LLDPE bags, and three packs were heated in boiling water (2 L) until the internal temperature reached 80±2°C for 5 min, then cooled in iced water until the center's temperature lowered to 30°C. The cooked meat analogue samples were cut into pieces of 1.27 cm^3 cubes and subjected to evaluation.

Generic descriptive analysis (GDA) was performed based on the procedures previously used by Ergezer & Gokce [2011] and Sow & Grongnet [2010] with some modifications. Fifteen experienced panelists were recruited from the Faculty of Agro-Industry, Prince of Songkla University, Songkhla, Thailand. A total of 10 h of texture profiling training was completed by all panelists during 3 sessions prior to performing descriptive sensory evaluation of HMMA. The panelists were asked to list all descriptors related to appearance and texture that they would apply to describe HMMA during the first training session. They were allowed to engage in free discussion, while the leader acted as a facilitator to guide and organize the process without participating in the profiling. At the end of the first session, the descriptive terms, including visual fibrous strand, roughness, hardness, and the number of chews, were selected for use in the subsequent training on scoring each attribute.

Table 2. Texture lexicon used for profiling the texture of high-moisture meat analogues (HMMA).

Term	Definition	Technique	Reference	Scale
Visual fibrous strand	Amount of fibrous strand	Breaking a strip and assessing the amount of fibrous strands	Chicken breast boiled for 20 min	5
			HMMA with 55% MC	10
			HMMA with 65% MC	15
Roughness	Size of fiber at sample surface after first bite	Bite through sample 1 time with molars and assess the surface sensation by tongue	HMMA with 65% MC	4.5
			HMMA with 60% MC	7
			HMMA with 55% MC	13
Hardness	The force required to compress the sample	Compress or bite through sample 1 time with molars or incisors	Egg white (Hard cooked)	2.5
			HMMA with 65% MC	6
			HMMA with 55% MC	8
			Peanut (Cocktail type, Planters)	9
			Almonds (Shelled)	11
Number of chews	The number of chews required to prepare the sample for swallowing	Chew the sample and count the number of chews required to swallow	Chicken breast boiled for 20 min	20
			Chicken breast boiled for 40 min	30
			HMMA with 55% MC	40

MC, feed moisture content.

In the second session, the sample set (HMMA produced with low (55%) and high (65%) feed moisture content) and reference food samples were served, along with definitions and instructions for evaluating the selected textural attributes of HMMA. Sensory attribute scoring was practiced by the panelists using reference food items and cooked HMMA samples (**Table 2**). A 15-cm unstructured line scale ranging from 0 (lowest) to 15 (highest) was applied for evaluation, except the number of chews, established with a simple count. During training, reference samples were fixed on the scale, while the meat analogue sample sets were fixed through consensus. The purpose of the final session was to monitor the panelists' performance and to calibrate the consensus intensity scores. Then, 12 trained panelists were selected at the end of the last training session for sensory analysis due to their high accuracy during training and following calibration. GDA of the 11 experimental HMMAs was conducted over 3 sessions, with 4–5 samples in each session. The samples were coded with three–digit random numbers and served to the panelists in a random presentation order.

For acceptance test, 50 consumer-type panelists with age of 20–60 who commonly consume plant-based food products were recruited from the Songkhla province, Thailand. The panelists judged for appearance of visual fibrous strand (visual observation by tearing the sample into half), hardness (bite completely through the sample between the molar teeth), toughness, and overall liking using a 9-point hedonic scale. The samples were served as described previously. Bottled water was provided to the panelists to rinse their mouths between sample evaluations.

The study involving human participants was reviewed and approved by the Research Ethics Committee under the Research and Development Office, Prince of Songkla University (PSU-HREC-2023-024-1-1).

Statistical analysis

Analysis of variance (ANOVA) for regression, the coefficient of determination (R^2) and lack of fit for the mathematical models were analyzed using Design Expert version 13 (Stat-Ease, Inc., Minneapolis, MN, USA). The significance of the differences was defined at $p<0.05$. Pearson correlation analysis was conducted between sensory parameters. All analyses were performed using SPSS statistic program (version 28.0 for Windows, SPSS Inc., Chicago, IL, USA).

RESULTS AND DISCUSSION

Appearance

The images of meat analogues made with different barrel temperatures and feed moisture contents are shown in **Figure 1**. All meat analogue samples developed layered and fibrous structures (meat-like texture). When tearing the samples, they separated into long and aligned fibrous strands rather than breaking into breaking-like brittle materials, indicating an anisotropic internal structure similar to the muscle fiber of cooked meat, such as chicken breast. During extrusion under high temperature

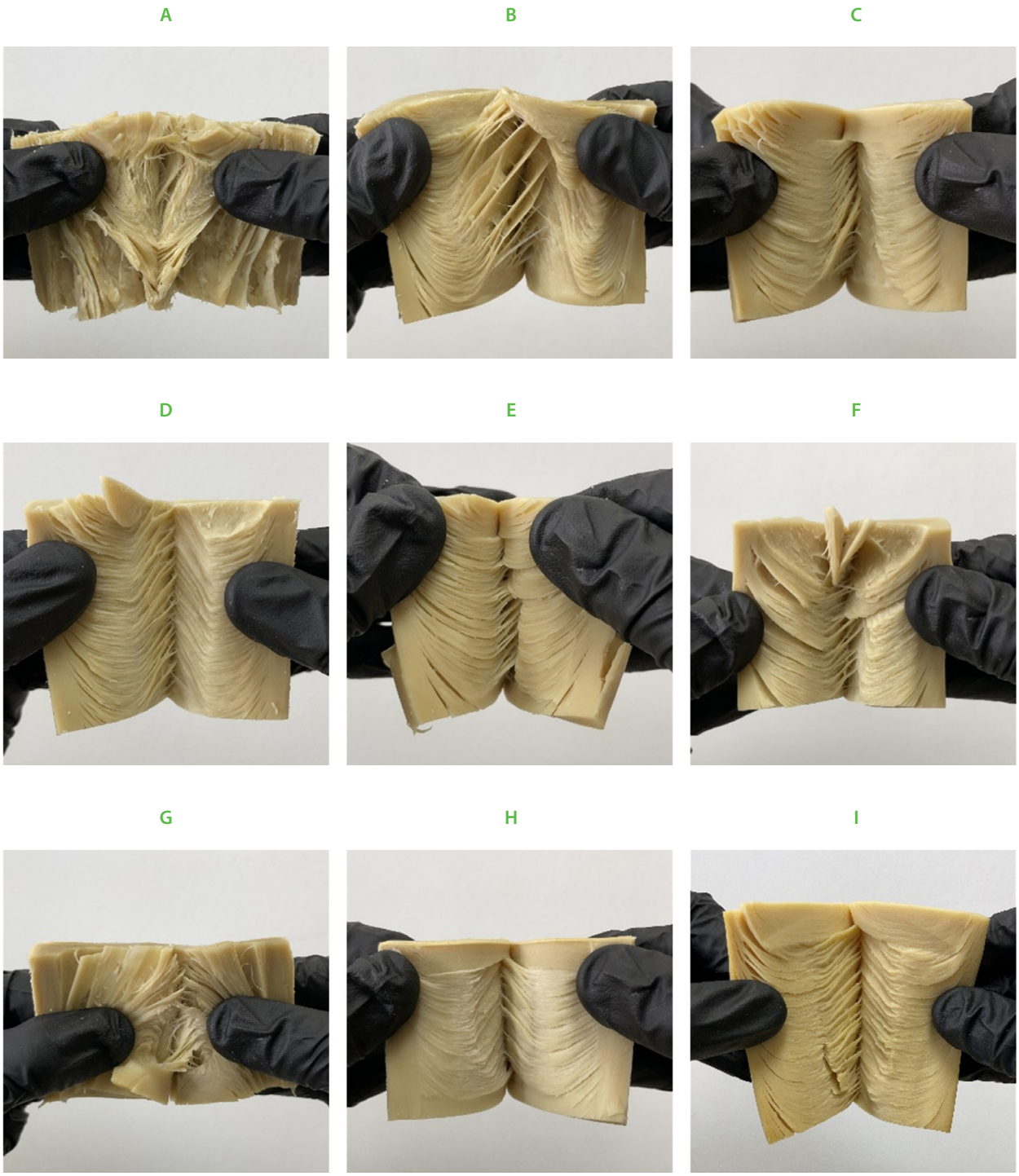

Figure 1. Appearance of high-moisture meat analogues produced using a blend of mung bean protein isolate and wheat gluten (70:30, *w/w*) at different barrel temperatures (BT, °C) and feed moisture contents (MC, %, *w/w*): (**A**) 140BT-55MC, (**B**) 160BT-55MC, (**C**) 140BT-65MC, (**D**) 160BT-65MC, (**E**) 135.86BT-60MC, (**F**) 164.14BT-60MC, (**G**) 150BT-52.93MC, (**H**) 150BT-67.07MC, and (**I**) 150BT-60MC.

and dynamic shear, proteins unfold from their native spherical conformation, leading to chain breakage, exposure of sulfhydryl groups, and reduced hydrogen bond stability. Shear stress, pressure drop, and moisture evaporation at the die promote molecular chain alignment and stretching. Subsequently, the cooling die stabilizes the extrudate structure by enhancing hydrogen and disulfide bonding, resulting in a more disordered protein network and the formation of rigid, interlaced fibrous structures [Sun *et al.,* 2023]. Meat analogues with a high feed moisture content (60, 65 and 67.07%, **Figure 1C–F** and **H–I**) showed thinner, denser, and more numerous fibrous strands than those produced with a low feed moisture content (52.93 and 55%, **Figure 1 A–B** and **G**). These results are consistent with the findings of Chen *et al.* [2010], who reported that feed moisture content had a significant impact on the texture of HMMA from soy protein, with the optimal fibrous structure observed at 60% feed moisture content.

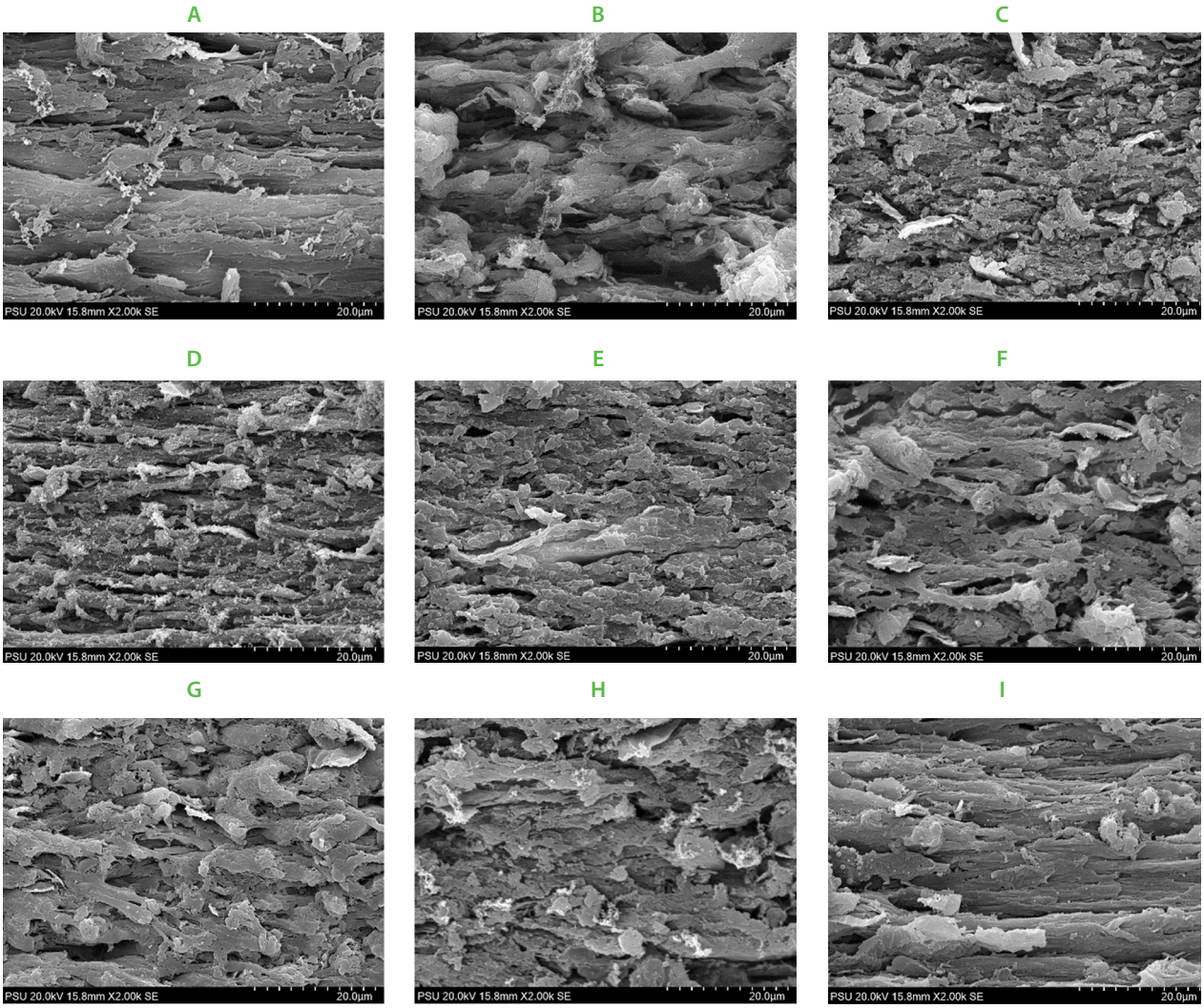

Figure 2. Scanning electron micrographs of high-moisture meat analogues produced using a blend of mung bean protein isolate and wheat gluten (70:30, *w/w*) at different barrel temperatures (BT, ºC) and feed moisture contents (MC, %, *w/w*). (**A**) 140BT-55MC, (**B**) 160BT-55MC, (**C**) 140BT-65MC, (**D**) 160BT-65MC, (**E**) 135.86BT-60MC, (**F**) 164.14BT-60MC, (**G**) 150BT-52.93MC, (**H**) 150BT-67.07MC, and (**I**) 150BT-60MC.

They also suggested that the meat analogue had more fibrous structure when increasing the moisture content from 28 to 60%. Gulzar *et al*. [2025] also pointed out that a higher extrusion moisture level (65%) enhanced the formation of fibrous texture of soy protein-based HMMA compared to 50% level. Moisture content plays the roles of lubricant, plasticizer, and reactant during extrusion process, while also facilitating protein molecular unfolding and structural rearrangement and increasing the flexibility and mobility of protein chains [Ryu, 2020; Sun *et al*., 2023]. Nevertheless, the meat analogue with the highest moisture content (67.07%, **Figure 1H**) exhibited a less fibrous structure than the samples with 60% and 65% feed moisture contents (**Figure 1C-F** and **I**), as characterized by fibers that adhered to each other and were not clearly defined. Lin *et al*. [2000] reported that the structure of HMMA from soy protein and wheat gluten became more directionally aligned with moisture content decreasing from 70% to 60%. Additionally, Liu & Hsieh [2008] revealed that when moisture content ranged from 60.11 to 72.11%, the well-defined fiber orientation of meat analogue was found only at 60.11%. Moreover, Sun *et al*. [2023] suggested that excessive moisture content leads to incomplete texturization of extrudates, which may be attributed to protein dilution, reduced energy required for structural disruption, and increased molecular flexibility and fluidity. These effects limit the exposure of reactive groups in protein structures, thereby reducing protein aggregation and cross-linking. From these phenomena, it could be concluded that moisture could facilitate protein unfolding and molecular alignment during the extrusion process; however, the positive effect of moisture on fibrous structure development has its limitations.

Nevertheless, extrusion temperature exhibited no significant impact on the appearance of the meat analogue (**Figure 1**). This is similar to the results of previous studies on the production of HMMA from pea proteins, which revealed that the effect of barrel temperature on meat analogue properties was relatively minor compared to the effect of feed moisture content [Sun *et al*., 2023; Zhang & Ryu, 2023].

Table 3. Firmness in a penetration test, crosswise strength and lengthwise strength of shear force, and degree of texturization of high-moisture meat analogues produced using a blend of mung bean protein isolate and wheat gluten (70:30, *w/w*) at different barrel temperatures (BT, °C) and feed moisture contents (MC, %, *w/w*).

Treatment	Firmness (N)	Crosswise strength (N)	Lengthwise strength (N)	Degree of texturization
140BT-55MC	91.8±8.3	7.8±2.3	9.9±1.2	1.4±0.6
160BT-55MC	108.8±4.4	6.7±1.9	12.3±0.5	2.0±0.6
140BT-65MC	46.8±5.5	4.6±1.0	6.5±0.5	1.5±0.4
160BT-65MC	53.9±11.4	7.8±0.4	7.9±0.4	1.0±0.1
135.86BT-60MC	72.0±4.8	9.9±1.9	9.6±1.0	1.0±0.3
164.14BT-60MC	68.9±7.5	6.1±1.4	9.2±0.6	1.6±0.5
150BT-52.93MC	105.3±11.7	8.4±2.6	9.4±1.2	1.3±0.5
150BT-67.07MC	33.5±2.0	3.1±0.4	4.6±0.2	1.5±0.2
150BT-60MC*	67.7±5.6	9.8±1.2	10.5±1.4	1.1±0.2

Values are mean ± standard deviation (n=10). *Treatment was carried out in triplicate.

Table 4. Parameters of texture profile analysis of high-moisture meat analogues produced using a blend of mung bean protein isolate and wheat gluten (70:30, *w/w*) at different barrel temperatures (BT, °C) and feed moisture contents (MC, %, *w/w*).

Treatment	Hardness (N)	Springiness	Cohesiveness	Chewiness (N)	Resilience
140BT-55MC	342±23	0.84±0.03	0.67±0.02	194±16	0.35±0.01
160BT-55MC	390±22	0.89±0.06	0.75±0.01	260±19	0.41±0.01
140BT-65MC	198±11	0.95±0.02	0.73±0.02	136±10	0.36±0.01
160BT-65MC	284±27	0.90±0.03	0.74±0.02	188±20	0.39±0.02
135.86BT-60MC	250±17	0.91±0.03	0.73±0.02	167±13	0.37±0.02
164.14BT-60MC	276±13	0.92±0.02	0.78±0.02	197±9	0.43±0.01
150BT-52.93MC	340±26	0.86±0.05	0.71±0.01	207±19	0.37±0.01
150BT-67.07MC	164±5	0.92±0.03	0.70±0.02	106±5	0.36±0.01
150BT-60MC*	288±18	0.89±0.05	0.75±0.02	194±25	0.39±0.02

Values are means ± standard deviation (n=10). *Treatment was carried out in triplicate.

Microstructure

The microstructure images (at 2,000× magnification) of the meat analogues obtained under different extrusion conditions were displayed in **Figure 2**. The results were aligned with images of HMMA appearance shown in **Figure 1**. The meat analogues with low feed moisture contents of 52.93% (**Figure 2G**) and 55% (**Figure 2A–B**) exhibited larger fiber strands with multiple segmented layers and cavity structures, while those with high feed moisture contents of 60% (**Figure 2E–F** and **I**) and 65% (**Figure 2C-D**) showed thinner fibrous strands with greater continuity, smaller pores, and a lower pore number. The sample with 67% feed moisture (**Figure 2H**) demonstrated a layered and less fibrous structure. The effect of extrusion temperature on the microstructure of meat analogues was lesser when compared with that of feed moisture content. At a lower feed moisture content (55%) and barrel temperatures of 150 and 160°C (**Figure 2G** and **B**), the samples showed larger fibrous strands, whereas the samples processed at 140°C (**Figure 2A**) exhibited more compact strand alignment. Our study results are consistent with findings from previous studies reporting that the influence of extrusion temperature was significant only under low feed moisture conditions [Lin *et al*., 2000; Zhang & Ryu, 2023]. In particular, higher extrusion temperatures were associated with enhanced protein denaturation, molecular disassembly, and protein realignment under shear [Sun *et al*., 2023].

Textural properties

The effects of barrel temperature and feed moisture content on HMMA textural properties are presented in **Table 3** and **Table 4**. The results of the ANOVA, including R^2 values, model significance

Table 5. Predictive regression models and goodness-of-fit of the response variables for high-moisture meat analogues produced using a blend of mung bean protein isolate and wheat gluten (70:30, *w/w*) at different barrel temperatures (X_1) and feed moisture contents (X_2).

Analysis	Response variable	Regression model	R^2	Probability of model	Lack of fit
Penetration test	Firmness	$Y = 7265.38 + 251.98\ X_1 - 2565.68\ X_2$	0.9475	Sig	NS
Texture profile analysis	Hardness	$Y = 28780.89 + 2180.79\ X_1 - 6358.48\ X_2$	0.8448	Sig	NS
	Springiness	$Y = 0.90 + 1.768 \times 10^{-003}\ X_1 + 0.026 - 0.025\ X_1\ X_2$	0.5879	NS	NS
	Cohesiveness	$Y = 0.75 + 0.020\ X_1 + 4.482 \times 10^{-003}\ X_2 - 0.017\ X_1\ X_2 - 1.042 \times 10^{-003}\ X_1^2 - 0.026\ X_2^2$	0.7883	NS	NS
	Chewiness	$Y = 18871.25 + 2054.73\ X_1 - 3475.42\ X_2$	0.7424	Sig	NS
	Resilience	$Y = 0.39 + 0.022\ X_1 - 3.018 \times 10^{-003}\ X_2 - 7.500 \times 10^{-003}\ X_1\ X_2 + 2.083 \times 10^{-003}\ X_1^2 - 0.015\ X_2^2$	0.8614	Sig	NS
Shear force measurement	Crosswise strength	$Y = 9.76 - 0.41\ X_1 - 1.20\ X_2 + 1.08\ X_1\ X_2 - 0.92\ X_1^2 - 2.04\ X_2^2$	0.7917	NS	Sig
	Lengthwise strength	$Y = 10.46 + 0.42\ X_1 - 1.82\ X_2 - 0.26\ X_1\ X_2 - 0.30\ X_1^2 - 1.49\ X_2^2$	0.9042	Sig	NS
	Degree of texturization	$Y = 1.32 + 0.12\ X_1 - 0.072\ X_2 - 0.26\ X_1\ X_2$	0.4420	NS	NS
Sensory descriptive analysis	Visual fibrous strand	$Y = 14.47 + 0.69\ X_1 + 2.16\ X_2 - 0.11\ X_1\ X_2 - 1.46\ X_1^2 - 1.86\ X_2^2$	0.8824	Sig	Sig
	Hardness	$Y = 6.91 + 0.31\ X_1 - 1.15\ X_2$	0.7346	Sig	NS
	Roughness	$Y = 5.57 - 0.26\ X_1 - 3.52\ X_2 + 0.31\ X_1\ X_2 + 2.20\ X_1^2 + 1.03\ X_2^2$	0.9746	Sig	NS
	Number of chews	$Y = 35.51 + 0.025\ X_1 - 7.22\ X_2$	0.8335	Sig	NS
Acceptance test	Appearance	$Y = 6.42 - 0.021\ X_1 + 0.53\ X_2$	0.8557	Sig	NS
	Hardness	$Y = 5.70 - 0.21\ X_1 + 0.80\ X_2$	0.7117	Sig	NS
	Toughness	$Y = 5.84 - 0.24\ X_1 + 0.72\ X_2$	0.6762	Sig	NS
	Overall liking	$Y = 5.88 - 0.15\ X_1 + 0.83\ X_2$	0.7712	Sig	NS

Sig, statistical significance at $p<0.05$; NS, non-significant.

(*p*-values), and lack-of-fit statistics for the textural properties of HMMA as influenced by barrel temperature and feed moisture content, are presented in **Table 5**. ANOVA indicated that the feed moisture content significantly affected all texture parameters, except resilience, while barrel temperature was only significant to chewiness and resilience ($p<0.05$). However, both variables had no impact on springiness, cohesiveness, shear force (crosswise strength), and the degree of texturization ($p\geq0.05$).

The response surface of product firmness as function of extruder barrel temperatures and feed moisture contents is shown in **Figure 3A**. The highest product firmness was found for the meat analogues extruded with lower feed moisture contents (52.93% and 55%). On the other hand, the meat analogues extruded with high feed moisture contents (65% and 67.07%) showed lower firmness regardless of barrel temperature (**Table 3**).

The impact of barrel temperatures and feed moisture contents on meat analogue TPA parameters, including hardness chewiness, and resilience, are shown in **Figure 3B–D**. Hardness showed a progressive decrease with an increasing feed moisture content. The sample extruded with high moisture contents (65% and 67.07%) showed lower hardness, with the lowest value found for the sample produced with the highest feed moisture content (**Table 4**). These results align with firmness determination results and are in agreement with the findings of Lin *et al*. [2000], who revealed that the feed moisture content had a greater influence on overall product texture compared to extrusion temperature. The results of chewiness test followed the same trend as those of hardness (**Figure 3**, **Table 4**). The highest value was found for the meat analogue with 55% feed moisture content extruded at 160°C barrel temperature. The resilience of HMMA samples was slightly affected, with values ranging from 0.35 to 0.43. Nevertheless, it was not possible to apply the predicted models for springiness and cohesiveness, as they had low R^2 values and lacked statistical significance in probability of the model (**Table 5**), which are generally regarded as unreliable for predictive purposes [Koocheki *et al*., 2009; Myers & Montgomery, 2002].

The degree of texturization (DT) indicates the formation of a fibrous structure with values greater than 1. The force required to cut across the meat analogues in the lengthwise strength is higher than that in the crosswise strength [Chen *et al*., 2010]. According to data in **Table 5**, the predicted model of DF and crosswise strength shear force could not be applied due to statistical insignificance of the model or low R^2 value. The effects of extruder barrel temperatures and feed moisture contents on the shear force (lengthwise strength) of HMMAs are shown in **Figure 3E**. All samples extruded at a high moisture content exhibited the formation of a fibrous structure because of showing a value of more than 1 by Meullenet Owens razor shear blade (knife blade) (**Table 3**). Among these, the highest DT was found in 160BT-55MC, which was consistent with the microstructure shown in **Figure 2**. The low extrusion moisture increased friction and shear within the cooling die, resulting in a higher velocity gradient and enhanced fibrous structure formation [Lin *et al*., 2000]. Chen *et al*. [2010] reported that moisture content significantly affected the degree of texturization, and the most well-developed fibrous structure was observed in soybean meat analogue extruded at 60% feed moisture. Regarding extrusion temperature, many studies have suggested that barrel temperature significantly affected texture attributes only at lower moisture contents [Lin *et al*., 2000]. Additionally, Kitabatake *et al*. [1985] found that extrusion temperature had a minimal influence on product texture when soy protein isolate meat analogue was processed at a feed moisture content above 70%.

Sensory analysis

Descriptive analysis

The results of descriptive sensory analysis are provided in **Table 6**. The predicted equations, coefficients of determination (R^2), probability of models, and lack of fit of models obtained for the effect of the extrusion process on attributes of descriptive analysis (visual fibrous strand, hardness, roughness, and number of chews) are depicted in **Table 5**. According to ANOVA of regression, the predicted visual fibrous strand model could not be applied due to a substantial lack of fit in the model ($p<0.05$). The response surfaces created from the predicted models as shown in **Figure 3** revealed that only feed moisture content significantly affected all sensory descriptors ($p<0.05$). Regardless of barrel temperature, hardness and the number of chews increased with a decreasing extrusion moisture content. These results were in agreement with hardness determined by TPA and firmness determined in the penetration test as discussed above. Furthermore, roughness and the number of chews were positively correlated with hardness (correlation coefficient, $r=0.83$ and 0.92, respectively, $p<0.05$), indicating strong positive relationships, whereby increases in roughness and chew number were associated with increased hardness. The higher roughness and the number of chews were found for the meat analogues with a low feed moisture content, while the lowest roughness, the number of chews, and hardness were shown for the meat analogue with a high feed water content (150BT-67.07MC).

For the visual fibrous strand, the score ranging from 11.5 to 15.0 was found in the meat analogue with a medium and high feed moisture (60–67.07%), while those with low moisture contents (52.93% and 55%) received the lowest scores ranging from 6.6 to 10.0 (**Table 5**). The fibrous strands of the sample with a high feed moisture were much finer compared to those of boiled chicken breast (score of 5) (**Table 2**).

Acceptance test

The predicted equations, coefficients of determination (R^2), probability of models, and lack of fit of models obtained for appearance, hardness, toughness, and overall liking determined in the acceptance test are depicted in **Table 5**. Models for the appearance, hardness, and overall liking were statistically significant ($p<0.05$), exhibited non-significant lack of fit ($p\geq0.05$), and had R^2 values greater than 0.7; thus, they were considered adequate and used to generate the response surface contour plots (**Figure 4**). All models were linear equations (**Table 5**). R^2

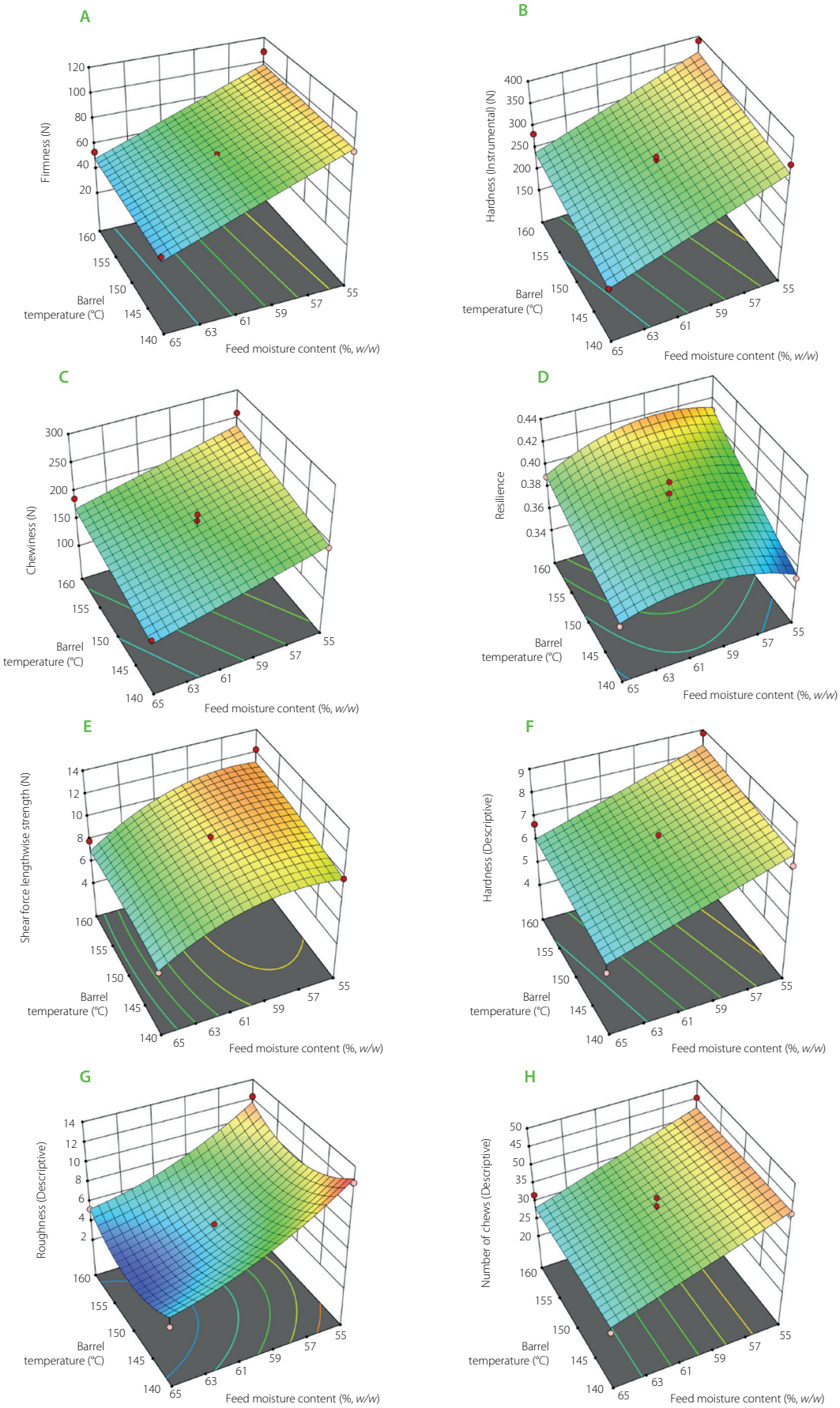

Figure 3. Response surface contour plots displaying the combined effect of barrel temperatures and feed moisture contents on texture parameters determined by texture profile analysis and penetration test, including firmness (**A**), hardness (**B**), chewiness (**C**), resilience (**D**), and shear force (lengthwise strength) (**F**), as well as by sensory descriptive analysis, including hardness (**G**), roughness (H), and number of chews (**I**) of high-moisture meat analogues produced using a blend of mung bean protein isolate and wheat gluten (70:30, *w/w*).

Table 6. Mean scores of descriptive sensory analysis and acceptance test of high-moisture meat analogues produced using a blend of mung bean protein isolate and wheat gluten (70:30, *w/w*) at different barrel temperatures (BT, ºC) and feed moisture contents (MC, %, *w/w*).

Treatment	Descriptive sensory analysis scores*				Acceptance test scores**			
	Hardness	Roughness	Visual fibrous strand	Number of chews	Appearance	Hardness	Toughness	Overall liking
140BT-55MC	7.3±0.9	12.5±0.9	6.6±1.3	42.1±4.6	5.9±1.8	6.0±1.6	6.2±1.7	6.0±1.7
160BT-55MC	8.9±0.9	12.3±0.9	10.0±0.0	45.4±9.8	5.9±1.6	4.7±2.1	4.8±2.2	4.8±1.9
140BT-65MC	5.1±0.7	4.3±1.0	12.0±1.4	26.8±5.3	6.7±1.4	6.6±1.6	6.7±1.8	6.7±1.6
160BT-65MC	6.7±0.9	5.3±1.3	15.0±0.0	32.0±8.3	6.8±1.6	6.1±1.8	6.1±2.2	6.4±1.8
135.86BT-60MC	7.8±0.8	11.2±1.9	12.1±1.5	39.0±10.0	6.9±1.4	6.1±1.6	6.2±1.7	6.3±1.6
164.14BT-60MC	7.2±0.9	9.1±1.5	11.5±1.4	33.1±7.6	6.7±1.7	6.2±1.9	6.4±1.7	6.5±1.7
150BT-52.93MC	8.0±0.6	12.4±1.2	8.6±1.8	42.8±8.6	5.8±1.9	4.4±2.0	4.7±2.0	4.7±2.0
150BT-67.07MC	4.6±0.9	3.3±0.9	13.4±1.8	22.3±6.4	7.3±1.5	7.2±1.6	7.2±1.6	7.4±1.5
150BT-60MC***	6.9±1.0	5.6±1.2	14.4±0.7	35.8±7.3	6.5±1.6	5.6±1.9	5.8±1.8	5.8±1.8

Values are mean ± standard deviation (*n=12 or **n=50). ***Treatment was carried out in triplicate.

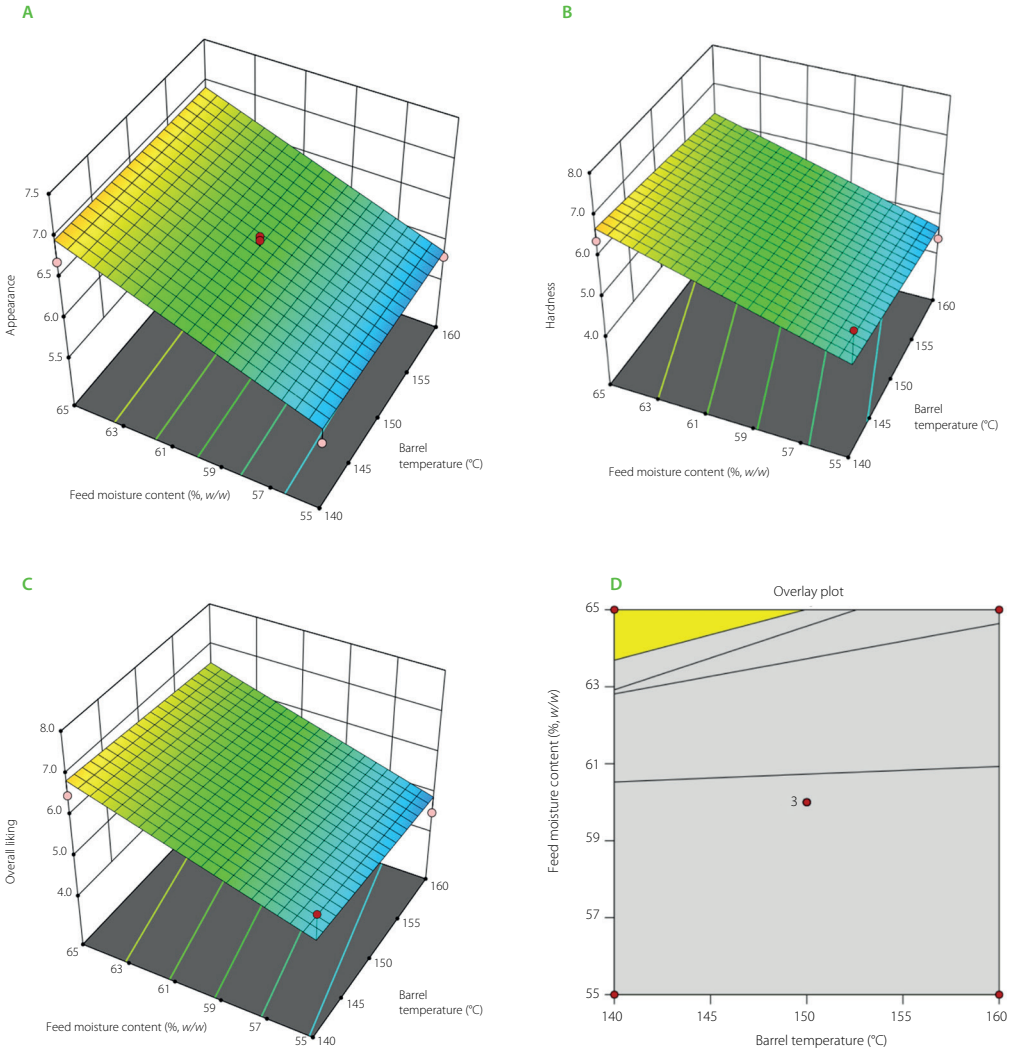

Figure 4. Response surface contour plots of acceptance scores including appearance (**A**), hardness (**B**), and overall liking (**C**) of high-moisture meat analogues produced using a blend of mung bean protein isolate and wheat gluten (70:30, *w/w*) at different barrel temperatures and feed moisture contents. The optimum region (yellow shade) that obtained high appearance, hardness, and overall liking score levels (>6.5, >6.5, and >6.5, respectively) (**D**).

values determined for all attributes ranged from 0.6762 to 0.8557, implying that the model explained 67.62% to 85.57% of the total variance. Feed moisture content was identified as the key factor affecting appearance, hardness, toughness, and overall liking, as indicated by its higher coefficient values in the predictive regression models compared to those of barrel temperature. The liking scores of all attributes of the meat analogues tended to increase with an increasing extrusion moisture content (**Table 6**). This finding indicated that the panelists preferred the meat analogue with soft and easy-to-chew texture. Previous studies have suggested that increasing extrusion moisture content significantly reduced hardness, springiness, cohesiveness, and chewiness in both soy- and pea protein-based products [Chen *et al*., 2010; Zhang & Ryu, 2023]. In extrusion process, the feed moisture content is considered the most influential factor on both the system and the characteristics of the meat analogue. On the contrary, extrusion temperature showed no effect ($p \geq 0.05$) on all attributes in the acceptance test. To determine the optimum region, a contour plot showing predicted scores of appearance, hardness, and overall liking (each at least 6.5, close to maximum values) was used to identify the optimal formulation range. The optimum region (yellow shaded area in **Figure 4D**) corresponding to 140°C barrel temperature and 65% feed moisture content had the highest desirability of 0.644. Verification of the predicted model showed that the observed acceptance scores for appearance, hardness, and overall liking were 6.7±1.4, 6.4±1.6, and 6.5±1.6, respectively. The experimental errors, compared with the predicted values, ranged from 1.20% to 2.08%.

CONCLUSIONS

MBP and WG blend was successfully used to develop high-moisture meat analogue using a co-rotating twin screw extruder. The results indicate that feed moisture content was the most influential factor affecting the development of fibrous microstructure, as well as textural and sensory properties of the product. Increased feed moisture promoted protein alignment and enhanced the formation of a well-defined fibrous structure, which contributed to improved texture and overall acceptability. However, feed moisture contents higher than 65% led to adverse effects on fibrous structure formation. The optimized conditions for producing MBP and WG based HMMA with the highest acceptability were: barrel temperature of 140°C and 65% feed moisture content. The findings provide valuable insights into the role of processing conditions in HMMA development and offer practical guidance for optimizing product quality in industrial applications.

ACKNOWLEDGEMENTS

The authors would like to thank the Faculty of Agro-Industry, Prince of Songkla University, for providing access to research facilities. The authors are also grateful to the National Metal and Materials Technology Center (MTEC) for assistance in extrusion process.

RESEARCH FUNDING

This research was supported by National Science, Research and Innovation Fund (NSRF) and Prince of Songkla University (Grant No. AGR6505031C), and by the PSU-Graduate Studies Scholarship (PSU_PHD2563-04) and Overseas Thesis Research Grant for Graduate Students (OTR 2567-003) from the Graduate School, Prince of Songkla University.

CONFLICT OF INTERESTS

The authors declare that they have no conflict of interests.

OTHER INFORMATION

The study involving human participants was reviewed and approved by the Research Ethics Committee under the Research and Development Office, Prince of Songkla University (PSU--HREC-2023-024-1-1).

ORCID IDs

K. Kijroongrojana https://orcid.org/0000-0002-8981-796X
K. Mektun https://orcid.org/0009-0002-9699-4566

REFERENCES

1. Anwar, F., Latif, S., Przybylski, R., Sultana, B., Ashraf, M. (2007). Chemical composition and antioxidant activity of seeds of different cultivars of mungbean. *Journal of Food Science*, *72*(7), S503-S510. https://doi.org/10.1111/j.1750-3841.2007.00462.x
2. Arizton (2024). Plant-based meat market - Global outlook & forecast 2024--2030 (online). (Accessed: October 20, 2020). https://www.arizton.com/market-reports/plant-based-meat-market--size-analysis
3. Bourne, M.C. (2002). Chapter 7: Sensory methods of texture and viscosity measurements. In M.C. Bourne (Ed.), Food Texture and Viscosity: Concept and Measurement. Academic Press. London, pp. 257-291. https://doi.org/10.1016/B978-012119062-0/50007-3
4. Chen, F.L., Wei, Y.M., Zhang, B., Ojokoh, A.O. (2010). System parameters and product properties response of soybean protein extruded at wide moisture range. *Journal of Food Engineering*, *96*(2), 208-213. https://doi.org/10.1016/j.jfoodeng.2009.07.014
5. Chiang, J.H., Loveday, S.M., Hardacre, A.K., Parker, M.E. (2019). Effects of soy protein to wheat gluten ratio on the physicochemical properties of extruded meat analogues. *Food Structure*, *19*, art. no. 100102. https://doi.org/10.1016/j.foostr.2018.11.002
6. Dahiya, P.K., Linnemann, A.R., Van Boekel, M.A.J.S., Khetarpaul, N., Grewal, R.B., Nout, M.J.R. (2015). Mung bean: Technological and nutritional potential. *Critical Reviews in Food Science and Nutrition*, *55*(5), 670-688. https://doi.org/10.1080/10408398.2012.671202
7. Du, M., Xie, J., Gong, B., Xu, X., Tang, W., Li, X., Li, C., Xie, M. (2018). Extraction, physicochemical characteristics and functional properties of Mung bean protein. *Food Hydrocolloids*, *76*, 131-140. https://doi.org/10.1016/j.foodhyd.2017.01.003
8. Ergezer, H., Gokce, R. (2011). Comparison of marinating with two different types of marinade on some quality and sensory characteristics of turkey breast meat. *Journal of Animal and Veterinary Advances*, *10*(1), 60-67.
9. Gulzar, S., Tagrida, M., Martín-Belloso, O., Soliva-Fortuny, R. (2025). Optimizing high-moisture meat analogue textures through artificial intelligence: The effect of sorbitol in soy protein concentrate blends. *LWT – Food Science and Technology*, *217*, art. no. 117416. https://doi.org/10.1016/j.lwt.2025.117416
10. Hwang, N.K., Gu, B.J., Zhang, Y., Ryu, G.H. (2024). Possibility of isolated mung bean protein as a main raw material in the production of an extruded high-moisture meat analog. *Foods*, *13*(14), art. no. 2167. https://doi.org/10.3390/foods13142167
11. Joshi, V.K., Kumar, S. (2015). Meat analogues: Plant based alternatives to meat products – a review. *International Journal of Food and Fermentation Technology*, *5*(2), 107-119. https://doi.org/10.5958/2277-9396.2016.00001.5

12. Kitabatake, N., Megard, D., Cheftel, J.C. (1985). Continuous gel formation by HTST extrusion-cooking: Soy proteins. *Journal of Food Science*, *50*(5), 1260-1265.
https://doi.org/10.1111/j.1365-2621.1985.tb10457.x
13. Koocheki, A., Taherian, A.R., Razavi, S.M.A., Bostan, A. (2009). Response surface methodology for optimization of extraction yield, viscosity, hue and emulsion stability of mucilage extracted from *Lepidium perfoliatum* seeds. *Food Hydrocolloids*, *23*(8), 2369-2379.
https://doi.org/10.1016/j.foodhyd.2009.06.014
14. Lin, S., Huff, H., Hsieh, F. (2000). Texture and chemical characteristics of soy protein meat analog extruded at high moisture. *Journal of Food Science*, *65*(2), 264-269.
https://doi.org/10.1111/j.1365-2621.2000.tb15991.x
15. Liu, K., Hsieh, F.H. (2008). Protein-protein interactions during high-moisture extrusion for fibrous meat analogues and comparison of protein solubility methods using different solvent systems. *Journal of Agricultural and Food Chemistry*, *56*(8), 2681-2687.
https://doi.org/10.1021/jf073343q
16. Mubarak, A.E. (2005). Nutritional composition and antinutritional factors of mung bean seeds (*Phaseolus aureus*) as affected by some home traditional processes. *Food Chemistry*, *89*(4), 489-495.
https://doi.org/10.1016/j.foodchem.2004.01.007
17. Myers, R.H., Montgomery, D.C. (2002). Response surface methodology: Process and Product Optimization Using Designed Experiments. 2nd edition. John Willey & Sons, Inc.. New York, USA.
18. Plattner, B.J., Hong, S., Li, Y., Talavera, M.J., Dogan, H., Plattner, B.S. Alavi, S. (2024). Use of pea proteins in high-moisture meat analogs: Physicochemical properties of raw formulations and their texturization using extrusion. *Foods, 13*(8), art. no. 1195.
https://doi.org/10.3390/foods13081195
19. Ryu, G. (2020). Chapter 7: Extrusion cooking of high-moisture meat analogues. In G.M. Ganjyal (Ed.), Extrusion Cooking. 2nd edition, Woodhead Publishing, Cambridge, UK, pp. 205-224.
https://doi.org/10.1016/B978-0-12-815360-4.00007-9
20. Samard, S., Gu, B., Ryu, G. (2019). Effects of extrusion types, screw speed and addition of wheat gluten on physicochemical characteristics and cooking stability of meat analogues. *Journal of the Science of Food and Agriculture*, *99*(11), 4922-4931.
https://doi.org/10.1002/jsfa.9722
21. Seetapan, N., Raksa, P., Limparyoon, N., Srirajan, S., Makmoon, T., Israkarn, K., Gamonpilas, C., Methacanon, P., Fuongfuchat, A. (2023). High moisture extrusion of meat analogues using mung bean (*Vigna radiata* L.) protein and flour blends: investigations on morphology, texture and rheology. *International Journal of Food Science and Technology*, *58*(4), 1922-1930.
https://doi.org/10.1111/ijfs.16334
22. Sow, T.M.A., Grongnet, J.F. (2010). Sensory characteristics and consumer preference for chicken meat in Guinea. *Poultry Science*, *89*(10), 2281-2292.
https://doi.org/10.3382/ps.2010-00679
23. Sun, D., Zhang, B., Zhou, C., Ren, W., Wu, M. (2023). Effect of high-moisture extrusion process on quality attribute and fibrous formation mechanism of pea protein: Insight into dynamic changes of textural protein. *Innovative Food Science and Emerging Technologies*, *89*, art. no. 103486.
https://doi.org/10.1016/j.ifset.2023.103486
24. Theng, A.H.P., Tarique, M., Ong, D.S.M., Chiang, J.H., Rasul, S., Yuliarti, O. (2025). Evaluating the effects of insoluble dietary fibres on pea protein-based extruded meat analogues. *International Journal of Biological Macromolecules, 311*(Part 1), art. no. 143715.
https://doi.org/10.1016/j.ijbiomac.2025.143715
25. Zahari, I., Ferawati, F., Helstad, A., Ahlström, C., Östbring, K., Rayner, M., Purhagen, J.K. (2020). Development of high-moisture meat analogues with hemp and soy protein using extrusion cooking. *Foods*, *9*(6), art. no. 772.
https://doi.org/10.3390/foods9060772
26. Zhang, T., Dou, W., Zhang, X., Zhao, Y., Zhang, Y., Jiang, L., Sui, X. (2021). The development history and recent updates on soy protein-based meat alternatives. *Trends in Food Science & Technology, 109*, 702–710.
https://doi.org/10.1016/j.tifs.2021.01.060
27. Zhang, Y., Ryu, G.H. (2023). Effects of process variables on the physicochemical, textural, and structural properties of an isolated pea protein-based high-moisture meat analog. *Foods*, *12*(24), art. no. 4413.
https://doi.org/10.3390/foods12244413
28. Zhao, Y., Li, K., Zhang, X., Zhang, T., Zhao, J., Jiang, L., Sui, X. (2024). Protein blend extrusion: Crafting meat analogues with varied textural structures and characteristics. *Food Chemistry, 460*(Part 3), art. no. 140709.
https://doi.org/10.1016/j.foodchem.2024.140709

ORIGINAL ARTICLE
http://journal.pan.olsztyn.pl

Polish Journal of Food and Nutrition Sciences
2026, Vol. 76, No. 2, 202–214
DOI: 10.31883/pjfns/221784
ISSN 1230-0322, e-ISSN 2083-6007

Heat-Induced Aging Improvements in Sensory Quality, Antioxidant and Anti-Inflammatory Activities of *Allium schoenoprasum* L. Bulbs

Nguyen H.K. Nguyen[1]†, Nam Q. Tran[1]†, Nghia T. Nguyen[2], Bao M.N. Nguyen[1], Ngoc N. Nguyen[1], Ha L. Nguyen[3]*

[1]Faculty of Applied Science and Technology, Nguyen Tat Thanh University, 300A Nguyen Tat Thanh Street, Xom Chieu Ward, Ho Chi Minh City, Vietnam
[2]Biotechnology Center of Ho Chi Minh City, 2374 Do Muoi Street, Trung My Tay Ward, Ho Chi Minh City, Vietnam
[3]Institute of Applied Sciences, HUTECH University, 475A Dien Bien Phu Street, Thanh My Tay Ward, Ho Chi Minh City, Vietnam

This study investigated the effects of heat-induced aging on the nutritional composition, physicochemical properties, sensory profiles, and biological activities of *Allium schoenoprasum* L. (AS) bulbs over a 7-day period. Key parameters evaluated included instrumental color, texture, bioactive compound content (total phenolics and total flavonoids), antioxidant capacity (ABTS$^{\bullet+}$ scavenging activity and ferric reducing antioxidant power, FRAP), and anti-inflammatory potential (bovine serum albumin denaturation inhibition). The results demonstrated that thermal aging for 7 days resulted in a significant reduction in moisture content (from 65.18 to 23.33 g/100 g fresh weight, FW) and a transition to a distinct black color (L^* value decreased from 76.91 to 26.94). Thermal treatment induced increases in contents of reducing sugars and total soluble solids. These shifts effectively enhanced the flavor profile and overall sensory acceptability (score increased from 5.57 to 8.29). Importantly, although total phenolic and total flavonoid contents initially declined (days 1–2), they substantially increased during the later stages of aging (days 3–7). This accumulation of phenolic compounds resulted in a significant enhancement in antioxidant capacity, evidenced by increases in ABTS$^{\bullet+}$ scavenging activity and FRAP. Conversely, the specific anti-inflammatory capacity of the aged AS bulbs was significantly lower compared to the fresh samples. These findings provide critical insights into the dynamic physicochemical transformations of AS during aging, assisting manufacturers in optimizing processing parameters to develop high-quality black AS products with targeted functional properties.

Keywords: bioactive compounds, color parameters, *in vitro* bioactivity, radical scavenging, textural properties, thermal processing

INTRODUCTION

Allium schoenoprasum L. (AS), a member of the subfamily Alliaceae and genus *Allium*, is cultivated in many countries, such as Vietnam, France, and Canada [Singh *et al*., 2018]. This edible chive plant grows from bulbs (1 cm wide and 2–3 cm long) and has pale purple flowers, so it can be found in gardens as ornamental plant or in local markets as food products [Zdravković-Korać *et al*., 2010]. The AS young leaves and bulbs are commonly used as a spice in many dishes, such as dumplings, salads, and dairy products. Different AS organs are also used in traditional medicine to improve conditions such as sore throat, flu, and cold [Parvu *et al*., 2014; Singh *et al*., 2018]. Due to its bioactive compounds,

***Corresponding Author:**
*Corresponding Author: email: **nl.ha@hutech.edu.vn** (Dr. H.L. Nguyen)
†These authors had equal contribution to this work

Submitted: 24 December 2025
Accepted: 13 May 2026
Published on-line: 8 June 2026

AS has anticancer, antihypertensive, anti-inflammatory, anthelminthic, antibacterial, and antioxidant activities [Singh *et al*., 2018]. The AS bulbs are especially rich in phenolic compounds, with flavonoids being a major class. They were also reported to contain sulfur compounds, such as diethanol disulfide, dimethyl trisulfide, and methyl pentyldisulfide, responsible for antioxidant and antibacterial activity [Tran *et al*., 2024].

Allium plants, especially garlic, have a pungent flavor. Therefore, excessive consumption of garlic can lead to stomach irritation and bad breath (halitosis) [Ryu & Kang, 2017]. Different processes have been applied to overcome these disadvantages of fresh garlic. Among them, aging under conditions of high humidity (60–90%) and temperature (40–60°C) for a long time has been found to have significant effects in stimulating the metabolism of biological compounds and enhancing the functional properties of garlic [Utama *et al*., 2024]. The reactions occurring during aging, with enzymatic browning and non-enzymatic browning (Maillard reaction) being the main reactions, can result in an increase in the content of melanoidins, phenolic compounds, proteins, organosulfur compounds, and reducing sugars [Chang *et al*., 2020; Utama *et al*., 2024]. Furthermore, the aging process imparts a sweeter taste and chewier texture to black garlic while limiting the pungent taste characteristic of fresh garlic. While the characteristic black color is the primary indicator of successful aging, excessive thermal treatment can lead to over-carbonization (an undesirable dull, burnt appearance), loss of biological activity, or the development of a bitter taste [Kelebek *et al*., 2025].

AS can serve as an alternative to garlic and onion because it shares similar physical and biological properties with these two plants. However, consuming excessive amounts of AS can lead to digestive issues and halitosis, similar to the effects of garlic [Zdravković-Korać *et al*., 2010]. Thermal aging, a process involving the prolonged exposure of raw materials to controlled high temperatures and humidity without chemical additives, is a promising processing method that can mitigate the sensory drawbacks of fresh AS and enhance its bioavailability. However, a significant knowledge gap remains. Although the physicochemical and bioactive transformations during the thermal aging of garlic have been extensively documented [Kelebek *et al*., 2025; Ryu & Kang, 2017], the systematic application of this process to AS remains critically underexplored. Therefore, this study aimed to evaluate the changes in the quality of AS bulbs over a 7-day heat-induced aging period. Specifically, changes in nutritional composition, color, physicochemical characteristics, texture parameters, sensory qualities, bioactive compound contents, and antioxidant and anti-inflammatory activities were investigated during the 7-day aging process. Finally, Pearson's correlation coefficient was used to examine the relationships between these properties.

MATERIALS AND METHODS

Materials

Fresh *A. schoenoprasum* (AS) bulbs at optimal ripening stage were collected in 2025 (February to May) from local supermarkets in Di An ward, Ho Chi Minh City, Vietnam. Damaged bulbs were removed and the remaining ones were cleaned before aging.

Production of aged (black) *Allium schoenoprasum* L.

Fresh AS bulbs (approximately 1.5 kg) were aged using an NK-686 apparatus (Ho Chi Minh City, Vietnam) with controlled temperatures and relative humidity of 65–75°C and 70–80%, respectively. No additional treatments were applied during the 7 days of aging. A representative sample of approximately 100 g of AS bulbs was randomly collected after each aging day to prepare for subsequent analysis.

Proximate analysis

The AOAC International standard procedures were used to determine the proximate composition of AS bulbs [AOAC, 2005]. Moisture, crude fat, crude protein, crude fiber, and ash contents were determined by AOAC 950.46, AOAC 922.06, AOAC 979.09, AOAC 962.09 and AOAC 942.05 methods, respectively. Carbohydrate content was calculated based on Equation (1):

$$\text{Carbohydrates} = 100 - (\text{Fat} + \text{Protein} + \text{Ash} + \text{Fiber}) \quad (1)$$

Moisture content was expressed in fresh weight (FW) of AS bulbs, and calculations of the remaining results were based on dry weight (DW) of AS bulbs.

Color analysis

The AS bulb color values in the CIElab color space (L^*, darkness/lightness; a^*, greenness/redness; b^*, blueness/yellowness) were measured using a CR-400 device (Konica Minolta, Osaka, Japan). The total color difference (ΔE) between fresh and aged AS bulbs was calculated based on Equation (2):

$$\Delta E = \sqrt{(L^*_t - L^*_f)^2 + (a^*_t - a^*_f)^2 + (b^*_t - b^*_f)^2} \quad (2)$$

where: L^*_f, a^*_f, b^*_f are the color values of fresh AS bulbs (day 0) and L^*_t, a^*_t, b^*_t are the color values of AS samples after aging.

Physicochemical analysis

Preparation of *Allium schoenoprasum* L. filtrate

AS bulbs (10 g) were ground and mixed with distilled water at a solid-to-solvent ratio of 1:10 (*w/v*). The slurry was then ultrasonicated using a PRO 150S device (Asonic, Ljubljana, Slovenia) for 30 min at a controlled temperature of 35±2°C. Finally, the slurry was filtered through Whatman No.1 filter paper, and the filtrate was used for subsequent physicochemical analyses.

pH and total soluble solid determination

The pH of the AS filtrate was measured based on the activity of H_3O^+ ions using an HI2211 instrument (Hanna Instruments, Woonsocket, RI, USA), while the content of total soluble solids (TSS) expressed in °Brix was determined using an HI96801 instrument (Hanna Instruments, Woonsocket, RI, USA). The analyses were repeated three times at 25°C.

Titratable acidity determination

The acid-base titration method was used to determine AS samples' titratable acidity (TA) [Islam *et al*., 2013]. A phenolphthalein solution (0.1%, *w/w*) was added to the AS filtrate diluted with distilled water. The mixture was then titrated with a 0.1 M NaOH solution until a pink color persisted for 30 s. TA was calculated using Equation (3):

$$TA = \frac{V_{NaOH} \times 0.1 \times V_1 \times 0.064}{V_2 \times m} \quad (3)$$

where: V_{NaOH} is the volume of the NaOH solution used for titration (mL), V_1 is the volume filled up (mL), V_2 is the volume of extract (mL), 0.1 is the normality of NaOH (M), 0.064 is the conversion factor for citric acid equivalent, and m is the mass of the AS sample used to filtrate the preparation (g). The results were expressed as mg of citric acid equivalent *per* 100 g of fresh weight (mg/100 g FW).

Reducing sugar determination

The reducing sugar (RS) content of AS samples was determined by the colorimetric method with 3,5-dinitrosalicylic acid (DNS) in an alkaline medium [Miller, 1959], with some minor modifications. Briefly, 30 g of potassium sodium tartrate tetrahydrate was dissolved in 50 mL of deionized water. On the other hand, 1 g of DNS was dissolved in 20 mL of 2 M NaOH. The entirety of both solutions was completely combined and gently heated to form a homogeneous mixture. After cooling to room temperature, the mixture was filled up to 100 mL with distilled water to prepare the final DNS reagent. Then, 1 mL of DNS reagent was added to 2 mL of the AS filtrate and mixed thoroughly. The reaction mixture was incubated in a water bath at 95°C for 5 min. Subsequently, the mixture was rapidly cooled under running tap water, and the absorbance of the samples was immediately measured at 540 nm using a UV–Vis spectrophotometer (Cary 60, Agilent, Penang, Malaysia). Glucose at various working concentrations (0–1,000 µg/mL) was used to construct the standard curve. The results were expressed as mg of glucose equivalent *per* g of AS bulb DW.

Texture analysis

The texture of the AS bulbs was evaluated using a texture analyzer (TA.XTplusC.0001, Stable Micro Systems Ltd., Surrey, UK) equipped with a P/75 cylindrical probe (7.5 mm diameter). A two-cycle compression test was performed with a strain of 20%. The pre-test and post-test speeds were set to 0.1 cm/s, while the test speed was 0.5 cm/s. From the obtained force-time curves, several texture parameters were determined. Specifically, hardness was defined as the maximum peak force attained during the first compression cycle. Springiness was evaluated as the ratio of the time duration of the second compression to that of the first compression. Cohesiveness was calculated as the ratio of the positive force area during the second compression to that of the first compression. Gumminess was defined as the energy needed to break down a semi-solid sample prior to swallowing. Resilience, which indicates the instantaneous ability of the sample to recover its original height, was evaluated as the ratio of the withdrawal work to the compression work during the first compression cycle.

Preliminary sensory evaluation

A preliminary sensory evaluation was conducted to assess the changes in the physical and sensory characteristics of AS samples during the heat-induced aging process. The sensory panel consisted of 14 members, comprising laboratory staff and university students (7 men and 7 women, aged 20 to 35) from the Faculty of Applied Science and Technology, Nguyen Tat Thanh University (Ho Chi Minh City, Vietnam), who were familiar with the sensory evaluation of thermally aged *Allium* products. The sensory attributes, including color, degree of dryness, texture, flavor, taste, and overall sensory quality, were evaluated using a 9-point rating scale. The corresponding meanings assigned to the scale were: 1 – extremely poor, 2 – very poor, 3 – poor, 4 – slightly poor, 5 – fair/acceptable, 6 – slightly good, 7 – good, 8 – very good, and 9 – excellent [Yuan *et al*., 2022]. The AS samples were coded with three-digit random numbers and presented to the panelists in a randomized order. Purified water was provided to the panelists to cleanse their palates between sample tastings. The evaluation exclusively involved the tasting of thermally aged AS samples prepared without the addition of any harmful chemicals. All participants were healthy adult volunteers. Prior to the evaluation, all panelists were fully informed about the purpose of the study and the sample preparation methods, and they provided their informed consent to participate.

Total phenolic content, total flavonoid content, and biological activity analysis

Preparation of *Allium schoenoprasum* L. extract

The AS bulbs were ground and extracted with a 70% (*v/v*) ethanol solution at a solid-to-solvent ratio of 1:10 (*w/v*). The mixture was ultrasonicated for 30 min using a PRO 150S device (Asonic, Ljubljana, Slovenia) at a controlled temperature of 35±2°C. The suspension was filtered to obtain the *A. schoenoprasum* extract (ASE). The ASE was used directly for the phytochemical content determinations and biological activity assays without further evaporation, and all results were expressed on a bulb DW basis. Preliminary range-finding tests were conducted to determine the optimal extract volumes applied in the subsequent assays, ensuring that all absorbance readings fell strictly within the linear range of their respective standard curves.

Total phenolic content determination

The method with the Folin-Ciocalteu reagent in alkaline medium was applied to estimate the total phenolic content (TPC) of AS bulbs [Pirca-Palomino *et al.*, 2024; Singleton & Rossi, 1965]. Briefly, 200 µL of ASE were reacted with 1 mL of the 10% (*w/v*) Folin-Ciocalteu reagent. After 5 min, the mixture was reacted with 800 µL of a 7.5% (*w/v*) Na_2CO_3 solution. After 1 h, the absorbance of the solution at 765 nm wavelength was estimated using a Cary 60 UV–Vis spectrophotometer (Agilent). Gallic acid solutions at various concentrations (0–0.1 mg/mL) were used to construct the standard curve. TPC was expressed as mg gallic acid equivalents (GAE) *per* 100 g of AS bulb DW.

Total flavonoid content determination

The flavonoid-aluminum complexation method was applied to estimate the total flavonoid content (TFC) of AS bulbs [Miliauskas *et al.*, 2004; Pirca-Palomino *et al.*, 2024]. Briefly, 500 µL of ASE were mixed with 100 µL of 1% (*w/v*) $AlCl_3{\times}6H_2O$ solution, 100 µL of 1 N CH_3COOK solution, and 4.3 mL of ethanol absolute. After 30 min, the absorbance of the solution was recorder at a wavelength of 415 nm using a Cary 60 UV–Vis spectrophotometer (Agilent). Quercetin solutions at various concentrations (0–0.1 mg/mL) were used to construct the standard curve. TFC was expressed as mg quercetin equivalents (QE) *per* 100 g of AS bulb DW.

ABTS assay

The discoloration reaction of the pre-generated, blue-green 2,2'-azino-bis(3-ethylbenzothiazoline-6-sulfonic acid) (ABTS) radical cations by antioxidants was used to estimate the free radical scavenging capacity of AS bulbs [Raczkowska *et al.*, 2024; Re *et al.*, 1999]. Briefly, 500 µL of ASE were mixed with 1,500 µL of a solution of generated $ABTS^{\bullet+}$ calibrated to an absorbance of 1.1. After 30 min, the mixture absorbance was measured at wavelength of 734 nm using the Cary 60 UV–Vis spectrophotometer (Agilent). Trolox solutions at various concentrations (0–0.01 mg/mL) were used to construct the standard curve. $ABTS^{\bullet+}$ scavenging activity of AS bulbs was expressed as mg Trolox equivalents (TE) *per* 100 g AS bulb DW.

Ferric reducing antioxidant power assay

The reduction of Fe^{3+} complexed with 2,4,6-tripyridyl-*s*-triazine (TPTZ) (light yellow) to Fe^{2+}-TPTZ complex (blue) was applied to estimate the ferric reducing antioxidant power (FRAP) of AS bulbs [Benzie & Strain 1996; Nguyen *et al.*, 2025]. Briefly, 20 mL of an $FeCl_3$ solution (0.02 M) were mixed with 20 mL of a TPTZ solution (0.01 M) and 200 mL of a CH_3COONa solution (0.3 M) to form an FRAP reagent (FR). Then, FR (10 mL) was reacted with 0.3 mL of ASE. After 10 min, the absorbance of the solution was estimated at 593 nm using a Cary 60 UV–Vis spectrophotometer (Agilent). $FeSO_4$ solutions at various concentrations (0–3 mg/mL) were used to construct the standard curve. FRAP of AS samples was expressed as mg $FeSO_4$ *per* 100 g AS bulb DW.

Anti-inflammatory capacity determination

The anti-inflammatory capacity of the AS bulbs was evaluated by bovine serum albumin (BSA) denaturation inhibition assays [Rahman *et al.*, 2015]. Briefly, 50 µL of ASE at specific concentrations (0–28.96 µg/mL for fresh AS bulbs and 0–48 µg/mL for 7-day aged AS bulbs) were added to 450 µL of a 1% (*w/v*) BSA solution in phosphate-buffered saline (PBS; pH 6.3). The mixture was incubated at 37°C for 30 min, then the temperature was gradually increased to 57°C and kept for another 5 min. Then, all samples were removed and allowed to cool for 15–20 min. After cooling, 2.5 mL of PBS (pH 6.3) were added to each sample, and the absorbance was measured at 255 nm using a Cary 60 UV–Vis spectrophotometer (Agilent). Distilled water was used instead of ASE in the test control, which represented 100% protein denaturation. The product control consists of 450 µL of distilled water and 50 µL of ASE. Equation (4) was used to calculate the percentage inhibition of protein denaturation:

$$\%\ \text{Inhibition} = 100 - \left(\frac{A - B}{C} \times 100\right) \quad (4)$$

where: A is the optical density of the test solution (extract and BSA), B is the optical density of the product control (extract and water), and C is the optical density of the test control (water and BSA). Analysis was done in triplicate. The extract concentration required to achieve a 50% inhibition of protein denaturation was denoted as the IC_{50} value. This parameter was calculated by applying linear regression to the dose-response curve.

Statistical analysis

All determinations were performed three times independently on samples from each collection day. Data are expressed as the mean and standard deviation. Statistical analyses were performed using IBM SPSS Statistics 22 (IBM Corp., Armonk, NY, USA). Prior to the analysis of variance (ANOVA), the normality of the data distribution and the homogeneity of variances were verified using the Shapiro-Wilk test and Levene's test, respectively. Statistically significant differences among the mean values were determined using a one-way ANOVA followed by Tukey's post hoc test at a significance level of $p<0.05$. Pearson correlation between all determined parameters was also analyzed.

RESULTS AND DISCUSSION

Proximate composition of *Allium schoenoprasum* L. bulbs

Changes in the proximate composition of AS bulbs during heat-induced aging were investigated in fresh and aged samples. The moisture content of fresh AS bulbs (day 0) and AS samples aged for 1 day did not differ significantly ($p\geq0.05$) (**Table 1**). However, extending the aging time resulted in a significant ($p<0.05$) decrease in the moisture content of AS bulbs to 23.33 g/100 g FW. During aging, the decrease in moisture content was due to the effect of high temperature, which is a common

Table 1. Proximate composition of *Allium schoenoprasum* L. bulbs during heat-induced aging.

Time (days)	Moisture (g/100 g FW)	Crude fat (g/100 g DW)	Crude protein (g/100 g DW)	Ash (g/100 g DW)	Crude fiber (g/100 g DW)	Carbohydrates (g/100 g DW)
0	65.18±2.05^{a}	1.26±0.01^{c}	7.51±0.26^{b}	0.46±0.02^{c}	2.36±0.09^{a}	88.40±0.24^{a}
1	64.46±2.71^{a}	1.28±0.02^{bc}	7.58±0.18^{b}	0.47±0.02^{c}	2.37±0.07^{a}	88.30±0.21^{a}
2	54.65±4.56^{b}	1.29±0.02^{abc}	8.08±0.12^{a}	0.51±0.01^{bc}	2.39±0.14^{a}	87.73±0.05^{b}
3	50.43±2.96^{bc}	1.33±0.05^{abc}	8.20±0.13^{a}	0.53±0.01^{ab}	2.42±0.06^{a}	87.52±0.11^{bc}
4	42.71±3.46^{cd}	1.35±0.04^{abc}	8.25±0.10^{a}	0.53±0.03^{ab}	2.42±0.04^{a}	87.44±0.14^{bc}
5	33.79±2.91^{de}	1.35±0.05^{abc}	8.28±0.11^{a}	0.55±0.02^{ab}	2.44±0.08^{a}	87.38±0.16^{bc}
6	27.46±3.11^{ef}	1.37±0.04^{ab}	8.31±0.12^{a}	0.57±0.01^{a}	2.47±0.07^{a}	87.28±0.02^{c}
7	23.33±3.22^{f}	1.38±0.02^{a}	8.37±0.13^{a}	0.58±0.01^{a}	2.47±0.04^{a}	87.20±0.09^{c}

Data are presented as the mean ± standard deviation (n=3). Different lowercase letters (a–f) indicate statistically significant differences (p<0.05) between different aging times, as determined by Tukey's test. FW, fresh weight; DW, dry weight.

phenomenon. Tahir *et al*. [2022] noted that the aging resulted in a decrease in moisture content from 64.30–67.50 g/100 g DW (fresh garlic) to 29.50–31.35 g/100 g DW (black garlic). In turn, the moisture content of 7 fresh garlic varieties (Havel, Rusák, Vekan, Ivan, Bjetin, Lukan, and Havran) ranged from 57.04 to 65.34 g/100 g DW, and the aging process reduced their moisture content to 33.52 to 42.52 g/100 g DW [Bedrníček *et al*., 2021]. The moisture content of fresh AS bulbs in our study (65.18 g/100 g FW) was within the ranges reported in the literature for conventional garlic (*Allium sativum* L.) [Bedrníček *et al*., 2021; Tahir *et al*., 2022], while differences were observed between aged AS and conventional garlic, which could be primarily due to biological differences between the *Allium* species (*A. schoenoprasum* versus *A. sativum*), coupled with inherent variations in bulb morphology. The differences could also result from the applied aging parameters [Afzaal *et al*., 2021]. It has been reported that the sensory quality, texture, and Maillard reaction product level of black garlic are determined by the moisture content [Najman *et al*., 2020; Yuan *et al*., 2022]. Therefore, monitoring the moisture content of aged AS bulbs may help control their quality characteristics.

The crude fat content of AS bulbs increased significantly during heat-induced aging (**Table 1**). This apparent increase is primarily attributed to the thermal disruption of the cellular matrix, which promotes the release and extractability of bound lipids. This observation is consistent with the trend reported in black garlic processing, where fat content increased from 0.15 to 0.60 g/100 g DW [Choi *et al*., 2008].

The crude protein content of AS bulbs after 7 days of aging was significantly (p<0.05) higher than that of the fresh AS bulbs and bulbs heat-treated for 1 day (**Table 1**). Tahir *et al*. [2022] suggested that enzyme activities during aging led to an increase in the protein content of two Pakistani garlic cultivars, with values increasing from 8.57 to 9.50 g/100 g (desi) and from 6.38 to 8.10 g/100 g (farmi).

The ash content of AS bulbs ranged from 0.46 to 0.58 g/100 g DW and increased over time during AS aging (**Table 1**). Meanwhile, although aging increased the crude fiber content of AS samples, the increase was not significant (p≥0.05). A similar increasing trend was reported in a study on *A. sativum* [Tahir *et al*., 2022]. This trend resulted from the thermal degradation of labile carbohydrates, which led to the concentration of the mineral fraction.

The aging process significantly decreased (p<0.05) the carbohydrate content of AS bulbs (**Table 1**). Fructans are documented as the predominant reserve carbohydrates in *Allium* species, accounting for over 75% of the total dry mass [Cheong *et al*., 2012]. Consequently, this overall reduction directly reflects the extensive degradation of these fructans into simpler saccharides *via* sequential enzymatic hydrolysis and non-enzymatic thermal cleavage [Afzaal *et al*., 2021].

Color properties of *Allium schoenoprasum* L. bulbs

Consumer perception of food quality is significantly influenced by product color, which in turn is linked to other food characteristics, such as pigment level and moisture content. Therefore, color is one of the critical indicators for quality control of black AS. In our study, the AS color parameter values decreased significantly (p<0.05) during 7 days of heat-induced aging (**Table 2**). The L^* value was 76.91 for fresh AS and 26.94 after 7 days of processing. The a^* and b^* values decreased from 6.36 to −1.82 and from 28.89 to 3.37, respectively. Correspondingly, the ΔE values increased (p<0.05) for aged AS bulbs. As shown in **Figure 1**, fresh AS was white and turned brown after 1 day of aging. The AS bulbs turned dark brown after 2 days and began to turn black after 3 days. Finally, the AS sample turned completely black after 7 days of aging, indicating that AS bulbs had entered the ripening stage.

Various biochemical reactions, such as the Maillard reaction and enzymatic browning reactions, occurred during aging.

Table 2. Color parameters of *Allium schoenoprasum* L. bulbs during heat-induced aging.

Time (days)	*L**	*a**	*b**	*ΔE*
0	76.91±1.67^{a}	6.36±0.07^{a}	28.89±0.81^{a}	–
1	55.21±0.44^{b}	4.61±0.35^{b}	21.28±0.55^{b}	23.09±1.38^{d}
2	42.45±0.89^{c}	2.46±0.14^{c}	16.23±1.18^{c}	36.93±2.52^{c}
3	40.38±1.54^{c}	1.88±0.13^{d}	10.13±1.00^{d}	41.33±2.60^{c}
4	35.18±0.57^{d}	0.90±0.03^{e}	7.42±0.04^{e}	47.26±1.03^{b}
5	34.78±1.71^{d}	0.36±0.04^{f}	6.32±0.21^{f}	48.18±1.01^{b}
6	31.78±2.17^{d}	−0.24±0.03^{g}	5.13±0.40^{g}	51.44±0.98^{b}
7	26.94±0.43^{e}	−1.82±0.16^{h}	3.37±0.49^{h}	56.72±1.40^{a}

Data are presented as the mean ± standard deviation (n=3). Different lowercase letters (a–h) indicate statistically significant differences (p<0.05) between different aging times, as determined by Tukey's test. *L**, darkness/lightness; *a**, greenness/redness; *b**, blueness/yellowness; *ΔE*, total color difference (compared to fresh bulbs).

Figure 1. Visual image of *Allium schoenoprasum* L. bulbs during heat-induced aging.

Among them, the Maillard reaction is the most important, as it is responsible for the color and flavor of foods. During the final stages of the Maillard reaction, high-molecular-weight melanoidins (brown pigment) are synthesized through a series of complex transformations, namely molecular rearrangements, condensation reactions, and polymerization [Wu *et al*., 2021]. The browning intensity of black garlic products is directly proportional to the content of melanoidins [Wu *et al*., 2021]. Therefore, longer aging time increases the content of melanoidins and intensifies garlic's black color. In addition to melanoidin, Maillard and caramelization reactions also produce 5-hydroxymethyl furfural, the content of which is also proportional to the aging time and browning intensity of garlic [Zhang *et al*., 2016]. These results demonstrate that an extended aging duration significantly enhances the browning intensity and black color of the product.

Physicochemical properties of *Allium schoenoprasum* L. bulbs

The pH value of the AS bulbs decreased significantly during 7 days of heat-induced aging (**Figure 2A**). In contrast, the TA value of the AS bulbs increased significantly over time. Several studies have observed similar trends during garlic aging [Tahir *et al*., 2022; Zhang

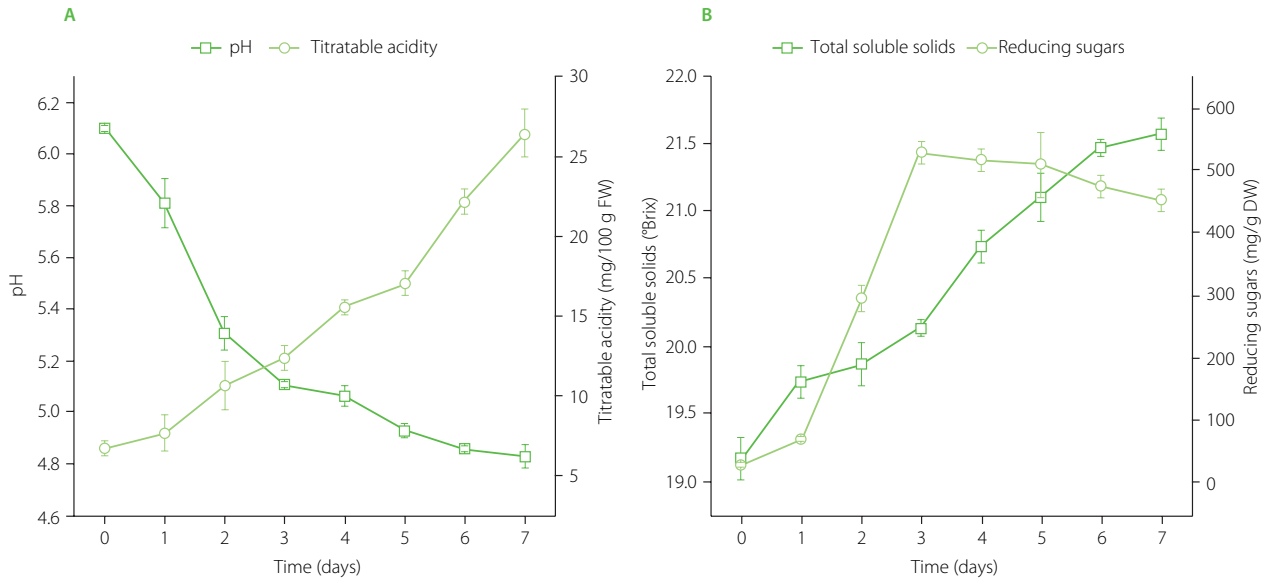

Figure 2. pH and titratable acidity (**A**) and contents of total soluble solids and reducing sugars (**B**) of *Allium schoenoprasum* L. bulb during heat-induced aging. FW, fresh weight; DW, dry weight.

et al., 2016]. Free alkaline amino groups of amino acids, peptides, and proteins are consumed in the Maillard reaction by reacting with reducing sugars, shifting the acid balance toward acidity. Furthermore, degradation of polysaccharides leads to an increase in the organic acid content, thus increasing the acidity of black garlic [Liang *et al*., 2015; Zhang *et al*., 2016]. The formation of organic acids not detected in fresh garlic, such as pyroglutamic, 3-hydroxypropionic, succinic, and formic acids, occurred during aging [Liang *et al*., 2015]. The low pH has its advantages as it helps stabilize the microbiological quality of black garlic [Ahmed & Wang, 2021].

The TSS of the AS bulbs increased significantly over time of the aging process (**Figure 2B**). In turn, the RS content of the AS bulbs exhibited a remarkable increase from 31.4 mg/g DW at day 0 to a peak of 516.5 mg/g DW at day 3, followed by a significant decrease to 452.4 mg/g DW by day 7. The significant increase in RS content during aging is a direct consequence of the breakdown of complex polysaccharides into simpler compounds [Afzaal *et al*., 2021; Li *et al*., 2015]. This transformation also contributes to the observed increase in TSS [Afzaal *et al*., 2021]. Initially, fructans undergo enzymatic hydrolysis into oligosaccharides, disaccharides, and monosaccharides, catalyzed by endogenous fructan exohydrolase [Cheong *et al*., 2012]. Although high temperatures eventually deactivate this native enzyme, further polysaccharide cleavage is driven by non-enzymatic thermal degradation during prolonged aging. This sequential mechanism results in monosaccharides (fructose and glucose) becoming the predominant saccharide fraction, which significantly enhances the characteristic texture and sweetness of black garlic [Afzaal *et al*., 2021; Cheong *et al*., 2012; Liang *et al*., 2015]. Furthermore, these reducing sugars serve as essential precursors for the non-enzymatic Maillard reaction [Afzaal *et al*., 2021; Li *et al*., 2015; Liang *et al*., 2015]. While the degradation of complex macromolecules into simpler compounds may enhance *in vitro* bioaccessibility, further physiological validation is required to confirm the impact of these chemical modifications on *in vivo* digestion.

Texture properties of *Allium schoenoprasum* L. bulbs

The changes in texture parameters of AS bulbs during heat-induced aging are shown in **Table 3**. The hardness and gumminess values decreased significantly ($p<0.05$) with aging of the bulbs. In contrast, the springiness value increased over time. The cohesiveness and resilience values of AS decreased ($p<0.05$) during the first 2 days of aging. However, they showed an increasing trend ($p<0.05$) in the last days of aging.

To the best of authors' knowledge, no study has investigated the textural properties (springiness, cohesiveness, gumminess, and resilience) of AS bulbs during aging. However, Bedrníček *et al*. [2021] noted that black garlic samples had a jelly-like texture and were softer than fresh garlic. The data also showed that the hardness of garlic samples decreased 11-fold after aging. Because of high temperature during aging, the thermal degradation of polysaccharides led to a reduction in the hardness of black garlic, while significantly increased its softness and elasticity [Li *et al*., 2020]. In addition, the weakening of the cell structure is also related to the decrease in moisture content during aging [Utama *et al*., 2024]. Yuan *et al*. [2022] noted that the hardness of garlic samples decreased after the first day of aging, but gradually increased from day 5 to day 10. This suggests that the black garlic samples were over-dried, which resulted in excessive loss of moisture content, thus leading to an increase in hardness during aging. The results of this study indicate that aging made black AS bulbs softer, more flexible, and more rigid while reduced their hardness. This suggests that black AS samples have a desirable texture for culinary appeal and commercial potential.

Table 3. Texture properties of *Allium schoenoprasum* L. bulbs during heat-induced aging.

Time (days)	Hardness (N)	Springiness	Cohesiveness	Gumminess (N)	Resilience
0	0.52±0.03^{a}	0.78±0.02^{f}	0.71±0.02^{a}	17.58±1.06^{a}	1.04±0.11^{a}
1	0.15±0.01^{b}	1.16±0.02^{f}	0.62±0.02^{ab}	2.39±0.22^{b}	0.77±0.07^{d}
2	0.09±0.01^{c}	4.83±0.24^{e}	0.48±0.02^{c}	1.63±0.05^{bc}	0.43±0.04^{e}
3	0.07±0.01^{cd}	5.71±0.24^{e}	0.55±0.04^{bc}	1.26±0.22^{c}	0.49±0.04^{e}
4	0.04±0.00^{de}	8.89±0.17^{d}	0.59±0.03^{abc}	0.83±0.07^{c}	0.52±0.03^{e}
5	0.03±0.00^{ef}	10.67±0.52^{c}	0.60±0.08^{ab}	0.78±0.08^{c}	0.53±0.04^{e}
6	0.02±0.00^{ef}	15.31±0.53^{b}	0.67±0.04^{ab}	0.55±0.08^{c}	0.60±0.08^{c}
7	0.01±0.00^{f}	18.77±1.06^{a}	0.70±0.05^{a}	0.55±0.04^{c}	0.64±0.01^{b}

Data are presented as the mean ± standard deviation (n=3). Different lowercase letters (a–f) indicate statistically significant differences (p<0.05) between different aging times, as determined by Tukey's test.

Table 4. Sensory properties of *Allium schoenoprasum* L. bulbs during heat-induced aging.

Time (days)	Color	Dry degree	Texture	Flavor	Taste	Overall sensory quality
0	6.07±0.62^{b}	5.50±0.65^{d}	5.36±0.50^{e}	5.00±1.11^{e}	4.86±0.77^{e}	5.57±0.51^{e}
1	6.21±0.43^{b}	5.57±0.94^{d}	6.07±0.62^{de}	5.36±0.50^{de}	5.07±0.92^{de}	5.71±1.07^{de}
2	6.29±0.61^{b}	5.71±0.99^{cd}	6.00±0.68^{de}	5.29±0.91^{de}	5.64±0.50^{cde}	5.50±0.65^{e}
3	7.57±0.65^{a}	6.21±0.58^{bcd}	6.07±0.92^{de}	6.36±0.50^{cd}	6.14±1.17^{cd}	5.93±1.00^{de}
4	7.57±0.85^{a}	6.79±1.05^{abc}	6.64±1.01^{cd}	7.00±0.68^{bc}	6.64±1.01^{bc}	6.57±0.51^{cd}
5	7.57±0.76^{a}	7.14±1.17^{ab}	7.07±1.07^{bc}	7.29±1.54^{abc}	7.64±1.15^{ab}	7.21±0.80^{bc}
6	7.64±0.84^{a}	7.36±1.28^{ab}	7.71±1.07^{ab}	7.86±0.86^{ab}	7.79±1.37^{a}	7.50±0.94^{ab}
7	7.71±0.99^{a}	7.43±1.22^{a}	8.21±0.58^{a}	8.14±0.95^{a}	8.43±0.51^{a}	8.29±0.47^{a}

Data are presented as the mean ± standard deviation (n=14). Different lowercase letters (a–e) indicate statistically significant differences (p<0.05) between different aging times, as determined by Tukey's test.

Sensory properties of *Allium schoenoprasum* L. bulbs

Sensory properties of food have a significant influence on its overall quality. Because chemical and physicochemical changes occur continuously during the heat-induced aging process, a preliminary sensory evaluation of the AS samples was performed to monitor the development of their organoleptic properties. All sensory scores of the AS bulbs improved continuously during aging (**Table 4**). The color scores of AS samples at the early aging stage were significantly lower (p<0.05) than those at the later stage. This was because AS samples began to turn black after 3 days and wholly turned to a uniform black color after 7 days. The decrease in moisture content led to a gradual increase in the dry degree of AS bulbs. However, the increase in the dry degree of AS samples at the later aging stage was insignificant (p≥0.05). In addition, the degradation of polysaccharides during aging also made the AS samples become gummy, soft, and jelly-like in texture. Therefore, their texture scores were significantly increased during 7 days of aging. The increase in organic acids, reducing sugar content, and the decrease in allicin content (a compound responsible for pungent taste) resulted in the AS samples having a characteristic sweet and sour taste after aging, thus increasing their flavor and taste scores [Li *et al*., 2015; Li *et al*., 2020]. Finally, the results also showed an increase in the overall sensory quality of the AS bulbs after 7 days of aging. This finding demonstrated that the aging process mitigated the characteristic pungent taste present in fresh AS samples and successfully enhanced the overall sensory profile of the black AS samples.

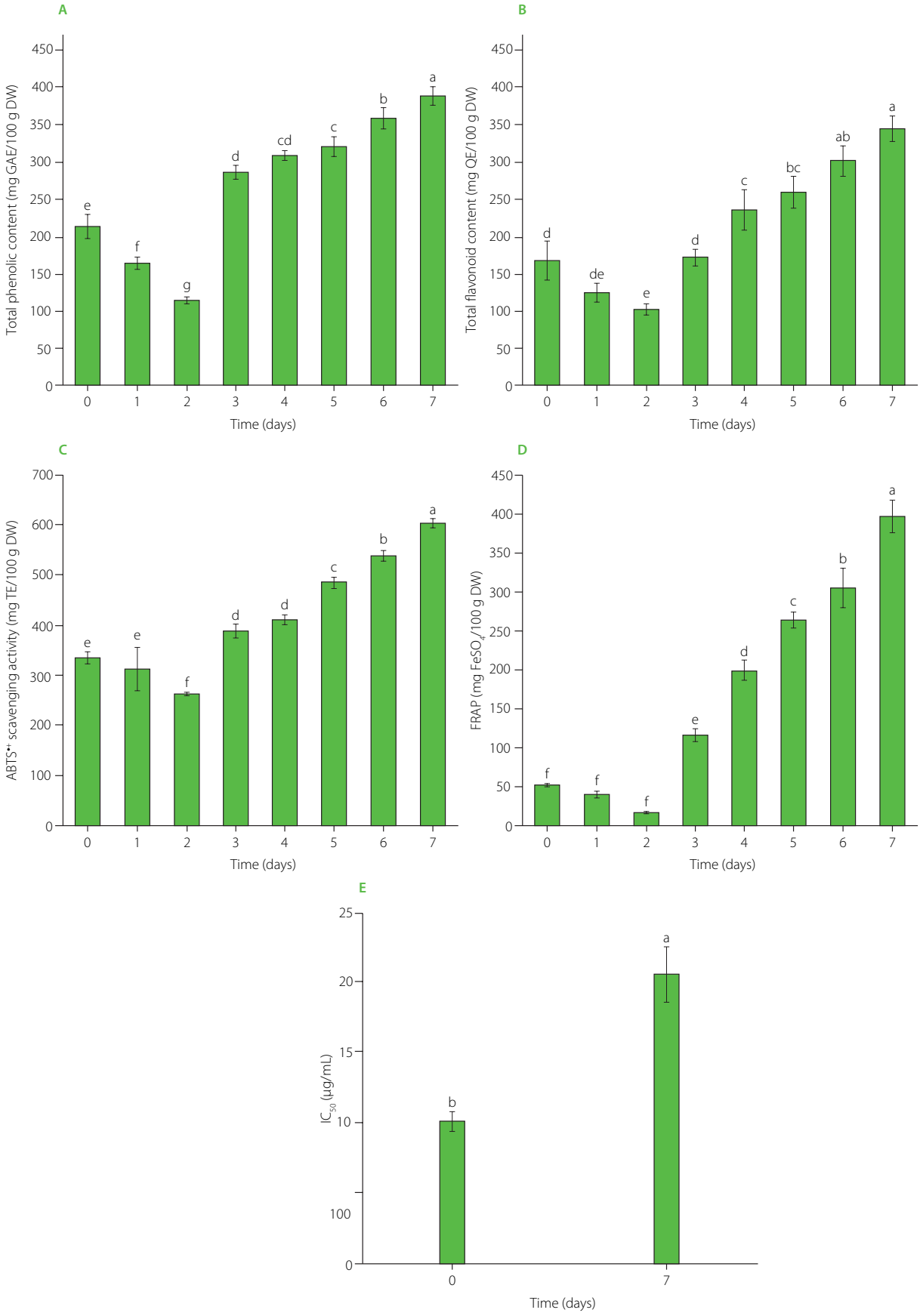

Figure 3. Total phenolic content (**A**), total flavonoid content (**B**), 2,2′-azino-bis (3-ethylbenzothiazoline-6-sulfonic acid) radical cation ($ABTS^{\bullet+}$) scavenging activity (**C**), ferric reducing antioxidant power (FRAP) (**D**), and inhibition of bovine serum protein denaturation (**E**) of *Allium schoenoprasum* L. during heat-induced aging. Data are presented as the mean and standard deviation (n=3). Different lowercase letters (a–f) indicate statistically significant differences (p<0.05) between different aging times, as determined by Tukey's test. GAE, gallic acid equivalents; QE, quercetin equivalents; TE, Trolox equivalents; IC_{50}, half-maximal inhibitory concentration; DW, dry weight.

Total phenolic and total flavonoid contents, and biological activity of *Allium schoenoprasum* L. bulbs

Contents of total phenolics and total flavonoids

The results indicate that the TPC and TFC of AS bulbs were significantly affected by aging (**Figure 3**). At the early stage of aging, TPC decreased significantly ($p<0.05$). In contrast, a significant ($p<0.05$) increase in TPC was observed at the late stage of aging. Similarly, TFC significantly ($p<0.05$) decreased from day 0 to day 2, followed by a significant ($p<0.05$) increase from day 3 to day 7. Under the influence of high temperature, oxidation reactions are accelerated, and covalent bonds are cleaved. Thus, phenolic compounds in agricultural products are degraded [Nguyen *et al*., 2025]. In addition, high humidity at the initial stage of aging also leads to increased activity of polyphenol oxidase and peroxidase, resulting in a recued phenolic content [Sun & Wang, 2018]. However, the decrease in humidity and pH at the later stage of aging led to enzyme inactivation, thus limiting the degradation of phenolics in AS samples [Toledano-Medina *et al*., 2016]. Moreover, polysaccharide depolymerization occurred during aging. Subsequently, phenolic compounds, including flavonoids and phenolic acids, are released from cell wall structures.

Antioxidant capacity

The content of bioactive compounds changes during aging, thus affecting the antioxidant capacity. The $ABTS^{\bullet+}$ scavenging activity of AS bulbs did not change significantly ($p\geq0.05$) during the first two days of aging (**Figure 3D**). Similarly, the FRAP values showed no significant ($p\geq0.05$) changes during the initial three days of the thermal process (**Figure 3E**). However, from day 3 to day 7, both $ABTS^{\bullet+}$ scavenging activity and FRAP increased significantly ($p<0.05$). The higher antioxidant capacity of AS bulbs after aging was consistent with results of previous studies on black garlic [Tahir *et al*., 2022]. The changes in the antioxidant capacity of AS samples over time followed a similar trend to the changes in TPC and TFC, indicating that phenolic compounds primarily influenced the antioxidant potential of AS bulbs. However, other AS bulb compounds could also affect their antioxidant capacity. The aging process leads to the conversion of allicin into water-soluble organosulfur compounds, thus increasing the antioxidant capacity of garlic [García-Villalón *et al*., 2016; Utama *et al*., 2024]. Moreover, melanoidins are known for their strong antioxidant capacity; longer aging times also lead to increased melanoidin content and antioxidant capacity of the garlic [González-Ramírez *et al*., 2022].

Anti-inflammatory capacity

Arthritis and inflammatory responses are closely related to the phenomenon of tissue protein denaturation [Aidoo *et al*., 2021]. The anti-inflammatory potential of fresh AS (day 0) and black AS (day 7) bulbs was evaluated through their capacity to inhibit the heat-induced denaturation of bovine serum albumin. As shown in **Figure 3F**, fresh AS bulbs exhibited significantly lower IC_{50} values ($p<0.05$) compared to black AS samples, indicating a reduction in specific anti-inflammatory potential following the thermal aging process. Interestingly, this trend contrasts with the observed enhancement in antioxidant capacity. In *Allium* species, anti-inflammatory activity is predominantly attributed to heat-sensitive organosulfur compounds, rather than phenolic compounds [Jeong *et al*., 2016]. Therefore, the severe thermal degradation of these organosulfur compounds during prolonged aging directly contributes to the reduced efficacy in preventing BSA denaturation. However, extrapolating these *in vitro* BSA denaturation results directly to *in vivo* systems is highly limited. Actual physiological anti-inflammatory efficacy depends on complex cellular immune responses and the gastrointestinal bioavailability of these compounds, necessitating further *in vivo* or cell-based model studies.

Pearson correlation

The correlations among the proximate composition, color parameters, physicochemical parameters, sensory scores, and antioxidant capacity of the AS bulbs during aging are illustrated in **Figure 4**. Exact correlation coefficients are detailed in **Table S1** in Supplementary Materials. The IC_{50} values (representing anti-inflammatory activity) were not included in the correlation matrix, as two sampling points (days 0 and 7) provide insufficient degrees of freedom for valid correlation modeling. The results demonstrated that moisture content was significantly negatively correlated with the sensory attributes and antioxidant capacities. Conversely, nutrient contents, such as crude fat, crude protein, ash, crude fiber, and carbohydrates, all exhibited positive correlations with these parameters. Among the sensory attributes, the sensory scores for color showed a significant negative correlation with the instrumental L^*, a^*, and b^* values. Simultaneously, ΔE exhibited a significant positive correlation with the sensory color scores.

The results also indicated that moisture content correlated negatively with dry degree and texture, whereas springiness showed a significant positive correlation with these two parameters. Regarding flavor and taste, the sensory scores were significantly and positively correlated with reducing sugars, titratable acidity, carbohydrates, crude protein, crude fat, and TSS, while being negatively correlated with pH values.

Overall, the antioxidant capacities of AS were negatively correlated with L^*, a^*, and b^* values, while showing a positive correlation with ΔE. Finally, TPC and TFC exhibited a strong positive correlation with the ABTS and FRAP assay results. These findings demonstrate that the accumulated phenolic compounds are highly effective at neutralizing free radicals and providing reducing power *via* electron donation [Karnjanapratum *et al*., 2021].

CONCLUSIONS

The changes in the chemical composition, physicochemical properties, sensory profiles, and biological activities of AS bulbs during the heat-induced aging were comprehensively determined in this study. The results demonstrated that aging reduced the moisture content, leading to the concentration of crude fat,

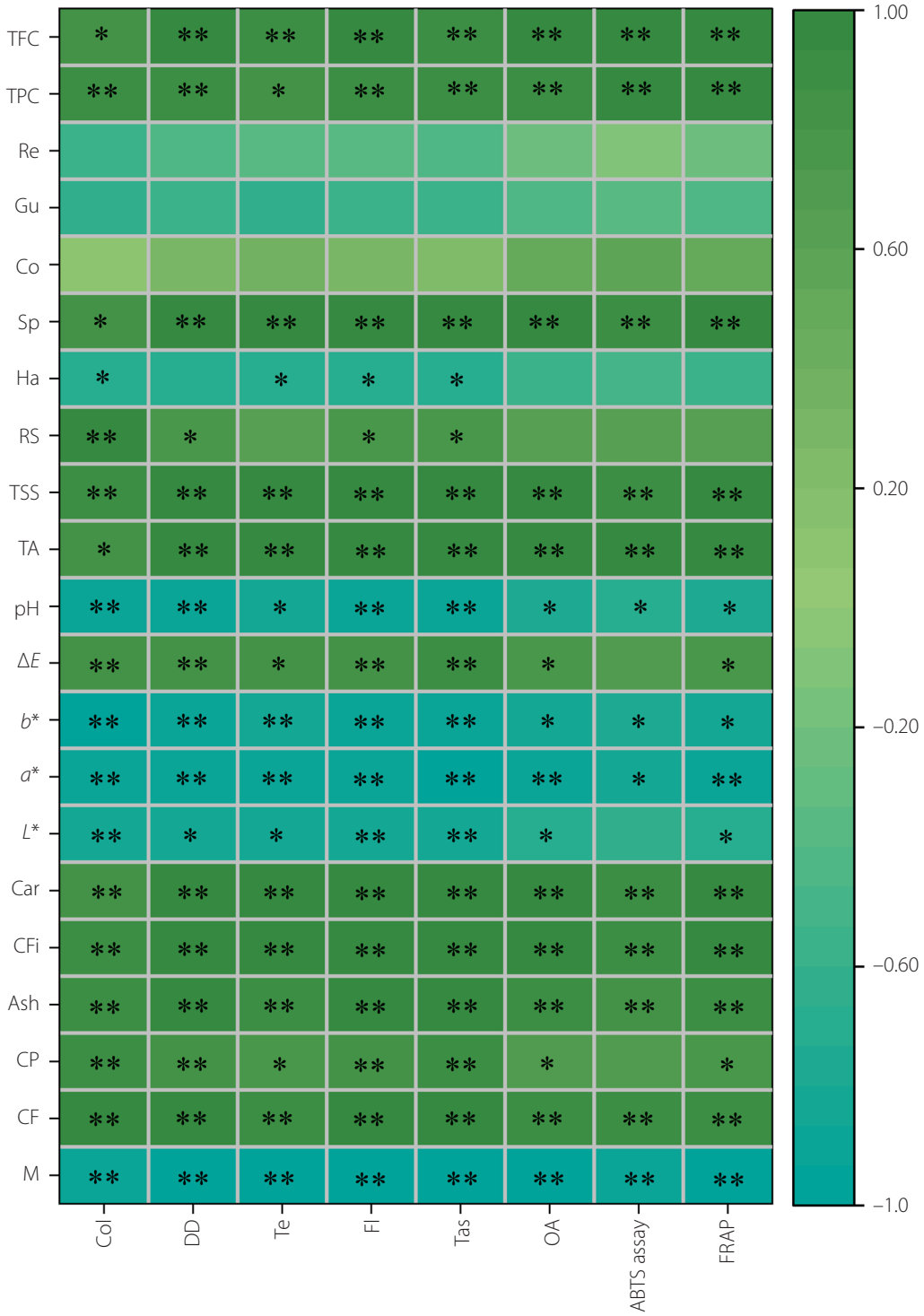

Figure 4. Pearson's correlogram of parameters determined for *Allium schoenoprasum* L. bulbs during heat-induced aging. M, moisture; CF, crude fat; CP, crude protein; CFi, crude fiber; Car, carbohydrates; *L**, darkness/lightness; *a**, greenness/redness; *b**, blueness/yellowness; Δ*E*, total color difference; TA, titratable acidity; TSS, total soluble solids; RS, reducing sugars; Ha, hardness; Sp, springiness; Co, cohesiveness; Gu, gumminess; Re, resilience; TPC, total phenolic content; TFC, total flavonoid content; Col, color; DD, dry degree; Te, texture; Fl, flavor; Tas, taste; OSQ, overall sensory quality; ABTS assay, 2,2′-azino-bis (3-ethylbenzothiazoline-6--sulfonic acid) assay; FRAP, ferric reducing antioxidant power. Correlations are significant at $p \leq 0.05$ (*) or at $p \leq 0.01$ (**).

protein, ash, and fiber, whereas carbohydrate levels significantly declined. The AS bulbs turned completely black after 7 days of treatment. The concurrent increases in reducing sugars, TSS, and titratable acidity, alongside the reduction in pH, significantly improved the sensory attributes of the aged samples. During the aging process, there was a significant increase in the content of phenolic compounds (TPC and TFC). As a result, the antioxidant capacity ($ABTS^{\bullet+}$ scavenging activity and FRAP) of the AS bulbs was significantly enhanced. However, compared to the fresh AS, the specific anti-inflammatory capacity of the aged samples

decreased. Pearson's correlation analysis confirmed that the improvement in sensory properties (color, flavor, and taste) was strongly associated with the decreases in instrumental color values (L^*, a^*, b^*), as well as the increases in reducing sugars, titratable acidity, carbohydrates, crude protein, crude fat, and TSS. Additionally, the enhanced sensory texture scores were linked to decreases in moisture, hardness, gumminess, and resilience, and increases in springiness and cohesiveness. While this study provides a knowledge of the chemical and physicochemical changes occurring in AS bulbs during a 7-day aging period, the effects of different pretreatment methods should be further investigated to optimize the functional and nutritional quality of black AS.

ACKNOWLEDGEMENTS

The authors would like to thank Nguyen Tat Thanh University for creating favorable conditions that made it possible to effectively finish the research.

RESEARCH FUNDING

No funding was received for this research.

CONFLICT OF INTERESTS

There is no conflict of interest, according to the authors.

SUPPLEMENTARY MATERIALS

The following are available online at **https://journal.pan.olsztyn.pl/Heat-Induced-Aging-Improvements-in-Sensory-Quality-Antioxidant-and-Anti-Inflammatory,221784,0,2.html**; **Table S1.** Correlation coefficients of the indicators.

ORCID IDs

B.M.N. Nguyen https://orcid.org/0009-0007-7609-9616
H.L. Nguyen https://orcid.org/0009-0008-3435-6028
N.H.K. Nguyen https://orcid.org/0000-0002-5582-0343
N.N. Nguyen https://orcid.org/0000-0001-6240-0868
N.T. Nguyen https://orcid.org/0000-0001-7646-8230
N.Q. Tran https://orcid.org/0009-0007-5814-5316

REFERENCES

1. Afzaal, M., Saeed, F., Rasheed, R., Hussain, M., Aamir, M., Hussain, S., Mohamed, A.A., Alamri, M.S., Anjum, F.M. (2021). Nutritional, biological, and therapeutic properties of black garlic: a critical review. *International Journal of Food Properties, 24*(1), 1387-1402. **https://doi.org/10.1080/10942912.2021.1967386**
2. Ahmed, T., Wang, C.K. (2021). Black garlic and its bioactive compounds on human health diseases: A review. *Molecules*, *26*(16), art. no. 5028. **https://doi.org/10.3390/molecules26165028**
3. Aidoo, D.B., Konja, D., Henneh, I.T., Ekor, M. (2021). Protective effect of bergapten against human erythrocyte hemolysis and protein denaturation *in vitro*. *International Journal of Inflammation, 2021*(1), art. no. 1279359. **https://doi.org/10.1155/2021/1279359**
4. AOAC (2005). *Official Methods of Analysis* (17th ed.). The Association of Official Analytical Chemists, Rockville, MD, USA.
5. Arzanlou, M., Bohlooli, S. (2010). Introducing of green garlic plant as a new source of allicin. *Food Chemistry*, *120*(1), 179-183. **https://doi.org/10.1016/j.foodchem.2009.10.004**
6. Bedrníček, J., Laknerová, I., Lorenc, F., de Moraes, P.P., Jarošová, M., Samková, E., Tříska, J., Vrchotová, N., Kadlec, J., Smetana, P. (2021). The use of a thermal process to produce black garlic: Differences in the physicochemical and sensory characteristics using seven varieties of fresh garlic. *Foods*, *10*(11), art. no. 2703. **https://doi.org/10.3390/foods10112703**
7. Benzie, I.F.F., Strain, J.J. (1996). The ferric reducing ability of plasma (FRAP) as a measure of "antioxidant power": the FRAP assay. *Analytical Biochemistry, 239*(1), 70–76. **https://doi.org/10.1006/abio.1996.0292**
8. Chang, W.C.W., Chen, Y.T., Chen, H.J., Hsieh, C.W., Liao, P.C. (2020). Comparative UHPLC-Q-Orbitrap HRMS-based metabolomics unveils biochemical changes of black garlic during aging process. *Journal of Agricultural and Food Chemistry*, *68*(47), 14049-14058. **https://doi.org/10.1021/acs.jafc.0c04451**
9. Cheong, K.L., Yan, F., Huang, X. (2012). Enymologic characterization of garlic fructan exohydrolase. *Journal of Food Biochemistry*, *36*(2), 248-253. **https://doi.org/10.1111/j.1745-4514.2010.00532.x**
10. Choi, D.J., Lee, S.J., Kang, M.J., Cho, H.S., Sung, N.J., Shin, J.H. (2008). Physicochemical characteristics of black garlic (*Allium sativum* L.). *Journal of the Korean Society of Food Science and Nutrition*, *37*(4), 465-471 (in Chinese, English abstract). **https://doi.org/10.3746/jkfn.2008.37.4.465**
11. García-Villalón, A.L., Amor, S., Monge, L., Fernández, N., Prodanov, M., Muñoz, M., Inarejos-García, A.M., Granado, M. (2016). *In vitro* studies of an aged black garlic extract enriched in S-allylcysteine and polyphenols with cardioprotective effects. *Journal of Functional Foods*, *27*, 189-200. **https://doi.org/10.1016/j.jff.2016.08.062**
12. González-Ramírez, P.J., Pascual-Mathey, L.I., García-Rodríguez, R.V., Jiménez, M., Beristain, C.I., Sanchez-Medina, A., Pascual-Pineda, L.A. (2022). Effect of relative humidity on the metabolite profiles, antioxidant activity and sensory acceptance of black garlic processing. *Food Bioscience*, *48*, art. no. 101827. **https://doi.org/10.1016/j.fbio.2022.101827**
13. Islam, M.K., Khan, M.Z.H., Sarkar, M.A.R., Absar, N., Sarkar, S.K. (2013). Changes in acidity, TSS, and sugar content at different storage periods of the postharvest mango (*Mangifera indica* L.) influenced by Bavistin DF. *International Journal of Food Science*, *2013*(1), art. no. 939385. **https://doi.org/10.1155/2013/939385**
14. Jeong, Y.Y., Ryu, J.H., Shin, J.H., Kang, M.J., Kang, J.R., Han, J., Kang, D. (2016). Comparison of anti-oxidant and anti-inflammatory effects between fresh and aged black garlic extracts. *Molecules, 21*(4), art. no. 430. **https://doi.org/10.3390/molecules21040430**
15. Karnjanapratum, S., Supapvanich, S., Kaewthong, P., Takeungwongtrakul, S. (2021). Impact of steaming pretreatment process on characteristics and antioxidant activities of black garlic (*Allium sativum* L.). *Journal of Food Science and Technology*, *58*(5), 1869-1876. **https://doi.org/10.1007/s13197-020-04698-7**
16. Kelebek, H., Sasmaz, H.K., Kilic-Buyukkurt, O., Selli, S. (2025). Functional and physicochemical properties during the transition from fresh to black garlic: a comparative review. *Discover Molecules*, *2*(1), art. No. 33. **https://doi.org/10.1007/s44345-025-00036-6**
17. Li, F., Cao, J., Liu, Q., Hu, X., Liao, X., Zhang, Y. (2020). Acceleration of the Maillard reaction and achievement of product quality by high pressure pretreatment during black garlic processing. *Food Chemistry*, *318*, art. no. 126517. **https://doi.org/10.1016/j.foodchem.2020.126517**
18. Li, N., Lu, X., Pei, H., Qiao, X. (2015). Effect of freezing pretreatment on the processing time and quality of black garlic. *Journal of Food Process Engineering*, *38*(4), 329-335. **https://doi.org/10.1111/jfpe.12156**
19. Liang, T., Wei, F., Lu, Y., Kodani, Y., Nakada, M., Miyakawa, T., Tanokura, M. (2015). Comprehensive NMR analysis of compositional changes of black garlic during thermal processing. *Journal of Agricultural and Food Chemistry*, *63*(2), 683-691. **https://doi.org/10.1021/jf504836d**
20. Miliauskas, G., Venskutonis, P.R., Van Beek, T.A. (2004). Screening of radical scavenging activity of some medicinal and aromatic plant extracts. *Food Chemistry, 85*(2), 231–237. **https://doi.org/10.1016/j.foodchem.2003.05.007**
21. Miller, G.L. (1959). Use of dinitrosalicylic acid reagent for determination of reducing sugar. *Analytical Chemistry, 31*(3), 426–428. **https://doi.org/10.1021/ac60147a030**
22. Najman, K., Sadowska, A., Hallmann, E. (2020). Influence of thermal processing on the bioactive, antioxidant, and physicochemical properties of conventional and organic agriculture black garlic (*Allium sativum* L.). *Applied Sciences, 10*(23), art. no. 8638. **https://doi.org/10.3390/app10238638**
23. Nguyen, N.H.K., Tran, N.Q., Nguyen, N.T., Nguyen, H.L. (2025). Impact of pretreatment solutions on the physicochemical and microbiological properties of dried Tu Quy mango (*Mangifera indica* L.). *Journal of Food Processing and Preservation*, *2025*(1), art. no. 8811106. **https://doi.org/10.1155/jfpp/8811106**

24. Parvu, A.E., Parvu, M., Vlase, L., Miclea, P., Mot, A.C., Silaghi-Dumitrescu, R. (2014). Anti-inflammatory effects of *Allium schoenoprasum* L. leaves. *Journal of Physiology and Pharmacology*, *65*(2), 309-315.
25. Pirca-Palomino, M., Malange, Y.I., Ramos-Escudero, F., Muñoz, A.M., Cancino-Chávez, K. (2024). Antioxidant properties, texture and sensory quality of sliced bread enriched with leaf powder from mango (*Mangifera indica*). *Polish Journal of Food and Nutrition Sciences*, *74*(4), 313-322. **https://doi.org/10.31883/pjfns/194599**
26. Raczkowska, E., Wojdyło, A., Nowicka, P. (2024). Effect of the addition of apple pomace and erythritol on the antioxidant capacity and antidiabetic properties of shortbread cookies. *Polish Journal of Food and Nutrition Sciences*, *74*(2), 147-161. **https://doi.org/10.31883/pjfns/187941**
27. Rahman, H., Chinna Eswaraiah, M., Dutta, A. (2015). *In-vitro* anti-inflammatory and anti-arthritic activity of *Oryza sativa* var. Joha Rice (an aromatic indigenous rice of Assam). *J. Agric. & Environ. Sci*, *15*(1), 115-121.
28. Re, R., Pellegrini, N., Proteggente, A., Pannala, A., Yang, M., Rice-Evans, C. (1999). Antioxidant activity applying an improved ABTS radical cation decolorization assay. *Free Radical Biology and Medicine, 26*(9-10), 1231-1237. **https://doi.org/10.1016/S0891-5849(98)00315-3**
29. Ryu, J.H., Kang, D. (2017). Physicochemical properties, biological activity, health benefits, and general limitations of aged black garlic: A review. *Molecules, 22*(6), art. no. 919. **https://doi.org/10.3390/molecules22060919**
30. Singh, V., Chauhan, G., Krishan, P., Shri, R. (2018). *Allium schoenoprasum* L.: a review of phytochemistry, pharmacology and future directions. *Natural Product Research, 32*(18), 2202-2216. **https://doi.org/10.1080/14786419.2017.1367783**
31. Singleton, V.L., Rossi, J.A. (1965). Colorimetry of total phenolics with phosphomolybdic-phosphotungstic acid reagent. *American Journal of Enology and Viticulture, 16*, 144–158. **https://doi.org.10.5344/ajev.1965.16.3.144**
32. Sun, Y.E., Wang, W. (2018). Changes in nutritional and bio-functional compounds and antioxidant capacity during black garlic processing. *Journal of Food Science and Technology*, *55*(2), 479-488. **https://doi.org/10.1007/s13197-017-2956-2**
33. Tahir, Z., Saeed, F., Nosheen, F., Ahmed, A., Anjum, F.M. (2022). Comparative study of nutritional properties and antioxidant activity of raw and fermented (black) garlic. *International Journal of Food Properties*, *25*(1), 116-127. **https://doi.org/10.1080/10942912.2022.2026954**
34. Toledano-Medina, M.A., Pérez-Aparicio, J., Moreno-Rojas, R., Merinas-Amo, T. (2016). Evolution of some physicochemical and antioxidant properties of black garlic whole bulbs and peeled cloves. *Food Chemistry*, *199*, 135-139. **https://doi.org/10.1016/j.foodchem.2015.11.128**
35. Tran, A.S.N., Pham, V.H., Duong, C.D., Bui, Q.T.P. (2024). Extraction conditions, chemical composition and biological activity of essential oil of *Allium schoenoprasum* L. bulb from Quang Tri province, Vietnam. *Food Chemistry Advances*, *4*, art. no. 100574. **https://doi.org/10.1016/j.focha.2023.100574**
36. Utama, G.L., Rahmi, Z., Sari, M.P., Hanidah, I.i. (2024). Psychochemical changes and functional properties of organosulfur and polysaccharide compounds of black garlic (*Allium sativum* L.). *Current Research in Food Science, 8*, art. no. 100717. **https://doi.org/10.1016/j.crfs.2024.100717**
37. Wu, J., Jin, Y., Zhang, M. (2021). Evaluation on the physicochemical and digestive properties of melanoidin from black garlic and their antioxidant activities *in vitro*. *Food Chemistry, 340*, art. no. 127934. **https://doi.org/10.1016/j.foodchem.2020.127934**
38. Yuan, X., Wang, Z., Liu, L., Mu, D., Wu, J., Li, X., Wu, X. (2022). Changes of physicochemical properties in black garlic during fermentation. *Fermentation*, *8*(11), art. no. 653. **https://doi.org/10.3390/fermentation8110653**
39. Zdravković-Korać, S., Milojević, J., Tubić, L., Ćalić-Dragosavac, D., Mitić, N., Vinterhalter, B. (2010). Somatic embryogenesis and plant regeneration from root sections of *Allium schoenoprasum* L. *Plant Cell, Tissue and Organ Culture*, *101*(2), 237-244. **https://doi.org/10.1007/s11240-010-9682-z**
40. Zhang, X., Li, N., Lu, X., Liu, P., Qiao, X. (2016). Effects of temperature on the quality of black garlic. *Journal of the Science of Food and Agriculture*, *96*(7), 2366-2372. **https://doi.org/10.1002/jsfa.7351**

ORIGINAL ARTICLE
http://journal.pan.olsztyn.pl

Polish Journal of Food and Nutrition Sciences
2026, Vol. 76, No. 2, 215–227
DOI: 10.31883/pjfns/221951
ISSN 1230-0322, e-ISSN 2083-6007

Metabolomic Insights into Bee Bread Antiviral Activity Against Influenza A Virus

Karolina Matejczuk[1], Marika Mróz[2], Tilemachos G. Dimitriou[3], Barbara Kusznierewicz[2], Dimitris Mossialos[3], Piotr Szweda[1]

[1]Department of Pharmaceutical Technology and Biochemistry, Faculty of Chemistry, Gdansk University of Technology, Narutowicza Street 11/12, 80-233, Gdansk, Poland
[2]Department of Chemistry, Technology and Biotechnology of Food, Faculty of Chemistry, Gdansk University of Technology, Narutowicza Street 11/12, 80-233, Gdansk, Poland
[3]Microbial Biotechnology, Molecular Bacteriology-Virology Laboratory, Department of Biochemistry and Biotechnology, School of Health Sciences, University of Thessaly, 42500 Larissa, Greece

Bee bread (BB) is a natural apicultural product that exerts a broad spectrum of biological activities, including antimicrobial properties. The identification of novel antiviral agents is of considerable importance in light of the ongoing global impact of viral pathogens, particularly the influenza A virus (IAV). This study evaluated the antiviral efficacy of eighteen BB aqueous extracts against IAV H1N1 using Madin-Darby canine kidney (MDCK) cells. The cytotoxicity of the extracts varied significantly, ranging from 1.33 to 15.97 µL/mL. Real-time PCR analysis revealed a notable decline in a viral RNA copy number after the treatment with BB extracts, indicating inhibition of viral replication. The half maximal inhibitory concentration (IC_{50}) of extracts ranged from 0.13 to 1.09 µL/mL. Selectivity index (SI) showed significant variability, spanning from 2.13 to 47.68. Furthermore, BB samples revealed total phenolic content (TPC) ranging from 4.08 to 6.10 mg GAE/g, and total flavonoid content (TFC) between 0.22 and 0.97 mg QE/g. A significant negative correlation was observed between IC_{50} and SI, whereas no significant associations were found between IC_{50}, or SI and TPC or TFC indicating that activity profiles of the extracts were independent of phenolic and flavonoid contents. Ultra-performance liquid chromatography–high-resolution mass spectrometry (UPLC-HRMS) profiling confirmed that bee bread contained a diverse set of bioactive metabolites, including flavonoids, phenolic acids, amino acids, lipids, and carbohydrate derivatives, supporting its potential as a multifunctional natural product. When combined with antiviral assays, these compositional insights suggest that the antiviral activity of bee bread likely results from the collective action of multiple compound classes rather than a single dominant group.

Keywords: antiviral agents, antiviral potential, bee products, flavonoids, phytochemicals

ABBREVIATIONS

BB, bee bread; CC_{50}, 50% cytotoxic concentration; GAE, gallic acid equivalent; IAV, influenza A virus; IC_{50}, half maximal inhibitory concentration; MDCK, Madin-Darby canine kidney cells; MEM, minimal essential medium; MTT, 3-(4,5-dimethylthiazol-2-yl)-2,5-diphenyltetrazolium bromide; PBS, phosphate buffer saline; QE, quercetin equivalent; SDS, sodium dodecyl sulfate; TFC, total flavonoid content; TPC, total phenolic content; UPLC-HRMS, ultra-performance liquid chromatography–high-resolution mass spectrometry.

***Corresponding Author:**
E-mail: **karolina.matejczuk@pg.edu.pl** (Dr. K. Matejczuk)

Submitted: 27 December 2025
Accepted: 18 May 2026
Published on-line: 9 June 2026

INTRODUCTION

Viral infections remain a constant and serious challenge to global health, playing a major role in both morbidity and mortality worldwide [Asma *et al*., 2022]. Despite considerable progress in modern medicine, the continuous emergence and re-emergence of viral pathogens, coupled with the ever-present risk of pandemics, underscore the urgent need for effective antiviral strategies [Márquez-Bandala *et al*., 2025]. Current antiviral therapies, while crucial, often face limitations such as the development of drug resistance and the potential for adverse side effects [Lam & Baumgarth, 2019]. This makes the exploration of alternative and complementary approaches essential, particularly those derived from natural sources, which may offer improved safety profiles and novel mechanisms of action.

Throughout history, diverse civilizations have utilized bee products, including honey, propolis, bee pollen, and bee bread, for their therapeutic properties, notably in the treatment of infections. This rich history of folk medicine has spurred a growing scientific interest in the bioactive compounds present in these bee-derived products and their potential health benefits [Asma *et al*., 2022]. Modern research aims to validate these traditional applications and to identify the specific components responsible for their observed effects.

Among these bee products, bee bread stands out as a particularly intriguing product. It is formed through a natural process within the honeycomb cells, where worker bees collect pollen from flowers and mix it with honey or nectar and their own salivary secretions [Bakour *et al*., 2022]. This mixture then undergoes fermentation, transforming it into bee bread. The resulting bee bread boasts a rich nutritional composition, including significant amounts of proteins, carbohydrates, lipids, amino acids, vitamins, and minerals [Aylanc *et al*., 2023; Ćirić *et al*., 2022]. Furthermore, bee bread contains a variety of bioactive compounds, such as polyphenols (mainly flavonoids), and enzymes, which presumably contribute to its therapeutic potential [Mărgăoan *et al*., 2019]. Besides being crucial in bee bread production, the fermentation process may also enhance bee bread bioavailability and bioactivity compared to bee pollen.

Bee products, including honey, propolis, bee venom or royal jelly, possess antiviral potential against DNA and RNA viruses. Their mechanism of action involves decreasing viral load, viral replication inhibition, reduction of DNA synthesis, or reduced adhesion to the host cells [Otręba *et al*., 2025]. Furthermore, the antiviral effects of bee products, such as honey and propolis, are primarily attributed to a diverse array of bioactive secondary metabolites, specifically phenolic compounds (flavonoids and phenolic acids), as well as specialized molecules like methylglyoxal and organic acids [Asma *et al.,* 2022; Otręba *et al*., 2025]. Although other bee products, like honey and propolis, have been extensively studied in this context, research on the antiviral potential of bee bread remains relatively limited [Asma *et al*., 2022]. However, initial *in vitro* studies have provided evidence that bee bread may inhibit mammalian viruses, including influenza A virus [Asoutis Didaras *et al*., 2022; Dimitriou *et al*., 2023]. These initial findings provide a strong rationale for further investigation of the antiviral activity of bee bread, particularly against clinically important human pathogens, such as the influenza virus.

The main goal of this research was to explore the antiviral potential of eighteen bee bread samples derived from Polish apiaries against influenza A H1N1 virus. Its second aim was metabolomic analysis of bee bread extracts and an attempt to identify individual compounds or groups of compounds that are responsible for this antiviral effect.

MATERIALS AND METHODS

Chemicals, reagents, and cell cultures

All chemicals and reagents were purchased from commercial sources. Minimal essential medium supplemented with Earle's balanced salts and fetal bovine serum was obtained from Biosera (France). Bradford reagent, phosphate buffer saline (PBS), sodium dodecyl sulfate (SDS), 3-(4,5-dimethylthiazol-2-yl)-2,5--diphenyltetrazolium bromide (MTT), TPCK trypsin, sodium nitrite, aluminum chloride, sodium hydroxide, quercetin, formic acid, and acetonitrile were bought from Merck (Darmstadt, Germany). Ethanol and HCl were bought from POCH (Gliwice, Poland). Syringe filters (0.22 µm, Millex) were purchased from Millipore (Billerica, MA, USA). Ultrapure water (18.0 MΩ) was produced using the Milli-Q Advantage A10 System (Millipore, Billerica, MA, USA). Madin-Darby canine kidney (MCDK) cells were obtained from Vircell (Granada, Spain), and the clinical influenza A H1N1 strain was provided by Dr. Nikolaos Siafakas (ATTIKON General University Hospital of Athens, Greece). M30F2/08 and M264R3/08 primers were obtained from Eurofins Genomics (Ebersberg, Germany), and FastGene Scriptase II from Nippon Genetics (Tokyo, Japan).

Sample preparation

The investigation of antiviral potential of bee bread included 18 samples (n=18) of dried polyfloral bee bread (BB) pellets derived from apiaries located in different regions of Poland (products were collected from 2020 to 2022). Sample identifiers (BB1–BB18) follow the original laboratory coding; numbers BB5 and BB12 were not assigned at the collection stage. All tested BB samples were firstly homogenized in a ceramic mortar. Extracts were prepared for MTT and antiviral assays according to the protocol described previously by Dimitriou *et al*. [2023]. The BB samples were suspended in a minimum essential medium (MEM) at a 1:10 ratio (*w/w*) and incubated for 1 h at ambient temperature. Afterwards, the mixtures were centrifuged (10,000×*g*, 10 min), and supernatants were filtered through 0.22 µm syringe filters. The obtained MEM extracts were stored at 4°C for further analysis.

For total phenolic content and total flavonoid content (TPC and TFC, respectively) determination, the BB samples were dissolved with MilliQ water in a 1:5 ratio (*w/w*) and incubated for 2 h on a rotary shaker at ambient temperature and 100 rpm. Subsequently, suspensions were centrifuged at 10,000 rpm (corresponding to approximately 8,400×*g*) for 10 min and filtered

using 0.22 µm syringe filters. The obtained aqueous BB extracts were stored at 4°C for further analysis.

Cell viability assay

Cytotoxicity of the analyzed BB samples against MCDK cells was determined with the MTT colorimetric method [Asoutis Didaras *et al*., 2022]. The MCDK cells were seeded in the wells of 96-well plates in MEM supplemented with 2% fetal bovine serum followed by 24 h of incubation at 37°C. Afterwards, the MEM medium was removed, and 100 µL of each BB MEM extract were added into cells – the final concentrations of BB MEM extracts in the wells were in the range from 0.25 to 32 µL/mL. Subsequently, the Madin-Darby canine kidney (MDCK) cells treated with BB extracts were incubated for 24 h at 37°C. Then, 20 µL of an MTT solution (2.5 mg/mL) were added into each well, and the plates were incubated for 1 h at 37°C. MTT is converted into crystalline formazan as a result of the enzymatic reduction of the tetrazolium salt by mitochondrial dehydrogenases, yielding an insoluble product that precipitates within metabolically active cells. After incubation, 100 µL of the MTT solvent (10% SDS and 0.01 M HCl) were added into wells in order to dissolve the formed formazan crystals. The measurement was taken at 570 nm using a microplate reader.

Antiviral activity assay

Antiviral activity of BB against influenza A H1N1 virus was assessed with the cell culture assay following the protocol published previously [Dimitriou *et al*., 2023]. The MDCK cells and the dilutions of BB MEM extracts, ranging from 0.25 to 32 µL/mL, were prepared as described in the cell viability assay section. The virus stock of influenza A virus (IAV) in MEM was prepared in a 1:10 ratio (*v/v*) with the addition of 1 µg/mL of TPCK trypsin. Afterwards, the virus stock was mixed with BB MEM extracts in a 1:1 ratio (*v/v*). The positive control was virus stock mixed with MEM in a 1:1 ratio (*v/v*) and the negative control was just the MEM medium. Subsequently, all the mixtures were incubated for 1 h at 37°C. After incubation, the medium was removed from 96-well plates containing MCDK cells, and 200 µL of the prepared mixtures (virus stock with BB extracts, positive and negative control) were added into the wells. All samples were tested in triplicate. The plates containing BB extracts and both negative and positive controls were incubated at 37°C and examined daily for the development of cytopathic effect (CPE). Afterwards, the plates were stored at –80°C for further analysis.

RNA extraction was performed to isolate the viral RNA from infected MDCK cell cultures after exposure to the analyzed extracts [Dimitriou *et al*., 2023]. Because influenza A is an RNA virus, extracting its genome is essential for downstream quantification. Real-time PCR targeting the M gene of the virus was then used to measure the remaining viral RNA copies, thereby indicating how strongly each sample of BB extract inhibited viral replication or directly inactivated the virus. A reverse transcription assay was performed using an M30F2/08 primer targeting the M gene segment 5′-ATGAGYCTTYTAACCGAGGTCGAAACG-3′ (Eurofins Genomics) and FastGene Scriptase II (Nippon Genetics) according to the manufacturer's protocol. The synthesized cDNA was stored at –80°C for further analysis.

Antiviral activity was determined by comparative real-time PCR according to protocols provided in earlier works [Asoutis Didaras *et al*., 2022; Dimitriou *et al*., 2023]. The relative concentration of viral titer in MCDK cells incubated with different concentrations of BB extracts compared to the viral titer in the control sample (MCDK cells incubated with the virus without any supplementation with BB extract) was calculated targeting the M gene segment M30F2/08 5′-ATGAGYCTTYTAACCGAGGTCGAAACG-3′/ /M264R3/08 5′-TGGACAAANCGTCTACGCTGCAG-3′ [Eisfeld *et al*., 2014]. The comparative real-time PCR was conducted using an Eco48 instrument (PCRmax, Staffordshire, United Kingdom) according to the following protocol: 95°C for 2 min, 40 cycles of 95°C for 5 s and 60°C for 30 s followed by a melting curve analysis step. Cycle threshold (Ct) values were used to calculate the relative concentration as a means of $2^{-\Delta Ct\,(Control\text{-}Sample)}$, according to EcoStudy (PCRMax).

Calculation of cytotoxicity concentration, half maximal inhibitory concentration, and selectivity index

In this study, the MTT assay was used to calculate cytotoxicity concentration (CC_{50}) of the analyzed BB extracts against MDCK cells. CC_{50} is the concentration of the agent (in this case: BB extracts) that reduces the uninfected cell viability by 50% [Cavalli *et al*., 2012]. The absorbance values obtained for each concentration of BB extracts were normalized to the untreated cell control. A dose–response curve was generated by plotting sample concentration against the percentage of viable cells (GraphPad Prism 10, GraphPad Software, Inc., La Jolla, CA, USA), and the CC_{50} value was defined as the concentration that reduced cell viability to 50% of the control.

For the estimation of the antiviral potential of BB extracts, the calculation of the half maximal inhibitory concentration (IC_{50}) was used, and it is a measure of the effectiveness of a compound in inhibiting biological/biochemical function. [Hendriks, 2010]. The IC_{50} was determined on the basis of quantitative real-time PCR data. The relative amount of viral RNA in each condition was calculated in comparison to the positive control. Dose–response curves were then generated in GraphPad Prism 10 (GraphPad Software) by plotting sample concentration against the percentage reduction in viral RNA levels. The IC_{50} value was defined as the concentration of the sample that produced a 50% decrease in viral RNA quantity relative to the untreated virus control.

The selectivity index (SI), defined as the ratio of cytotoxicity to antiviral activity [McGaw *et al*., 2014], was calculated considering both CC_{50} and IC_{50}.

Total phenolic content and total flavonoid content determination

The total phenolic content (TPC) of the BB aqueous extracts was quantified using the Folin–Ciocalteu method, following the protocol described previously [Pełka *et al*., 2021] with small

modifications. Briefly, 50 µL of the Folin–Ciocalteu reagent, diluted at 1:10 (*v/v*) with deionized ultrapure water, were combined with 10 µL of the BB aqueous extract. After 5-min incubation, 40 µL of a 7.5% sodium carbonate solution (Na_2CO_3) were added, followed by 100 µL of ultrapure water to obtain the final reaction volume of 200 µL. The mixture was incubated for 30 min at ambient temperature, and, subsequently, absorbance was measured at 725 nm using a microplate reader (TECAN Spark 10M, Grödig, Austria). The calibration curve was plotted with fresh gallic acid standard solutions in the range of concentrations from 0 to 2.0 mg/mL. The TPC in BB aqueous extracts was expressed as mg of gallic acid equivalent (GAE) *per* g of the product. All measurements were conducted in triplicate.

The total flavonoid content (TFC) was determined using a modified version of the method reported previously [Gull *et al*., 2018]. Briefly, 125 µL of distilled water were dispensed in the wells of a 96 well-plate and mixed with 25 µL of BB aqueous extracts and 10 µL of 5% $NaNO_2$. After 5 min of incubation at room temperature, 15 µL of 10% $AlCl_3$ were added, and the plate was incubated 30 min at ambient temperature in the dark. After incubation, 50 µL of 1M NaOH were added. Subsequently, absorbance was read at 510 nm using a microplate reader (TECAN Spark 10M). TFC was calculated using a quercetin calibration curve (concentration of quercetin from 0 to 1.0 mg/mL), and results were expressed as mg of quercetin equivalent (QE) *per* g of the product. All measurements were performed in triplicate.

Metabolomic analysis using ultra-performance liquid chromatography–high-resolution mass spectrometry

Ultra-performance liquid chromatography–high-resolution mass spectrometry (UPLC-HRMS) analysis enabled the comprehensive profiling and tentative identification of compounds of diverse classes in bee bread based on their chromatographic behavior, accurate precursor ion masses, and characteristic fragmentation patterns. The gathered tandem mass spectrometry (MS/MS) data were compared with reference fragmentation patterns, exact masses, and structural annotations available in the Human Metabolome Database (HMDB), PubChem, and previously published literature which provided spectral libraries, reported MS/MS data, and structural information necessary for tentative compound identification.

Aqueous extracts were prepared by suspending raw bee bread material in MilliQ water at a ratio corresponding to 200 mg of the starting material *per* mL of the solvent (*w/v*). The suspensions were vortexed, allowed to extract, and the soluble fraction was collected after filtration through 0.22 µm syringe filters. The filtrates were subsequently analyzed using the UPLC-HRMS technique as described in a previous work with small modifications [Litewski *et al*., 2024]. A quality control (QC) sample was prepared by combining equal aliquots of all bee bread extracts included in the study. The QC mixture was processed and analyzed in the same manner as the individual samples. QC injections were used to monitor UPLC-HRMS system stability, assess analytical reproducibility, and support data normalization during metabolomic analysis. The UltiMate 3000 UHPLC system by Thermo Scientific Dionex (Waltham, MA, USA) composed of a quaternary pump, a well plate autosampler, a column compartment equipped with a 100 Å Luna Omega Polar C18 column (150×2.1 mm, 1.6 µm, Phenomenex, Torrance, CA, USA), and a diode array detector was used. It was coupled with a high-resolution Thermo Q-ExactiveTM Focus quadrupole-Orbitrap mass spectrometer, manufactured by Thermo (Bremen, Germany). The entire chromatographic system was managed using Chromeleon 7.2.8 software from Thermo Fisher Scientific (Waltham, MA, USA).

The chromatographic separation was performed using a mobile phase consisting of (A) water acidified with formic acid (0.1%, *v/v*) and (B) acetonitrile acidified with formic acid (0.1%, *v/v*). The system operated at a constant flow rate of 0.3 mL/min. The gradient elution began at 5% solvent B and increased linearly to 25% B over the first 5 min. It then continued to rise gradually, reaching 50% B at 18 min, followed by a rapid increase to 80% B at 19 min. The gradient then progressed to 100% B by the 25 min and was held constant at this level until 30 min. The initial mobile phase was run for 7 min to condition the column. The injection volume of the samples was 4 µL. The analytes were ionized using heated electrospray ionization (HESI) operated in both positive and negative ion modes. The sheath, auxiliary, and sweep gas flow rates were set to 35, 15, and 3 bar, respectively. Ionization was performed with a spray voltage of 2.5 kV, and the S-lens radio frequency (RF) level was maintained at 50. The capillary temperature was adjusted to 350°C, while the heater was set to 300°C. For the full mass spectrometry (MS) scan, the mass range covered 120 to 1,200 *m/z* with a resolution of 70,000 full width at half maximum (FWHM). The automatic gain control (AGC) target was 2×10^5, and the maximum injection time was 100 ms. MS2 parameters included a resolution of 17,500 FWHM, an isolation window of 3 *m/z*, a collision energy of 30 eV, an AGC target of 1×10^6, and a maximum injection time of 100 ms. Data processing was performed using Compound Discoverer 3.3 software (Thermo Fisher Scientific) and Freestyle 1.3 software (Thermo Fisher Scientific). Compound identification was performed using the Compound Discoverer 3.3 workflow, which included accurate mass matching, isotopic pattern evaluation, and MS/MS fragmentation pattern comparison against spectral libraries (mzCloud and ChemSpider). Putative identifications were assigned based on mass accuracy, retention time behavior, and fragmentation similarity.

Statistical analysis

The presented data are shown as the means and standard deviation (SD) derived from three measurements. The Shapiro-Wilk test of normality was used to determine data distribution. One-way ANOVA (α=0.05) was run separately on TPC and TFC to assess total variance, followed by pairwise comparisons using Tukey's honestly significant difference (HSD) test. Statistical groupings were derived using a custom compact letter display approach based on non-significant Tukey comparisons ($p\geq0.05$), assigning

alphabetical labels in descending mean order. Statistical analysis of TPC and TFC results was conducted by Python (version 3.13.5, Python Software Foundation, Wilmington, DE, USA) with stats model package (version 0.14.5, NumFOCUS, Austin, TX, USA). A correlation analysis was performed to investigate the associations among cytotoxicity (CC_{50}), antiviral activity (IC_{50}), selectivity index (SI), and phytochemical parameters (TPC and TFC). Because the data were not normally distributed, non-parametric Spearman rank correlation coefficients (r_s) were employed to evaluate monotonic relationships between the measured parameters. Corresponding *p*-values were calculated to determine the statistical significance of each correlation. All analyses were conducted using two-tailed tests. Statistical analysis of the metabolomics data was conducted using MetaboAnalyst 6.0 (https://www.metaboanalyst.ca, accessed on June 11, 2025). Principal component analysis (PCA) was performed to assess overall variation in the data and to visualize clustering patterns among the sample groups. Differential metabolite analysis between the samples showing the greatest variation in biological activity was performed based on a $\log_2$ fold change (FC)≥2. A significance threshold of $p \leq 0.1$ was applied to distinguish differential metabolites from non-significant ones.

RESULTS AND DISCUSSION

Antiviral potency of bee bread extracts

The cell viability assay with the use of an MTT dye was performed to estimate the toxicity level of BB MEM extracts on MCDK cells. The cytotoxicity was expressed as CC_{50} and varied from 1.33 to 15.97 µL/mL for all tested samples (**Table 1**). The least toxic BB sample was BB20 (15.97 µL/mL) followed by BB3 (11.80 µL/mL).

The results obtained after comparative real-time PCR revealed a decreasing copy number of IAV H1N1 after the treatment with the BB MEM extracts. The half minimum inhibitory concentration (IC_{50}) of the samples that exhibited antiviral activity was in the range from 0.13 µL/mL (BB13) to 1.09 µL/mL (BB7 and BB15). The IC_{50} values differed among the tested BB samples, indicating that the antiviral activity of BB might depend on the botanical origin and/or the chemical composition of BB.

The calculation of selectivity index (SI) was performed taking into consideration both CC_{50} and IC_{50} values. According to Cavalli

Table 1. Antiviral profile (CC_{50}, IC_{50}, and SI values) of bee bread (BB) aqueous extracts.

BB sample	Sample location	CC_{50} (µL/mL)	IC_{50} (µL/mL)	SI
BB1	Legnica	2.22±0.62	0.15±0.04	14.93
BB2	Malbork	5.65±0.48	0.34±0.14	16.66
BB3	Bielsko-Biała	11.80±1.12	0.40±0.16	29.66
BB4	Cychry	3.24±0.57	0.64±0.22	5.07
BB6	Czaplinek	3.79±0.74	1.08±0.76	3.52
BB7	Mielec	3.18±0.45	1.09±0.32	2.93
BB8	Mielec	6.74±1.79	0.49±0.00	13.67
BB9	ND	7.81±1.78	0.49±0.06	16.05
BB10	Brusy	5.56±1.87	0.29±0.13	19.52
BB11	Częstochowa	5.27±0.99	0.17±0.02	31.47
BB13	Malbork	2.59±0.33	0.13±0.07	20.41
BB14	Suchorzew	3.51±0.57	0.55±0.32	6.44
BB15	Miłogoszcz	2.32±0.49	1.09±0.82	2.13
BB16	Miłogoszcz	3.19±1.06	0.29±0.03	10.91
BB17	Majdan Starowiejski	5.58±0.94	0.53±0.01	10.51
BB18	Warka	1.33±0.21	0.25±0.01	5.29
BB19	Modzele	3.09±0.44	0.31±0.16	9.89
BB20	Gajewo	15.97±1.05	0.34±0.42	47.68

The extracts were tested in triplicate and the results are shown as mean ± standard deviation. ND, no data; CC_{50}, 50% cytotoxic concentration; IC_{50}, 50% inhibitory concentration; SI, selectivity index.

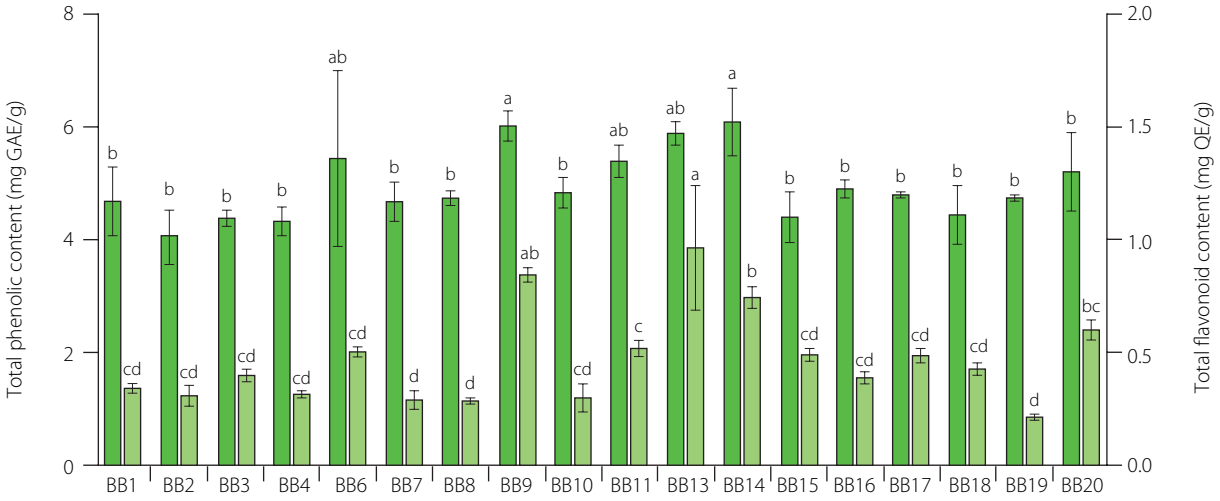

Figure 1. Total phenolic and total flavonoid content of bee breads (BB). The results are presented as mean (n=3). Error bars represent standard deviation. Different lowercase letters above each bar denote significant differences among samples according to Tukey's honestly significant difference post-hoc test at $p<0.05$. GAE, gallic acid equivalent; QE, quercetin equivalent.

et al. [2012], higher SI values indicate a safer and more effective sample. The SI values were between 2.13 and 47.68, thus they were highly variable (over 20-fold). However, four samples revealed SI values higher than 20 meaning that the IC_{50} value was more than 20 times lower than the corresponding CC_{50} value. These findings provide evidence supporting the antiviral activity of BB. Due to the limited number of studies on the antiviral properties of bee bread, assessing accurately its effectiveness against influenza remains challenging. Nevertheless, all the SIs calculated for BB extracts in this study are comparable with the SI values obtained for aqueous extracts of BB presented by Dimitriou *et al*. [2023]. Antiviral activity of other bee products, such as honey, propolis or bee venom, has been described well. These products act through several mechanisms, such as blocking viral entry, inhibiting replication, providing direct virucidal effects, and stimulating the host's immune response [Asma *et al*., 2022]. For honey, IC_{50} values ranged from 3.2 mg/mL (Manuka honey) to 11.3 mg/mL (range honey) with SI values from 22.9 to 7.1, respectively [Otręba *et al*., 2025]. Honey demonstrates potent anti-influenza activity by directly deactivating viral particles before infection and utilizing bioactive metabolites, like flavonoids and phenolic acids, to block viral attachment and entry into host cells [Otręba *et al*., 2025]. Furthermore, specialized components, such as methylglyoxal, inhibit the assembly and maturation of new virions, while the product's low pH and high osmolality provide a physicochemical barrier that suppresses viral replication [Kontogiannis *et al*., 2022]. In the case of propolis, this apicultural product exhibits notable antiviral activity against influenza A virus, with reported IC_{50} values ranging from 19.5 to 111.6 µg/mL [Otręba *et al*., 2025]. Its antiviral mechanism involves the inhibition of viral adsorption and entry into host cells, coupled with the suppression of intracellular replication through the downregulation of viral mRNA synthesis. Additionally, specific secondary metabolites, such as 3,4-dicaffeoylquinic acid, confer indirect antiviral protection by modulating host immune responses, including the upregulation of TRAIL expression to promote the elimination of infected cells and the enhancement of protective antibody titers [Asma *et al*., 2022]. These findings position bee bread within the broader spectrum of antiviral bee products, suggesting that its bioactivity may follow similar mechanistic patterns. Although the potency varies among samples, the overall antiviral profile of BB aligns with the established antiviral potential observed for other bee products.

Total phenolic and total flavonoid contents of bee breads

Phenolic compounds, including flavonoids, exhibit health-promoting potential, including anti-inflammatory, anti-cancer, and antimicrobial activities [Stachelska *et al*., 2025]. Flavonoids are a group of phenolic compounds that are widely present in bee products, including bee bread. In this research, TPC of BB ranged from 4.08 to 6.10 mg GAE/g, and TFC was in the range from 0.22 to 0.97 mg QE/g (**Figure 1**). In our previous work, TPC values varied from 16.88 to 20.18 mg GAE/g; however, it involved ethanolic extracts of bee bread [Pełka *et al*., 2021]. The study of Mohammed *et al*. [2022] proved that 70% ethanol was the best solvent for the extraction of phenolic compounds. Nevertheless, despite its lower extraction efficiency, water is non-toxic and, hence, is considered a safer alternative to ethanol, particularly in the context of antiviral activity. Concerning the TFC, in the study of Sawicki *et al*. [2022], bee bread methanolic extracts contained approximately 5 mg of QE/mL. What is more, Mayda *et al*. [2020] presented data on the total flavonoid content ranging from 1.81 to 3.74 mg of QE/g BB, depending on botanical origin. Nevertheless, TFC of BB can be highly variable, as reported for BB collected in Romania, which was lower, between 0.45 to 1.86 mg QE/g [Ilie *et al*., 2024]. This difference between samples might be attributed to diverse botanical origin and extraction methods.

A correlation analysis was performed to further explore potential relationships among cytotoxicity, antiviral activity, selectivity index, and the phytochemical characteristics of the extracts (TPC and TFC), Because the Shapiro–Wilk test indicated that the variables did not follow a normal distribution, non-parametric Spearman rank correlation coefficients (r_s) were applied. The analysis revealed a significant negative correlation between IC_{50} and SI (r_s=–0.6636, p=0.0034), as well as IC_{50} and CC_{50} (r_s=0.1806, p=0.4709), demonstrating that the extracts with stronger antiviral potential (lower IC_{50} values) were associated with higher selectivity indexes and that the antiviral activity of the extracts was not driven by cytotoxicity. No statistically significant correlations (p>0.05) were observed between IC_{50}, or SI and the TPC or TFC, suggesting that the antiviral and cytotoxic properties of the extracts were not directly dependent on their phenolic content within the tested range. Although phenolics are often highlighted as key contributors to the bioactivity of bee-derived products, bee bread is known to possess a far more diverse profile of bioactive compounds. Its fermentation process and mixed botanical origin generate a complex matrix enriched not only in phenolics but also in peptides, amino acids, lipids, carbohydrates, and various secondary metabolites [Bakour *et al*., 2022; Ćirić *et al*., 2022]. Due to its chemical diversity, it is likely that the antiviral activity results from the combined or interacting effects of multiple metabolite classes rather than being driven solely by phenolic compounds. Because TPC and TFC obtained through colorimetric assays offer only broad approximations of the total phenolic and total flavonoid content, they do not provide insight into the specific compounds present. Therefore, a more detailed characterization of the extracts by UPLC-HRMS was performed.

Chemical composition of bee bread aqueous extracts

This analytical approach facilitated the annotation of 218 metabolites in BB aqueous extracts analyzed in both negative and positive ionization, that were classified into ten principal categories. These included 45 flavonoids; 39 amino acids, peptides and analogs; 33 carbohydrates and carbohydrate conjugates; 33 lipids; 22 phenylpropanoids and derivatives; 13 nucleic acid components; 11 organoheterocyclic compounds; 8 alkaloids and their derivatives; 5 carboxylic acids; and 9 other compounds (**Figure 2**). Representative total ion chromatograms (TICs) of the pooled QC sample, acquired in both ionization modes, are shown in **Figure 3**, illustrating the overall complexity of the analyzed BB extracts. Detailed annotations, including retention time, formula, mass error, diagnostic fragment ions and relative abundances, are summarized in **Table S1** in Supplementary Materials.

Flavonoid glycosides, particularly derivatives of kaempferol, quercetin, isorhamnetin, and myricetin, were the most prevalent in bee bread (**Figure 2**, **Table S1**), which is consistent with

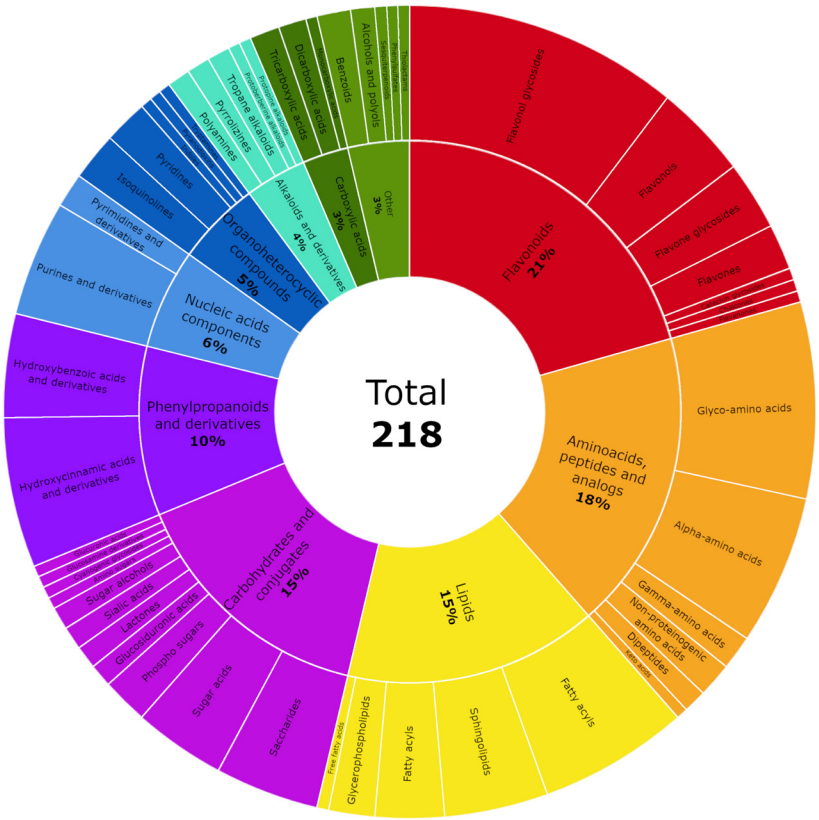

Figure 2. A sunburst plot showing the classification of the bee bread metabolites tentatively identified by ultra-performance liquid chromatography–high-resolution mass spectrometry (UPLC-HRMS) analysis. Refer to **Table S1** in Supplementary Materials for the full information on the metabolites shown in this plot.

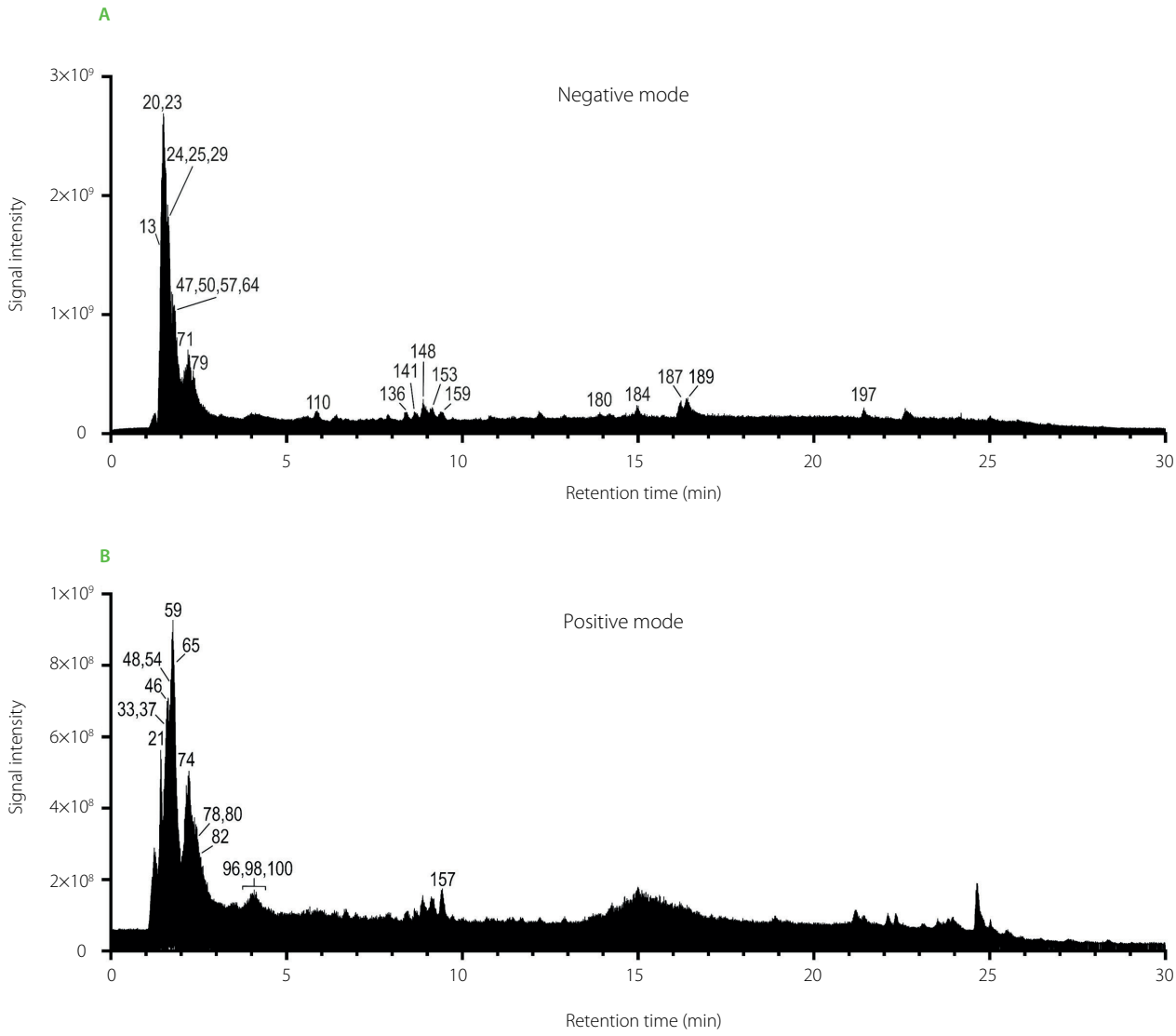

Figure 3. Total ion chromatograms (TICs) of the pooled quality control (QC) sample of bee bread extracts acquired in a negative ion mode (**A**) and a positive ion mode (**B**). For peak identities, see **Table S1** in Supplementary Materials.

findings reported by Bakour *et al*. [2019]. Their identification was based on aglycone $[M–H]^-$ ions (*m/z* 285.04, 301.03, 315.05, and 317.02, respectively) and diagnostic neutral losses of sugar moieties. Kaempferol was identified as the most abundant flavonoid in the majority of the analyzed bee bread extracts and was highlighted by Ilie *et al*. [2024], together with quercetin and caffeic acid, as one of the key contributors to the antimicrobial activity of bee bread. Phenylpropanoids and derivatives identified in bee bread comprised simple phenolic acids, their glycosylated derivatives, and various polyamine conjugates. Caffeic, *p*-coumaric, ferulic, vanillic, protocatechuic, gentisic, salicylic, and 4-hydroxybenzoic acids were annotated from their $[M–H]^-$ ions and typical decarboxylation and demethylation fragments, while glycosylated forms showed neutral loss of hexose units. Polyamine conjugates bearing caffeoyl, feruloyl, or coumaroyl residues produced fragment ions corresponding to putrescine or spermidine backbones. These phenolamides, which have been reported in bee products, are increasingly recognized for their antioxidant and anti-inflammatory potential [Qiao *et al*., 2023; Zhang *et al*., 2025].

Another major group of metabolites identified in bee bread consisted of amino acids, peptides, and their analogues (**Figure 2**, **Table S1**). During fermentation, pollen proteins undergo enzymatic and microbial transformation into more bioavailable forms, resulting in elevated levels of free amino acids and short peptides. Specific amino acids, such as tryptophan and arginine, have been proposed as indicators of the botanical origin of the pollen, while the overall amino acid profile can offer insights into the geographical origin of bee bread [Bakour *et al.,* 2022]. In the analyzed bee bread extracts, the most intense signals corresponded to *N*-(1-deoxy-1-fructosyl) derivatives – Amadori rearrangement products (ARPs) – which are key intermediates formed during the early stages of the Maillard reaction. Although ARPs are rarely found in nature without thermal processing, they are commonly

detected in bee products. In honey, for example, their levels have been reported to gradually increase during storage [Yan *et al.*, 2023]. Several free amino acids were annotated based on the typical neutral losses (*e.g.*, H_2O, NH_3, COOH), ammonium ions, or side-chain-specific fragment ions. The most intense signals were observed for isoleucine and phenylalanine, both being essential amino acids, which is consistent with previous reports indicating that essential amino acids constitute a major part of the bee bread amino acid pool [Urcan *et al.*, 2021].

Lipids identified in bee bread included glycerophospholipids, sphingolipids, fatty acid derivatives, and acylcarnitines (**Figure 2**, **Table S1**). Sphinganine, sphingosine, phytosphingosine, and ceramides with varying acyl chain lengths were detected, suggesting active lipid remodeling and potential microbial or enzymatic transformations during pollen fermentation. Glycerophosphocholine, a common phospholipid in bee products and previously reported in bee bread [Darwish *et al.*, 2022], was confirmed by the diagnostic phosphocholine fragment ion at *m/z* 184.07, while glycerophosphoinositol and related phospholipids were identified from characteristic headgroup and fatty acyl ions. Linoleic acid, one of the major fatty acids in bee bread [Kaplan *et al.*, 2016], together with its hydroxy- and hydroperoxy-derivatives (*e.g.*, 9,10-DiHODE, 15,16-DiHODE, 9-HPODE), reflected both the high polyunsaturated fatty acid content and oxidative/enzymatic transformations occurring during fermentation and storage. These lipid species are nutritionally relevant and may contribute to the anti-inflammatory and cardioprotective potential attributed to bee bread [Bakour *et al.*, 2022]. Carbohydrates represent another major class of metabolites in bee bread, including simple sugars, sugar alcohols, sugar acids, and numerous phosphorylated saccharides (**Figure 2**, **Table S1**). Phosphorylated derivatives, such as mannose phosphate, glucose 1-phosphate, and bisphosphorylated hexoses (D-glucose 2,6-bisphosphate, D-fructose 2,6-bisphosphate), were identified from sequential phosphate losses and diagnostic phosphate fragments, reflecting active carbohydrate metabolism in the bee bread matrix.

Gluconic acid, a product of glucose oxidation by glucose oxidase and a representative of the sugar acids class, was the most abundant compound detected across all analyzed bee bread extracts (**Table S1**), which is consistent with findings from previous reports on bee products [Aksoy *et al.*, 2024]. Its predominance is biologically relevant, as it is a primary contributor to the acidic pH of bee bread, which plays a key role in its antimicrobial and preservative properties through direct pH reduction and synergistic interactions with hydrogen peroxide and phenolic compounds [Çelik *et al.*, 2022]. Several other sugar acids, including arabinonic, galactaric, glucuronic, and tartaric acids, were also annotated. Low-molecular-weight organic acids, such as malic, quinic, isocitric, and citric acids, commonly reported in bee products, were detected alongside methylsuccinic acid, a methylated derivative of succinic acid not previously described in bee bread. In contrast, acetic, lactic, succinic, and oxalic acids were not detected, due to the mass cutoff of 120 Da applied in the analytical method, rather than their actual absence in the bee bread matrix. Notably, the organic acid profile of bee products remains understudied despite its potential as a quality and authenticity marker [Aksoy *et al.*, 2024; Çelik *et al.*, 2022].

Metabolomic analysis of bee bread extracts

Principal component analysis was used to visualize the variation in metabolomic profiles between the studied bee bread samples (**Figure 4**). In the negative mode, the first principal component (PC1) explained 18.1% of the total variance, while

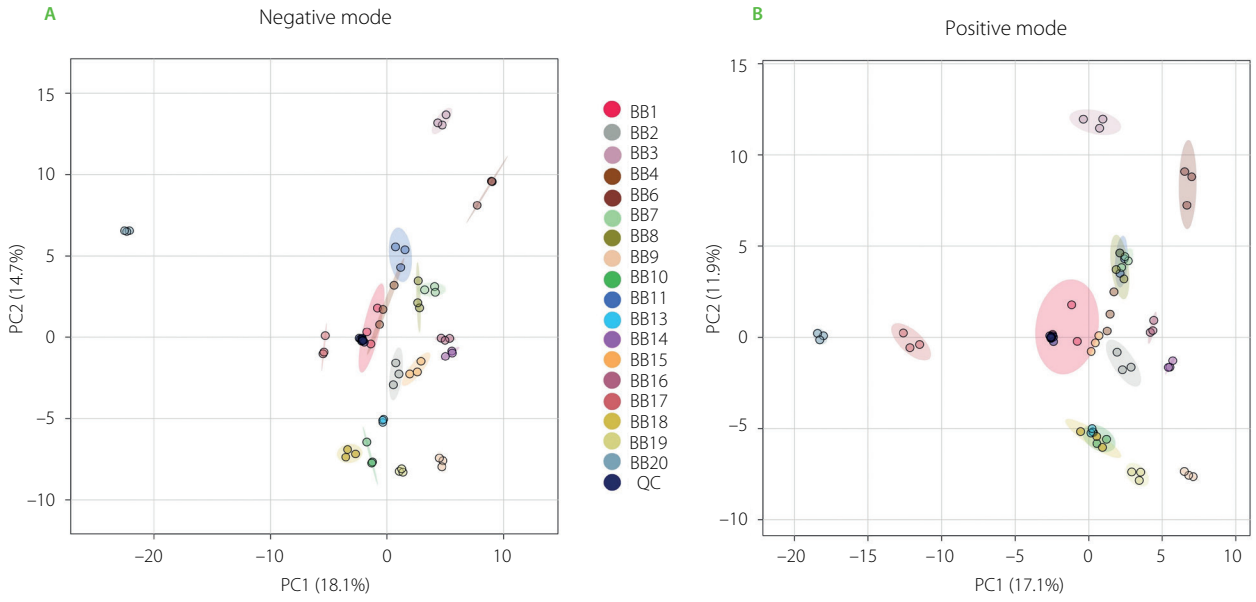

Figure 4. Results of principal component analysis (PCA) of the bee bread (BB) metabolomic data gathered from ultra-performance liquid chromatography–high-resolution mass spectrometry (UPLC-HRMS) analysis in a negative (**A**) and a positive ionization mode (**B**). QC, quality control sample.

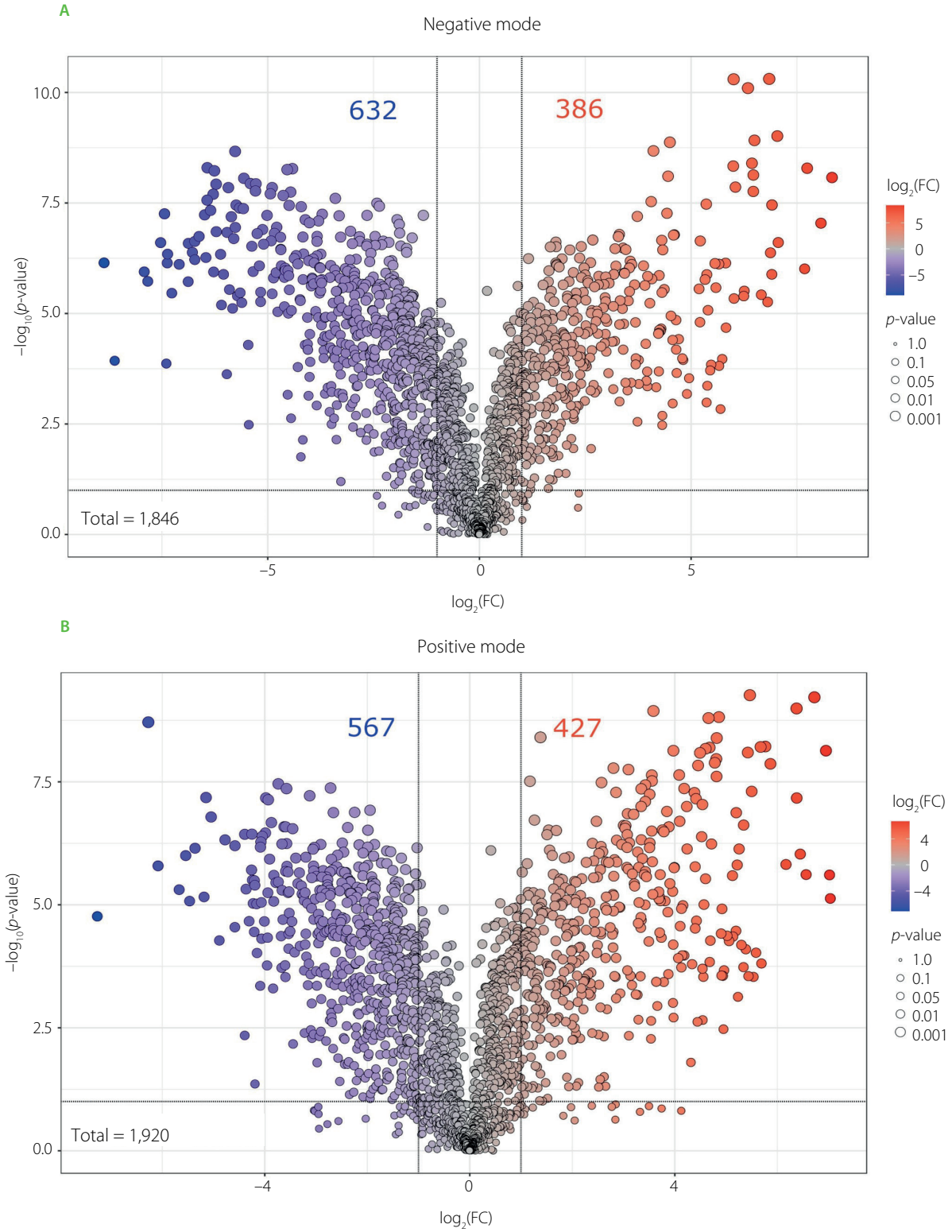

Figure 5. Volcano plots combining the results of fold change (FC) analysis and *t*-tests comparing metabolomic profiles of two bee bread samples with the highest (BB20, red dots) and lowest (BB15, dark blue dots) antiviral activity determined as the selectivity index.

the second component (PC2) accounted for 14.7% of the total variance. In the positive mode, PC1 and PC2 explained 17.1% and 11.9% of the total variance, respectively. In both modes, the QC sample was clustered tightly near the center of the plot, indicating good reproducibility of the measurements and overall analytical stability of the UPLC-HRMS system. The sample located furthest to the left on both the negative and positive mode PCA (BB20) was most distinct from all other samples in terms of its overall metabolomic profile. This pronounced separation suggests that BB20 possesses unique metabolic characteristics, encouraging further investigation into the factors contributing to its divergence from the other samples. Other groups also

formed well-defined clusters, but were positioned closer to the center, which suggests that their profiles are more similar to the overall dataset average. The limited overlap between clusters highlights that PCA effectively distinguishes the metabolomic profiles of the groups of compounds. This separation implies that the underlying metabolic differences between groups are substantial enough to be captured by the first two principal components.

While PCA provides an overview of the separation between sample groups based on their overall metabolomic profiles, volcano plots were used to identify specific features that are significantly different between the most contrasting samples – BB20 (red dots), being the most active against IAV, and BB15 (dark blue dots), being the least active (**Figure 5**). The upper extremes of the plot (both left and right) emphasize data points that exhibit substantial fold changes along with a strong statistical significance, marking them prime subjects for further analysis. In the negative ionization mode, out of 1,846 detected features, 632 showed a significant decrease and 386 showed a significant increase in BB20 compared to BB15. In turn, 1,920 features were detected in the positive ionization mode, with 567 showing significantly decreased abundance and 427 significantly increased abundance in BB20.

In the negative ionization mode, the compound that deviated the most from other compounds in BB20 sample (log_2(FC)>8) was quercetin 3-*O*-diglucosyl-*N*-acetylglucoside (**Table S1**, **Figure 5**). Quercetin and its derivatives are recognized for their antiviral efficacy against a wide array of viruses, including major respiratory pathogens such as influenza A virus, respiratory syncytial virus (RSV), rhinovirus (RV), and SARS-CoV-2 [Manjunath & Thimmulappa, 2022]. Their antiviral mechanism primarily involves interference with the viral entry by altering virion surface proteins. Consequently, quercetin may be used as a preventive agent or be used in combination with other pharmacological agents to enhance antiviral activity, potentially reducing toxicity and side effects of co-administrated agents [Di Petrillo *et al*., 2022]. Besides this compound, luteolin, isorhamnetin, kaempferol derivatives, and other quercetin-related flavonoids were also detected in the BB20 sample. These flavonoids exhibit a broad spectrum of biological activities, encompassing antiviral potential against many groups of viruses, such as influenza A virus [Dong *et al*., 2014; Ninfali *et al*., 2020; Yan *et al*., 2019]. Importantly, the synergistic effects of flavonoid mixtures may enhance their antiviral efficacy, underscoring the need for further investigation into their comprehensive qualitative and quantitative profiles [Ninfali *et al*., 2020]. On the other hand, in the BB15 sample, in both positive and negative ionization we found outliers belonging to the group of flavonoids, such as kaempferol, isorhamnetin, narcissin, and their derivatives. Despite the presence of flavonoids with established antiviral activity [Badshah *et al*., 2021], this particular sample exhibited the weakest antiviral effect in the comparative analysis. This discrepancy may be attributed to several factors, including a low content of active flavonoids, limited bioavailability, or antagonistic interactions with other matrix components that may suppress antiviral efficacy.

Furthermore, lactoyl amino acids, such as *N*-lactoyl-methionine and *N*-lactoyl-leucine, were identified in the BB20 sample (**Table S1**). Lactoyl amino acids, derived from amino acids, might indirectly affect immune responses by influencing amino acid metabolism [Naja *et al*., 2025]. However, there is no evidence for their direct antiviral potential. In the study conducted by Dimitriou *et al*. [2023], proteinaceous fractions isolated from bee bread demonstrated substantial antiviral activity against IAV. Although the detailed chemical composition of these fractions was not characterized, the reported high selectivity indexes imply the presence of bioactive compounds beyond commonly characterized flavonoids or phenolic acids. Our UPLC-HRMS analysis further revealed the presence of amino acids and related derivatives, potentially originating from peptide-based structures that remained unidentified due to their complex fragmentation patterns. The occurrence of such peptides and proteinaceous compounds may be attributed to the metabolic activity of microbial communities related to bee bread, such as lactic acid bacteria [Asoutis Didaras *et al*., 2024]. These bioactive peptides and proteins are hypothesized to contribute to the antiviral efficacy observed. Accordingly, comprehensive proteomic profiling of bee bread extracts may help explain the functional contribution of peptide-derived components in their therapeutic applications.

Surprisingly, analysis in the positive ionization mode revealed a considerable presence of organoheterocyclic compounds (**Table S1**). Among them, raphanusamide – a naturally occurring metabolite in *Raphanus sativus* L. (radish) – is associated with the plant's phototrophic response [Chen *et al*., 2023]. Other alkaloids were identified as well, including palaudine, *S*-reticuline, salsolinol, protopine, and venoterpine, that were earlier found in many plants belonging to Loganiaceae, Papaveraceae Juss., and Cornaceae families [Deng *et al*., 2021; Jafaar *et al*., 2021]. While alkaloids are known to exhibit diverse biological properties, *i.e.*, they possess antioxidant and anti-inflammatory activity and the ability to inhibit DNA and RNA synthesis, determining a viral replication blockage [Ponticelli *et al*., 2023], the data regarding antiviral activity of particular alkaloids found in our study remain limited. Hence, future research could exploit their presence and concentration in order to determine the botanical origin of BB.

On the other hand, in the BB15 sample, the compounds that deviated the most from other compounds (log_2(FC)<-7) were lipid derivatives, such as polyhydroxy fatty acids (9,10,13-trihydroxystearic acid, 9,10,12,13-tetrahydroxyoctadecanoic acid (sativic acid)), oxylipins (DiHODEs, 9-HOTrE), and lactobionic acid (**Table S1**, **Figure 5**). Despite exhibiting diverse biological functions [Harlina *et al*., 2024; Olajide & Cao, 2022], these bioactive lipid derivatives have not been evaluated for their antiviral potential.

Interestingly, in the positive ionization mode, lysophosphatidylcholine (LysoPC, 18:3/0:0) (**Table S1**, **Figure 5**) appeared as the most pronounced outlier in BB15. It has been implicated in enhancing influenza A virus replication by modulating the host cellular environment through MAPK, JNK, and PI3K/AKT signaling pathways [Cha *et al*., 2024]. Thus, its presence may be particularly significant in the context of lower antiviral potential of bee bread.

Nevertheless, the results obtained underscore the complexity of natural matrices, where both pro- and antiviral agents can be present simultaneously. As a result, it seems essential to assess the overall biological impact of the entire metabolite profile, rather than focusing solely on individual components, since their combined interactions may influence the final bioactivity.

CONCLUSIONS

This study demonstrates that aqueous extracts of bee bread possess notable antiviral activity against influenza A virus (H1N1), where 11 out of the 18 studied samples showed selective antiviral action (SI>10). The observed antiviral effects were likely influenced by the complex chemical composition of bee bread, which includes a diverse array of flavonoids, phenolic acids, amino acids, lipids, and carbohydrate derivatives. Metabolomic profiling *via* UPLC-HRMS revealed 218 distinct compounds, with flavonoids representing the most abundant (45 compounds; 20.6% of all annotated features) and structurally diverse class, dominated by flavonol glycosides. Flavonoids showed the greatest inter-sample variability in relative abundance among all chemical classes (4.2–13.3% of total peak area), with kaempferol and quercetin derivatives collectively accounting for over 60% of total flavonoid peak area, suggesting their key role in the observed variation of antiviral activity across samples. Notably, quercetin derivatives and other flavonoids with known antiviral properties were found in the most active samples. Additionally, 39 amino acid-related compounds (17.9% of total annotated features) and the presence of unidentified high-mass compounds suggest the potential involvement of bioactive peptides, possibly originating from microbial fermentation processes. These findings support the hypothesis that both phenolic and proteinaceous compounds contribute to the antiviral efficacy of bee bread. Further proteomic investigations are, however, needed to elucidate the identity and functional role of peptide-based compounds. Overall, bee bread emerges as a promising functional food supporting viral infection treatment, meriting continued exploration for therapeutic applications.

RESEARCH FUNDING

The research was funded by grant UMO-2022/45/N/NZ9/02710 financed by National Science Centre (Poland).

CONFLICT OF INTERESTS

There is no conflict of interest, according to the authors.

SUPPLEMENTARY MATERIALS

The following are available online at **https://journal.pan.olsztyn.pl/Metabolomic-Insights-into-Bee-Bread-Antiviral-Activity-Against-Influenza-A-Virus,221951,0,2.html**; **Table S1**. Chemical composition of bee bread samples after UPLC-MS/MS analysis.

ORCID IDs

T.G. Dimitriou **https://orcid.org/0000-0001-5413-3069**
B. Kusznierewicz **https://orcid.org/0000-0001-8138-3872**
K. Matejczuk **https://orcid.org/0000-0003-2523-8165**
D. Mossialos **https://orcid.org/0000-0003-3753-4287**
M. Mróz **https://orcid.org/0000-0003-2791-3363**
P. Szweda **https://orcid.org/0000-0001-8291-5148**

REFERENCES

1. Aksoy, A., Altunatmaz, S.S., Aksu, F., Tokatlı Demirok, N., Yazıcı, K., Yıkmış, S. (2024). Bee bread as a functional product: Phenolic compounds, amino acid, sugar, and organic acid profiles. *Foods*, *13*(5), art. no. 795. **https://doi.org/10.3390/foods13050795**
2. Asma, S.T., Bobiş, O., Bonta, V., Acaroz, U., Shah, S.R.A., Istanbullugil, F.R., Arslan-Acaroz, D. (2022). General nutritional profile of bee products and their potential antiviral properties against mammalian viruses. *Nutrients*, *14*(17), art. no. 3579. **https://doi.org/10.3390/nu14173579**
3. Asoutis Didaras, N., Dimitriou, T., Daskou, M., Karatasou, K., Mossialos, D. (2022). *In vitro* assessment of the antiviral activity of Greek bee bread and bee collected pollen against Enterovirus D68. *Journal of Microbiology, Biotechnology and Food Sciences*, *11*(4), art. no. e4859. **https://doi.org/10.55251/jmbfs.4859**
4. Asoutis Didaras, N., Karaiskou, I., Nikolaidis, M., Siaperopoulou, C., Georgi, I., Tsadila, C., Karatasou, K., Amoutzias, G.D., Mossialos, D. (2024). Contribution of microbiota to bioactivity exerted by bee bread. *Pharmaceuticals*, *17*(6), art. no. 761. **https://doi.org/10.3390/ph17060761**
5. Aylanc, V., Falcão, S.I., Vilas-Boas, M. (2023). Bee pollen and bee bread nutritional potential: Chemical composition and macronutrient digestibility under *in vitro* gastrointestinal system. *Food Chemistry*, *413*, art. no. 135597. **https://doi.org/10.1016/j.foodchem.2023.135597**
6. Badshah, S.L., Faisal, S., Muhammad, A., Poulson, B.G., Emwas, A.H., Jaremko, M. (2021). Antiviral activities of flavonoids. *Biomedicine & Pharmacotherapy*, *140*, art. no. 111596. **https://doi.org/10.1016/j.biopha.2021.111596**
7. Bakour, M., Fernandes, Â., Barros, L., Sokovic, M., Ferreira, I.C.F.R., Lyoussi, B. (2019). Bee bread as a functional product: Chemical composition and bioactive properties. *LWT – Food Science and Technology*, *109*, 276–282. **https://doi.org/10.1016/j.lwt.2019.02.008**
8. Bakour, M., Laaroussi, H., Ousaaid, D., El Ghouizi, A., Es-Safi, I., Mechchate, H., Lyoussi, B. (2022). Bee bread as a promising source of bioactive molecules and functional properties: An up-to-date review. *Antibiotics*, *11*(2), art. no. 203. **https://doi.org/10.3390/antibiotics11020203**
9. Cavalli, R., Donalisio, M., Bisazza, A., Civra, A., Ranucci, E., Ferruti, P., Lembo, D. (2012). Enhanced antiviral activity of acyclovir loaded into nanoparticles. *Methods in Enzymology, 509*, pp. 1–19. **https://doi.org/10.1016/B978-0-12-391858-1.00001-0**
10. Çelik, S., Gerçek, Y.C., Özkök, A., Ecem Bayram, N. (2022). Organic acids and their derivatives: minor components of bee pollen, bee bread, royal jelly and bee venom. *European Food Research and Technology*, *248*(12), 3037–3057. **https://doi.org/10.1007/s00217-022-04110-y**
11. Cha, M.-H., Choi, H.-J., Ma, J.-Y. (2024). Lysophosphatidylcholines promote influenza virus reproduction through the MAPK/JNK pathway in PMA-differentiated THP-1 macrophages. *International Journal of Molecular Sciences*, *25*(12), art. no. 6538. **https://doi.org/10.3390/ijms25126538**
12. Chen, C., Kim, R.H., Hwang, K.T., Kim, J. (2023). Chemical compounds and bioactivities of the extracts from radish (*Raphanus sativus*) sprouts exposed to red and blue light-emitting diodes during cultivation. *European Food Research and Technology*, *249*(6), 1551–1562. **https://doi.org/10.1007/s00217-023-04235-8**
13. Ćirić, J., Haneklaus, N., Rajić, S., Baltić, T., Lazić, I.B., Đorđević, V. (2022). Chemical composition of bee bread (perga), a functional food: A review. *Journal of Trace Elements and Minerals*, *2*, art. no. 100038. **https://doi.org/10.1016/j.jtemin.2022.100038**
14. Darwish, A., Abd El-Wahed, A., Shehata, M., El-Seedi, H., Masry, S., Khalifa, S., Mahfouz, H., El-Sohaimy, S. (2022). Chemical profiling and nutritional evaluation of bee pollen, bee bread, and royal jelly and their role in functional fermented dairy products. *Molecules*, *28*(1), art. no. 227. **https://doi.org/10.3390/molecules28010227**

15. Deng, A.-P., Zhang, Y., Zhou, L., Kang, C.-Z., Lv, C.-G., Kang, L.-P., Nan, T.-G., Zhan, Z.-L., Guo, L.-P., Huang, L.-Q. (2021). Systematic review of the alkaloid constituents in several important medicinal plants of the Genus *Corydalis*. *Phytochemistry*, *183*, art. no. 112644.
https://doi.org/10.1016/j.phytochem.2020.112644
16. Dimitriou, T.G., Asoutis Didaras, N., Barda, C., Skopeliti, D., Kontogianni, K., Karatasou, K., Skaltsa, H., Mossialos, D. (2023). Antiviral activity of beebread, bee-collected pollen and artificially fermented pollen against influenza A virus. *Foods*, *12*(10), art. no. 1978.
https://doi.org/10.3390/foods12101978
17. Di Petrillo, A., Orrù, G., Fais, A., Fantini, M. C. (2022). Quercetin and its derivates as antiviral potentials: A comprehensive review. *Phytotherapy Research*, *36*(1), 266–278.
https://doi.org/10.1002/ptr.7309
18. Dong, W., Wei, X., Zhang, F., Hao, J., Huang, L., Zhang, C., Liang, W. (2014). A dual character of flavonoids in influenza A virus replication and spread through modulating cell-autonomous immunity by MAPK signaling pathways. *Scientific Reports, 4*, art. no. 7237.
https://doi.org/10.1038/srep07237
19. Eisfeld, A.J., Neumann, G., Kawaoka, Y. (2014). Influenza A virus isolation, culture and identification. *Nature Protocols*, *9*(11), 2663–2681.
https://doi.org/10.1038/nprot.2014.180
20. Gull, T., Sultana, B., Anwar, F., Nouman, W., Mehmood, T., Sher, M. (2018). Characterization of phenolics in different parts of selected *Capparis* species harvested in low and high rainfall season. *Journal of Food Measurement and Characterization*, *12*(3), 1539–1547.
https://doi.org/10.1007/s11694-018-9769-5
21. Harlina, P.W., Maritha, V., Yang, X., Dixon, R., Muchtaridi, M., Shahzad, R., Nur'Isma, E.A. (2024). Exploring oxylipins in processed foods: Understanding mechanisms, analytical perspectives, and enhancing quality with lipidomics. *Heliyon*, *10*(16), art. no. e35917.
https://doi.org/10.1016/j.heliyon.2024.e35917
22. Hendriks, B.S. (2010). Functional pathway pharmacology: chemical tools, pathway knowledge and mechanistic model-based interpretation of experimental data. *Current Opinion in Chemical Biology*, *14*(4), 489–497.
https://doi.org/10.1016/j.cbpa.2010.06.167
23. Ilie, C.I., Spoiala, A., Geana, E.I., Chircov, C., Ficai, A., Ditu, L.M., Oprea, E. (2024). Bee bread: A promising source of bioactive compounds with antioxidant properties – First report on some antimicrobial features. *Antioxidants*, *13*(3), art. no. 353.
https://doi.org/10.3390/antiox13030353
24. Jafaar, H.J., Isbilen, O., Volkan, E., Sariyar, G. (2021). Alkaloid profiling and antimicrobial activities of *Papaver glaucum* and *P. decaisnei*. *BMC Research Notes*, *14*(1), art. no. 348.
https://doi.org/10.1186/s13104-021-05762-x
25. Kaplan, M., Karaoglu, Ö., Eroglu, N., Silici, S. (2016). Fatty acids and proximate composition of beebread. *Food Technology and Biotechnology*, *54*(4).
https://doi.org/10.17113/ftb.54.04.16.4635
26. Kontogiannis, T., Dimitriou, T.G., Didaras, N.A., Mossialos, D. (2022). Antiviral activity of bee products. *Current Pharmaceutical Design*, *28*(35), 2867–2878.
https://doi.org/10.2174/1381612828666220928110103
27. Lam, J.H., Baumgarth, N. (2019). The multifaceted B cell response to influenza virus. *The Journal of Immunology*, *202*(2), 351–359.
https://doi.org/10.4049/jimmunol.1801208
28. Litewski, S., Koss-Mikołajczyk, I., Kusznierewicz, B. (2024). Comparative analysis of phytochemical profiles and selected biological activities of various morphological parts of *Ligustrum vulgare*. *Molecules*, *29*(2), art. no. 399.
https://doi.org/10.3390/molecules29020399
29. Manjunath, S.H., Thimmulappa, R.K. (2022). Antiviral, immunomodulatory, and anticoagulant effects of quercetin and its derivatives: Potential role in prevention and management of COVID-19. *Journal of Pharmaceutical Analysis*, *12*(1), 29–34.
https://doi.org/10.1016/j.jpha.2021.09.009
30. Mărgăoan, R., Strant, M., Varadi, A., Topal, E., Yücel, B., Cornea-Cipcigan, M., Campos, M.G., Vodnar, D.C. (2019). Bee collected pollen and bee bread: Bioactive constituents and health benefits. *Antioxidants*, *8*(12), art. no. 568.
https://doi.org/10.3390/antiox8120568
31. Márquez-Bandala, A.H., Gutierrez-Xicotencatl, L., Esquivel-Guadarrama, F. (2025). Pathogenesis induced by influenza virus infection: Role of the early events of the infection and the innate immune response. *Viruses*, *17*(5), art. no. 694.
https://doi.org/10.3390/v17050694
32. Mayda, N., Özkök, A., Ecem Bayram, N., Gerçek, Y.C., Sorkun, K. (2020). Bee bread and bee pollen of different plant sources: determination of phenolic content, antioxidant activity, fatty acid and element profiles. *Journal of Food Measurement and Characterization*, *14*(4), 1795–1809.
https://doi.org/10.1007/s11694-020-00427-y
33. McGaw, L.J., Elgorashi, E.E., Eloff, J.N. (2014). Chapter 8: Cytotoxicity of African medicinal plants against normal animal and human cells. In V. Kuete (Ed.), *Toxicological Survey of African Medicinal Plants*, Elsevier, pp. 181–233.
https://doi.org/10.1016/B978-0-12-800018-2.00008-X
34. Mohammed, E.A., Abdalla, I.G., Alfawaz, M.A., Mohammed, M.A., Al Maiman, S.A., Osman, M.A., Yagoub, A.E.A., Hassan, A.B. (2022). Effects of extraction solvents on the total phenolic content, total flavonoid content, and antioxidant activity in the aerial part of root vegetables. *Agriculture*, *12*(11), art. no. 1820.
https://doi.org/10.3390/agriculture12111820
35. Naja, K., Hedaya, L., Elashi, A.A., Rizzo, M., Elrayess, M.A. (2025). N-Lactoyl amino acids: Emerging biomarkers in metabolism and disease. *Diabetes Metabolism Research and Reviews*, *41*(5), art. no. e70060.
https://doi.org/10.1002/dmrr.70060
36. Ninfali, P., Antonelli, A., Magnani, M., Scarpa, E.S. (2020). Antiviral properties of flavonoids and delivery strategies. *Nutrients*, *12*(9), art. no. 2534.
https://doi.org/10.3390/nu12092534
37. Olajide, T.M., Cao, W. (2022). Exploring foods as natural sources of FAHFAs – A review of occurrence, extraction, analytical techniques and emerging bioactive potential. *Trends in Food Science & Technology*, *129*, 591–607.
https://doi.org/10.1016/j.tifs.2022.11.005
38. Otręba, M., Marek, Ł., Stojko, J., Rzepecka-Stojko, A. (2025). Bee products as alternatives in the treatment of viral infections. *Journal of the Science of Food and Agriculture, 106*(1), 33-54.
https://doi.org/10.1002/jsfa.70017
39. Pełka, K., Otłowska, O., Worobo, R.W., Szweda, P. (2021). Bee bread exhibits higher antimicrobial potential compared to bee pollen. *Antibiotics*, *10*(2), art. no. 125.
https://doi.org/10.3390/antibiotics10020125
40. Ponticelli, M., Bellone, M.L., Parisi, V., Iannuzzi, A., Braca, A., de Tommasi, N., Russo, D., Sileo, A., Quaranta, P., Freer, G., Pistello, M., Milella, L. (2023). Specialized metabolites from plants as a source of new multi-target antiviral drugs: a systematic review. *Phytochemistry Reviews*, *22*(3), 615–693.
https://doi.org/10.1007/s11101-023-09855-2
41. Qiao, J., Feng, Z., Zhang, Y., Xiao, X., Dong, J., Haubruge, E., Zhang, H. (2023). Phenolamide and flavonoid glycoside profiles of 20 types of monofloral bee pollen. *Food Chemistry*, *405*(Part A), art. no. 134800.
https://doi.org/10.1016/j.foodchem.2022.134800
42. Sawicki, T., Starowicz, M., Kłębukowska, L., Hanus, P. (2022). The profile of polyphenolic compounds, contents of total phenolics and flavonoids, and antioxidant and antimicrobial properties of bee products. *Molecules*, *27*(4), art. no. 1301.
https://doi.org/10.3390/molecules27041301
43. Stachelska, M.A., Karpiński, P., Kruszewski, B. (2025). A comprehensive review of biological properties of flavonoids and their role in the prevention of metabolic, cancer and neurodegenerative diseases. *Applied Sciences*, *15*(19), art. no. 10840.
https://doi.org/10.3390/app151910840
44. Urcan, A.C., Criste, A.D., Dezmirean, D.S., Bobiş, O., Bonta, V., Dulf, F.V., Mărgăoan, R., Cornea-Cipcigan, M., Campos, M.G. (2021). Botanical origin approach for a better understanding of chemical and nutritional composition of bee bread as an important value-added food supplement. *LWT – Food Science and Technology*, *142*, art. no. 111068.
https://doi.org/10.1016/j.lwt.2021.111068
45. Yan, H., Ma, L., Wang, H., Wu, S., Huang, H., Gu, Z., Jiang, J., Li, Y. (2019). Luteolin decreases the yield of influenza A virus *in vitro* by interfering with the coat protein I complex expression. *Journal of Natural Medicines, 73*(3), 487–496.
https://doi.org/10.1007/s11418-019-01287-7
46. Yan, S., Zhang, M., Yuan, Y., Mu, G., Xu, H., Zhao, T., Wang, Y., Xue, X. (2023). Chaste honey in long term-storage: Occurrence and accumulation of Maillard reaction products, and safety assessment. *Food Chemistry*, *424*, art. no. 136457.
https://doi.org/10.1016/j.foodchem.2023.136457
47. Zhang, J., Qiao, J., Zhang, Y., Zhu, H., Haubruge, E., Liu, L., Dong, J. (2025). Di-*p*-coumaroyl spermidine from bee pollen alleviates chronic nonbacterial prostatitis. *Food Science & Nutrition*, *13*(6), art. no. e70467.
https://doi.org/10.1002/fsn3.70467

INSTRUCTIONS FOR AUTHORS

SUBMISSION. Original contributions relevant to food and nutrition sciences are accepted on the understanding that the material has not been, nor is being, considered for publication elsewhere. All papers should be submitted and will be processed electronically via Editorial Manager system (available from PJFNS web site: http://journal.pan.olsztyn.pl). On submission, a corresponding author will be asked to provide: Cover letter; Files with Manuscripts, Tables, Figures/Photos; and Names of two potential reviewers (one from the author's homeland – but outside author's Institution, and the other from abroad). All papers which have been qualified as relevant with the scope of our Journal are reviewed. All contributions, except the invited reviews are charged. Proofs will be sent to the corresponding author and should be returned within one week since receipt. No new material may be inserted in the text at proof stage. It is the author's duty to proofread proofs for errors.

Authors should very carefully consider the preparation of papers to ensure that they communicate efficiently, because it permits the reader to gain the greatest return for the time invested in reading. Thus, we are more likely to accept those that are carefully designed and conform the instruction. Otherwise, papers will be rejected and removed from the online submission system.

SCOPE. The Polish Journal of Food and Nutrition Sciences publishes original, basic and applied papers, and reviews on fundamental and applied food research, preferably these based on a research hypothesis, in the following Sections:

Food Technology:
- Innovative technology of food development including biotechnological and microbiological aspects
- Effects of processing on food composition and nutritional value

Food Chemistry:
- Bioactive constituents of foods
- Chemistry relating to major and minor components of food
- Analytical methods

Food Quality and Functionality:
- Sensory methodologies
- Functional properties of food
- Food physics
- Quality, storage and safety of food

Nutritional Research:
- Nutritional studies relating to major and minor components of food (excluding works related to questionnaire surveys)

"News" section:
- Announcements of congresses
- Miscellanea

OUT OF THE SCOPE OF THE JOURNAL ARE:
- Works which do not have a substantial impact on food and nutrition sciences
- Works which are of only local significance i.e. concern indigenous foods, without wider applicability or exceptional nutritional or health related properties
- Works which comprise merely data collections, based on the use of routine analytical or bacteriological methods (i.e. standard methods, determination of mineral content or proximate analysis)
- Works concerning biological activities of foods but not providing the chemical characteristics of compounds responsible for these properties
- Nutritional questionnaire surveys
- Works related to the characteristics of foods purchased at local markets
- Works related to food law
- Works emphasizing effects of farming / agricultural conditions / weather conditions on the quality of food constituents
- Works which address plants for non-food uses (i.e. plants exhibiting therapeutic and/or medicinal effects)

TYPES OF CONTRIBUTIONS. *Reviews*: (at least: 30 pages and 70 references) these are critical and conclusive accounts on trends in food and nutrition sciences; *Original papers*: (maximally: 30 pages and 40 references) these are reports of substantial research; *Reports on post and forthcoming scientific events, and letters to the Editor* (all up to three pages) are also invited (free of charge).

REVIEW PROCESS. All scientific contributions will be peer-reviewed on the criteria of originality and quality. Submitted manuscripts will be preevaluated by Editor-in-Chief and Statistical Editor (except for review articles), and when meeting PJFNS' scope and formal

requirements, they will be sent to a Section Editor who upon positive preevaluation will assign at least two reviewers from Advisory Board Members, reviewers suggested by the author or other experts in the field. Based on the reviews achieved, Section Editor and Editor-in--Chief will make a decision on whether a manuscript will be accepted for publication, sent back to the corresponding author for revision, or rejected. Once a manuscript is sent back to the corresponding author for revision, all points of the reviews should be answered or rebuttal should be provided in the Explanation letter. The revised manuscripts will be checked by Section Editor and by the original reviewers (if necessary), and a final decision will be made on acceptance or rejection by both Section Editor and Editor-in-Chief.

Polish Journal of Food and Nutrition Sciences uses CrossCheck's iThenticate software to detect instances of similarity in submitted manuscripts. In publishing only original research, PJFNS is committed to deterring plagiarism, including self-plagiarism.

COPYRIGHT LICENSE AGREEMENT referring to Authorship Responsibility and Acknowledgement, Conflict of Interest and Financial Disclosure, Copyright Transfer, are required for all authors, i.e. *Authorship Responsibility and Acknowledgement*: Everyone who has made substantial intellectual contributions to the study on which the article is based (for example, to the research question, design, analysis, interpretation, and written description) should be an author. It is dishonest to omit mention of someone who has participated in writing the manuscript ("ghost authorship") and unfair to omit investigator who have had important engagement with other aspects of the work. All contributors who do not meet the criteria for authorship should be listed in an Acknowledgments section. Examples of those who might be acknowledged include a person who provided purely technical help, writing assistance, or a department chairperson who provided only general support. Any financial and material support should also be acknowledged. *Conflict of Interest and Financial Disclosure*: Authors are responsible for disclosing financial support from the industry or other conflicts of interest that might bias the interpretation of results. *License to Publish*: All articles published on the website of Polish Journal of Food and Nutrition Sciences are available in the Open Access format, meaning they are freely accessible online without charge to anyone, anywhere.

Since volume 75, Authors publish their works under the Creative Commons Attribution 4.0 License (CC BY 4.0). Pursuant to the License terms, Authors retain the copyright and full publishing rights without restrictions. The License permits unrestricted use, distribution and reproduction, provided that the original work is cited. The specific license terms of use are available on https://creativecommons.org/licenses/by/4.0/

In volumes 64–74, Authors published their works under the Creative Commons Attribution-NonCommercial-NoDerivs Licenses (CC BY-NC-ND) 3.0 and 4.0, pursuant to which they retained the copyright, and other proprietary rights relating to the article, such as patent rights, to use the substance of the article in future own works, including lectures and books, to reproduce the article for own purposes, provided the copies are not intended for commercial re-use or for share of the adapted and derivative versions. The specific license terms of use are available on http://creativecommons.org/licenses/by-nc-nd/3.0 and http://creativecommons.org/licenses/by-nc-nd/4.0.

In earlier volumes (47–63), Authors published their works under Copyright Transfer License, pursuant to which they retained the right to revise, adapt, prepare derivative works, present orally, or distribute the work provided that all such use was for the personal noncommercial benefit of the author(s) and was consistent with any prior contractual agreement between the publisher and authors.

A manuscript will not be published once the signed form has not been submitted to the Editor with the manuscript revised after positive reviews.

CHANGES TO AUTHORHIP. Authors are expected to consider carefully the list and order of authors before submitting their manuscript and provide the definitive list of authors at the time of the original submission. Any addition, deletion or rearrangement of author names in the authorship list should be made only before the manuscript has been accepted and only if approved by the journal Editor. To request such a change, the Editor must receive the following from the corresponding author: (a) the reason for the change in author list and (b) written confirmation (e-mail, letter) from all authors that they agree with the addition, removal or rearrangement. In the case of addition or removal of authors, this includes confirmation from the author being added or removed.

ETHICAL APPROVAL OF STUDIES AND INFORMED CONSENT. For all manuscripts reporting data from studies involving human participants or animals, formal approval by an appropriate institutional review board or ethics committee is required and should be described in the Methods section. For those investigators who do not have formal approval from ethics review committees, the principles outlined in the Declaration of Helsinki should be followed. For investigations of humans, state in the Methods section the manner in which informed consent was obtained from the study participants (i.e., oral or written). Editors may request that authors provide documentation of the formal review and recommendation from the institutional review board or ethics committee responsible for oversight of the study.

UNAUTHORIZED USE. Unauthorized use of the PJFNS name, logo, or any content for commercial purposes or to promote commercial goods and services (in any format, including print, video, audio, and digital) is not permitted by IAR&FR PAS.

MANUSCRIPTS. A manuscript in English must be singlesided, preferably in Times New Roman (12) with 1.5-point spacing, without numbers of lines. The Editor reserves the right to make literary corrections and to make suggestions to improve brevity. English is the official language. The English version of the paper will be checked by Language Editor. Unclear and unintelligible version will be returned for correction.

Every paper should be divided under the following headings in this order: a **Title** (possibly below 150 spaces); the **Name(s)** of the author(s) in full. In paper with more than one author, the asterisk indicates the name of the author to whom correspondence and inquiries should be addressed, otherwise the first author is considered for the corre-spondence. Current full postal address of the indicated corresponding author or the first author must be given in a footnote on the title page; the **Place(s)** where the work was done including the institution name, city, country if not Poland. In papers originated from several institu-tions the names of the authors should be marked with respective superscripts; the **Key words** (up to 6 words or phrases) for the main topics of the paper; an **Abstract** (up to 250 words for regular papers and reviews) summarizing briefly main results of the paper, no literature references; an **Introduction** giving essential background by saying why the research is important, how it relates to previous works and stating clearly the objectives at the end; **Materials and Methods** with

sufficient experimental details permitting to repeat or extend the experiments. Literature references to the methods, sources of material, company names and location (city, country) for specific instruments must be given. Describe how the data were evaluated, including selection criteria used; **Results and Discussion** presented together (in one chapter). Results should be presented concisely and organized to supplement, but not repeat, data in tables and figures. Do not display the data in both tabular and graphic form. Use narrative form to present the data for which tables or figures are unnecessary. Discussion should cover the implications and consequences, not merely recapitulating the results, and it must be accomplished with concise **Conclusions**; **Acknowledgements** should be made to persons who do not fill the authorship criteria (see: Authorship forms); **Research funding** should include financial and material support; **Conflict of Interests**: Authors should reveal any conflicts of interest that might bias the interpretation of results; **Other information** including Generative AI use declaration and other important information (See Editorial Policy section for details on the journal website). **References** as shown below.

REFERENCES each must be listed alphabetically at the end of the paper (each should have an Arabic number in the list) in the form as follows: **Periodicals** – names and initials of all the authors, year of publication, title of the paper, journal title as in Chemical Abstracts, year of publication, volume, issue, inclusive page numbers, or article id.; **Books** – names and initials of all the authors, names of editors, chapter title, year of publication, publishing company, place of publication, inclusive page numbers; **Patents** – the name of the application, the title, the country, patent number or application number, the year of publication.

For papers published in language other than English, manuscript title should be provided in English, whereas a note on the original language and English abstract should be given in parentheses at the end.

The reference list should only include peer-reviewed full-text works that have been published or accepted for publication. Citations of MSc/PhD theses and works unavailable to international Editors, Reviewers, and Readers should be limited as much as possible.

References in the text must be cited by name and year in square parentheses (e.g.: one author – [Tokarz, 1994]; two authors – [Słonimski & Campbell, 1987]; more than two authors – [Amarowicz *et al*., 1994]). If more than one paper is published in the same year by the same author or group of authors use [Tokarz, 1994a, b]. Unpublished work must only be cited where necessary and only in the text by giving the person's name.

Examples:

Article in a journal:

Słonimski, B.A., Campbell, L.D., Batista, E., Howard B. (2008). Gas chromatographic determination of indole glucosinolates. Journal of Science and Food Agriculture, 40(5), 131–143.

Asher, A., Tintle, N.L., Myers, M., Lockshon, L., Bacareza, H., Harris, W.S. (2021). Blood omega-3 fatty acids and death from COVID-19: A pilot study. *Prostaglandins, Leukotrienes and Essential Fatty Acids, 166*, art. no. 102250.

Book: Weber, W., Ashton, L., Milton, C. (2012). Antioxidants – Friends or Foes? 2nd editition. PBD Publishing, Birmingham, UK. pp. 218–223.
Chapter in a book: Uden, C., Gambino, A., Lamar, K. (2016). Gas chromatography. In M. Queresi, W. Bolton (Eds.), CRC Handbook of Chromatography, CRC Press Inc., Boca Raton, Florida, USA, pp. 44–46.

ABBREVIATIONS AND UNITS. Abbreviations should only be used when long or unwieldy names occur frequently, and never in the title; they should be given at the first mention of the name. Metric SI units should be used. The capital letter L should be used for liters. Avoid the use of percentages (% g/g,% w/w; Mol%; vol%), ppm, ppb. Instead, the expression such as g/kg, g/L, mg/kg, mg/mL should be used. A space must be left between a number and a symbol (e.g. 50 mL not 50mL). A small x must be used as multiplication sign between numeric values (e.g. 5 × 102 g/mL). Statistics and measurements should be given in figures, except when the number begins a sentence. Chemical formulae and solutions must specify the form used. Chemical abbreviations, unless they are internationally known, Greek symbols and unusual symbols for the first time should be defined by name. Common species names should be followed by the Latin at the first mention, with contracting it to a single letter or word for subsequent use.

FIGURES should be submitted in separate files. Each must have an Arabic number and a caption. Captions of all Figures should be provided on a separate page "Figure Captions". Figures should be comprehensible without reference to the text. Self-explanatory legend to all figures should be provided under the heading "Legends to figures"; all abbreviations appearing on figures should be explained in figure footnotes. Three-dimensional graphs should only be used to illustrate real 3D relationships. Start the scale of axes and bars or columns at zero, do not interrupt them or omit missing data on them. Figures must be cited in Arabic numbers in the text.

TABLES should be submitted in separate files. They should be as few in number and as simple as possible (like figures, they are expensive and space consuming), and include only essential data with appropriate statistical values. Each must have an Arabic number and a caption. Captions of all Tables should be provided on a separate page "Table Captions". Tables should be self-explanatory; all abbreviations appearing in tables should be explained in table footnotes. Tables must be cited in Arabic numbers in the text.

PUBLICATION FEE. Since 16th December 2024, a standard publication fee has been established at the rate of 500 EUR (plus VAT if applicable, e.g. for private persons). For Polish Authors an equivalent fee was set at 1950 PLN +23%VAT. The fee applies irrespective of the number of pages and tables/figures in the manuscript. Payment instructions will be sent to Authors via e-mail with acceptance letter.

Information on publishing and subscription is available from:

Ms. Joanna Molga
Editorial Office of Pol. J. Food Nutr. Sci.
InLife Institute of Animal Reproduction and Food Research, Polish Academy of Sciences, Trylińskiego 18, 10-683 Olsztyn, Poland
phone (48 89) 500 32 45
e-mail: pjfns@pan.olsztyn.pl; http://journal.pan.olsztyn.pl

Nutrition